**NTNU – Trondheim**
Norwegian University of
Science and Technology

# Wet Gas Compressor Surge Detection

Marie Rennemo Jellum

Master of Energy and Environmental Engineering
Submission date: June 2013
Supervisor: Lars Eirik Bakken, EPT
Co-supervisor: Tor Bjørge, EPT

Norwegian University of Science and Technology
Department of Energy and Process Engineering

NTNU
Norges teknisk-
naturvitenskapelige universitet

Institutt for energi- og prosessteknikk

EPT-M-2013-59

# MASTEROPPGAVE

for

Stud.techn. Marie Rennemo Jellum

Våren 2013

**Deteksjon av surge i våtgasskompressorer**
*Wet gas compressor surge detection*

**Bakgrunn**
De fleste store felt i Nordsjøen er utbygd med tradisjonell teknologi. Fokus har i de senere år skiftet mot mindre og mer fjerntliggende felt med begrenset infrastruktur. Utvikling og drift av slike felt krever ny kostnadseffektiv teknologi. Et helt sentralt element her er havbunnsbasert brønnkompresjon for å frakte brønnstrømmen direkte til land, eller mer fjerntliggende prosesseringsanlegg offshore.
Teknologien kan i enkelte tilfelle eliminere behovet for offshore prosessanlegg, noe som kan gi en formidabel kostnadsreduksjon. De fleste leverandører av turbomaskiner satser derfor på utvikling av havbunnsbaserte våtgasskompressorer. Noen få prototype konsepter eksisterer og det foregår i dag utstrakt testing og validering av teknologien.
Ved NTNU er det bygd opp en rigg for å teste våtgass kompressorer og analysere de grunnleggende mekanismene relatert til våtgass kompresjon. Riggen er unik og sentral i blant annet analyser av ustabilitet i våtgass strømning.

**Mål**
Basert på litteratur og tidligere eksperimentelt arbeid i våtgass kompresjonsrigg er det et mål å dokumentere fenomener relatert til våtgass surge. Spesielt vektlegges bruk av transiente trykkmålinger for å validere ustabiliteter i våtgass strømningsregime hvor sensorer kan ligge i væskefilmen lang kanalene.

**Oppgaven bearbeides ut fra følgende punkter:**

1. Litteraturstudie for å dokumentere hvordan ulike trykksensorer responderer på aerodynamisk ustabilitet i våtgass strømning.

2. Prosjektere laboratorierigg for å validere trykksensorers evne til å detektere trykkpulsasjoner i forbindelse med våtgass surge og stall.

3. Dokumentere hvordan optimal sensor for surgedeteksjon kan benyttes til pålitelig anti surge kontroll av havbunnsbasert våtgasskompressor.

" - "

Senest 14 dager etter utlevering av oppgaven skal kandidaten levere/sende instituttet en detaljert fremdrift- og eventuelt forsøksplan for oppgaven til evaluering og eventuelt diskusjon med faglig ansvarlig/veiledere. Detaljer ved eventuell utførelse av dataprogrammer skal avtales nærmere i samråd med faglig ansvarlig.

Besvarelsen redigeres mest mulig som en forskningsrapport med et sammendrag både på norsk og engelsk, konklusjon, litteraturliste, innholdsfortegnelse etc. Ved utarbeidelsen av teksten skal kandidaten legge vekt på å gjøre teksten oversiktlig og velskrevet. Med henblikk på lesning av besvarelsen er det viktig at de nødvendige henvisninger for korresponderende steder i tekst, tabeller og figurer anføres på begge steder. Ved bedømmelsen legges det stor vekt på at resultatene er grundig bearbeidet, at de oppstilles tabellarisk og/eller grafisk på en oversiktlig måte, og at de er diskutert utførlig.

Alle benyttede kilder, også muntlige opplysninger, skal oppgis på fullstendig måte. For tidsskrifter og bøker oppgis forfatter, tittel, årgang, sidetall og eventuelt figurnummer.

Det forutsettes at kandidaten tar initiativ til og holder nødvendig kontakt med faglærer og veileder(e). Kandidaten skal rette seg etter de reglementer og retningslinjer som gjelder ved alle (andre) fagmiljøer som kandidaten har kontakt med gjennom sin utførelse av oppgaven, samt etter eventuelle pålegg fra Institutt for energi- og prosessteknikk.

Risikovurdering av kandidatens arbeid skal gjennomføres i henhold til instituttets prosedyrer. Risikovurderingen skal dokumenteres og inngå som del av besvarelsen. Hendelser relatert til kandidatens arbeid med uheldig innvirkning på helse, miljø eller sikkerhet, skal dokumenteres og inngå som en del av besvarelsen. Hvis dokumentasjonen på risikovurderingen utgjør veldig mange sider, leveres den fulle versjonen elektronisk til veileder og et utdrag inkluderes i besvarelsen.

I henhold til "Utfyllende regler til studieforskriften for teknologistudiet/sivilingeniørstudiet" ved NTNU § 20, forbeholder instituttet seg retten til å benytte alle resultater og data til undervisnings- og forskningsformål, samt til fremtidige publikasjoner.

Besvarelsen leveres digitalt i DAIM. Et faglig sammendrag med oppgavens tittel, kandidatens navn, veileders navn, årstall, instituttnavn, og NTNUs logo og navn, leveres til instituttet som en separat pdf-fil. Etter avtale leveres besvarelse og evt. annet materiale til veileder i digitalt format.

☐ Arbeid i laboratorium (vannkraftlaboratoriet, strømningsteknisk, varmeteknisk)
☐ Feltarbeid

NTNU, Institutt for energi- og prosessteknikk, 14. januar 2013

Olav Bolland
*Instituttleder*

Lars E Bakken
*Faglig ansvarlig/veileder*

Medveileder;
- Tor Bjørge, Statoil/NTNU

# PREFACE

This thesis was written during my final semester at NTNU, and marks the end of my Energy and Environmental Engineering Master Program. I can't believe it's already over… I am so grateful for all the people who have helped me along the way. Friends, family, teacher, you've all been amazing. I have had a great supervisor, Professor Lars Eirik Bakken, and would like to thank him for guidance and valuable help during the pre-project and the work with the thesis. I would also like to thank Tor Bjørge, my co-supervisor, and Ole Jørgen Nydal professor in multiphase pipeflow at NTNU.

Finally, I have to thank my father Edgar Jellum. Thank you dad! You have been a tremendous support and my biggest motivator. Thank you for love and encouragement, for always being positive, and for always believing in me. Words cannot express how much this has meant to me.

# SUMMARY

The development of wet gas compressors for installation subsea is key to increase the recovery of oil and gas from the Norwegian Continental Shelf. Safe operation of the compressor depends on understanding of how wet gas affects the behavior of the machine. The compressor operating range is limited by stall and surge, and it is therefore particularly important to determine how liquid will affect the inception of these phenomena. Measuring pressure transients within the compressor or in the inlet and discharge pipe are widely used in experimental investigation of stall and surge. Spectral analysis of the pressure signal is used to detect aerodynamic instabilities in compressor. Pressure measurements are also an important part of the anti-surge control systems, and it is used for continuous condition monitoring of the machine. It is therefore important to determine how liquid affect the pressure measurements.

This thesis consists of three main parts. The first part describes and explains stall and surge, and introduces various pressure measurement techniques that can be used to measure pressure transients in centrifugal compressors. Piezoelectric and piezoresistive pressure sensors are well suited to this. They have a wide operating range, high stability and sensitivity, and are very robust. Pressure sensitive paint (PSP) and stress-sensitive films (S3F) are interesting alternatives. These techniques measure global surface pressure, which is very useful when investigating complex flow fields.

The second part investigates how wet gas affects compressor stability, and how liquid presence affect pressure measurements in wet gas flows. Results from the test facility for wet gas compression at NTNU have shown that wet gas has a stabilizing effect on the compressor. Unfortunately, it is difficult to interpret the measurements due to large uncertainties around how liquid affects pressure measurements. Liquid presence may cause suppression and/or enhancement of certain frequencies, and also introduce additional frequencies that are specifically related to the dynamic characteristic of the liquid phase. The existing literature on this particular topic is very limited, but evaluation of various multiphase experiments has given some insight. It has been shown experimentally that droplets entrained in a gas phase dampen out pressure fluctuations. High frequency components will be most affected, but experiments have also shown significant dampening of frequencies down to 100 Hz. The presence of a liquid film is believed to cause amplification of random frequencies in the lower

frequency range. Turbulence and vortex formation causes a chaotic and highly dynamic flow pattern in the film, and this will affect the pressure measured at the wall. The liquid film will also reduce the performance of PSP and make the use of S3F more complicated. Piezoelectric and piezoresistive pressure sensors will not be directly affected. To increase the understanding of how liquid affects the pressure measurements in wet gas flows an experiment is planned to examine how thin liquid films will affect the surface pressure in wet gas flows. More knowledge in this field is important for future research of wet stall and surge.

The economical consequences of stall and surge are massive. In particular if the compressor is installed subsea. Safe running of the compressors is therefore dependent on a anti-surge system that prevents the compressor from becoming unstable. The final part of the report investigates anti-surge control in subsea compression, and how the performance of different systems is affected by liquid. Surge control based on surge avoidance is currently the safest and most reliable technique. However, the performance of these systems is significantly reduced in wet gas compression. Liquid changes the compressor characteristic, and affects the wear and tear of the machine. Liquid presence will also reduce the accuracy of flow, pressure and temperature measurements. By installing dynamic pressure sensors inside the compressor or outside in the connected pipeline, condition monitoring of the machine could be significantly improved. However, due to the challenging subsea environment and the high requirements to sensor performance, it is difficult to finding an optimal sensor is challenging. It is also difficult to determine where the sensors should be installed. This requires knowledge of how the liquid is distributed in the compressor, and will also depend on detailed knowledge of the liquid will affect the pressure measurement

# SAMMENDRAG

Utvikling av våtgasskompressorer for installering subsea er viktig for å øke utvinningen av olje of gass fra norsk sokkel. Sikker drift av kompressoren krever kunnskap om hvordan væske vil påvirke maskinen. Kompressorens driftsområdet er begrenset av stall og surge, og det er derfor spesielt viktig å finne ut hvordan disse fenomenene blir påvirket av våtgass. Måling av trykkvariasjoner inne i kompressoren eller i innløps- og utløpsrøret er mye brukt i eksperimentell undersøkelse av stall og surg. Spektralanalyse av trykksignalet blir brukt for å detektere ustabiliteter i kompressoren. Trykkmålinger er også en viktig del av anti-surge kontroll systemer, og det er brukt for kontinuerlig overvåking av kompressoren. Det er derfor viktig at å bestemme hvordan våtgass påvirker trykkmålinger.

Denne rapporten består av tre hoveddeler. Den første delen beskriver og forklarer stall og surge, og introduserer ulike trykkmåle teknikker som kan brukes til å måle trykktransienter i sentrifugalkompressorer. Piezoelektriske og piezoresistive trykksensorer er godt egnet til dette. De har et bredt driftsområde, høy stabilitet og sensitivitet, og er veldig robuste, og er svært godt egnet til dette. Trykksensitiv maling (PSP) og stress-sensitive filmer (S3F) er interessante alternativer. Disse teknikkene måler globalt overflatetrykk, noe som er svært nyttig når man undersøker komplekse strømningsfelt.

Den andre delen undersøker hvordan våtgass påvirker kompressor stabilitet, og hvordan væske påvirker trykkmålinger i våtegass strømning. Resultater fra testriggen for våtgasskompresjon ved NTNU har vist at våtgass ha en stabiliserende effekt på kompressoren. Desverre er det vanskelig å tolke målingene på grunn av stor usikkerhet rundt hvordan væske påvirker trykkmålingene. Væske kan føre til undertrykkelse og / eller forsterkning av visse frekvenser, og også innføre ytterligere frekvenser knyttet til den dynamiske karakteristikk av væskefasen. Eksisterende litteatur på dette området er begrenset, men evaluering av ulike flerfase eksperimenter har gitt noen innsikt. Det er vist eksperimentelt at draper i gassfasen demper ut trykkvariasjoner. Trykkomponenter med høy frekvens vil være mest påvirket, men eksperimenter har også vist betydelig demping av frekvenser ned til 100 Hz. Væskefilmer er antatt å forårsake amplifikasjon av tilfeldige frekvenser i det nedre frekvensområde. Turbulens og vortex dannelse forårsaker en svært dynamisk strømningsbilde i filmen, og dette vil påvirke trykket målt ved veggen. Væskefilmen vil også redusere ytelsen til PSP og gjøre bruk av S3F mer komplisert.

Piezoelektriske og piezoresistive trykksensorer vil ikke bli direkte påvirket. For å øke forståelsen av hvordan væske påvirker trykkmålinger i våtgass strømninger er det planlagt et eksperiment for å undersøke hvordan tynne væskefilmr vil påvirke overflatetrykk i en våtgasstrøm. Mer kunnskap på dette feltet er viktig for framtidig forskning av våtgass stall og surge.

De økonomiske konsekvensene av stall og surge er betydelige. Spesielt hvis kompressoren er installert subsea. Sikker drift av maskinen er derfor avhengig av anti-surge systemer som hindrer kompressoren fra å bli ustabil. Den siste delen av rapporten undersøker anti-surge kontroll i subsea komprimering, og hvordan ytelsen til forskjellige systemer påvirkes av væske. Surge kontroll basert på surge-avoidance er i dag den sikreste og mest pålitelige teknikken, men ytelsen til disse systemene er betydelig redusert i våtgasskompresjon. Våtgass endrer kompressorkarakteristikken, og påvirker slitasje av maskinenen. Væsken vil også redusere nøyaktigheten av volumstrøm, trykk- og temperaturmålinger. Ved å installere dynamiske trykksensorer inni kompressorens eller i rørledningen utenfor, kan overvåkingen av maskinen bli vesentlig forbedret. På grunn av røffe subsea-omgivelser og høye krav til ytelse, er det en stor utfordring å finne en egnet sensor. Det er også vanskelig å bestemme hvor sensoren bør monteres. Dette krever kunnskap om hvordan væsken er fordelt i kompressoren, og vil også være avhengig av detaljert kunnskap om hvordan væsken vil påvirke trykkmålingen.

# NOMENCLATUR

## SYMBOLS

| | | |
|---|---|---|
| A | Area | [$m^2$] |
| C | Absolute velocity | [m/s] |
| C | Capacitance | [F] |
| D | Diffusivity coefficient | [$m^2$/s] |
| D | Displacement | [m] |
| $D_h$ | Hydraulic diameter | [m] |
| F | Force | [N] |
| G | Gauge factor | [] |
| I | Luminescent intensity | [cd] |
| K | Bulk modulus | [Pa] |
| L | Length | [m] |
| $M_e$ | Mobility | [$m^2$/V·s] |
| $N_e$ | Number of charge carriers | [] |
| P | Pressure | [Pa] |
| $\dot{Q}$ | Volume-flow | [$m^3$/s] |
| R | Specific Gas constant | [KJ/Kg·K] |
| R | Resistance | [Ω] |
| $S_V$ | Sensitivity | [V·m/N] |
| U | Rotational velocity | [m/s] |
| V | Relative velocity | [m/s] |
| V | Velocity | [m/s] |
| V | Volume | [$m^3$] |
| V | Voltage | [V] |
| | | |
| a | Speed of Sound | [m/s] |
| a | Attenuation coefficient | [$m^{-1}$] |
| b | Width | [m] |
| b | Depth | [m] |
| e | Electron charge | [C] |

| | | |
|---|---|---|
| d | Cylinder diameter | [m] |
| f | Frequency | [Hz] |
| f | Vortex shedding frequency | [Hz] |
| h | Thickness | [m] |
| h | Height | [m] |
| l | Length | [m] |
| $\dot{m}$ | Mass flow | [kg/s] |
| t | Time | [s] |
| x | Position | [m] |
| | | |
| Ma | Mach Number | [] |
| Re | Reynolds Number | [] |
| St | Stouhal Number | [] |
| | | |
| α | Area fraction | [] |
| δ | Density ratio | [] |
| δ | Thickness | [m] |
| ε | Strain | [] |
| ζ | Resistivity | [Ω·m] |
| κ | Ratio of specific heat capacity | [] |
| μ | Shear module | [Pa] |
| μ | Viscosity | [kg/s·m] |
| ρ | Density | [$kg/m^3$] |
| υ | Kinematic viscosity | [$m^2/s$] |

## SUBSCRIPTS

| | |
|---|---|
| d | Diameter |
| e | Charge |
| e | Entrance length |
| g | Gas |
| h | Homogenous |
| i,j | Arbitrary phases |
| l | Liquid |
| s | Constant entropy |
| s | Slit |

| | |
|---|---|
| p | Distance to pressure senor |
| w | Wall |
| w | Water |
| | |
| N | Normal |
| T | Tangential |
| V | Voltage |
| | |
| amb | Ambient |
| dyn | Dynamic |
| sal | Surge avoidance line |
| si | Superficial, arbitrary phase |
| sg | Superficial, gas phase |
| sl | Superficial, liquid phase |
| sl | Surge line |
| stag | Stagnation |
| stat | Static |
| tot | Total |
| | |
| 1 | Impeller inlet |
| 2 | Impeller outlet |
| 3 | Diffuser inlet |
| 4 | Diffuser outlet |
| ∞ | Freestream |

# ABBRIVATIONS

| | |
|---|---|
| AA | Anodized Aluminum |
| DTC | Discharge Time Constant |
| ESD | Electro-Static Discharge |
| GMF | Gas Mass Fraction |
| GVF | Gas Volume Fraction |
| ICP | Integrated Circuit Piezoelectric. This is a registered trademark of the PCB Group, Inc., parent company of PCB Piezotronics |

| | |
|---|---|
| MEMS | Micro-Electro-Mechanical-Systems |
| PC | Polymer/Ceramic |
| PIV | Particle Image Velocimetry |
| PSP | Pressure-Sensitive Paint |
| SM | Surge Margin |
| SOI | Silicon-On-Insulation |
| S3F | Surface-Stress-Sensitive Film |
| TLC | Thin Layer Chromatography |

# PRESSURE SENSOR TERMONOLOGY

The field of measuring calls for well and clearly defined terms, and specifications should be given in a universally understandable way in order to avoid all misunderstandings and misinterpretations. Various sensor manufacturers have their own terminology, which sometimes differ greatly from each other, and this can cause problems when choosing sensor for a specific application. The different sensor-related terms used in this document is listed below.

| TERM | EXPLANATION |
|---|---|
| Measurand | The physical quantity, property or condition, in this case *pressure*, which is measured. |
| Sensor/Transducer | A device that provides a usable output in response to the specified measurand. |
| Output | The signal (electrical, optical, mechanical etc.) produced by the sensor/transducer. The output is a function of the applied measurand. |
| Sensing element | The part of the sensor/transducer which responds directly to the measurand |
| Transduction element | The portion of the sensor/transducer in which the output originates. |
| Range | The measurand values, over which the sensor is intended to measure, indicated upper and lower values. |
| Span | The algebraic difference between the limits of the range. |

| | |
|---|---|
| Overload | The maximum magnitude of the measurand that can be applied to the sensor without causing change in performance beyond a specified tolerance. |
| Environmental Conditions | Values of specified external conditions such as temperature, absolute pressure, shock, vibrations, humidity etc., that when exposed to, the sensor must perform as specified. |
| Threshold | The smallest change in the measurand that will result in a measurable change in the senor output. |
| Resolution | The magnitude of output step changes as the measurand is continuously varied over the range. |
| Sensitivity | The ratio of the change in sensor output to a change in the value of the measurand. |
| Gage Factor | Strain sensitivity |
| Linearity | A linear output means that the measurand is proportional to the output. The linearity is thus the closeness of a calibration curve to a specified straight line. |
| Repeatability | The ability of a sensor to reproduce the output readings when the same measurand value is applied under the same conditions. |
| Stability | The ability of the sensor to retain its performance characteristics for a long period of time. |
| Error | The mathematical difference between the indicated value (output) and the true value of the measurand. |

| | |
|---|---|
| Accuracy | The ratio of error to output span, often given in percentage of the output span. |
| Dynamic Characteristics | The characteristics of a sensor that relate to the sensor response to variations of the measurand with time. |
| Natural Frequency | The frequency of free oscillations of the sensing element of a fully assembled sensor. The natural frequency is excited by a very short pulse of the measurand. The sensing element will oscillate at its the natural frequency, but the amplitude if the oscillations will decrease exponentially according to the damping factor. The damping factor, in conjunction with the natural frequency, determines the limit of the frequency response and the response time characteristics of the sensor. |
| Resonant Frequency | The measurand frequency at which the senor responds with the maximum output amplitude. |
| Frequency Response | The change with frequency of the output/measurand amplitude ratio and the phase difference between output and measurand, for a sinusoidally varying measurand applied to the sensor within specified range of measurand frequency. The frequency range of the sensor must always be wide enough to cover all the frequencies that will occur in the measurand to be measured. In electro-mechanical pressure sensors the upper usable frequency limit is usually taken as 1/3 of the natural frequency or the resonant frequency. |
| Response Time | The time required for the output of the sensor to reach a value normally specified as 98% of the final output value when exposed to a step change in the measurand. The response time characteristics of the sensor are determined by the natural frequency in conjunction with the damping factor of the sensor. |

# CONTENT

# LIST OF FIGURES

# LIST OF TABLES

# 1 INTRODUCTION

This chapter explains the background and motivation for the work conducted, and also gives a presentation of the scope of the thesis and the report structure.

## 1.1 BACKGROUND AND MOTIVATION

Gas activities make up a growing share of the petroleum sector, and provide the Norwegian state with considerable revenues. Natural gas stands for more than 25% of all energy utilization in Europe, and Norway is one of the main suppliers. In 2011 the energy content of the exported gas was about eight times that of the normal Norwegian production of electricity (Norwegian Petroleum Directorate 2012). However, as the largest and most profitable fields are being emptied, petroleum production from the Norwegian shelf is declining. In order to counteract this trend, and be able to meet the future energy demand, increased recovery from existing fields and also production from less profitable and more remote fields, are necessary.

Subsea compression is a key technology leap towards improving the recovery rate and lifetime of mature gas fields. The gas is compressed on the seabed causing the pressure in the pipes to rise. This means that the gas will flow more easily, and that more gas can be retrieved from the reservoir. When considering production from remote fields, subsea compression of the well stream will eliminate the use of expensive platform solutions, and enable long pipelines and potentially direct landing of the well stream. The well stream typically contains gas, liquid and particles. In traditional systems liquid and particles are removed from the gas before compression. Dry gas enters the centrifugal compressor, while a pump handles the liquid fraction. This requires large and often complex separation and filtering systems that must be monitored and maintained. Filters must be changed, and separation tanks and connecting pipelines repaired, and this is a major drawback when considering implementation subsea.

Wet gas compression would eliminate the need of cumbersome separation systems. If liquid flow rates are small, gas and liquid could be compressed simultaneously and significantly reduce the system complexity and the need of maintenance. However wet gas compression introduces other challenges. Liquid presence affects the performance of the compressor, and

will also alter the inception and evolution of rotating stall and surge. These are complex phenomena, but a fundamental understanding of the prevailing flow mechanisms, and how they affect compressor stability is necessary in order to design reliable and cost-efficient compression systems. Experimental testing has indicated that liquid presence improves the stability of the machine, but the results also revealed that liquid has significant impact on instruments used to detect and distinguish between the different instabilities. Measurement of pressure transients is typically used to identify incipient surge and the onset of rotating stall. Wet gas is believed to influence these measurements, but an understanding of the overall effect has not been established. This is of big concern when analyzing the pressure measurement. There is a big risk of misinterpretation of the measurements, and this can result in misunderstanding the actual condition of the machine. Effort should therefore be made to identify and investigate the different multiphase mechanisms that will influence pressure and pressure measurement in wet gas flows.

Stall and surge can cause breakdown of the compressor and damage the connected pipelines. This is critical if the components are installed subsea. Subsea compression is therefore dependent on safe, reliable and robust anti-surge systems that prevent the machine from unstable operations. The performance of these systems depends on several factors, but accurate measurement of flow, pressure and temperature is key to good protection. If liquid affects the measurements, the performance of the system is reduced, and the system will offer less protection. A fundamental understanding of liquid impact on wet gas measurements is therefor essential to the development of wet gas compression systems for subsea installations.

## 1.2 SCOPE OF THESIS

This report investigates different topics related to aerodynamic instabilities in wet gas compressors. Stall and surge will be explained, and wet gas impact on these phenomena will be evaluated. The main focus, however, is given the use of transient pressure measurement for detection of incipient surge and rotating stall in wet gas compressors. Four different pressure measurement techniques; piezoelectric and piezoresistive pressure sensors and pressure sensitive paints and surface stress sensitive films, will be explained, and their suitability for measuring unsteady pressure in turbomachines evaluated. An extensive literature study has also been performed in order to establish how liquid presence affects pressure and pressure measurements in wet gas flows. Different multiphase mechanisms that are considered as significant to wet gas measurements will be explained and discussed, and their impact on pressure measurements in wet gas compressors will be indicated. The report will also give a detailed description of an experiment planned to investigate the ability of

flush mounted pressure sensors to respond to pressure fluctuations in wet gas flows. The experiment will focus on investigating pressure components generated in thin liquid films, and how this will affect the pressure signal measured beneath the film. Anti-surge control in wet gas compressors, and challenges related to installing these systems subsea, is the final topic. Liquid impact on pressure measurement is significant to the performance of these systems, and this will be highlighted.

The work presented in the report is based on the findings in the pre-project, *Wet Gas Compressor Stall and Surge* (Jellum 2012), and the result of the literature search.

## 1.3 REPORT STRUCTURE

The main content of the different chapters are summarized below.

- **CHAPTER 2** gives a general introduction to pressure and different pressure measurement techniques. The operational principals of the centrifugal compressor are presented, and fundamental concepts from multiphase flow theory are introduced.

- **CHAPTER 3** explains and describes the different aerodynamic instabilities encountered in the centrifugal compressor. The chapter also gives an introduction to anti-surge control.

- **CHAPTER 4** gives a comprehensive description of piezoelectric and piezoresistive pressure sensor. The two techniques are compared, and the different advantages and disadvantages indicated.

- **CHAPTER 5** describes the pressure sensitive paint (PSP) and surface stress sensitive film (S3F) method. The chapter also indicates how these techniques can be used to measure unsteady pressure in turbomachines.

- **CHAPTER 6** investigates liquid impact on compressor stability, and also how liquid presence affects pressure and pressure measurements in wet gas flows.

- **CHAPTER 7** describes an experiment planned to investigate how the presence of thin liquid films affect surface pressures in wet gas flows. This is considered as key to avoid misinterpretation of the pressure measurements in wet gas compressors.

- **CHAPTER 8** deals with surge control in wet gas compressors. The chapter investigates how liquid presence affects the performance of different anti-surge systems, and also presents challenges related to implementing these systems subsea. The various anti-surge techniques are compared in order to find the best solution.

- **CHAPTER 9** summarizes the main findings that can be drawn from the previous chapters.

- **CHAPTER 10** presents a recommendation for future work and other concluding remarks.

Chapter 2-5 gives presents a lot of general theory, but this provided to give a more complete understanding of the techniques and phenomena described in the report. Chapter 6,7 and 8 are the most important chapters. Derivation of mathematical expressions, Matlab codes and pressure sensor datasheet is given in the Appendix.

# 2 FUNDAMENTAL THEORY

This chapter will serve as the theoretical background for the subsequent investigation of wet gas impact on pressure sensors used to measure unsteady pressure in centrifugal compressors. The chapter is divided into three main parts. The first part will give a brief description of the centrifugal compressor and the fundamental operating principals. For more details the reader is encourage to review the pre-project, *Wet Gas Compressor Stall and Surge* (Jellum 2012). The second part gives an introduction to pressure and pressure measurements. The physical meaning of this property will be described, and different methods of measuring pressure will be listed. Pressure measurement in rotation machinery is also discussed. The last part presents different multiphase flow concepts.

## 2.1 THE CENTRIFUGAL COMPRESSOR

Compressors used in the process industry are required to have a smooth operation, a large tolerance to process fluctuations, and a high reliability. The centrifugal compressor, often referred to as "the workhorse of the process industry", fulfills all of these requirements. Figure 2.1 shows a picture of a single-stage and a multi-stage centrifugal compressor.

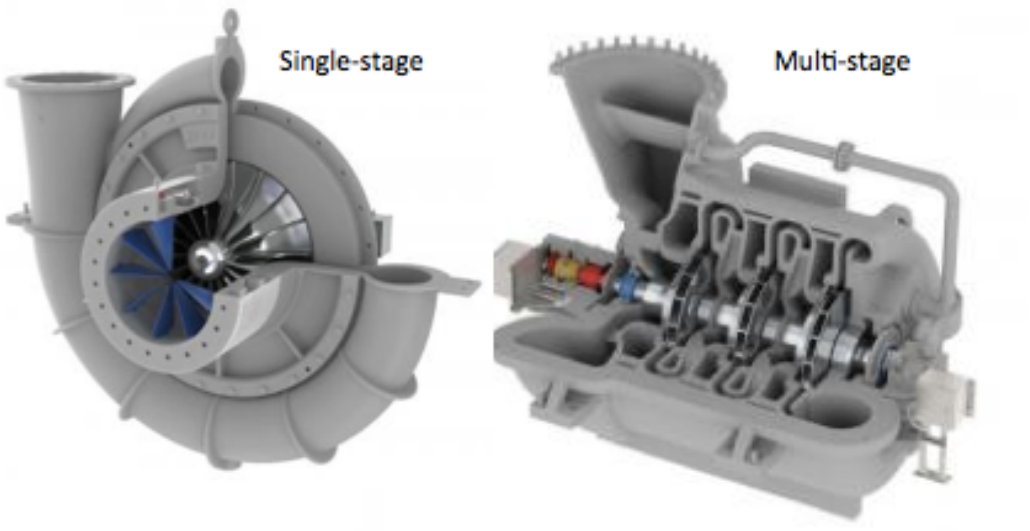


Figure 2.1: The centrifugal compressor (Nu-Way Energy)

The centrifugal compressor essentially consists of a stationary casing containing a rotating impeller, followed by a diverging channel known as the diffuser. The impeller imparts a high velocity to the flow, and the diffusor, vaned or vaneless, decelerates the gas with a consequent rise in static pressure. No *work* is done in the diffuser. All energy transfer between the flow and the compressor takes place in the impeller where momentum is transferred to the flow from the rotating impeller blades. The gas enters the impeller eye axially, and is then whirled around in high velocity before it leaves the vanes of the impeller disc in a radial direction. In order to obtain the centripetal acceleration and thus radial equilibrium at any point in the flow, the static pressure in the flow must increase from impeller eye to impeller tip (Gravdahl and Egeland 1999) Figure 2.2 illustrates how the absolute velocity and the pressure change from compressor inlet to outlet.

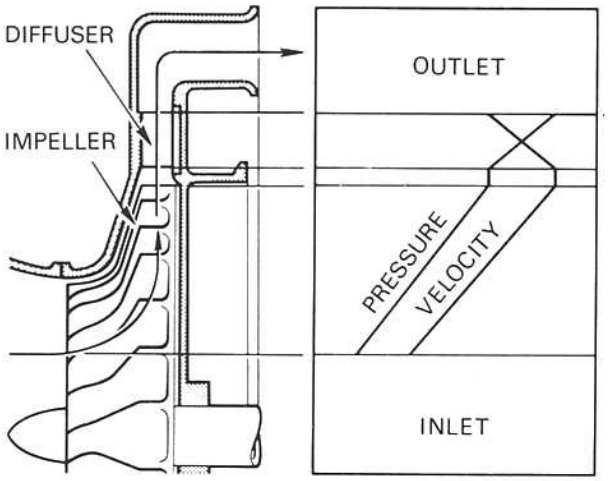


Figure 2.2: Pressure and velocity variation in a centrifugal compressor stage (Boyce 1993)

The overall performance of a compressor may be specified by curves of delivery pressure and delivery temperature plotted versus mass flow for various fixed values of rotational speed (Saravanamuttoo, et al. 2009). This is called a *compressor performance characteristic*. The curves may be plotted as compressor head (H) versus volume flow (Q) with contour lines for various values of efficiency superimposed upon the plot. Figure 2.3 shows a typical compressor characteristic. The figure illustrates how the compressor operating range is limited by choking at high volume flow, and surge at low volume flow, when moving along a constant speed curve. At zero volume flow the pressure ratio will have some value A. This value corresponds to the centrifugal pressure head produced by the action of the impeller on the gas trapped between the vanes. Increasing the volume flow, following the dotted line representing the *theoretical* characteristic, the pressure ratio will increase due to the contribution of pressure rise coming from the diffuser. At some point B, efficiency

approaches its maximum value, and maximum pressure ratio is also achieved. Further increase in volume flow will reduce the pressure rise. The gas angels will no longer match the vane angels resulting in breakaway of the flow (separation), and a rapid decrease in efficiency. Following the dotted line from E to C, the pressure rise drops to zero, and all power is absorbed in overcoming internal frictional resistance (Saravanamuttoo, et al. 2009)

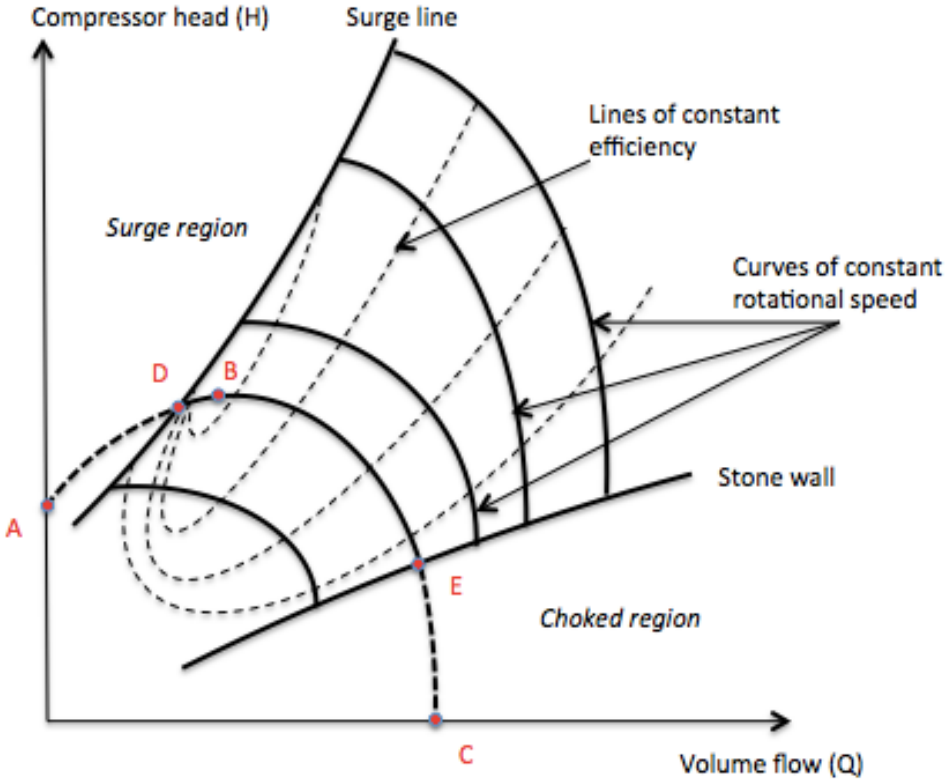


Figure 2.3: Compressor performance characteristic

Operating at the dotted part of the curve is not possible in reality. The useful operation range is limited by choking at high mass flow when sonic velocity is reached in some component, and at low mass flows by the onset of surge or rotating stall. Left of the *surge line,* in the *surge region,* the compressor will be highly unstable. Compressor operations in this region are associated with sudden drops in delivery pressure, and violent aerodynamic pulsations that are transmitted throughout the machine. Unstable compressor operation is highly unwanted, and may cause severe damage to the compressor and auxiliaries due to the large thermal and mechanical loads involved. Vibration induced by unstable operation may propagate to the rest of the compression system, and also result in unacceptable levels of noise. However, even though it is dangerous to operate the compressor near the surge line, it is desirable to do so because of the high performance and efficiency obtained there.

## 2.2 INTRODUCING PRESSURE AND PRESSURE MEASUREMENTS

### 2.2.1 WHAT IS PRESSURE?

Fluid pressure is defined as the measure of force per unit area exerted by a fluid, acting perpendicularly to any surface it contacts. This definition is given in equation 2.2.1. The standard SI unit for pressure measurement is Pascal (Pa), which is equivalent to one Newton per square meter.

$$P \stackrel{\text{def}}{=} \frac{F}{A} \tag{2.2.1}$$

Pressure measurements can be divided into three different categories: *absolute pressure, gage pressure* and *differential pressure*. The absolute pressure is the difference between the pressure at a given point in a fluid and the absolute zero of pressure or a perfect vacuum. Gage pressure is the measurement of the difference between the absolute pressure and the local atmospheric pressure, while differential pressure is simply the difference between two unknown pressures (Heeley 2005).

There are also different types of fluid systems and fluid pressures. In a *static system*, the fluid is at rest, while in a *dynamic system,* the fluid is moving. The pressure measured in a static system is the *static pressure*. In an ideal gas, the static pressure can be derived by applying the ideal gas law:

$$P_{stat} = \rho RT \tag{2.2.2}$$

The static pressure increases with depth in the fluid, and acts equally in all directions. The increase in pressure at a deeper depth is essentially the effect of the weight of the fluid above that depth. This is expressed in the hydrostatic pressure equation:

$$P(h) = P_{h=0} + \rho g h \tag{2.2.3}$$

If the working fluid is a gas, this pressure increase is in most cases negligible since the density and therefore the weight of the fluid is much smaller than the pressure being applied to the system (Heeley 2005).

In a dynamic system, pressure typically is defined using three different terms: *static, dynamic and total pressure*. The static pressure is independent of the fluid movement, and is the same pressure as the pressure that is measured in a static system. The dynamic pressure is associated with the velocity of the fluid, and is equal to the kinetic energy per unit volume of a fluid particle. Dynamic pressure is one of the terms of Bernoulli's equation, which can be derived from the conservation of energy for a fluid in motion. In incompressible fluid dynamics the dynamic pressure is defined according to equation 2.2.4.

$$P_{dyn} = \frac{1}{2}\rho V^2 \tag{2.2.4}$$

By assuming ideal gas and applying the definition of acoustic speed and Mach number, the definition of dynamic pressure can be extended to also include compressible flows. This is given in equation 2.2.5.

$$\rho = \frac{P_{stat}}{RT}, \qquad a = \sqrt{\frac{\kappa RT}{m}}, \qquad Ma = \frac{V}{a}$$

$$P_{dyn} = \frac{1}{2}\kappa P_{stat} Ma^2 \tag{2.2.5}$$

Total pressure is simply the static pressure plus the dynamic pressure:

$$P_{tot} = P_{stat} + P_{dyn} \tag{2.2.6}$$

Figure 2.4 shows how the different pressure terms can be measured in a dynamic system.

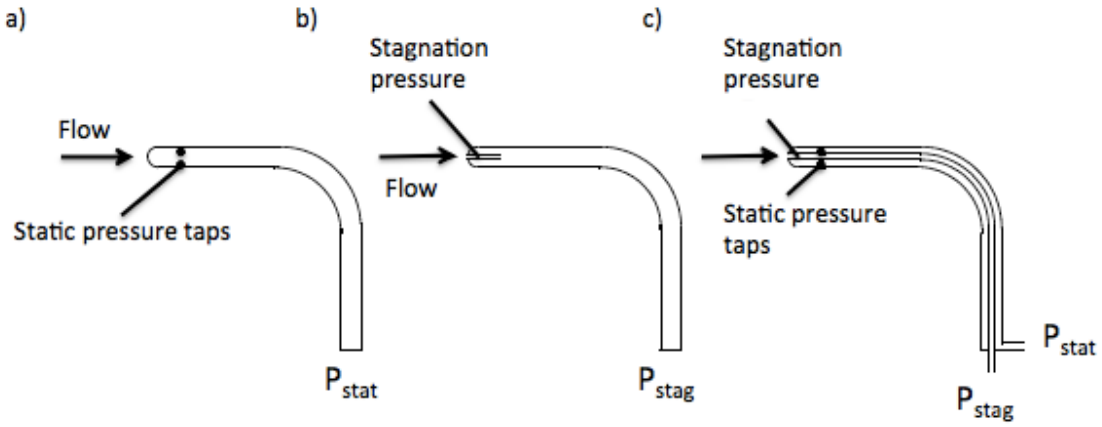


Figure 2.4: Static, total and dynamic pressure measurements

Under steady-state conditions, accurate static pressures may be measured by tapping into the fluid stream perpendicular to the fluid flow. This is illustrated in figure 2.4a). Figure 2.4.b) shows how to measure stagnation pressure. The stagnation pressure is the value obtained when a flow is decelerated to zero velocity in an isentropic process. All the kinetic energy is converted into a pressure that can be measured. If the flow is incompressible, stagnation pressure and total pressure is the same. The stagnation pressure is a vector quantity that depends on both magnitude and direction for the total measured value. For accurate measurements, it is important that the Pitot probe or impact tube is aligned parallel to the flow field with the tip of the tube pointing directly into the flow. When dynamic pressure measurement is desired, the total and static pressures are measured and then subtracted to obtain the dynamic pressure. Figure 2.4.c) shows a pitot-static pressure probe, which combines static pressure taps with the basic pitot tube, and can measures the three different pressures.

Transient or unsteady systems, are systems with changing conditions such as pressures, flow rates etc. Depending on the rate of change, accurate measurements can be very difficult to obtain. If the pressure measurement system has a faster response time than the rate of change in the system, the system can be treated as quasi-steady-state, and the measurements will be about as accurate as steady-state measurements. However, if the pressure changes faster than the response time of the system, accurate measurements are not possible to achieve. This is similar to taking photos. If the measurement is assumed to be a snap shot of what is happening in the system, one must be able to take the picture faster than the rate of change. Otherwise the picture; hence the measurement, will be blurred (Heeley 2005).

### 2.2.2 An Introduction to Different Pressure Measurement Techniques

Pressure may be measured using a variety if different techniques, and as with most measurands, pressure measurement methods have varying suitability for different applications. Pressure range, sensitivity, dynamic response and cost all vary by several orders of magnitude from one instrument design to the next.

Mechanical pressure gauges and electromechanical pressure sensors incorporate an elastic sensing element called a force-summing device that changes shape under the effect of applied pressure. The shape change is then converted to a displacement. The sensing element may be a diaphragm, a piston, a bourdon tube, a capsule, or a set of bellows. The most commonly used Bourdon tubes and diaphragms. In mechanical gauges, the motion generated in the sensing element by the applied pressure is converted by mechanical linkage into dial or

pointer movement. In electromechanical gauges the motion generated by the sensing element is transformed into an electrical signal. Electromechanical gauges are much more useful and adaptable than mechanical gauges, especially when applied in data acquisition and control systems. In well-designed sensors, the electrical output is directly proportional to the applied pressure over a wide pressure range. Depending on the dynamic characteristics of the sensor, electromechanical sensors are suitable for measuring unsteady and rapidly changing pressure (Wilson 2003). Electromechanical sensors will be described in details in chapter 4.

The pressure measurements can be taken at finite locations, or across a continuous surface. Pressure-Sensitive Paint (PSP) allows for measuring pressure over a continuous surface. The paint contains luminescent molecules that fluoresce to different intensities depending on the air pressure. The luminescent intensity is also utilized in surface stress sensitive films (S3F). In this case the intensity depends on the thickness of the film, with again depends on the applied pressure. PSP and S3F will be described in details in chapter 5.

There are numerous other ways of deriving the fluid pressure. A conservative estimate would be that there might be over 50 technologies and at least 300 companies making pressure sensors worldwide (Thermal-FluidsCentral). Optical sensors use the physical change of an optical fiber to detect strain due to applied pressures Thermal sensors use the changes in thermal conductivity of a gas due to density changes to measure pressure. Resonant sensors use the changes in resonant frequency in a sensing mechanism to measure stress, or changes in gas density, caused by applied pressure (Wilson 2003).

### 2.2.3 Data Acquisition In Rotating Machinery

The flow structure in the centrifugal compressor is inherently unsteady with contributions both from periodic variations due to the relative alignment between rotating and stationary parts and large-scale instabilities such as stall and surge, as well as turbulence. The pressure sensors in operating machines are generally installed in the inlet and/or discharge piping, and the pressure data is therefore obtained in a stationary frame of reference. This requires special data-acquisition and averaging procedures in order to distinguish between periodic and turbulent fluctuations. The phase-locked ensemble-averaging technique consists of conditionally sampling a time series of data obtained over many revolutions based on the impeller phase. A signal from a shaft encoder is typically used to synchronize the sensor time series with the phase of the machine. The sensor is triggered based on the signal from the shaft encoder. Varying the delay between the shaft encoder pulse and the timing of data acquisition, can sample different phases. ( Tropea, Yarin and Foss 2007).

## 2.3 MULTIPHASE FLOW

### 2.3.1 WET GAS FUNDAMENTALS

Wet gas is defined by the industry as gas containing a maximum of 5% liquid on a *volume* basis. Owing to large variations in density, the liquid fraction on a *mass* basis can be more than 50%. The gas volume fraction (GVF) and the gas mass fraction (GMF) describe the liquid content of the flow. Equation 2.3.1 and 2.3.2 expresses GVF and GMF respectively.

$$GVF = \frac{\dot{Q}_g}{\dot{Q}_g + \dot{Q}_l} \tag{2.3.1}$$

$$GMF = \frac{\dot{m}_g}{\dot{m}_g + \dot{m}_l} \tag{2.3.2}$$

The area fraction is used to indicate how much of the flowing area occupied by a particular phase. The area fraction of an arbitrary phase *i* is given in equation 2.3.3.

$$\alpha_i = \frac{A_i}{A_{tot}} \tag{2.3.3}$$

In single-phase flow it is custom to define the instantaneous average velocity as volume flow divided by the pipe cross-sectional area (Bratland 2010). In this way, the average velocity directly reflects the volume flow. In multi-phase flow, however, the part of the area occupied by one particular phase varies in space and time, so the flow is no longer proportional to the velocity at a given point. By defining superficial velocities for gas and liquid, this problem can be solved.

$$V_{si} = \alpha_i V_i \tag{2.3.4}$$

$V_i$ is the average velocity in the cross-sections occupied by phase *i*. The volumetric flow of phase *i* is then given by:

$$\dot{Q}_\iota = A_i V_i \tag{2.3.5}$$

Inserting equation 2.3.3 and 2.3.5 in 2.3.4 yields:

$$V_{si} = \frac{\dot{Q}_l}{A_{tot}} \tag{2.3.6}$$

By inspection it is clear that the superficial velocity is proportional to, and directly reflects, the volumetric flow. The superficial velocity can be regarded as the average instantaneous velocity the phase would have had if it occupied the whole cross-sectional area (Bratland 2010).

Another important parameter in wet gas compression is the *density ratio* between gas and liquid. This parameter gives an indication of the phase interactions of the flow and the ability of the liquid to follow the gas streamlines. By evaluating the density ratio, the possibilities for phase separation, and the ability of the liquid droplets to respond to the gas flow can be estimated.

$$\delta = \frac{\rho_g}{\rho_l} \tag{2.3.7}$$

### 2.3.2 Flow Regimes

Multiphase flow can take many different forms, and in order to do calculations and estimations it is necessary to determine on a suitable flow regime. Flow regime maps are useful tools for getting an overview over which flow regimes we can expect for a particular set of input data (Bratland 2010). Figure 2.5 on the next page shows a typical flow map for horizontal pipe flow. The flow within a centrifugal compressor differs a lot from flow through a pipe, but the flow map can still be used as an indication on what flow regime to expect. Due to its high gas velocities and small liquid content, the internal compressor flow pattern in wet gas compression is typically described as annular flow. Characterized as annular multiphase flow. Liquid flows as a thin film on internal walls and a dense droplet spray in the core.

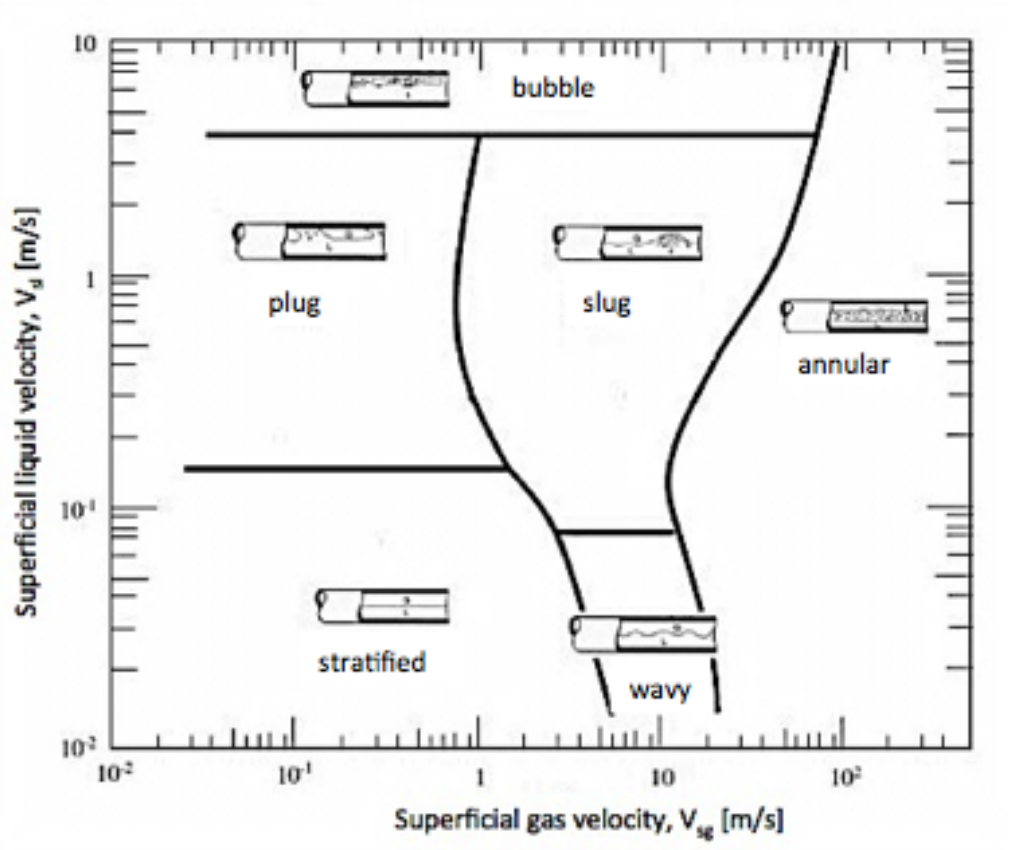


Figure 2.5: Flow regimes in horizontal pipes (Mandhane, Gregory and Aziz 1974)

### 2.3.3 Modeling Wet Gas Flow

As the flow moves through the compressor, the distribution if the liquid film, i.e. he film thickness, and also the concentration and size of the droplets will vary. Centrifugal forces, gravity and friction will affect the phases differently in the different compressor components, making it close to impossible to establish any mathematical description of the flow. The distribution of droplets and liquid film is also expected to very over the cross section, adding further complexity to problem.

The homogenous flow model concerns with the dynamics of multiphase flow in which the relative motion between the phases can be neglected. This is applicable if the flow is sufficiently well mixed and therefore the disperse particle size sufficiently small so as to eliminate any significant relative motion. The homogenous flow model also assumes that there is no temperature difference between the phases. Following the procedure given by Bratland (2010) the governing conservation equations in such a flow can be modeled as

single-phase equations by simply using average values of the thermodynamic properties. Equation 2.3.8 shows how to calculate the homogenous density.

$$\rho_h = \alpha_g \rho_g + \left(1 - \alpha_g\right)\rho_l \tag{2.3.8}$$

The homogenous flow model can as a first approximation, model many bubbly flows and mist flows. However, this is not the case for annular flow. When considering compressible flows in which a gaseous continuous phase is seeded with droplets, like the core flow in annular flows, it is necessary to evaluate the relative motion between disperse and continuous phases (Brennen 2005). The homogenous flow model can thus only be used to establish a base state. Perturbation methods must then be applied to examine the phenomena that constitute departure from single-phase flow mechanics. This way of describing the flow is only suitable if the relative motion and temperature differences are very small.

Wood's model can be used to estimate the speed of sound in multiphase flow. He evaluated the impact of introducing liquid to a gas flow. According to Wood's model, increased water content tends to lower the relative speed of sound. The model, given in equation 2.3.9, is based upon the assumption of homogenous flow.

$$\frac{a^2|_{\alpha_g}}{a^2|_{\alpha_g=1}} = \frac{1 + \dfrac{1-\alpha_g}{\alpha_g}}{1 + \dfrac{1-\alpha_g}{\alpha_g} \cdot \dfrac{\rho_l}{\rho_g}} \tag{2.3.9}$$

# 3 AERODYNAMIC INSTABILITIES

In order to secure stable operation of the compressor, and to prevent the machine from degradation and the possibility of severe damages, understanding of stall and surge and also the flow mechanisms behind the phenomena is essential. Choosing the correct instrumentation for identification and control of stall and surge phenomena requires knowledge of the characteristic behavior of the flow.

This chapter will give a description of the different types of aerodynamic instabilities typically encountered in a centrifugal compressor. This involves explanation of stall and surge, and also a description of the characteristic pressure signatures associated with these phenomena. The chapter will also give a brief description of different anti-surge techniques. The chapter is divided into five main parts. The first part gives a general introduction to the concept of unstable compressor operations, while part two, three and four give a more detailed explanation of stall and surge phenomena. Anti-surge control is introduced in the final part.

## 3.1 PRINCIPALS OF UNSTABLE COMPRESSOR OPERATIONS

Surge and stall are highly unwanted phenomena causing several unwanted effects in the centrifugal compressor: introduction of thermal and mechanical loads, oscillations and lowered pressure rise and efficiency. Depending on the type and severity of the instability, the forces involved may cause structural damages to the compressor, and in the worst-case scenario cause complete breakdown of the machine. Re-start of the entire compression system machine will often be necessary in order to regain stable operation.

The stability of a system is understood as the systems ability to regain its initial condition when subjected to a small disturbance. The compressor is unstable when the pressure ratio gradient is positive, and stable when the pressure ratio gradient is negative. This can be explained by considering a compressor operating between two pressure reservoirs and equipped with a downstream throttling valve. Imagine a sudden disturbance, in the form of partly closing the throttling valve and thereby temporarily reducing the volume flow. If the compressor is operating in the stable region, a drop in volume flow will be followed by an increase in delivery pressure. The increased delivery pressure will encourage an increased

flow through the throttle, and subsequently reduce the compressor delivery pressure and increase the compressor volume flow. The disturbance is *dampened*, and the compressor operating point will move back to its initial position. The system is self-compensating and thus inherently stable. On the other hand, if the compressor is operating in the unstable region, a decrease in volume flow will be followed by a decrease in delivery pressure. This will promote a reduction the flow through the throttling valve, and consequently move the compressor operating point further away from its initial position. The disturbance is *amplified*, and the system is inherently unstable (Gravdahl and Egeland 1999).

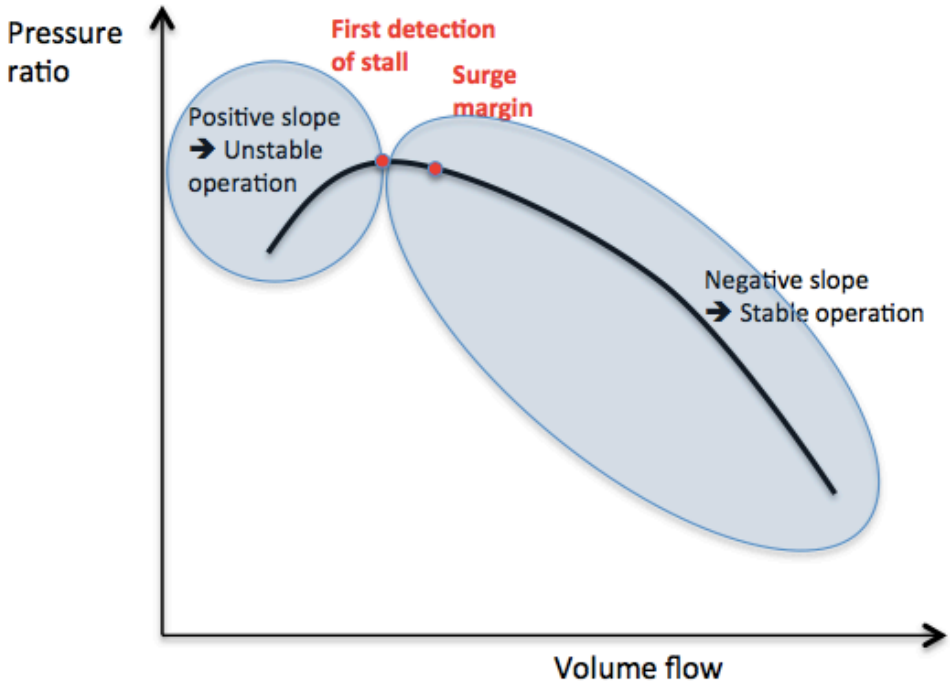


Figure 3.1: Different compressor operating regions

The regions of stable and unstable operation are indicated in figure 3.1. Evident from the figure instabilities within the machine arise when the volume flow is reduced beneath a certain limit. This point, typically known as the *surge point,* marks a definite change in the flow pattern in the compressor. As volume flow is reduced further, the compressor enters into either *stall* or *surge*. There are different categories of both surge and stall, but the phenomena are highly linked together. Boundary layer separation plays a major role in all types of instabilities, and is always present during unstable compressor operations. Boundary layer separation is explained in Appendix A.

## 3.2 ROTATING STALL

In the literature, the term *stall* is being used with a wide range of meanings. It is used for fully developed rotating stall, it can refer to the dynamic transient that initiates a surge, or it can be used to indicate heavily separated boundary layer flow over an airfoil (Boyce 1993). Compared to those of an axial compressor, the stall characteristics of a centrifugal compressor are far more complex and the literature is less extensive (T. Grüner 2012). Even though stall was detected for the first time in a centrifugal compressor, greatest interest and activity has been with the stall of axial compressors. This is partly explained by the complexity of the centrifugal stall characteristic, but also by the fact that with radial machines it is possible to operate quite satisfactorily with stall present. This tolerance to stalled regions is largely because the centrifugal effect causes so much of the pressure-rise, and this will be present even in the presence of rotating stall or other types of separated flows (Cumpsty 1989).

Regardless of its multiple meanings and complexity, stall refers to an operation mode in which parts of the compressor do not have an efficient energy transfer between the machine and the flow. The phenomenon is closely linked to boundary layer separation, this being in the blading of the impeller, or in the diffuser. The term *rotating stall* is used to highlight the distinctive circumferentially non-uniform flow pattern *rotating* around the annulus, often encountered when the compressor is operating in the stalled mode. One or more regions of stagnant flow, so- called stall-cells, travel around the circumference of the compressor at characteristic fraction of the shaft speed. (van Helvoirt 2007). Rotating stall is a mechanism that allows the compressor to adapt to a volume flow that, in reality, is too small. Instead of trying to share the limited flow evenly, the flow is unequally distributed over the circumference, resulting in deviating aerodynamic behavior, and thus a reduced performance of the machine. The stall cells reduce or completely block the flow, resulting in vibratory stresses and thermal lodes on the compressor blades. Moreover, rotating stall can induce *hysteresis* to the system, meaning that the flow rate has to be increased beyond the stall inception point in order to bring the compressor back to stable operation (van Helvoirt 2007).

There exist contradicting opinions in the literature on whether or not rotating stall is important for centrifugal compressors. Fully developed rotating stall induces vibrations in the impeller blades, and if the natural frequency of vibration of the blades coincides with the frequency at which the stall cell pass a blade, the result is resonance and the risk of mechanical failure due to fatigue. If the imbalance in blade loading is severe enough, the resulting non-uniform radial force distribution can also cause bending of the main shaft. If this happens there is a risk of the impeller blades hitting into the compressor casing, causing breakdown of the machine.

### 3.2.1 IMPELLER ROTATING STALL

Impeller stall is caused by boundary layer separation in the impeller channels at the suction side of the impeller blades. When the volume flow at the impeller inlet is reduced at constant rotational flow, the angle of attack to the impeller blade increases. This is illustrated in figure 3.2. When the angle of attack exceeds a certain limit, the flow passing the impeller blade can no longer follow the surface. The boundary layer thickens and separates causing formation of eddies and vortices in the impeller channel, and in some cases areas of reversed flow at the impeller outlet. The breakdown of the flow reduces the effective flow area, and thus limits the volume flow in the stalled blade passage.

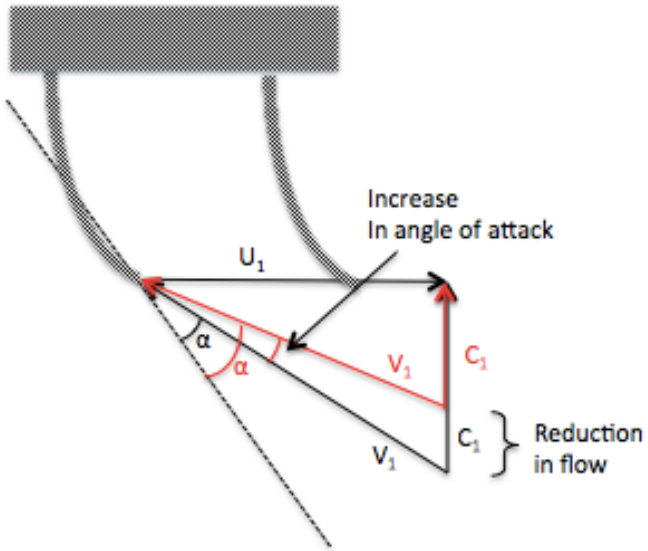


Figure 3.2: Velocity triangle at impeller inlet.

Impeller stall can be either *stationary* or, it can propagate from channel to channel, resulting in a stalled area that rotate around the impeller circumference. This type of impeller stall is known as *impeller rotating stall,* and figure 3.3 illustrates the physical mechanism behind the phenomenon. The figure shows a row of impeller blades. Suppose that there is a non-uniformity in the inlet flow such that a locally higher angle of attack, high enough to cause boundary layer separation, is produced on blade B. The separation at the suction surface of blade B causes a flow blockage between B and C. This blockage causes a diversion of the inlet flow away from blade towards A and C. The flow is deflected in such a way that channel C receives gas at an increased angle of attack, while channel A receives gas at a reduced angle of attack. Channel C the stalls, resulting in a reduction of angle of attack to channel B enabling the flow in this channel to recover. The stall passes from one channel to the next, propagating along the blade row. Seen from the impeller, i.e. in the relative frame of

reference, the stall cell is rotating in the opposite direction of the rotational speed. In the absolute frame, the stall cell is rotating in the same direction as the impeller, but at a lower speed (Gravdahl and Egeland 1999), (Saravanamuttoo, et al. 2009).

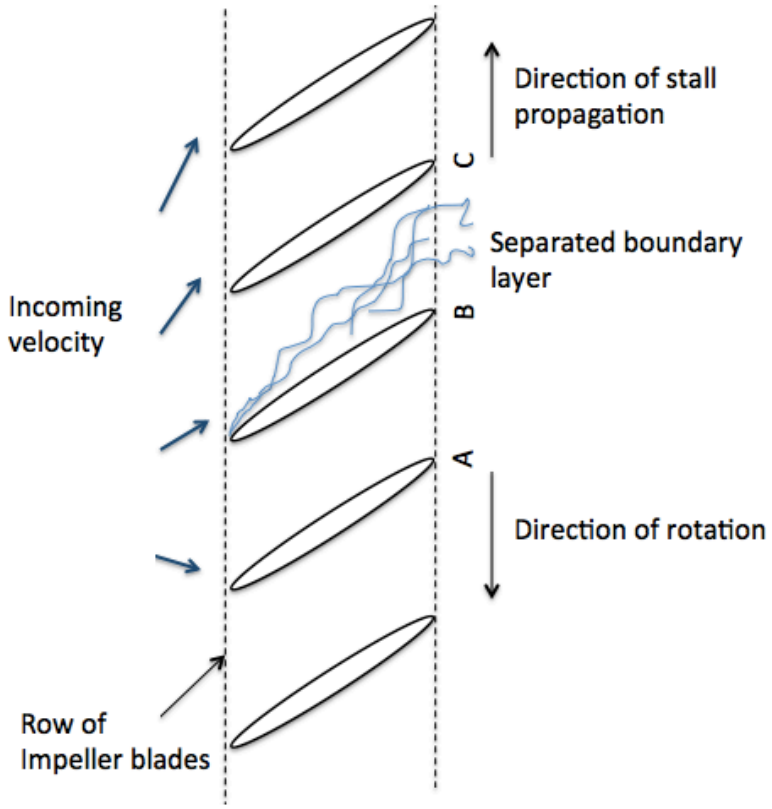


Figure 3.3: Rotating stall in Impeller

There exist different degrees of severity of the impeller stall. As already mentioned, the centrifugal compressor can operate quite well even if the impeller is stalled. At the same time, if a number of impeller blades stall simultaneously, causing a multiple of stall cells to rotate around the impeller, the resulting condition of the compressor can become quite close to surge. In addition, once an impeller begins to stall, only a small additional decrease in volume flow will stall the impeller completely. All the impeller channels will then suffer from flow blockage due to the formation of vortexes caused by separation of the boundary layer. Reversed flow will occur at the impeller outlet, causing the compressor to surge.

### 3.2.2 DIFFUSER ROTATING STALL

The diffuser is inherently unstable. Because of the increasing cross-sectional area towards the diffuser exit, the compressor flow experiences a tremendous adverse radial pressure gradient as it moves through the diffuser. Depending on the diffuser geometry and the flow rate, the radial pressure gradient set up may cause the flow to separate.

The inception and evolution of diffuser stall and rotating stall is very different in vaned diffusers compared to vaneless diffusers. Stall and rotating stall in vaned diffusers occur because of unacceptable high angles of attack to the diffuser vanes. The governing flow mechanisms are similar to those of impeller stall and rotating stall. In the vaneless diffuser however, stall is described as a three-dimensional boundary layer separation at the diffuser wall, and the likelihood of separation is primarily determined by the length of the flow path through the diffuser. A long flow path increases the amount of frictional losses, and thus promotes boundary layer separation. As indicated in figure 3.4, the length of the flow path increases with reduced volume flow. Reducing the volume flow means reducing the radial component of the absolute velocity, hence increasing the diffuser inlet angle $\alpha_3$. The length of the diffuser flow path is dependent on the inlet angle $\alpha_3$, and increases in a logarithmic manner with increased $\alpha_3$.

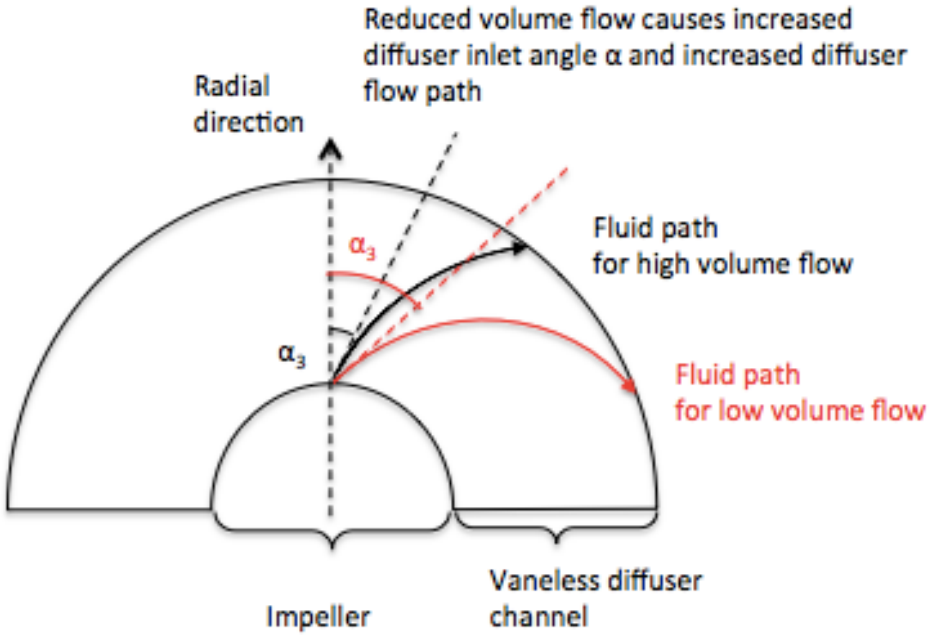


Figure 3.4: Flow path in diffuser channel at different volume flow

At a certain inlet angle, the *critical inlet angle* $\alpha_c$, instabilities start to arise within the diffuser. The value of $\alpha_c$ is highly dependent on the diffuser geometry, and a substantial amount of experimental work has been devoted to explore these dependencies. This is described in more details in the pre-project. The type flow mechanisms leading up to rotating stall will also depend on the diffuser geometry. For wide diffuser channels, diffuser rotating stall is associated with a two-dimensional core flow instability developing when the critical flow angle is reached. In narrow diffuser, wall friction becomes dominating, and diffuser rotating stall is associated with three-dimensional wall boundary layer instability. In narrow diffusers rotating stall is initiated by boundary layer separation at the diffuser wall. A narrow diffuser channel increases the magnitude of frictional losses, and as a result the flow becomes very sensitive to changes in the pressure gradient. If the flow is decelerated too fast, meaning that the pressure gradient increases, the flow might not be able to overcome both friction and pressure forces. If this is the case, the boundary layer separates from the wall, and diffuser stall is initiated (Dou and Mizuki 1998).

The stall cells in the vaneless diffuser can be described as *recirculated swirls* appearing in the flow. The *rotating* pattern of the stall cells is caused by interactions between a swirl and the rest of the flow. When a swirl or a stall cell starts to develop, the changed flow on the other side of the swirl causes the swirl to move in an oblique direction. Gradually additional stall cells start to emerge, causing a non-uniform flow pattern to rotate around the circumference of the diffuser. As the flow is reduced further, the stall cells increase in size, taking up more and more of the diffuser volume. Finally, the magnitude of stalled flow, rotating around the diffuser circumference, causes the compressor to surge (Sørvik 2012).

## 3.3 SURGE

Whereas the centrifugal compressor can operate fairly satisfactory with moderate stall present, surge oscillations can cause severe damages to the compressor and also induce vibration in other parts of the compression system. Surge oscillations are thus highly unwanted, and regarded as the aerodynamic instability mode of most concern in the centrifugal compressors [ (Gravdahl and Egeland 1999), (van Helvoirt 2007), (de Jager 1995)].

Surge is an axis-symmetrical oscillation of the flow through the compressor. The phenomenon is characterized by a limit cycle in the compressor characteristic. Surge causes large variations in the inlet and outlet conditions of the compressor, and large fluctuations in

pressure and system flow rate. According to Boyce (2001) the underlying cause of surge is aerodynamic stall, and some researchers claim that rotating stall is just a precursor to surge (Cumpsty 1989). However, experiments have also reported surge without any prior detection of stall. The two phenomena show fundamental differences. Rotating stall is characterized with a circumferentially non-uniform flow pattern, but with the average mass flow rate being approximately constant in time. Surge, on the other hand, causes an unsteady average mass flow, but the flow rate remains circumferentially uniform. Surge is a one-dimensional system instability, while rotating stall is a two-dimensional compressor instability.

Surge in a compressor occurs when the pressure across the compressor exceeds the pressure that the compressor can impart to the gas by the velocity conversion process. At the point the system pressure exceeds the compressor's pressure energy, the flow reverses through the compressor. The flow reversal causes the discharge pressure to drop and the suction pressure to rise. The drop in the system pressure differential allows the compressor flow to return to normal forward flow. This completes one surge cycle. If the conditions that provoked the original surge event have not changed, the surge cycles will repeat. It is common to distinguish between at least two types of surge: mild/classic surge and deep surge. Mild/classic surge is a phenomenon with oscillations in both pressure and flow in the compressor, while in deep surge, the mass flow oscillations have such a high amplitude, that full flow reversal occurs in the compression system (Gravdahl and Egeland 1999). Figure 3.5 shows a compressor characteristic with a deep surge cycle.

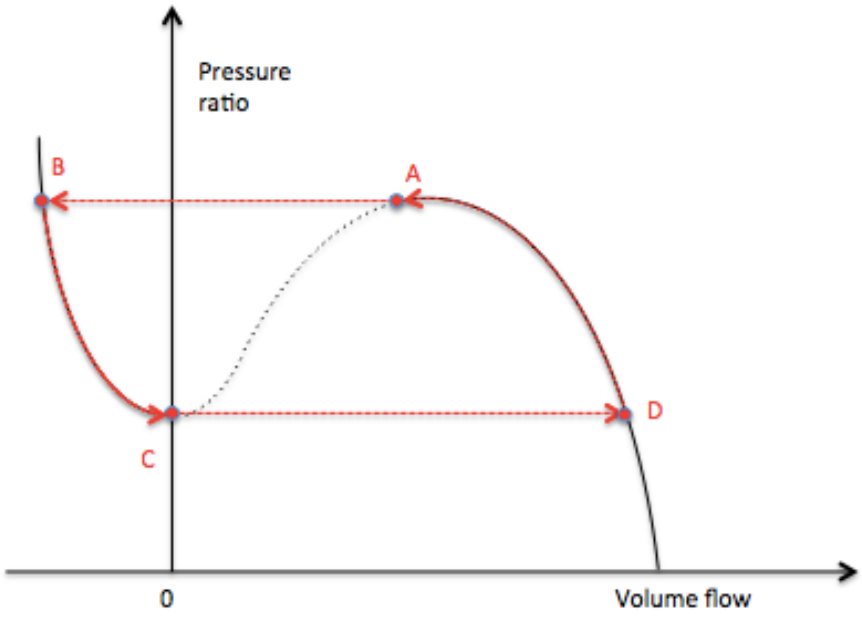


Figure 3.5: Deep surge cycle

Even for machine operating at stable conditions, unexpected events can occur that cause the compressor operating point to cross the surge line. Shutting off downstream processes or changing the production rate implies a load change that can cause the compression system to enter surge. Also worth mentioning is the effect of temporal changes in flow composition. This is common for compressors used in the production of oil and gas. Significant changes of gas composition cause the compressor characteristic, including the surge line, to change and hence surge can occur even if pressure rise and flow rate remains unchanged (van Helvoirt 2007).

## 3.4 STALL AND SURGE PRESSURE FLUCTUATIONS

Rotating impeller stall, rotating diffuser stall and surge each has a characteristic pressure signature. This can be used to indicate the aerodynamic condition of the compressors when operated in the unstable region. Measurement of pressure transients inside the compressor or in the inlet or discharge piping plays a major role in experimental investigation of stall and surge phenomena. Pressure measurements are also used in anti-surge control.

### 3.4.1 ROTATING STALL

Rotating stall is recognized as one or more regions of stagnant flow travelling around the circumference of the compressor at 10-90% of the shaft speed. Impeller rotating stall is recognized by sub-synchronous frequencies in the range of 50-80% of the rotational speed, while diffuser rotating stall is associated with frequencies in a somewhat lower range. The frequency of the vaneless diffuser rotating stall is typically in the range of 6 to 33% of the impeller rotational speed (T. Grüner 2012).

The rotating cells of stagnant flows induce pressure fluctuations with the same characteristic frequency. These pressure fluctuations act in the radial direction and the amplitude depends on both the rotational speed and the density of the flow. This is expressed in equation 3.4.1 (Tri-Sen Turbomachinery Controls).

$$\Delta P \approx \frac{1}{20}\rho U^2 \tag{3.4.1}$$

It is common to define the inception of rotating stall as the point where the pressure amplitude of the sub-synchronous pressure frequency becomes comparable with pressure variation caused by the passing of the impeller blades [(Kang and Kang 2003), (Ferrara,

Ferrara and Baladassarre 2004)]. Figure 3.6 shows the spectral content of the pressure signal when a centrifugal compressor is throttled into stalled operation. The compressor is operating at 9000RPM, and the pressure is measured at the diffuser wall.

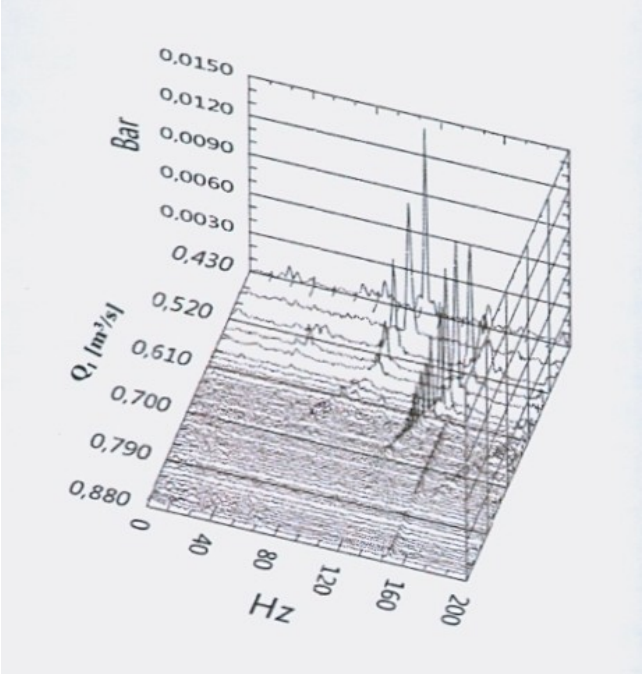


Figure 3.6: Frequency spectrum of diffuser pressure signal (T. Grüner 2012)

Two distinct stall frequencies can be recognized in the figure. Stall was first detected at $Q_1 = 0.69$ m3/s. with a characteristic frequency of approx. 90% of the rotational speed, and slightly increasing as the flow is reduced. It is overlapped by a second distinct stall frequency also increasing with reduced flow. The high stall frequency to rotational speed ratio indicates impeller rotating stall (T. Grüner 2012).

### 3.4.2 SURGE

The characteristic pressure pulsations associated with surge differs a lot from those corresponding to rotating stall. Firstly, unlike rotating stall, where pressure pulses act radially on the rotor shaft, the pressure pulsations accompanying surge act axially on the rotor. Secondly, pressure frequencies corresponding to surge are much lower. Only a few hertz compared to those of rotating stall that may approach several hundreds of hertz. In both rotating stall and surge, the frequency depends on the compressor speed, but in the case of surge the frequency is also dependent on the swallowing capacity of the system downstream of the compressor. Finally, the amplitudes of surge pressures are much higher than those of rotating stall. The magnitude will vary between mild and deep surge, but the pressure change

due to a deep surge is approximately ten times as big as the pressure change due to rotating stall. Equation 3.4.2 gives an approximation of the amplitude of surge pressure fluctuations (Tri-Sen Turbomachinery Controls).

$$\Delta P \approx \frac{1}{2}\rho U^2 \tag{3.4.2}$$

Ferrara, Ferrara, and Baladassarre (2004) performed several experimental investigations in order to evaluate the impact from diffuser geometry on the inception and evolution of rotating stall and surge in centrifugal compressors. The compressor model was instrumented with total and static pressure taps located at the model inlet, stage inlet, diffuser inlet and outlet and volute outlet. In addition, fast-responding dynamic pressure sensors were installed at the impeller inlet, at the diffuser inlet, at the diffuser mean radius and at the diffuser outlet. Figure 3.7 shows the pressure signals from three dynamic pressure sensors located at different sections in the compressor.

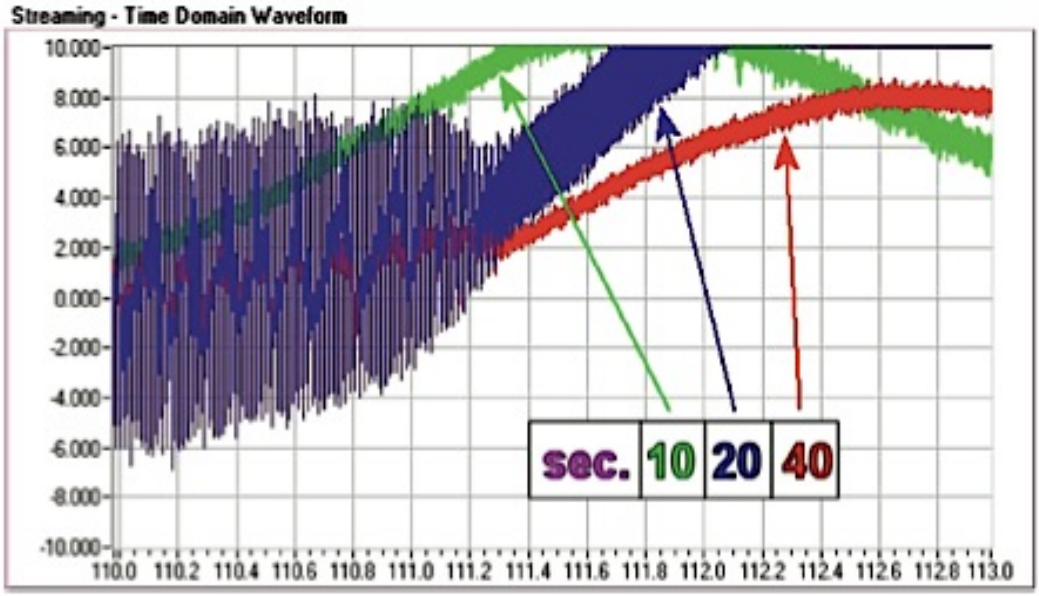


Figure 3.7:Transition from stall to surge (Ferrara, Ferrara and Baladassarre 2004)

The flow is continuously reduced by slowly closing the discharge throttle valve. The graph shows how the transient pressure develops from stall to surge. High-frequency pressure fluctuations associated with stall is transitioned into low frequency and high amplitude surge fluctuations when the flow is reduced. The pressure sensor installed at the impeller inlet (section 10) feels the typical surge pressure fluctuation earlier than the diffuser sensors (section 20 and 40). The figure clearly indicates the main differences between the stall and surge pressure signatures.

## 3.5 INTRODUCTION TO ANTI-SURGE CONTROL

The different techniques used to protect the compressor from unstable operation can be divided into three main methods: surge avoidance, surge detection and avoidance and surge suppression also referred to as active surge control. Focus is given surge avoidance and surge detection as these are the techniques that are discussed later in the report. Note that the word *surge* in the remainder of this chapter can be regarded as synonymous with rotating stall and surge.

### 3.5.1 SURGE AVOIDANCE

Traditionally surge control has been handled by using a control system that prevents the compressor from entering the unstable region left to the surge line. A surge avoidance line, also called the control line, is introduced some distance, e.g. 10% of the surge flow rate, away from the actual surge line. Figure 3.8 shows a compressor characteristic with the surge avoidance line indicated in red. The safety margin, or the surge margin *(SM)*, is applied to assure that the machine under no circumstances go into surge (Gravdahl and Egeland 1999).

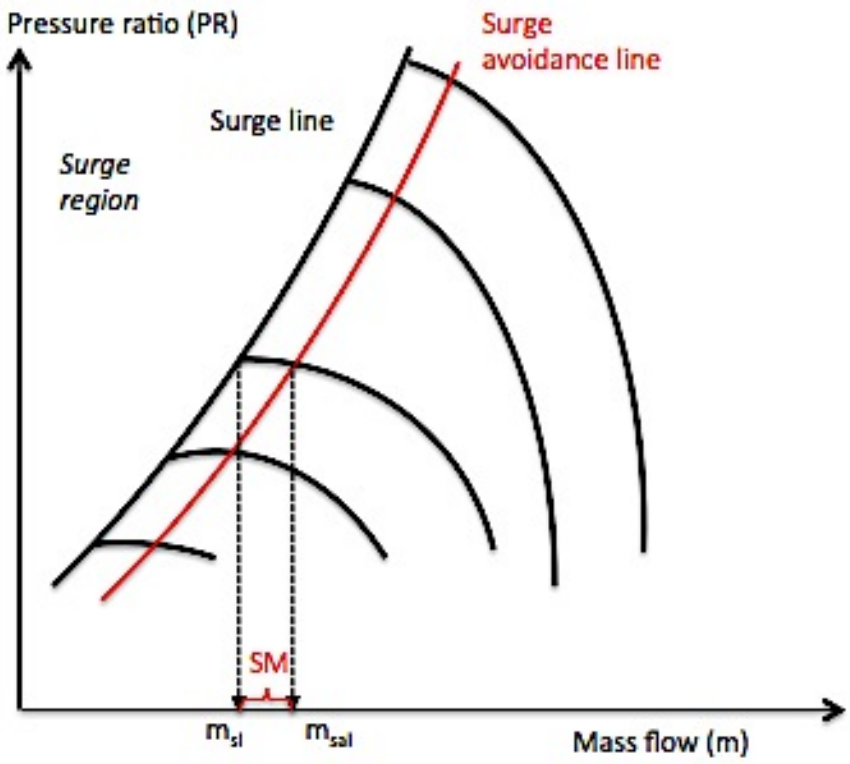


Figure 3.8: Surge avoidance

All surge avoidance schemes will operate on the following principles: If the working point of the compressor tend to cross the control line, i.e. if the distance between the working line and the surge line approaches the SM, some actuation device is activated and the working point is forced to stay to the right of the surge avoidance line. In centrifugal compression systems anti-surge valves where some of the compressed fluid is fed back to the compressor inlet are commonly used for surge avoidance. If the compressor operating point crosses the surge avoidance line, the anti-surge valve starts to open, thereby reducing the compressor pressure ratio and increasing the flow through the compressor. There exist different types of surge avoidance schemes, but the majority of newly designs utilize microprocessors or computer-based controllers. Parameters like flow, inlet and discharge pressure and temperatures, compressor speed and power, are measured, fed into the surge controller, and used to calculate the available surge margin. Figure 3.9 shows a typical surge avoidance scheme for industrial applications.

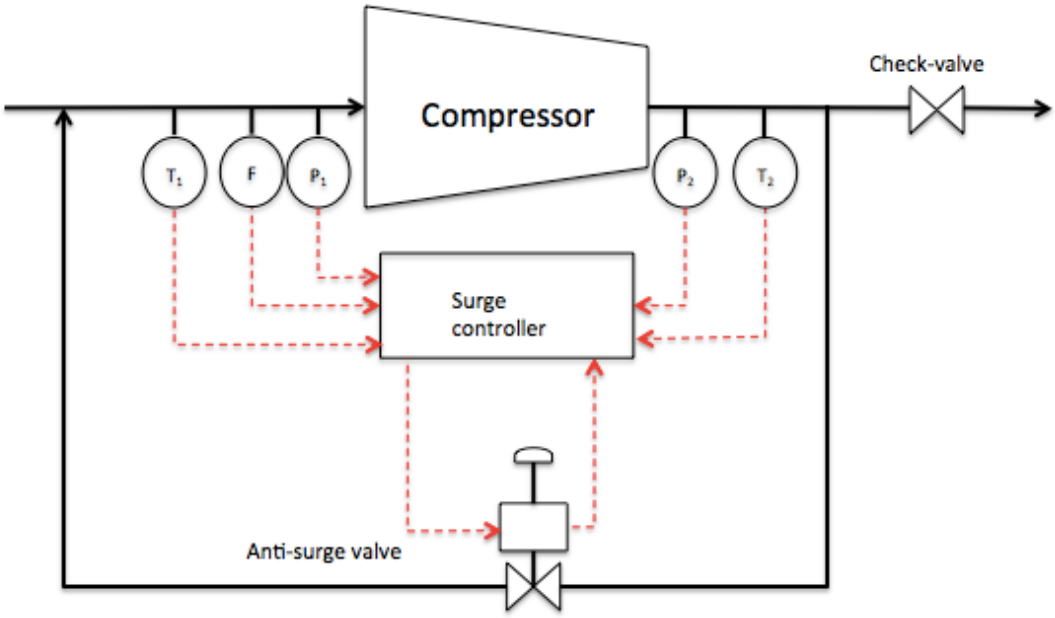


Figure 3.9: Surge avoidance scheme

The amount of margin required for a particular installation depends on a number of factors, and the amount of margin required to protect the compressor is not necessarily the same as the amount of margin required to protect the process. However, in a conventional compressor installation the most significant parameter that will affect the appropriate margin is the sizing and reaction time of the anti-surge valve. If the valve is inadequately sized or opens too slowly, a wider margin will be required to prevent surge. The reaction time of the surge valve also depends on the response time of flow meters, pressure sensors and other measurement devices used to determine the compressor operating point. In the past, about the only way to

evaluate the minimum margin requirement was to test the control system on the live process. In the last few years, however, the availability of rigorous, high fidelity dynamic simulation software has allowed anti-surge control system designers to evaluate the dynamics of the system and test the control system performance before the control system installed.

Surge control based on surge avoidance is the safest and most applied method. However, the system is very conservative, and the restriction of the feasible operating region unduly limits the capabilities of the compressor. The peak pressure rise for constant speed, representing the peak performance of the compressor, is located close to the surge line and cannot be reached when the safety margin is introduced. Regions of high efficiency lie close to, or may even encompass the surge line, and are thus also excluded from the operating range. In addition, the surge margin also limits the transient performance of the compressor as both acceleration and deceleration of the machine tends to drive the system towards the surge line (van Helvoirt 2007).

### 3.5.2 Surge Detection

In surge detection and avoidance, countermeasures to keep the operating point in the stable region are activated when the actual onset of surge is detected. This allows for operation closer to the surge line and thus enlarges the compressor operation envelope. Compared to avoiding surge by having a fixed surge margin, surge detection and avoidance makes it possible to run the machine in regions of higher efficiency and higher pressure-rise. However, to ensure safe compressor operation, knowledge of reliable surge precursors and also sophisticated instrumentation that can detect incipient surge, is required.

There are numerous innovative techniques and ideas for surge detection that are used for surge control purposes. Most of the successful techniques are based on monitoring various variations in flow, pressure, temperature, speed or other parameters at the compressor suction or discharge, along with their time derivatives or frequency of oscillations. These parameters are compared to threshold values defining the incipient surge and are fed to the surge controller. Surge detection based on measurements of pressures and pressure fluctuations is by far the most thoroughly investigated technique (Botros and Henderson 1994).

It is possible to distinguish between three main approaches to surge detection based on pressure measurements: Systems using the pressure signals directly, systems using time derivatives of pressure signals and systems based on measuring pressure fluctuations. An example of the first detection technique is surge detection based on measuring the pressure

difference between the hub side and shroud side pressure in the vicinity of the diffuser inlet. A controller compares the measured differential pressure to a set point value for surge control. The anti-surge valve is opened if the measured pressure difference is too big. Another method is based on measuring distortions in the total pressure in the inlet and outlet piping of the compressor. An example of the second technique is to monitor the time derivative of the discharge pressure. If a surge conditions is ensuing, the absolute value of the differentiated signal is greater than a reference value. The third and last technique is based on measuring pressure amplitudes and frequencies in or around the compressor (Botros and Henderson 1994). By monitoring the pressure fluctuations, both frequencies and amplitudes, flow instabilities can be detected, and adequate countermeasures can be activated.

### 3.5.3 INSTRUMENTATION

The performance of a surge control system depends the right choice and location of measurement devices. *Proper instrumentation is crucial for good system operability*. In surge avoidance schemes, the control system must be able to determine the available surge margin based on the compressor operating point in real time. The requirements to instrumentation in surge detection systems are even more stringent. These systems need reliable instruments that also are able to *detect* flow instabilities. The different detection schemes uses different approaches to predict surge, and it thus follow that the choice of instrumentation will vary correspondingly (Botros and Henderson 1994).

Uncertainty in pressure, temperature or flow measurements will cause the surge control system to over or under predict the occurrence of surge. In surge avoidance schemes, over predicting surge causes the compressor operation envelope to be limited by more than the allowable surge margin. Under predicting surge gives the control system less time to respond and activate countermeasures, and gives a reduction in the protection margin. In surge detection schemes, the compressor is already allowed to operate closer to the surge line, and the available time gap for the surge controller to activate countermeasures is already limited. As a consequence, under predicting surge is even more dangerous to the machine. In the worst-case scenario, inaccurate measurements can result in failure in detecting surge at all. This will leave the compressor unprotected.

Surge control in general also depends on the response time of transmitters and activators. The transmitter and the control system are at least required to respond to system changes as fast as the compressor surge rate. The surge rate depends on the compressor operating conditions, and will also be different for different compression systems. However, a general surge rate

can be estimated based on the flow rate through the system divided by the downstream volume. This is expressed in equation 3.5.1 (Brun and Nored 2008).

$$TR_{surge} \propto \frac{\dot{Q}}{V_p} \tag{3.5.1}$$

According to Brun and Nored (2008), the transmitter response time should be as fast as possible because compressors can approach surge rapidly. This is particularly true regarding emergency shut down situations, and this event should therefore be used to determine required minimum response time. In general the time response of a transmitter for the measurement of a process variable used in the surge control algorithm should be less than 100ms.

# 4 ELECTRO-MECHANICAL SENSORS

Pressure sensors based on electro-mechanical sensing and transduction techniques cover the main portion of the current, modern pressure sensor marked. Electro-mechanical pressure sensors are adaptable for a wide range of applications, and are especially useful when applied in data acquisition and control systems. In general, all commercially available electro-mechanical pressure sensors can be grouped into four categories, according to their sensing principles: optical, capacitive, piezoelectric, and piezoresistive. This chapter will focus on pressure measurements based on the *piezoelectric* and *piezoresistive* sensing principles. Piezoelectric and piezoresistive pressure sensors are commonly referred to as fast-response pressure sensors, dynamic pressure transducers or high-frequency pressure sensors, and sensors utilizing these technologies are widely used for measuring unsteady pressures and high frequency events. Piezoelectric and piezoresistive pressure sensors feature a wide operating range, high stability and sensitivity, and high ruggedness. This makes them very suitable for application in turbomachinery. Several papers also report on the use of piezoelectric and piezoresistive pressure sensors for detecting aerodynamic instabilities, i.e. stall and surge, in centrifugal compressors.

This chapter is divided into three main parts. The two first parts will give a description of piezoelectric and piezoresistive pressure sensors. The sensing and operational principals will be explained and different sensor designs will be presented. The third gives a comparison of the two techniques and presents the different advantages and disadvantages concerned with the two techniques.

## 4.1 PIEZOELECTRIC PRESSURE SENSORS

### 4.1.1 THE PIEZOELECTRIC EFFECT

*Piezoelectricity* is understood as a liner electromechanical interaction between the mechanical and electric state in crystalline materials without a center of symmetry. The word itself means electricity from pressure, and comes from the Greek word *piezin* meaning to press. The piezoelectric effect was discovered by the Curie brothers in 1880, but no practical use was attempted before Langvin conceived the idea of using thin plates of quartz to generate sound waves in water in 1917. This was the beginning of echo sounding (Fraden 2004)

We commonly divide the piezoelectric effect into a *direct* effect and a *converse* effect. Piezoelectric sensors utilize the direct effect. The direct piezoelectric effect refers to the generation of electric charge when a piezoelectric material is exposed to mechanical deformation. A piezoelectric material is like a pressure-sensitive capacitor. When tension or compression is exerted upon the material, electric charge accumulates on opposing surfaces creating an electrical potential difference or a voltage, across the material. This is illustrated in figure 4.1. The figure shows the displacement of electrical charge due to the deflection of the lattice in a naturally piezoelectric quartz crystal.

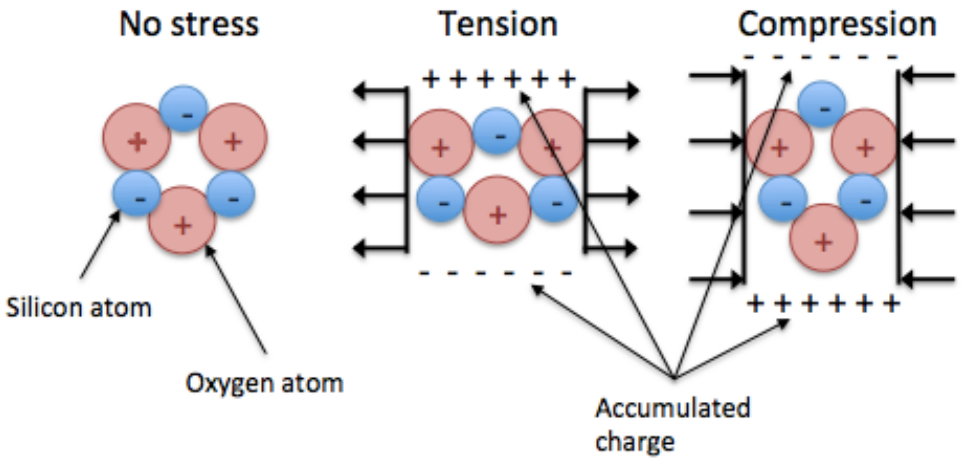


Figure 4.1: The direct piezoelectric effect in quartz

The converse piezoelectric effect describes the opposite situation, and means that the piezoelectric material is deformed when an electric voltage is applied. This effect is utilized in piezoelectric actuators and ultrasonic wave generators.

The generated voltage from a piezoelectric material with a thickness δ can be calculated according to equation 4.1.1.

$$V = S_v \cdot P \cdot \delta \tag{4.1.1}$$

The voltage sensitivity, $S_v$, depends on the piezoelectric material and the geometrical cut. (Gautschi 2002)

### 4.1.2 Piezoelectric Sensor Materials

Many materials, both natural and synthetic, exhibit piezoelectricity. However, only a rather restricted number of them have been proven suitable for transduction elements in piezoelectric sensors. Of the natural piezoelectric materials, the most frequently used are quartz, tourmaline and gallium orthophosphate. Quartz ($SiO_2$), either in its natural or high-quality, reprocessed form, is one of the most sensitive and stable piezoelectric materials available. Quartz can be used up to 573 °C, but the piezoelectric coefficients of quartz drops with increasing temperature, and the sensitivity of the sensors will thus be poorer at high temperature. Tourmaline works up to about 650 °C. (Gautschi 2002).

Of the synthetic materials, ceramics like lead zirconate titanate, barium titanate, and lead niobate are most extensively used. Piezoelectric ceramics display a very high sensitivity. Some of them exhibit piezoelectric coefficients up to over a 100 times higher than those of observed in single crystals. They can also be manufactured in many different shapes and with a broad range of values for the properties of interest. However, there are also drawbacks associated with using ceramics. Compared to single crystals like quartz and tourmaline, piezoelectric ceramics are not as stable, have a poorer electrical insulation resistance, and are much more temperature sensitive. The piezoelectric effect is not natural in these materials, and the degree of polarization will slowly decrease over time. This phenomenon is known as *aging,* and causes a reduction in sensitivity. Since piezoelectric ceramics are ferroelectrics, their electromechanical properties depend strongly on temperature. If the ceramics is exposed to high temperatures, the aging process will be significantly sped up. High temperature also alters the natural frequency response of piezoelectric ceramics. High temperature reduces the insulation resistance in the material, causing the electric charge to be drained out faster. Therefore, at high temperatures, piezoelectric ceramics cannot measure pressure fluctuations below 10-50 Hz.

Polymers are also used as piezoelectric materials. A polymer lacking symmetry known as polyvinylidene fluoride is commonly used, because it can be made into shapes that are impossible for solid material (Gautschi 2002).

### 4.1.3 Operational Principals and Sensor Design

Piezoelectric sensors are characterized by having a transduction element made up of a piezoelectric material. They are categorized as *active* pressures sensors, because no external energy is needed to get an output signal. When the piezoelectric material is exposed to

mechanical deformation, charge migration generates a voltage across the piezoelectric. To pick up this charge, conductive electrodes must be applied to specific surfaces. A piezoelectric sensor thus becomes a capacitor with a dielectric material, which is the piezoelectric material. The dielectric acts as a generator of electric charge, resulting in a voltage across the capacitor. Signal conditioning electronics then converts the voltage into signals that can be further processed (Fraden 2004).

Piezoelectric pressure sensors are a special form of force sensors. They usually have a diaphragm, which can be considered as the sensing element, that transmits the fluid pressure to the transduction element. In a well-designed pressure sensor the effective area of the diaphragm is constant. The force transmitted to the piezoelectric transduction element is therefore proportional to the acting pressure (Gautschi 2002).

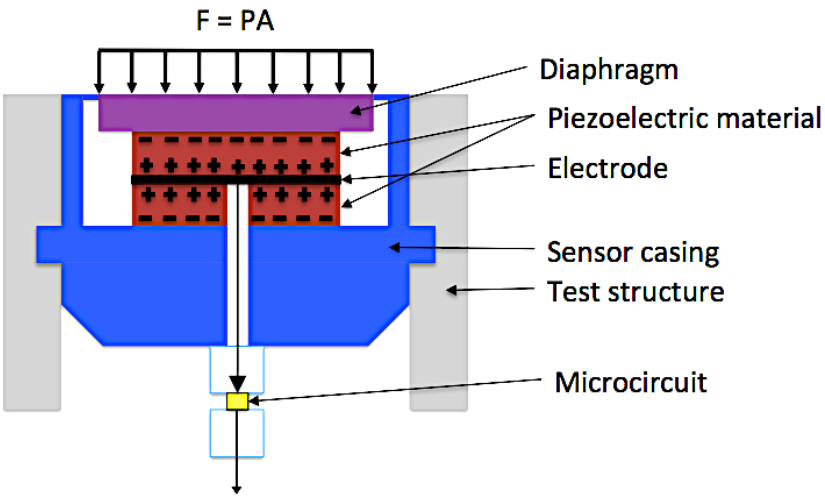


Figure 4.2: Typical pressure sensor structure with internal processing

A representation of a typical piezoelectric pressure sensor is shown in figure 4.2. The gray color represents the test structure. The purple color corresponds to the diaphragm, while the blue color corresponds to the sensor casing. The piezoelectric crystal, which is the transduction element in the sensor, is colored red, and the black electrode is where the charge from the crystals accumulates before it is conditioned by the yellow microcircuit.
Figure 4.3 illustrates a general-purpose sensor from PCB Piezotronics. This sensor has acceleration /vibration compensation and built in electronics. Figure 4.3b) indicates the sensor size accomplished by miniaturization

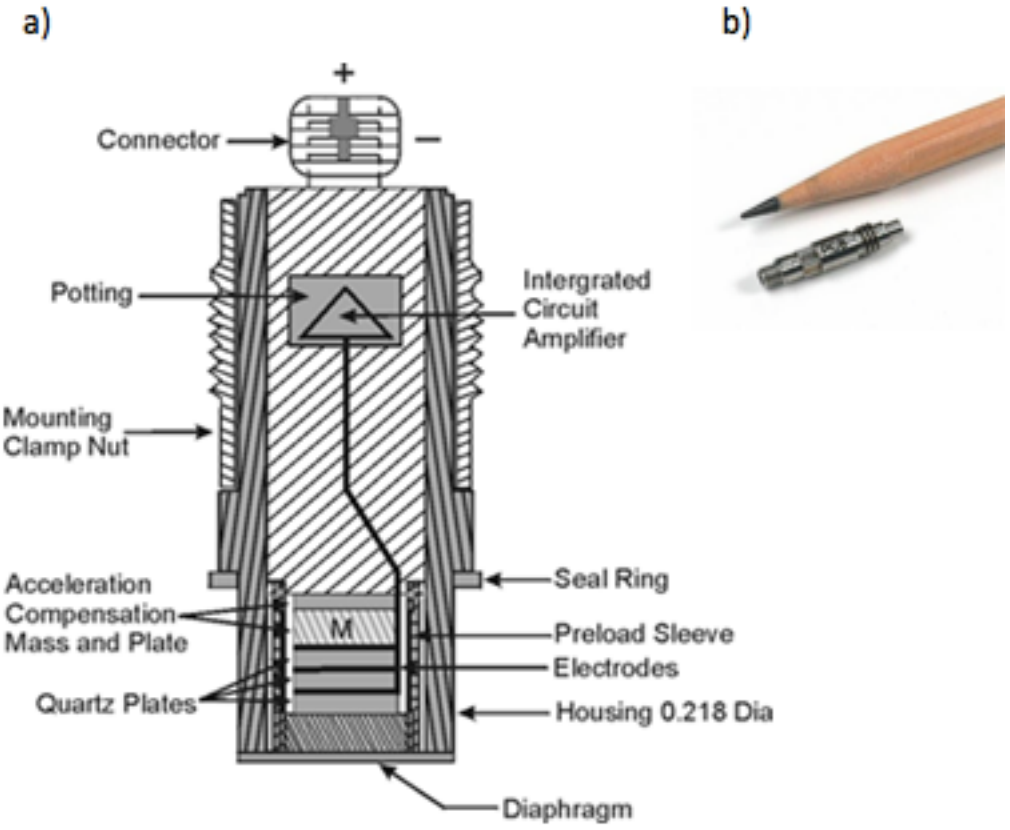


Figure 4.3: a) Typical ICP Quartz pressure sensor b) Subminiature ICP pressure sensor (PCB Piezotronics)

Figure 4.4 shows a similar type of sensor delivered by Kistler. The measured pressure acts through the steel diaphragm on the quartz crystal measuring element, which transforms the pressure into an electric charge. The stainless steel diaphragm is welded flush and hermetically to the stainless steel sensor housing.


Figure 4.4: Miniature acceleration-compensated piezoelectric pressure sensor (Kistler) and b) (PCB Piezotronics)

### 4.1.4 Dynamic vs. Static Measurements

The piezoelectric material generates an electric potential when pressure is applied. However, if the applied pressure remains constant, charge migration in the material and from its surroundings will nullify the charge separation in the piezoelectric material, and the electric charge will eventually leak to zero. Piezoelectric materials can therefore only measure dynamic events. They are not able to measure truly static events. They have a very poor *DC* accuracy but good *AC* accuracy (PCB Piezotronics).

The rate at which the charge leaks back to zero is dependent on the electrical insulation resistance of the piezoelectric material and the materials in contact with it. The charge leakage follows an exponential decay, and depending on the electrical characteristics of the system and also environmental factors like humidity and temperature, the time scale involved may be very short. The low-frequency monitoring capabilities of the system depend on the *Discharge Time Constant*, DTC. DTC is defined as the time required for a sensor or measuring system to discharge its signal to 37% of the original value, and is the product of the electrical capacitance and the electrical resistance of the measuring system. A large DTC allows for measuring long-duration pressure pulses and quasi-static pressure. The DTC of a piezoelectric pressure sensor can vary from just a few seconds up to more than 2000 seconds.

The DTC also limit the time available to take a fixed measurement. A general rule of thumb is that the signal loss and time elapsed over the first 10% of a DTC have a one-to-one relationship. This is illustrated in figure 4.5. If a sensor has a 500 second DTC, over the first 50 seconds, 10% of the original input signal decays. For 1% accuracy, data should therefore be taken in the first 1% of the DTC (PCB Piezotronics).

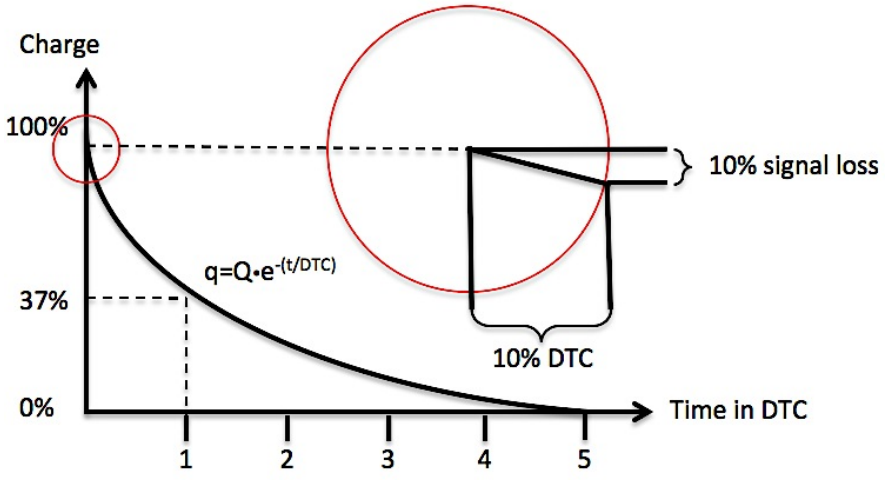


Figure 4.5: Piezoelectric signal exponential decay

### 4.1.5 INTERFACE ELECTRONICS

The output signal produced by the sensing and transduction elements must be conditioned prior to being analyzed by the chosen readout device. This includes conversion to a useful, low-impedance voltage signal, signal amplification/attenuation and filtering. The signal processing can be accomplished internal to the sensor by a microelectronic circuit, or external to the sensor. The two methods serve the same general function, but offer various advantages and disadvantages (PCB Piezotronics)

SENSORS WITH BUILT-IN ELECTRONICS

Figure 4.6 is equivalent diagram of a basic piezoelectric sensor with built in microelectronics. The measured pressure produces a quantity of charge, Δq, in the piezoelectric material. This charge is collected in the crystal capacitance, C, and forms a voltage according to the law of electrostatics:

$$\Delta V = \frac{\Delta q}{C} \tag{4.1.2}$$

Quartz exhibits a very low capacitance, which results in a high voltage output signal. This signal is suitable for signal condition with voltage amplifiers. The ICP pressure sensors incorporate a built-in MOSFET microelectronic amplifier to convert the high-impedance charge output into a low-impedance voltage signal. The gain of the amplifier determines the sensor sensitivity (PCB Piezotronics).

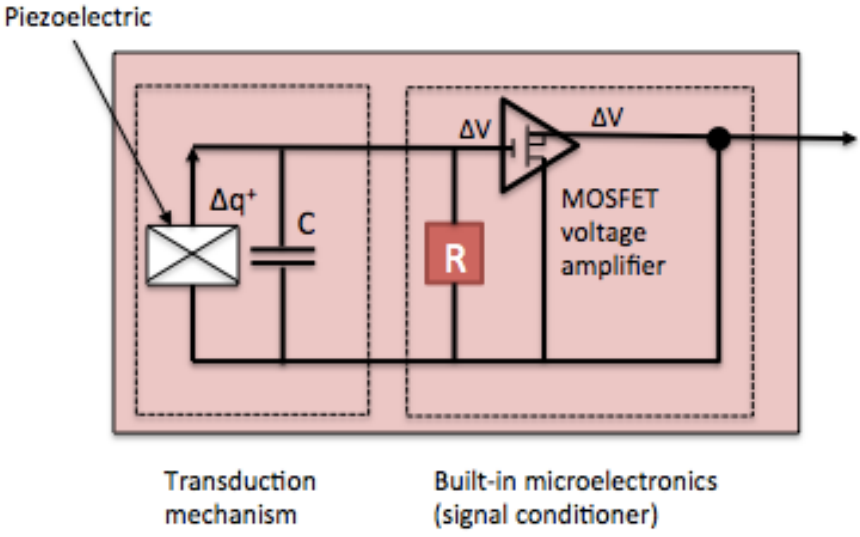


Figure 4.6: Sensor with built-in electronics

The characteristics of sensors with built-in electronics, i.e. the sensitivity and frequency range, are fixed within the sensor. This has both positive and negative consequences. The sensor characteristics will be independent of the supply voltage, which is an advantage. However, if the acting pressure is very low it can sometimes be necessary to increase the signal amplification in order to get an adequate resolution of the output signal. This is not possible with a built-in amplifier, which is a major drawback. Another disadvantage with internal electronics charge is that the built-in circuit is not as resistant to harsh environments as the sensing and transduction part of the sensor. The internal electronics will therefor limit the environmental range of the sensor. (PCB Piezotronics).

The main advantages with internal processing are low maintenance and easy usage. The sensor can be connected directly to the readout equipment, and in comparison with un-conditioned high impedance-signals, the low-impedance output signal can be transmitted over long distances with little loss in signal quality.

CHARGE MODE SENSORS

In charge mode sensors the conversion from a high-impedance charge output to a low-impedance voltage output is accomplished external to the sensor. It can be done directly by the input of the readout device, or by in-line voltage and charge amplifiers. Figure 4.7 illustrates a system with a basic charge mode sensor connected to a charge amplifier (PCB Piezotronics)

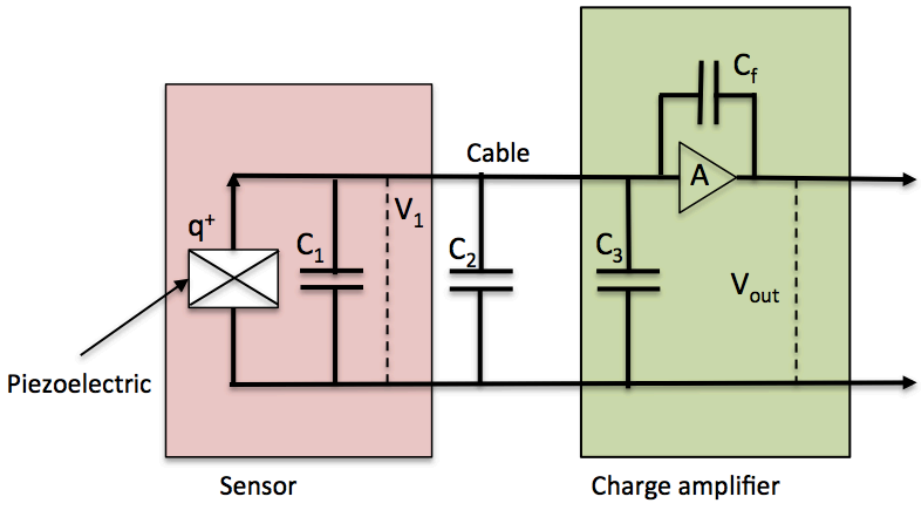


Figure 4.7: Charge mode sensor with charge amplifier

Charge mode systems with charge-amplifiers and charge mode systems with voltage-amplifiers have different advantages and disadvantages. Systems with voltage amplifiers are capable of linear operation at very high frequencies. Some of these systems have frequency limits exceeding 1 MHz, which makes them capable of detecting shock waves with rise times in the microsecond range. However, compared to equivalent charge amplified systems, voltage-amplified systems have a very high noise floor. This is a major drawback, especially when measuring small pressure variations. Sensors with built-in electronics and/or charge-amplified sensors are therefore typically used in these cases. There are also disadvantages with charge-amplified systems. The per-channel cost of charge-amplified instrumentation is typically very high, and it is also impractical to use charge-amplified systems above 50 or 100 kHz as the feedback capacitor exhibits filtering characteristics above this range (PCB Piezotronics).

.

External processing typically require more advanced and sophisticated instrumentation compared to internal processing. The high-impedance output signal is much more sensitive to environmental effects, and a special low-noise cables must be used in order to reduce the charge generated by cable motion, and minimize the noise caused by electro-magnetic and radio frequency interference. It is also very important to keep the input cable and connector to the charge or voltage amplifier dry and clean. Any change in the total capacitance or loss in insulation resistance due to contamination can radically alter the system characteristics. This often precludes the use of such systems in harsh or dirty environments unless extensive measures are taken to seal all cables and connectors. The cable length will also affect the signal quality. Operation over long cables is not advised since the capacitive loading of the cable may affect frequency response and introduce noise and signal distortion. Large capacitive cable loads may act as filters, and reduce the upper frequency limit (PCB Piezotronics).

A major benefit with external electronics is that the characteristics of the sensor are variable and can be changed by switching components in the external signal conditioner. When dealing with pressure fluctuations of very low amplitudes, this is a great advantage. By adjusting the signal amplification, a higher resolution can be achieved in the pressure range of interest. Since the electronics are external, charge mode sensors can also be used in very harsh environments, certain quartz models are capable of operation up to 540 °C (PCB Piezotronics).

## 4.2 PIEZORESISTIVE PRESSURE SENSORS

Although piezoelectric pressure sensors have been used in earlier year, the requirements in terms of sensor size and the objective of accurately measuring the static part of the pressure signal, have made focus turn towards piezoresistive pressure sensors. Piezoresistive sensors were among the first Micro-Electro-Mechanical-System (MEMS) devices, and are some of the most reported and developed micro-machined devices.

### 4.2.1 ORIGIN OF PIEZORESISTIVITY

The piezoresistive effect differs from the piezoelectric effect in the sense that the applied mechanical stress causes a change in the electrical resistance, not in the electric potential. This provides an easy and direct transduction mechanism between the mechanical and electrical domain. The piezoresistive effect was discovered by Lord Kelvin in 1856, but the development of piezoresistive materials did not kick off until the early 1950's, when the large piezoresistive effect in semiconducting materials like silicon and germanium was discovered. Today this is used in the MEMS field for a wide variety of sensing application, including pressure sensors (Barlian, et al. 2009).

The change in resistance is linearly related to the applied strain. This is expressed in equation 4.2.1. The proportional constant, G, is called the gauge factor. R is the original resistance of the material and ΔR is the change in resistance due to the applied strain ε.

$$\frac{\Delta \mathrm{R}}{R} = G \cdot \varepsilon \tag{4.2.1}$$

The electrical resistance of a conducting material depends on the geometrical dimensions, the length (l) and the cross-sectional area (A), as well as the specific resistivity (ζ) of the material. Changing any of these parameters will change the resistance. Equation 4.2.2 expresses the electrical resistance in an arbitrary conducting material.

$$R = \zeta \frac{l}{A} \tag{4.2.2}$$

In general all conducting materials exhibit a change in resistance with strain. However, due to significant changes in specific resistivity, the resistance change in semiconductors can be very large. The specific resistivity of a semiconductor is given in equation 4.2.3:

$$\zeta = \frac{1}{e \cdot N_e \cdot M_e} \tag{4.2.3}$$

The resistivity of semiconductors depends on the mobility ($M_e$) and number ($N_e$) of charge carriers. When strain is applied to a semiconductor, the average atomic spacing in the crystal lattice is changed. This affects the mobility of the charge carriers. The conducting band gaps are changed, making it easier or harder, depending on the material and strain, for electrons to be raised into the conduction band. The conduction band is the range of electron energies large enough to free an electron from binding with its atom and to move freely within the atomic lattice (Liu 2006).

### 4.2.2 Piezoresistive Sensor Materials

Piezoresistors are defined as materials whose *resistivity* changes with strain. Semiconductors like silicon and germanium are therefore true piezoresistors. The conductive properties, i.e. the resistivity, of a semiconductor can be modified by introducing impurities into the crystal lattice. This is known as *doping*. Controlled adding of impurities increases the number of charge carriers in the semiconductor, which again results in changing the electrical conductivity. By doping the semiconductor, the electrical conductivity may be varied by factors of thousands or millions. This has a great impact on the piezoresistive properties of the semiconductor. Figure 4.8 illustrates how the doping concentration affects the sensitivity and the temperature dependence in silicon (Barlian, et al. 2009).

Metal strain gauges can be used as transduction element in piezoresistive sensors, and they also offer some advantages over true piezoresistors:

- The need of doping and resulting lengthy process steps is eliminated.
- Metals can in general sustain a much greater elongation before fractured, and thus provide improved mechanical robustness.
- Metal resistors can be processed and deposited at much lower temperatures (Liu 2006).

In terms of gauge factors, metal strain gauges do not compare favorably with the true piezoresistors. Higher gauge factor means higher output for the same strain, or higher sensitivity relative to the stiffness and natural frequency of the transduction material. The subsequent description of piezoresistive pressure sensors will thus be limited to sensors using semiconducting materials as transduction elements.

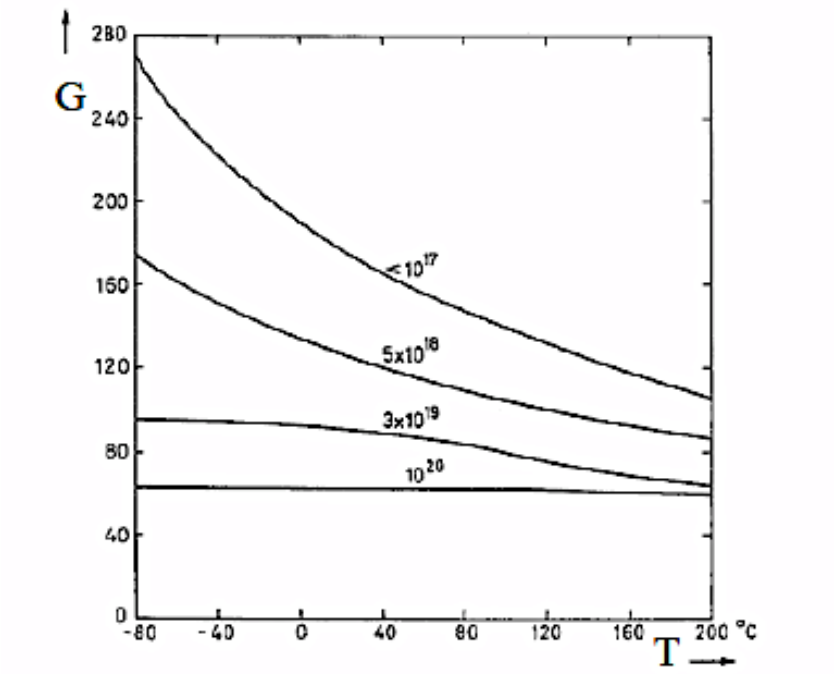


Figure 4.8: Influence of boron concentration on the sensitivity of P-type silicon (Kulite Semiconductor Products, Inc.)

### 4.2.3 Operational Principals and Sensor Design

Just like piezoelectric pressure sensors, piezoresistive sensors also consist of an elastic membrane or diaphragm and a detector that responds to an applied force. In piezoresistive pressure sensors the transduction element is made up of a piezoresistive material. Piezoresistors embedded in the elastic diaphragm transmits the force exerted on the diaphragm into a change in resistance. The piezoresistors can either be bonded to the diaphragm by an adhesive; *discrete gauges*, or they can be an integral part of the diaphragm; *integral gauges*. The diaphragm may be made from single-crystal silicon or diamond or CVD-based thin films. The integrated piezoresistors are formed by dopant diffusion, ion implantation, or doped epitaxy. When the diaphragm is deflected under pressure, maximum stress will occur at the edge of the membrane. In order to maximize the sensitivity of the sensor, the piezoresistors are thus usually located near the edges of the diaphragm.

The sensing and transduction element of a piezoresistive pressure sensor is illustrated in figure 4.9.

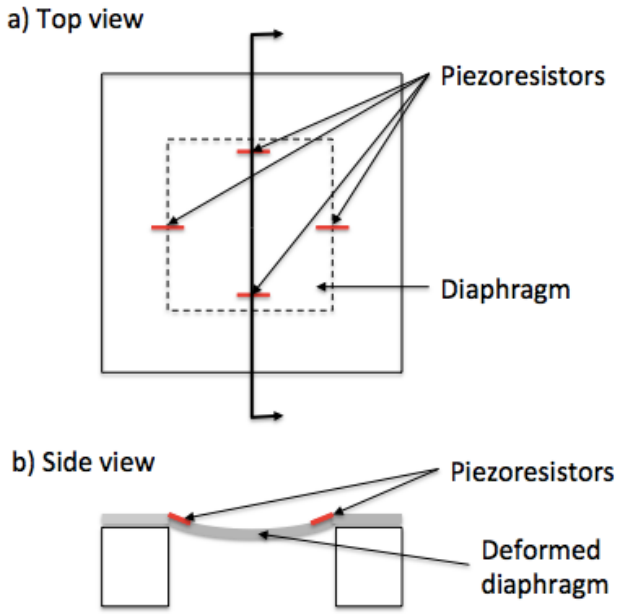


Figure 4.9: Sensing element of piezoresistive pressure sensor (Liu 2006)

To convert the strain-induced resistance-change of the piezoresistors into a voltage change, which can be measured directly and accurately with conventional instruments, the piezoresistors embedded in the diaphragm are connected together in a fully active *Wheatstone bridge circuit* (Barlian, et al. 2009). This is illustrated in figure 4.10.

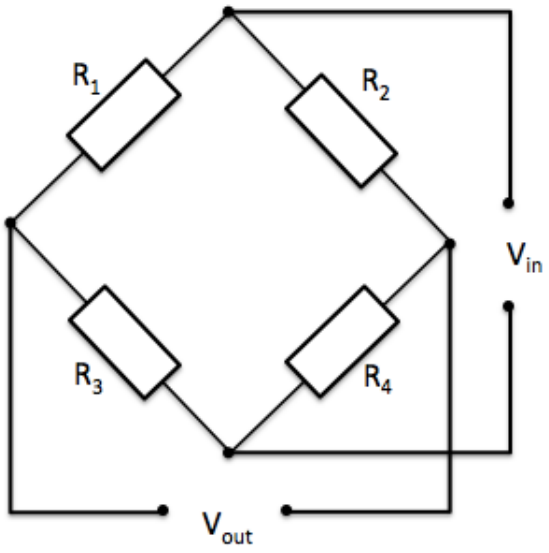


Figure 4.10: Wheatstone bridge circuit

The Wheatstone bridge configuration consists of four resistors connected in a loop. One or more of the resistors are *sensing* resistor, whose resistance changes when the diaphragm is deflected under pressure. The other resistors are made insensitive to strain by being located in regions with zero strain. The Wheatstone bridge is normally energized by applying a regulated voltage across two opposite corners. The output voltage will then be proportional to the product of the excitation voltage and the resistance changes of the strain gauges. Good circuit design dictates that whenever possible, the two adjacent arms of the bridge should change equally but in opposite directions under strain. This will eliminate temperature-induced changes from the output voltage. In figure 4.10 where all resistors are sensing resistors, this condition is achieved when $R_1$ and $R_4$, *the tension gauges* and $R_2$ and $R_3$, *the compression gauges*, are equal. For this special case equation the output voltage can be expressed according to equation 4.2.7:

$$\frac{V_{out}}{V_{in}} = \frac{\Delta R}{R} = G \cdot \varepsilon \qquad (4.2.7)$$

The output voltage is used as the actual measuring signal, and for visualization of the measured pressure.

In order to construct a pressure capsule from the sensing and transduction elements, it is necessary to support the elastic diaphragm on a pedestal. The purpose of the pedestal is to mechanically support the diaphragm, to isolate the sensing and transducing elements from mounting stress, to provide an overload stop when required and to configure the sensor reference pressure (Kulite Semiconductor Products, Inc.). Figure 4.11 shows a schematic diagram of an absolute pressure capsule diffused integrated sensor.

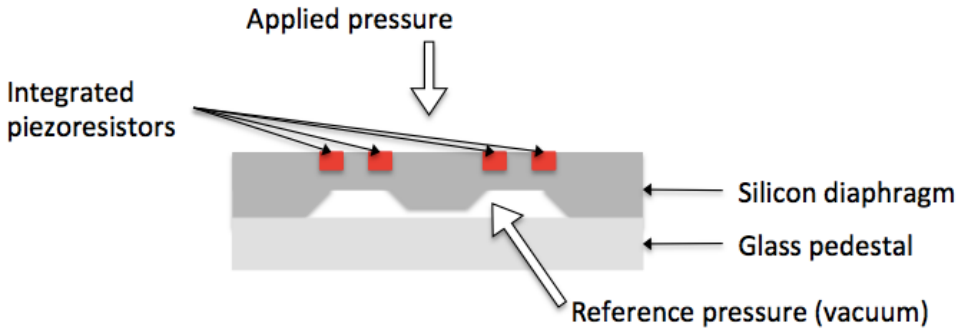


Figure 4.11: Complete Pressure capsule

Pressure capsules can be used without external casings, known as chip-on application or flush-mounted diaphragms, or they can be mounted in casings of different sizes and shapes. In many miniature pressure transducers the pressure capsule is located at the very front of the transducer, making them equivalent to flush-mounted diaphragms for true flush mounting of the diaphragms. Most of these models include a protective screen, designed to provide maximum protection of the diaphragm and at the same time cause minimum effect on the frequency response. Figure 4.12 illustrates one of these pressure sensors.

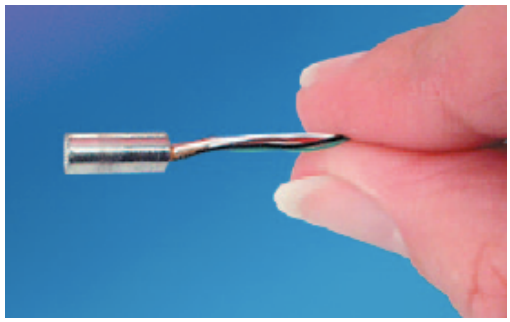

Figure 4.12: Miniature piezoresistive pressure transducer (Kulite Semiconductor Products, Inc.)

### 4.2.4 SOI Sensors and the Leadless Design

SOI SENSORS

The piezoresistors in a diffused silicon chip is typically electrically insulated form each other and the silicon diaphragm by reverse-bias p-n junctions. The p-n junction between the p-type piezoresistors and the n-type silicon diaphragm has a resistance characteristic that falls rapidly with temperature. At temperatures above 150°C to 200°C, the leakage currents within the Wheatstone bridge circuit will effectively bypass the piezoresistors, and the bridge will no longer measure the pressure accurately. The p-n junctions are also sensitive to light. For applications where pressure is measured in the presence of a detonation or other luminous events, the pressure sensor will generate an additional electrical output due to the light (Kulite Semiconductor Products, Inc.).

The SOI sensor (silicon-on-insulation) was developed to overcome the limitations of the p-n-junction isolation. In SOI sensors the piezoresistors are electrically insulated from the diaphragm material by a layer of silicon oxide, or by both a silicon oxide layer and a second

layer of glass. By replacing the p-n junction isolation, the temperature limit for continuous operation is extended to 538ºC. The SOI sensors are also insensitive to electro-magnetic interference and electrostatic discharge. (Kulite Semiconductor Products, Inc.) Figure 4.13 illustrates a traditional p-n junction type sensor. A schematic diagram of a dielectrically isolated fusion bonded sensor is given in figure 4.14.

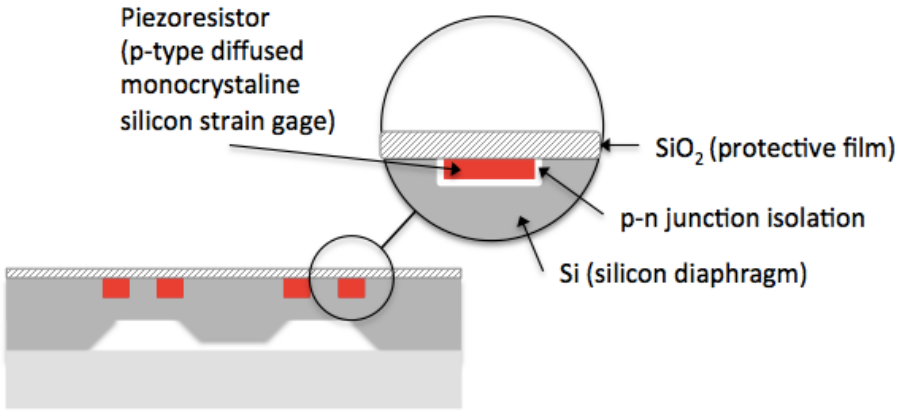


Figure 4.13: Diffused silicon chip with conventional p-n junction technology

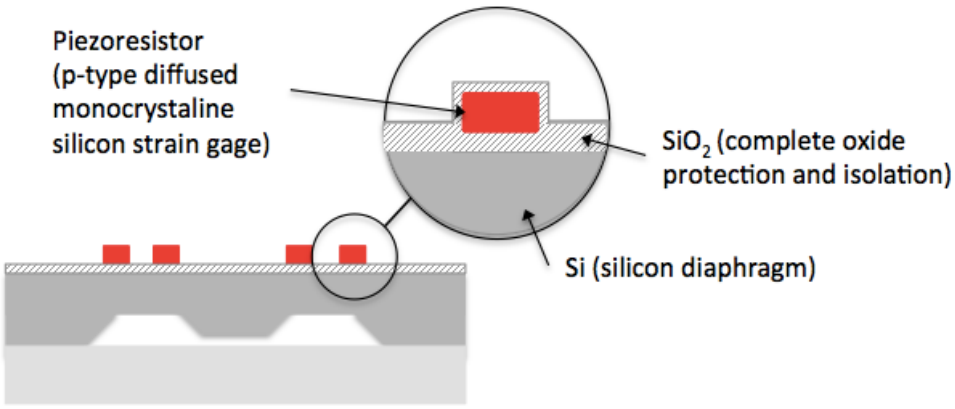


Figure 4.14: Fusion bonded sensor with SOI technology

THE LEADLESS DESIGN

Traditionally, electrical connection is made to the Wheatstone bridge on the silicon diaphragm by using very fine gold bond wires. This is illustrated in figure 4.15.

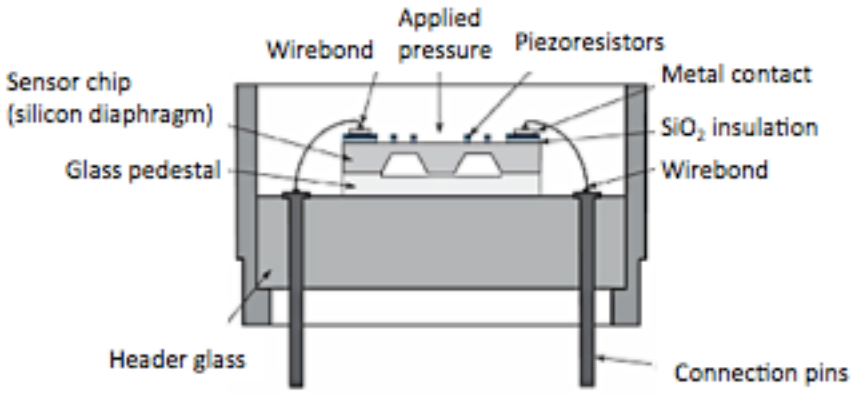


Figure 4.15: Wirebond connection design (Kulite Semiconductor Products, Inc.)

These wires and their welds are susceptible to failure due to fatigue under conditions of high vibration or rapid pressure cycling. If the pressure media is in direct contact with the stress-sensing network, which is the case in many pressure transducers, lead-outs and interconnections can also fail due to high temperatures and the presence of aggressive chemicals (Kulite Semiconductor Products, Inc.).

In the *leadless* design both wire bonding and direct contact between the active side of the diaphragm and the pressure medium has been eliminated. The pressure capsule is comprised of two main components, the *sensor chip* and a *cover wafer.* The assembly of the sensor chip and the cover wafer hermetically seals the piezoresistors and electrical interconnections from the surroundings, and the pressure medium only acts at the passive side of the diaphragm. The electrical connection to the sensing chip is made by using high temperature conductive glass-metal frits. By eliminating the gold bond wires and not exposing the sensor network and electrical contact areas to the environments and pressure media, the leadless sensors have a much higher ruggedness than the conventional design. They have a much higher tolerance to shock and vibrations, and also an improved temperature capability. A piezoresistive pressure sensor with a leadless design is illustrated in figure 4.16 (Kulite Semiconductor Products, Inc.).

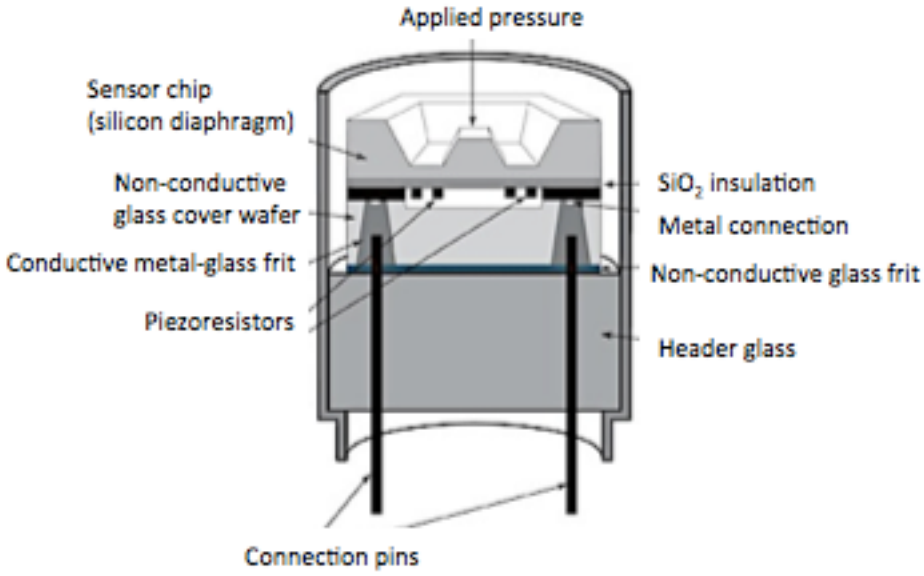


Figure 4.16: The leadless design (Kulite Semiconductor Products, Inc.)

### 4.2.5 Interface Electronics

Piezoresistive sensors are passive devices and require an external power supply to provide the necessary current or voltage excitation to operate the transducer. This energy source need to be well regulated and stable, since it may introduce sensitivity error and secondary effects that will cause errors in the output signal. However, even with a stable energy source that can provide a constant current or voltage supply, errors and spurious signals may appear at the transducer output due to variations in the line resistance caused by temperature changes. The line resistance affects the voltage drop between the sensor and the energy source, and variations the resistance may result in an unpredictable voltage/current at the sensor. These effects have most impact in remote sensing, when the distance between the sensor and the energy supply is big. (Kulite Semiconductor Products, Inc.).

Just like the output from a piezoelectric transducer, output from a piezoresistive transducer must be conditioned prior to being analyzed by the chosen readout device. A fully functional signal-processing unit consists of two stage-amplifiers, a compensation circuitry, and two forms of output (frequency and voltage) (Liu 2006). The millivolt output from the Wheatstone bridge can be amplified to a higher voltage level internal to the sensor, but signal amplification can also be accomplished in an external unit. The benefits and drawback concerned with the two approaches is similar to those of piezoelectric pressure sensors.

## 4.3 COMPARISON OF TECHNIQUES

The advantages and disadvantages of piezoelectric and piezoresistive pressure sensors are summarized in table B-1 and B-2 in Appendix B.

### 4.3.1 SIMILARITIES AND MINOR DIFFERENCES

Piezoelectric and piezoresistive pressure sensors share many of the same benefits and limitations. Both of the sensors are able to withstand harsh environments, and they have high rigidity. By using hermetically sealed sensor casings made of stainless steel or other materials that meets the corrosion requirements, and also protecting the sensing diaphragm with additional membranes measurement in aggressive fluids can be accomplished with both sensors. According to Gautschi (2002), the stiffness values of piezoelectric materials is in the order of $104 \cdot 10^9$ N/m$^2$ which is similar to that of many metals. They thus produce a high output signal with almost no deflection.

Furthermore, both piezoresistive and piezoelectric pressure sensors have a wide temperature range. SOI sensors and the leadless design allow for operation of piezoresistive sensors up to 538ºC. And by choosing quartz or tourmaline as piezoelectric, and also having external electronics or water-cooling, piezoelectric sensors can be used at similar temperatures. However, if operated outside their respective temperature range, both piezoresistive and piezoelectric pressure sensors will be affected. If exposed to very high temperatures, the performance of a piezoelectric sensor, piezoelectric ceramic in particular, is significantly reduced. The temperature will affect the sensor sensitivity by reducing the piezoelectric coefficients, and also cause a degradation of the low-frequency response of the sensor. High temperature reduces the insulation resistance in the piezoelectric, causing charge to be drained out at faster rate. *Aging* of piezoelectric materials, in particular non-natural piezoelectric materials, is also significantly sped up at high temperatures. However, according to Navabi (2010), the temperature sensitivity is more significant in piezoresistive sensor. The resistance of a piezoresistor increases with temperature by typically 10% per 100°F (≈38°C), and the strain sensitivity decreases with temperature by typically 2% per 100°F (Kulite Semiconductor Products, Inc.). There are ways of compensating for this temperature dependency. Kulite mentions circuit techniques using passive shunt or series resistor elements whose resistance is temperatures independent, and also adjustment of the bridge excitation voltage.

Piezoelectric and piezoresistive sensors can be miniaturized with micromachining and have very compact designs. In piezoelectric sensors, the amount of induced charge is proportional to sensor area and piezoelectric coefficients. As the sensor area shrinks, less charge is generated for the same applied pressure. Very little charge is generated if the sensors are intended to measure very small pressure signals. This makes the interface electronics particularly important in order to successfully measure pressure with MEMS scale piezoelectric sensors. Typically, the interface circuit in these sensors has an overall amplification of approximately a thousand. With such a large gain, minimize any unwanted feed-through and noise coming from the environment is very important. If not, this will easily saturate the circuit. The interface circuit should therefor be located close to the sensor in order to reduce the environmental effects (Kon, Oldham and Horowitz 2004). Piezoresistive pressure sensors can be miniaturized without any implication for the produced output. Recalled form chapter 4.2.1 the change in electrical resistance of a piezoresistor is caused by both geometrical effects and change in resistivity. However, since the change in resistivity by far exceeds the geometrical effects, the size of the piezoresistor is not relevant.

Both piezoelectric and piezoresistive sensors are very sensitive to strain. However, according to Gautschi (2002), piezoelectric sensors are more sensitive to strain than corresponding piezoresistive sensors. Evident from table 4-1 the strain sensitivity of piezoelectric sensors are about 50 000 times as big as those of equivalent piezoresistive sensors, and the threshold value is 10 times as big. A very small threshold value means that piezoelectric pressure sensors are able to detect and measure pressure pulses of very small amplitudes. The table also indicates that piezoelectric pressure sensors have a much higher span-to-threshold ratio, which indicates that piezoelectric sensors have a wider pressure range than the corresponding piezoresistive sensor. Due to constant improvement and development of the two measurement systems, it is difficult to compare the techniques.

| PRINCIPLE | Strain sensitivity | Threshold (1 to 100 Hz) | Span-to-threshold Ratio |
|---|---|---|---|
| PIEZOELECTRIC | 5 | 0.00001 | 100 000 000 |
| PIEZORESISTIVE | 0.0001 | 0.0001 | 2 500 000 |
| INDUCTIVE | 0.001 | 0.00005 | 2 000 000 |
| CAPACITIVE | 0.005 | 0.0001 | 750 000 |

Table 4-1: Comparison of stress sensitivity of different pressure measurement systems (Gautschi 2002)

Both of the sensors offer high stability, high reproducibility and high linearity of the dependence of the output on the measurand. The sensors are very reliable, and thus very suitable for implementation in control systems. On the downside, piezoelectric and piezoresistive sensors are intrusive methods, and if not care is taken during installation, mounting of the sensors may cause impact on the medium they measure. This will result in inaccurate measurements. Furthermore, it should also be mentioned that the sensors only provides a *point* measurements of the pressure. Obtaining full-field pressure measurement will require arrays of embedded pressure taps and a thus substantial amount of drilling in the test surface.

### 4.3.2 Main Differences

The main differences between piezoelectric and piezoresistive sensors are their dynamic characteristics and the electrical requirements. Piezoelectric sensors are active devices that generate charge due to external strain. No energy input is required to produce an output signal. Piezoresistive sensors require energy input to reveal the change in electrical resistance caused by the acting pressure.

Tsung and Han (2004) measured the dynamic characteristics of six pressure sensors of dissimilar design and structure. The performance of the different sensors was evaluated under the same experimental parameters, 10 bar and 600 Hz, using a pressure square-like wave generator. The dynamic performance of the sensors was compared by evaluating the response rate, overshoot and rise time of each sensor. The two piezoelectric sensors were very sensitive to pressure changes. The pressure raised up to about 10 times the preset value within an extremely short time, indicating an extremely quick time response. The impulse signals were followed by a "steady state" of 10 bar, which means that the pressure measurement of the two sensors are accurate. The two piezoresistive sensors showed less overshoot than the piezoelectric sensors, but a much slower time response. It was also difficult to distinguish between the impulse and the residual value, which resulted in a very inaccurate pressure measurement.

Table 4-2 summarizes the results for the piezoelectric and piezoresistive sensors. Sensor S1 and S2 are the piezoelectric sensors, while S4 and S6 are the piezoresistive sensors.

| SENSORS | S1 | S2 | S4 | S6 |
|---|---|---|---|---|
| Overshoot | 1000% | 950% | 400% | 280% |
| Rise time (ms) | 0.022 | 0.028 | 0.177 | 0.262 |
| Response rate (bar/s) | 4545 | 3571 | 565 | 382 |

Table 4-2: Dynamic characteristics of tested sensors (Tsung and Han 2004)

Piezoelectric and piezoresistive pressure sensors are frequently used to investigate the inception and evolution of aerodynamic instabilities in centrifugal compressors. Their high sensitivity and wide frequency range makes them appropriate for detecting and resolving the pressure fluctuations associated with unstable compressor operations. There are numerous articles reporting on the use of these sensors for unsteady pressure measurement in turbomachines, and several illustrative example were provided in the pre-project to this thesis. The reader is encouraged to review chapter 4 in *Wet Gas Compressor Stall and Surge* (Jellum 2012) for more details on the use of piezoelectric and piezoresistive pressure sensors in stall and surge detection.

Piezoresistive sensors are capable of measuring both dynamic and static pressures. Piezoelectric sensors cannot measure truly static events, but evident from the results of Tsung and Han (2004) they are much better at measuring high frequency signals. Piezoelectric sensors should be used when the frequencies encountered are very high, for instance when measuring pressure variations due to turbulence. They and can also be used to detect rotating stall. The pressure frequencies corresponding to surge are in the lower range, only a few hertz depending on the compression system. Piezoresistive sensors are therefore more suitable for measuring these fluctuations.

# 5 UNCONVENTIONAL TECHNIQUES

In order to increase the understanding of the complex flow interactions that occur within a centrifugal compressor, in particular the inception and evolution of stall and surge phenomena, knowledge of the global surface at different flow conditions would be very useful. Piezoelectric and piezoresistive pressure sensors can be used to investigate unsteady flow and pressure fields. However, since they only provide point measurements, the information will be limited. Traditional methods to measure global surface utilize embedded arrays of pressure taps. The spatial resolution of the measurement depends on the number and distribution of the pressure taps, and measurements of high resolution will require extensive drilling and a very complex sensor network. In this chapter, two alternative approaches; pressure-sensitive paint (PSP), surface-stress-sensitive films (S3F), will be described. These techniques measures global surface pressure. PSP and S3F require optical access to the model surface and an imaging device of high pixel resolution. The techniques are not meant for continuous monitoring and application in control system. However, for use in laboratory testing, they show great potential.

The chapter is divided into three main parts. The two first parts describe and explain the sensing and operational principles of PSPs and S3Fs. The third part provides some illustrative examples of the use of PSP for measuring unsteady surface pressure in turbomachinery.

## 5.1 PRESSURE-SENSITIVE PAINT (PSP)

Pressure measurements using PSP have been demonstrated in several challenging flow fields. The techniques have been used to measure the surface pressure of advanced compressor blades, and to measure the surface pressure of aircraft wings in flight. The PSP method is a relatively new technique, and conventional paint formulations were first applied in wind tunnel testing in the late 1980s and early 1990s. The great advantages of PSP include non-intrusive pressure measurements and high spatial resolution when compared to more conventional techniques like the flush-mounted piezoelectric and piezoresistive pressure sensors (Gregory, Asai, et al. 2008).

### 5.1.1 Operational Principals of PSP

PSP is an optical method of measuring surface pressure based on the *photoluminescent* behavior of certain oxygen-sensitive molecules. Photoluminescence is a process where a substance absorbs photons and then re-radiates photons to return to its initial state. Quantum mechanically, this can be described as an excitation to a higher energy state and then a return to a lower energy state accompanied by the emission of a photon. The luminophores absorbs energy at various efficiencies depending on the wavelength of the incident light, but most efficient wavelengths lie in the ultraviolet or blue range. The emitted light is typically shifted to longer wavelength, and lies in the red and green range. Figure 5.1 shows the Jablonski energy diagram depicting the vibrational and electronic states, and the photophysical processes associated with a typical luminescent molecule.

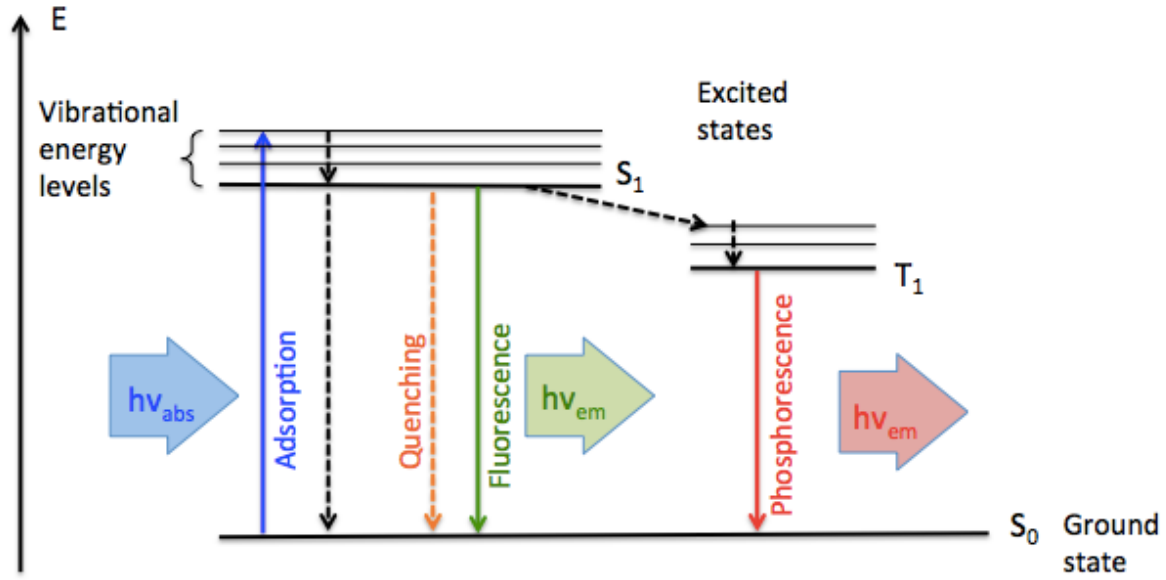


Figure 5.1: Jablonski energy diagram

A typical PSP is comprised of two main parts: the oxygen-sensitive luminescent molecules, and an oxygen-permeable binder to physically adhere these molecules to the model surface. When the painted surface is exposed to electromagnetic radiation, the luminophores are excited to an upper energy state. This energy is then released primarily through luminescence, which is the collective term for fluorescence and phosphorescence, and dynamic quenching. In PSPs', the rate at which the dynamic quenching process competes with the luminescence process, is dependent on the oxygen concentration in the paint. When an excited-state luminescent molecule interacts with an oxygen molecule, excess energy is transferred to a vibrational mode of the oxygen molecule, resulting in a radiationfree transition to the ground state. The higher the concentration of oxygen, the more of the excess energy is dissipated

through quenching. The light emitted by the paint can thus be measured to yield the oxygen concentration in the paint. The oxygen concentration in the paint is a function of the oxygen partial pressure at the test surface, which again depends on the local static pressure. An increase in the static pressure will give a corresponding increase in the oxygen partial pressure, which again results in a higher oxygen concentration in the paint.

The two energy dissipation methods – luminescence and oxygen quenching – are inversely proportional to one another. If the static pressure increases, the luminescent energy of the luminophores decreases. The light intensity emitted by the paint is therefore inversely proportional to the local pressure:

$$I_{surface} \propto \frac{1}{P_{surface}} \tag{5.1.1}$$

### 5.1.2 Measurement Technique

Conceptually a PSP system is composed of a PSP, an illumination or excitation source, a photodetector, and a long-pass filter. This is illustrated in figure 5.2.

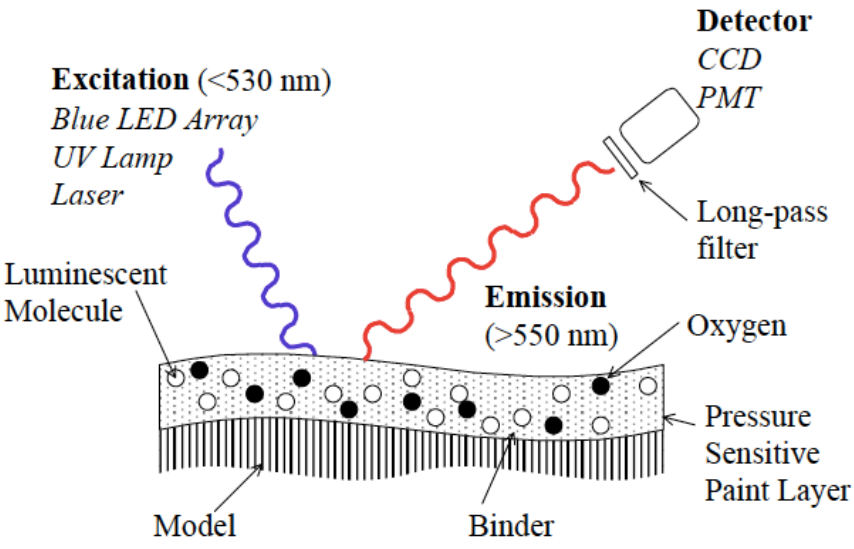


Figure 5.2: Basic PSP system (Innovative Sientific Solutions, Inc)

The PSP is distributed over the model surface and the surface is then illuminated by the excitation source causing the PSP luminophores to luminesce. Typical illumination sources include xenon arc lamps, LED arrays, UV lamps and lasers, and the excitation wavelength

range centers around 600nm. In order to produce accurate measurements, it is important for the illumination intensity to remain constant and for the illumination source to provide a relatively uniform illumination of the test surface. A photodetector is used to collect the luminescent energy from the PSP. Commonly used photodetectors in PSP testing include the photomultiplier tube (PMT) and the CCD camera. Important characteristics of good photodetectors are high efficiency at the wavelength of interest, and a low signal-to-noise ratio. Typically, PMT's are used for point measurements, while CCD cameras are used for global surface measurements. The input to the photodetector is optically filtered to eliminate all but the paint luminescence, and then the luminescent intensity is recorded and converted to pressure through the Stern-Volmer relation and a known reference condition (Gregory 2002).

### 5.1.3 Response Time and Sensitivity

In order to detect and measure the wide range of pressure frequencies and amplitudes involved in unsteady aerodynamic phenomena, sensitive and fast-responding pressure measurement systems are required. The luminescent process imposes the ultimate limit on the sensitivity and time response of the PSP, and the two luminescence processes; fluorescence and phosphorescence, exhibit different advantages and disadvantages. Fluorescence has a much quicker response compared to phosphorescence. The timescale for spontaneous fluorescence typically ranges from $10^{-10}$ to $10^{-6}$ s, while phosphorescence, involving more process steps, has a timescale in the range of $10^{-4}$ to $10^{4}$ s. Regarding sensitivity, the situation is the opposite. Dynamic quenching competes more effectively with the slower phosphorescence process than the faster fluorescence process. For a given change in oxygen concentration, the change in phosphorescence intensity is greater than the change in fluorescence intensity (Navarra 1997).

When measuring transient flow phenomena, especially high frequency events, the long phosphorescent lifetimes will usually not be compatible with the timing requirements. In order to resolve an unsteady pressure field with high precision, the time of the excitation and the subsequent lifetime if the paint must be well below the highest frequencies encountered. If imaging in a rotating frame, the time of the excitation and the subsequent lifetime of the paint must also occur within the data acquisition time required to image the rotating blade at a desired spatial resolution. This imposes stringent requirements to the temporal resolution of the paint. Fluorescent compounds are therefore usually chosen, even though phosphorescent compounds would give a more sensitive paint.

The sensitivity and time response of the paint also depends on the paint binder. The binders will typically have a somewhat limited openness to oxygen, which results in a slower response and a reduced sensitivity compared to the dynamic characteristic of luminescent process. Additional time is required for the oxygen molecules to permeate the binder, which gives less time for the oxygen to interact with the luminophores. Equation 5.1.2 expresses the relationship between the response time of the paint and the properties of the binder:

$$t_{PSP} \propto \frac{h^2}{D_{O_2}} \tag{5.1.2}$$

According to equation 5.1.2 improving the response time is accomplished by reducing the thickness of the binder layer, or by increasing the oxygen diffusivity of the binder material. Reducing the binder thickness is generally not advised. This will result in a reduction in the brightness of the luminescence, which again reduces the signal-to-noise ratio. Improving the paint response time should therefore be accomplished by increasing the oxygen diffusivity (Navarra 1997).

Finally it should also be mentioned that the paint sensitivity also depends on the absolute pressure at the test surface. By derivation of equation 5.1.3 with respect to pressure, a mathematical expression of the pressure sensitivity of the paint is obtained:

$$\frac{dI}{dP} \propto \frac{1}{P^2} \tag{5.1.3}$$

.

A standard approach to achieving high measurement accuracy is to increase the sensitivity of a gauge by measuring increments relative to a fixed value, e.g., using a differential pressure gauge instead of an absolute pressure gauge (Fonov, et al. 2006). PSPs' are essentially absolute pressure gauges, where the output signal, i.e. the luminescence intensity depends on an absolute pressure, rather than a pressure difference. This is major drawback when measuring very small pressure variations. Equation 5.1.3 shows that the pressure-sensitivity of the paint is inversely proportional to the square of the local pressure. Accurate pressure measurements are therefore difficult to obtain if the absolute local pressure is high. In particular if the pressure variations are small.

### 5.1.4 FAST-RESPONSE POROUS PSPS'

The development of PSPs' for unsteady pressure measurements has focused on improving the oxygen diffusivity of the binder material. The emergence of *porous* binder materials have been key to this development, and enabled measurements of unsteady pressure fluctuations on the order of 100 kHz (Gregory and Sullivan 2006). According to Nabavi (2010) flow fields with fundamental frequencies as high as 21 kHz have been successfully measured with porous PSP formulations. The structural difference between conventional binders and porous binders is indicated in figure 5.3.

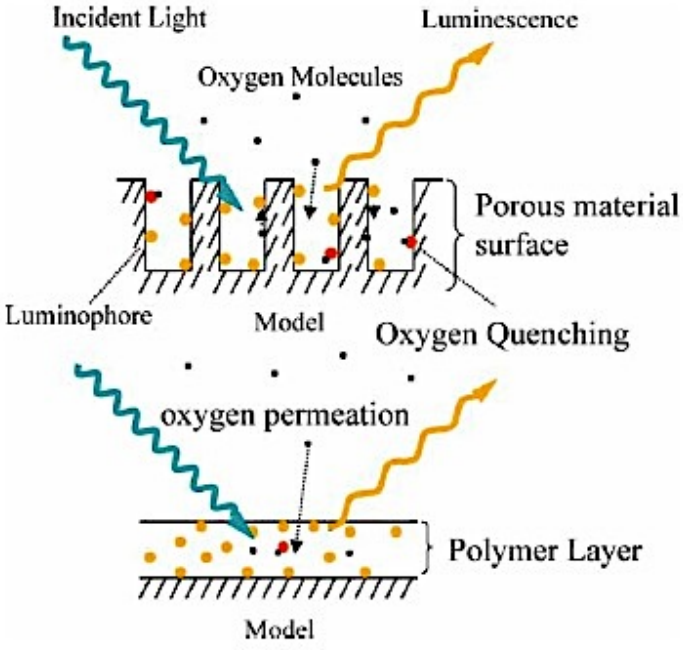


Figure 5.3: Porous PSP and conventional polymer-based PSP (Gregory, Asai, et al. 2008)

Conventional PSPs', using polymers as binder material, have a time response on the order of a few hundred milliseconds, or even a few seconds due to the diffusive characteristics of the polymer (Gregory 2002). The porous binder is characterized by an open structure that allows for greater interaction of oxygen molecules with the luminescent molecules. The common porous binders in use today include thin-layer chromatography plate (TLC-PSP), anodized aluminum (AA-PSP) and polymer/ceramic (PC-PSP). The different binders haves different advantages and disadvantages. TLC-plates are commercially available and fast and easy to prepare, but the plates are fragile and limited to use on flat or very simple shapes. Compared to TLC-PCP AA-PSP can be applied to curved and complex surfaces because the anodized aluminum layer can be formed on an arbitrary shape of aluminum. The binder is robust, and the surface roughness of the anodized layer is very small. The disadvantage of AA-PSP is that

it is difficult to anodize large models, and that only aluminum or titanium models can be used. PC-PSP can be applied to all types of surfaces. Compared to TLC-PSP and AA-PCP it reflects more luminescence, producing a brighter paint. According to Gregory et al. (2008) the response time of TLC-PSP and AA-PSP ranges from 10-100μs depending on the luminophores used, the layer thickness and some other parameters. Response times as low as 25μs have been reported on PC-PSP (Gregory, Asai, et al. 2008).

Gregory (2002) used a fluidic oscillator to investigate the ability of AA-PSP, PC-PSP and TLC-PSP to resolve an unsteady jet-flow field. Full-field measurements and point measurements were obtained with different paint samples, and the results were compared to hot-film probe measurements. The power spectrums of the pressure signals showed that the porous PSPs' were capable of responding to pressure fluctuations up to at least 40 kHz. This is well above the characteristic frequencies of stall and surge, and implies that paints can be used to investigate inception and evolution of stall and surge phenomena. The results also indicate that PC-PSP and TLC-PSP has slightly slower response compared to AA-PSP. (Gregory 2002)

### 5.1.5 PSBeads

PSP for surface pressure measurements have received a lot of attention in recent years, and due to significant improvements in frequency range and sensitivity, the PSP technology has become an advanced measurement technique also for measurement in unsteady flows. The need of measuring pressure globally and nonintrusively within a fluid flow, have motivated the development of PSBeads.

Kimura et al. (2006) synthesized oxygen sensitive polystyrene microspheres, doped with dual luminophores, and investigated the potential of using the microspheres to obtain the pressure distribution in 3D aerodynamic flows. Figure 5.4 illustrates the response time in the PSBeads to a jump in static pressure. Evident from the figure, the PSBeads' response to changes in oxygen is so fast that the luminescent intensity changes from initial to final value almost in the same amount of time as the pressure jump. According to Kimura et al (2006) the PSBeads' response to a pressure jump from vacuum to 1atm was within the measuring system resolution of 10ms. The diameters of the beads ranged from 1-5μm making them able to follow fluid flow accurately, and function as a pressure-sensitive airborne micro-particles providing an accurate non-intrusive imaging method for mapping the pressure distribution within a flow.

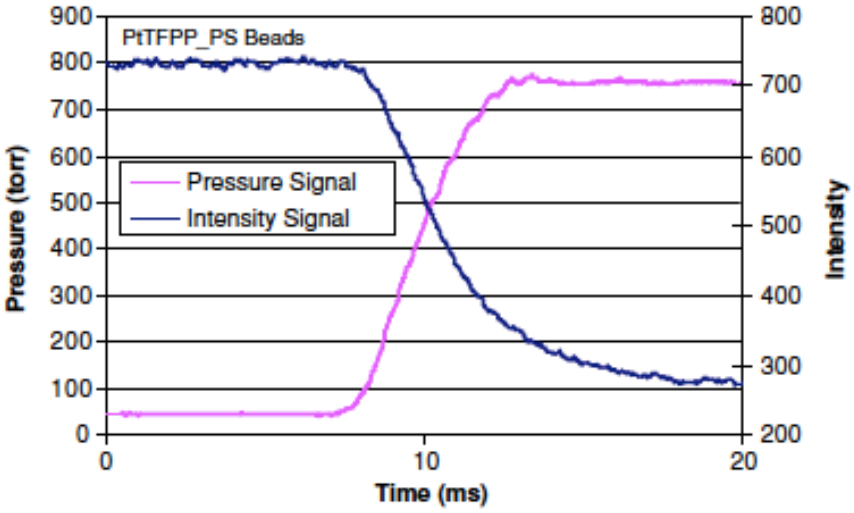


Figure 5.4: Response time for PSBeads to pressure jump (Kimura, et al. 2006)

The possibility of combining PSBead and PIV technologies to create a hybrid measurement system was presented by Abe, Okamoto and Madrame (2004). This system could potentially be used to, nonintrusively and simultaneously, resolve the global pressure distribution and the velocity field within a flowing fluid. PSBeads is an intriguing technique when considering the experimental investigation of aerodynamic instabilities inside the centrifugal compressor. The complex nature of the flow, both the boundary layer and the core flow, could be visualized at different operating conditions, and give a more comprehensive understanding of the different mechanism initiating stall and surge. Regarding wet gas compression, the PSBeads could also be used to model liquid droplets entrained in the core flow. This would indicate the droplet flow path through the compressor, which would be very useful in order to determine how the liquid is distributed in different parts of the machine.

## 5.2 SURFACE STRESS SENSITIVE FILMS (S3F)

Surface-stress-sensitive films are optical instruments for direct measurements of shear tension and pressure. The technique allows for simultaneous measurement of the global surface pressure and visualization of the surface flow. This is very useful, especially when understanding the physics of complex flows. The S3F measurements are not based on oxygen quenching, which eliminates the limitations associated with PSPs'. Compared to conventional PSPs', S3Fs' thus offer improved pressure sensitivity and frequency response, and do not require any oxygen in the test fluid. The technique can also be applied in incompressible flows (Fonov, et al. 2006).

### 5.2.1 Operational Principals of S3F

The basis of the S3F measurement is an elastic film of known thickness and shear modulus that deforms under the action of applied loads. The reaction of the film is monitored by imaging the surface, and then modeled by using a finite element analysis. This procedure results in a continuous distribution of shear tension and pressure over the filmed surface. The S3F consists of a thin and flexible elastomer film that has been embedded with markers and doped with luminescence molecules. When exposed to normal loads the film will deform, causing the local thickness of the film to be modified near the point of action. This can be measured by using the luminescent signal emitted from the film (Innovative Scientific Solutions, Inc). This is illustrated in figure 5.5.

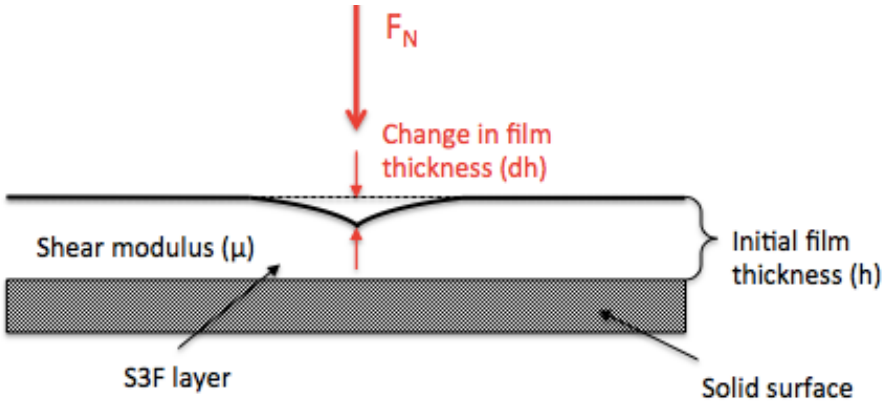


Figure 5.5: Film deformation due to normal loads

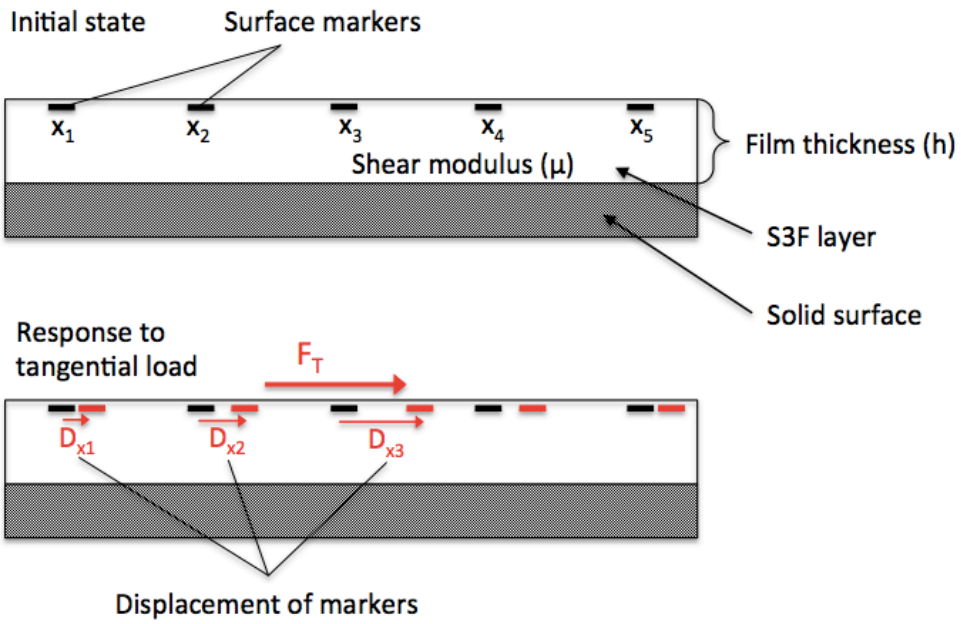


Figure 5.6: S3F exposed to tangential loads

Figure 5.6 shows the S3Fs' response to tangential loads. When the S3F is exposed to tangential loads, the film will deform, causing the film surface to undergo a tangential displacement. This displacement is visualized by considering the applied surface markers: as the film shears the surface is displaced, and the markers will be displaced correspondingly. The displacement is a function of the applied force, the film properties, the shear module of the film and the film thickness (Innovative Scientific Solutions, Inc).

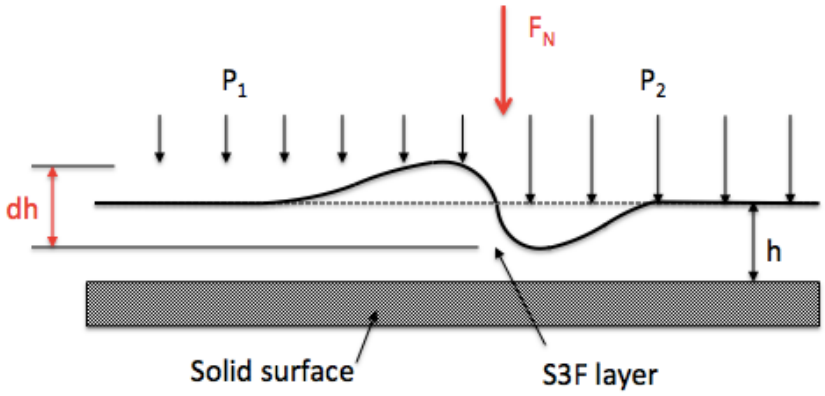


Figure 5.7: Film response to pressure

Figure 5.7 shows how the film responds to spatial variations in pressure. Pressure load $P_1$ and $P_2$ applied to adjacent surfaces will act to displace the material, resulting in a change in the local thickness according to equation 5.2.1. The intensity of the emitted luminescence is proportional to the change in film thickness, which is proportional to a pressure difference. The gauge factor, G, depends on the film properties, shear module and film thickness.

$$dh \sim G(P_2 - P_1) \tag{5.2.1}$$

The elastic film behaves in a similar manner as an incompressible fluid, and like standard fluids it will try to retain its original shape upon removal of the deformation force. It is also important to notice that the film will only react to *pressure gradients*; there must be a spatial variation in the normal load in order for the film to yield. As a consequence S3F is a gradient sensor, not an absolute pressure sensor (Fonov, et al. 2006).

Equation 5.2.1 and figure 5.5-7 is only a crude representation of the behavior of the film. In reality the determination of normal and tangential loads is more complicated. The deformation of the film due to normal loads includes *both* a normal response and a tangential response. Similarly, the response of the film due to a tangential load includes both a normal

and tangential response. The magnitude of the normal deformation is largest in the case of the applied normal load while the magnitude of the tangential deformation is largest in the case of the applied tangential load. However, according to Fonov *et. al* (2006) the amount of cross-talk between the components is on the order of 10-20 % of the main component, and in order to determine the original applied load, both of the deformation components must be measured.

### 5.2.2 Measurement Technique

The process of measuring pressure and shear is accomplished in two steps. First, the normal and tangential deformation of the film is optically measured. These deformations are then converted to forces using a physical stress/strain model of the film. The experimental setup for this S3F measurement system is shown in figure 5.8.

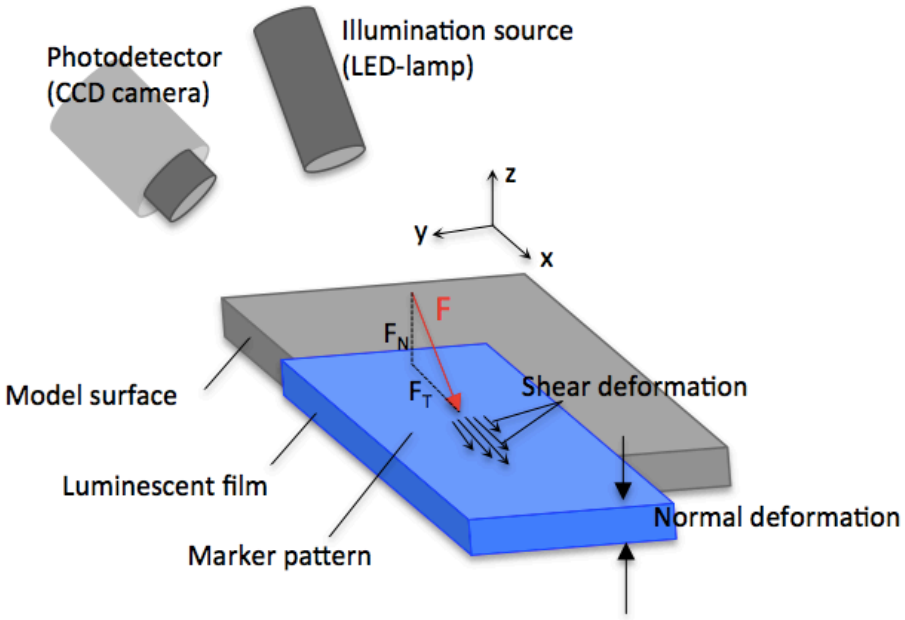


Figure 5.8: S3F experimental setup

All three components of deformation can be extracted from the images taken by the high-resolution CCD camera. The normal component is measured using the luminescence signal emitted from the film. Two images are acquired: an unloaded image and a loaded image. As luminescent output is proportional to the local film thickness, the ratio of the two images will be a linear function of film thickness. Since the unloaded film thickness is known value, the

image ratio represents an effective measurement of the film thickness. A variation in the film thickness indicates the presence of a pressure gradient. The tangential displacement measurement is accomplished using the same pair of images. The surface of the film is lightly scattered with small particles (markers) and the tangential displacement map is obtained by spatially cross-correlating the loaded and unloaded images. By superimposing the tangential displacement (vectors) and the thickness variations (color-map), a visualization of the flow can be produced. This image can then be converted to forces, i.e. pressure and shear components, by using the finite element analysis model (Innovative Scientific Solutions, Inc).

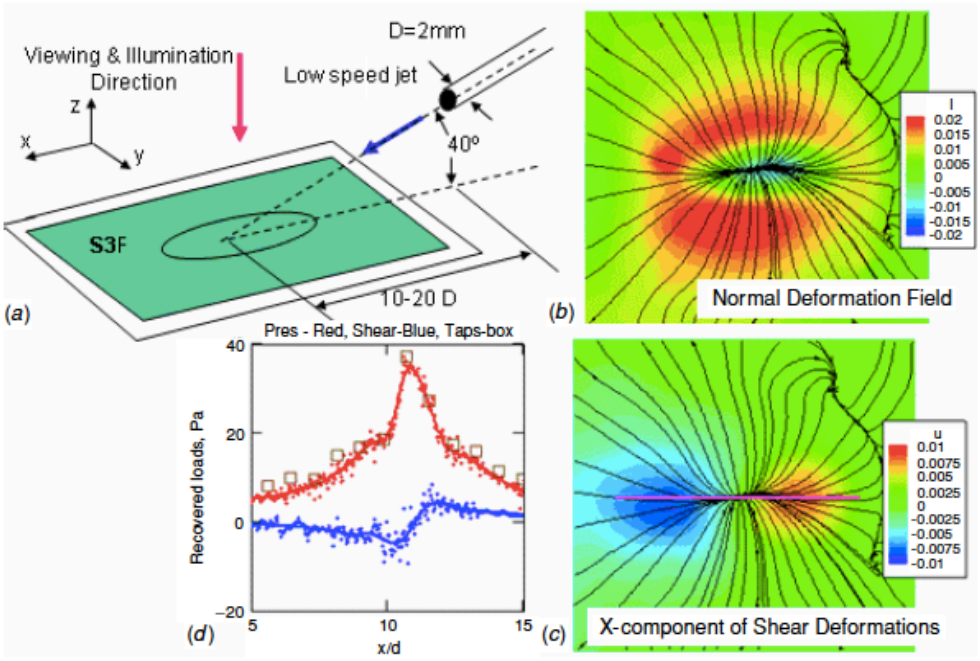


Figure 5.9: S3F in jet flow experiment (Fonov, et al. 2006)

Figure 5.9 illustrates an experiment using S3F to obtain the normal deformation, shear deformation and surface pressure distribution caused by a low speed jet flow. Comparing the recovered pressure loads to measurements from pressure taps at the surface, showed very good correspondence. This is illustrated in figure d). The read line represents pressure, the blue line represent shear, and the squares represent the pressure tap measurements. Figure a) and b) clearly show the great benefit of using S3Fs'. The color-maps indicate regions high/low pressure gradients and high/low shear, and the streamlines visualize the direction of the flow.

### 5.2.3 SENSITIVITY AND TIME RESPONSE

In contrast to PSPs', a S3F can be regarded as differential pressure gauges. The luminescent intensity is proportional to a pressure difference, and the pressure sensitivity is therefore constant.

$$\frac{dI}{dP} = C \tag{5.2.1}$$

By controlling the shear module and the thickness of the film, the sensitivity of the S3F can be tuned to detect very small pressure variations. Pressure sensitive films can resolve pressure differences as low as 2 Pa (Innovative Scientific Solutions, Inc). The sensitivity of the S3F should be adjusted in accordance with the range of the expected experimental surface forces. The maximum acceptable deformation of the surface should be kept low to minimize its influence on the flow-field.

The frequency response of the S3Fs' is limited by the natural frequency of the shear oscillation, and can be estimated according to equation 5.2.2:

$$f_0 = \frac{1}{2\pi}\sqrt{\frac{\mu}{\rho h^2}} \tag{5.2.2}$$

By changing $\mu \in [100–1000]$ Pa and $h \in [0.1–1]$ mm, it is possible to adjust the frequency response of the film in the range 0.3–10 kHz. This is approximately 100 times better than that of a conventional polymer PSP, and not that far from the response of the porous PSP (Fonov, et al. 2006) (Gregory, Asai, et al. 2008).

## 5.3 APPLICATION IN TURBOMACHINERY

There have been several studies involving the use of PSP for measurement of steady pressures in turbomachinery. By using pulsed illumination with a pulse-frequency matching the rotational speed, PSP have effectively been implemented for measurement of steady pressures in a rotating frame of reference (Fonov, et al. 2006). Snapshots of the same blade or the same machine part are superimposed in an image until sufficient light is accumulated to yield the pressure distribution.

Measuring non-periodic pressure fluctuations is much more challenging. The non-periodic behavior of the fluctuations eliminates the possibility of superimposing snapshots, and all the information on pressure field must be obtained from one single frame. This requires very high paint sensitivity, and a very bright paint in order to accumulated sufficient amounts of light. Gregory (2002) used PC-PSP in a turbocharger compressor to measure unsteady wall pressures, and steady and unsteady pressures on the rotating compressor blades. Figure 5.10 shows the experimental setup.

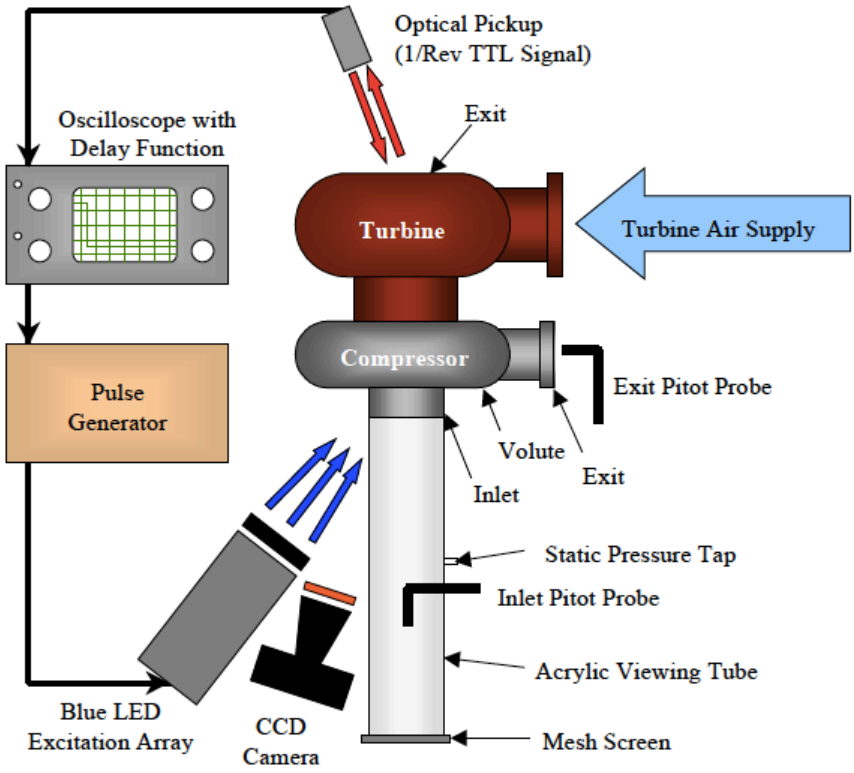


Figure 5.10:Experimental setup (Gregory 2002)

All the measurements were obtained at the same operating point in the compressor characteristic. In order to create a once-per-revolution unsteady inlet flow condition that is representative of situations like inlet distortions, rotating stall or surge, an acrylic divider plate was installed in the inlet tube. The effect of the inlet flow conditioning changes the effective velocity and the angle of attack that the impeller blade experiences. For unsteady PSP measurements one half of the tube was completely blocked, while a coarse mesh screen was installed in the other half to condition the flow. When there is complete flow blockage, the velocity triangle distorts such that the effective angle attack is increased, event to a point where the flow may separate.

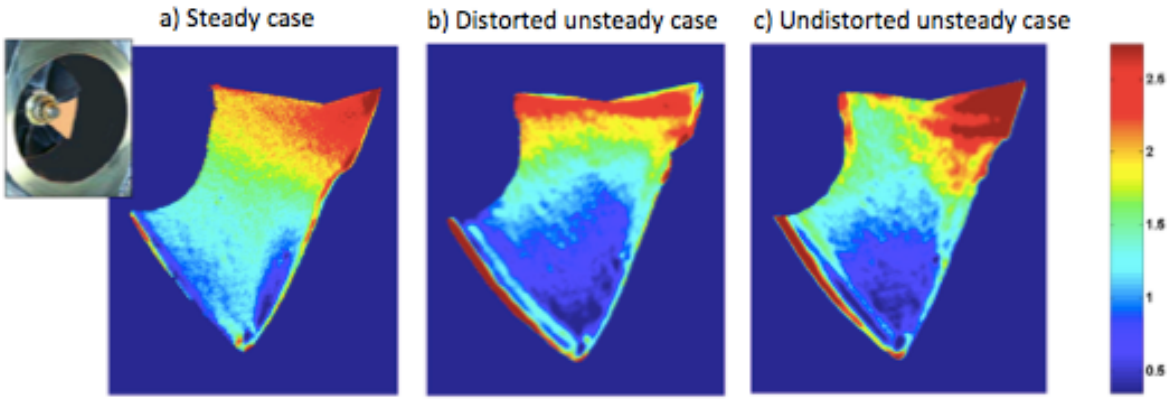


Figure 5.11: Pressure distributions of impeller blade (Gregory 2002)

Figure 5.11 shows the pressure distribution of a compressor blade. Figure a) shows the steady pressure distribution, while figure b) and c) shows two unsteady pressure distributions. In figure b) the blade is positioned behind the flow blockage, about to enter the half of the inlet tube where the inlet flow is passing through. Figure c) corresponds to the opposite position where the blade is about to enter behind the blocked part of the inlet tube. Figure 5.15a) shows how the pressure gradually increases along the blade surface, and corresponds to an ideal blade loading. The color-maps in figure b) and c) however, clearly show a big pressure rise at the very front of the blade followed by a pressure drop as the flow moves past the front portion of the blade. The effective angle of attack is no longer matching the blade geometry causing a reduced energy transfer between the impeller and the flow. The pressure distribution on the leading edge of the blade is quite similar in both cases. However, the pressure rise along the blade is less in the distorted case (b) than in the undistorted case (c) At approx. 40% of the chord the pressure distribution in the two cases starts to diverge. The pressure increases at a higher rate towards the trailing edge in the undistorted case. The pressure distribution for the undistorted case (**c**) is very similar to the steady flow conditions (a) (Gregory 2002).

Hayami et al. (2002) used the PSP method for pressure field measurements in a vaned diffuser during a surge condition. Figure 5.12 illustrates the experimental setup, while figure 5.13 shows a typical example of time sequence of visualized luminescent intensity images during a surge. The time t = 0 s corresponds to the onset of a surge, while T is the period of one surge cycle. A drastic change in luminescent intensity is recognized when the compressor enters a surge. The luminescent intensity is almost fixed in the upper part of every image, but according Hayami et al. (2002), this was because the excitation light did not pass through the window straight, and did not hit the upper PSP due to a thick and small window.

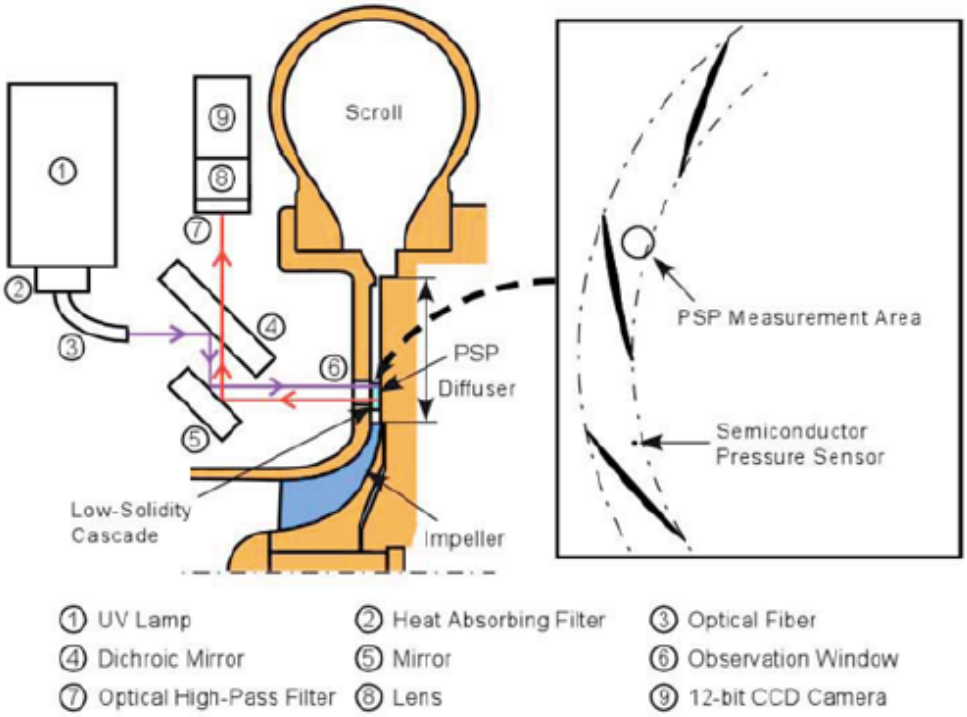


Figure 5.12: Meridional profile of the test compressor and the measurement system (Hayami, et al. 2002)

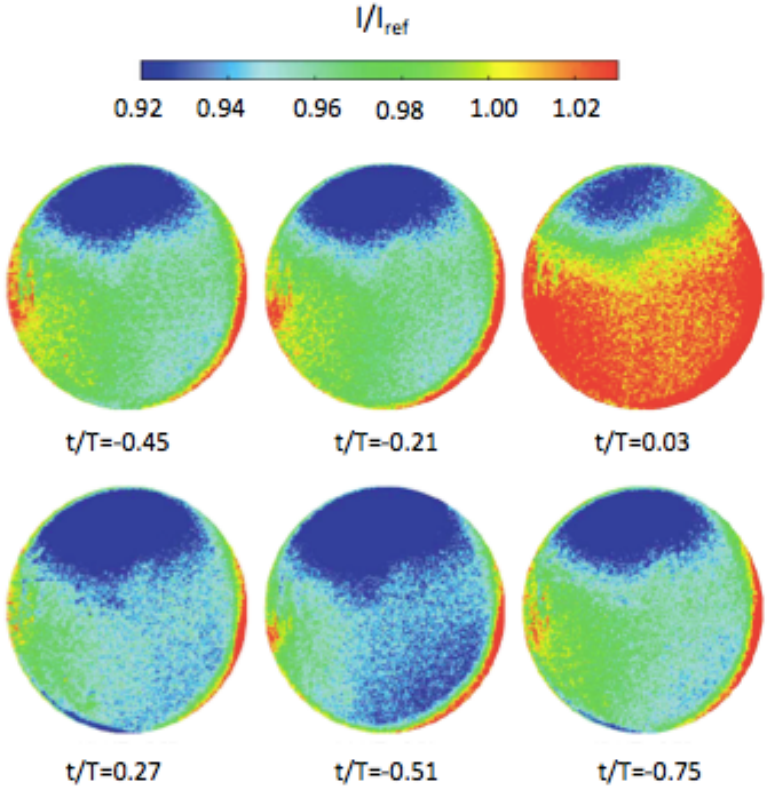


Figure 5.13: Time sequence of luminescent intensity (Hayami, et al. 2002)

The compressor was also equipped with piezoresistive pressure sensors. Figure 5.13 shows a comparison of the PSP measurements and the pressure measured by the high-frequency pressure sensor. The two measurements show the same characteristic pressure pattern.

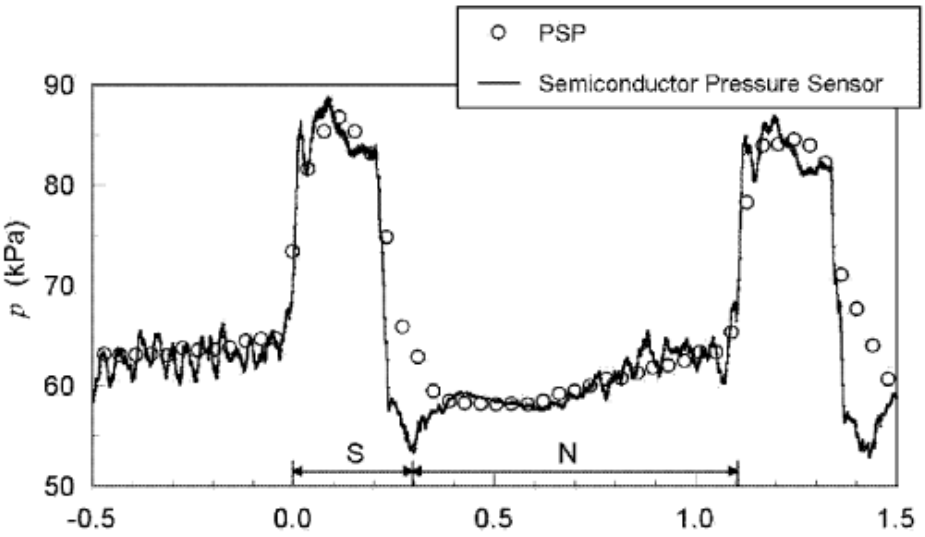


Figure 5.14: History of pressure fluctuations (Hayami, et al. 2002)

The author was unfortunately not able to find any examples of the application of SF3 in centrifugal compressors. However, the frequency range and pressure sensitivity demonstrated with this technique, indicate that S3F could be used to investigate the stall and surge phenomena. If successfully applied in the compressor, S3F would offer great insight into the aerodynamic behavior of the machine. Evaluation of color-maps and marker displacement from elastic films positioned throughout the machine would provide increased understanding of the inception and evolution of stall and surge phenomena. The onset and evolution of boundary layer separations could be investigated in terms of surface distributions of shear and pressure and flow direction. According to Forelines (2013), research scientist from Innovative Scientific Solutions, Inc.:

"*If optical access to the flow is accomplished, S3F could yield interesting data of wall shear profiles, both normal and tangential loads. However, unlike PSP, the S3F technique is not an off-the-shelf solution. One would have to engineer a wall pocket if defined depth, and the film must be made in various shear range depending on some expectations of wall shear.*"

# 6 WET GAS STALL AND SURGE

The initiation and evolution of aerodynamic instabilities in centrifugal compressors are highly complicated. The topic is challenging enough for dry gas applications, but the complexity is highly amplified by the presence of liquid. Wet gas alters the initiation and the evolution of aerodynamic instabilities, and the guidelines used to distinguish between different modes of unstable operation may not be applicable anymore. Liquid presence also has significant impact on pressure, and may also affect the performance of different pressure measurement techniques. Frequency spectra of pressure transient in wet gas flows have shown that the liquid presence alters the spectral content of the pressure signal, and significantly contributes to the pressure signal. A fundamental understanding of the different multiphase mechanisms, and how they affect the pressure, is currently not known. This makes analyzing the measurement very difficult, and is a severe draw back in wet gas compressor testing.

This chapter aims to discuss and explain different multiphase phenomena, and how they affect pressure measurements in wet gas flows. The chapter is divided into four main parts. The first part gives brief description of the liquid impact on compressor stability. This was investigated in the pre-project, and only the main findings are given here. Part two and three investigates liquid impact on pressure in wet gas flows. The influence from the droplet field and the liquid film will be treated separately. The fourth and final parts investigate liquid impact on the performance of the pressure measurement techniques presented in chapter 4 and 5.

## 6.1 LIQUID IMPACT ON COMPRESSOR STABILITY

Wet gas instabilities have only very recently been investigated, a fundamental understanding of the basic physical phenomena is still missing. However, in 2008 an experimental facility for wet gas compression was installed at NTNU, and this has led to interesting findings. Grüner (2012) investigated liquid impact on stall and surge. His results revealed that liquid presence causes the inception of instabilities to be delayed, and also alters the evolution of instabilities. Figure 6.1 show data from piezoresistive pressure sensors flush-mounted in the diffuser wall. Figure a) corresponds to dry gas compression, while figure b), c) and d) correspond to wet gas compression with increasing GMF.

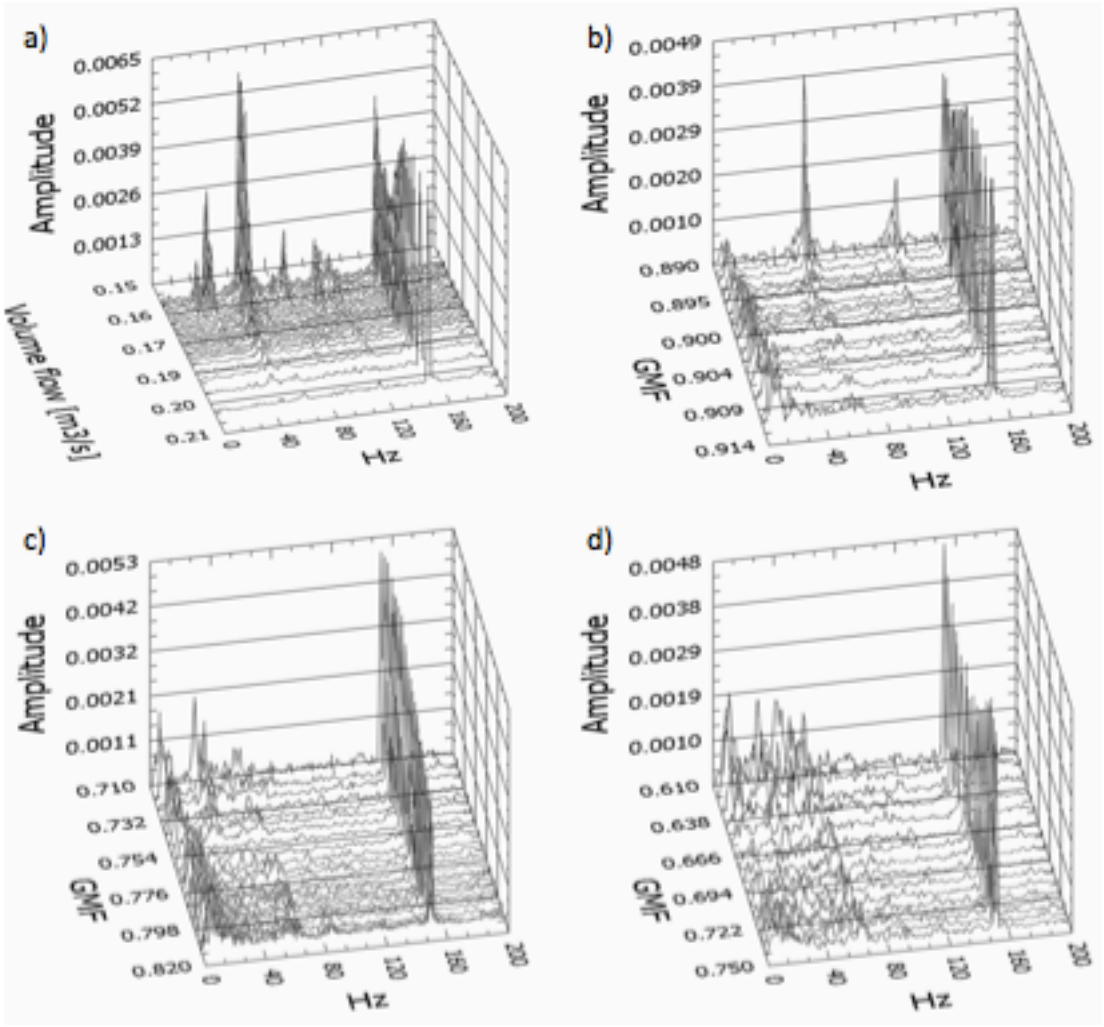


Figure 6.1: Liquid impact on inception and evolution of rotating diffuser stall (T. Grüner 2012)

At dry gas conditions (a) rotating stall developed at Q = 0.17m$^3$/s with a characteristic frequencies of approx. 33% of the rotational speed. Figure b) and c) show onset of rotating stall at Q = 0.15m$^3$/s and GMF = 0.89, and at Q = 0.12m$^3$/s and GMF = 0.72 respectively. Exact identification of instability onset was not possible in figure d) due to an excessive amplification of random frequencies. The inception and evolution of rotating stall is clearly dependent on GMF. When water is introduces in the flow the onset of rotating stall is delayed, and the characteristic frequency changes. When the water fraction increases, the compressor becomes more stable, and the characteristic stall frequency is reduced.

Grüner (2012) also demonstrated the increase in compressor stability by injecting liquid when operating at dry gas rotating stall. The test was performed at constant gas volume flow, and the result revealed an efficient suppression of the characteristic stall frequency when liquid was introduced in the flow. The waterfall graph in figure 6.2 illustrates the transient change in frequency spectrum when the GMF was reduced from 1.0 to 0.7.

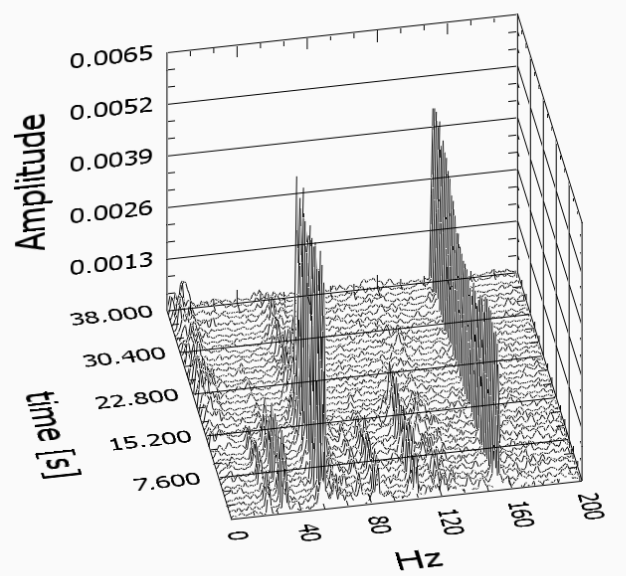


Figure 6.2: Water injection at rotating stall (T. Grüner 2012)

Both stall and surge happens subsequent to boundary layer separation, and the fundamentals of aerodynamic instability are thus mainly concerned with the boundary layer flow. The presence of liquid film and the droplets entrained in the core flow have significant impact on the boundary layer stability. The liquid flow will alter the gas flow due to phase interactions, and momentum exchange between the outer flow and the boundary layer and the boundary layer and the liquid film. The film creates additional surface roughness, causes the core flow to experience a different geometry, and reduces the area available to the core flow. Film atomization and droplet deposition will transfer momentum in out of the boundary layer. The prevailing processes will differ in the different compressor components, but the overall effect seems to improve the stability of the flow. Liquid impact on compressor stability and boundary layer separation was investigated in the pre-project*, Wet Gas Compressor Stall and Surg*e (Jellum 2012). The reader is encouraged to view that report for more information.

## 6.2 LIQUID IMPACT ON PRESSURE

Liquid presence will influence the onset and development of stall and surge, but multiphase effects is also expected to have significant impact on the spectral content of the pressure signal. The inherent non-homogeneity of wet gas flow fields will influence the propagation of pressure pulses in the gas phase, and flow dynamics in the liquid film is believed to have significant impact on the surface pressure. Liquid presence may cause suppression and/or enhancement of certain frequencies, and also introduce additional frequencies that are specifically related to the dynamic characteristic of the liquid phase. The different sources,

and the magnitude at which they change the frequency spectrum, are currently unknown, and his is a big challenge when investigating wet gas stall and surge phenomena. The liquid effects may result in misinterpretation of the spectrum analysis, and increase the risk of not identifying incipient stall and surge. In order for the sensors to report the actual condition in the gas phase, the liquid contribution should be eliminated from the signal. This calls for a comprehensive investigation of the different multiphase mechanisms, and how they affect pressure transients in wet gas flow fields.

### 6.2.1 Pressure Pulse Velocity in Wet Gas Flows

The speed at which a pressure pulse propagates through a medium is known as the acoustic speed or the speed of sound. The acoustic speed has different values in different substances, and the variations can be substantial depending on the physical properties of the different substances. For instance, the acoustic speed in water is about 4.3 times as big as in dry air at the same temperature.

In gas and liquids the pressure pulses propagate as compression waves, and the fluid's compressibility and density are the only important factors for the speed. Equation 6.2.1 gives the general expression for the speed of sound in a fluid:

$$a_{fluid} = \sqrt{\left(\frac{\partial P}{\partial \rho}\right)_s} = \sqrt{\frac{K}{\rho}} \tag{6.2.1}$$

K is the bulk modulus, and measures the substance's resistance to uniform compression. The equation shows how the pressure pulse velocity increases with decreasing compressibility and decreasing density. Adding liquid to a gas phase will increase the density, but the addition of liquid will also affect the compressibility of the fluid. The final result is hard to predict.

Wood's model for acoustic speed can be used to estimate the speed of sound in multiphase flows. The model reveal a significant reduction in the acoustic speed when liquid is introduced in the gas. The reduction in compressibility and increase in density affect the value in an additive manner. However, Wood's model is based on the assumption of homogenous flow, and is therefore a crude simplification of the actual conditions inside the compressor. Figure 6.3 shows how the gas volume fraction (GVF) will influence the speed of sound in a typical natural gas composition. The figure is based on the Wood's model.

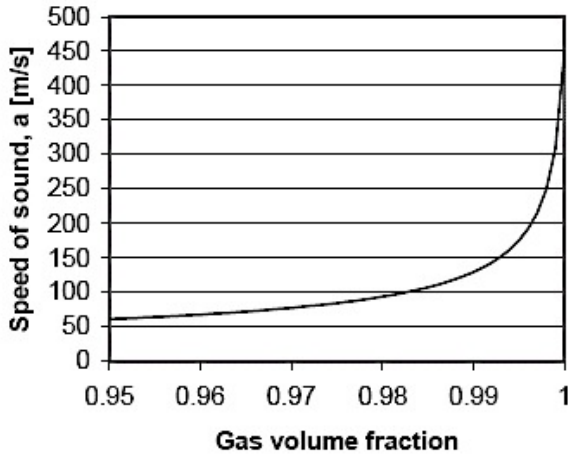


Figure 6.3: Speed of sound in typical natural gas composition at different values of GVF (T. Grüner, L. Bakken, et al. 2008)

Falk (1999) investigated the pressure pulse speed in different flow regime, and compared experimental results to Wood's model. Water and air were used as test fluids. For each test the shock tube sent out one pulse of compressed air, and the resulting pressure where measured by three flush mounted pressure transducers installed in different distance from the shock tube. The time delay between the pressure measurements was used to calculate the pressure pulse velocity. The result of the experiment is summarized in figure 6.4.

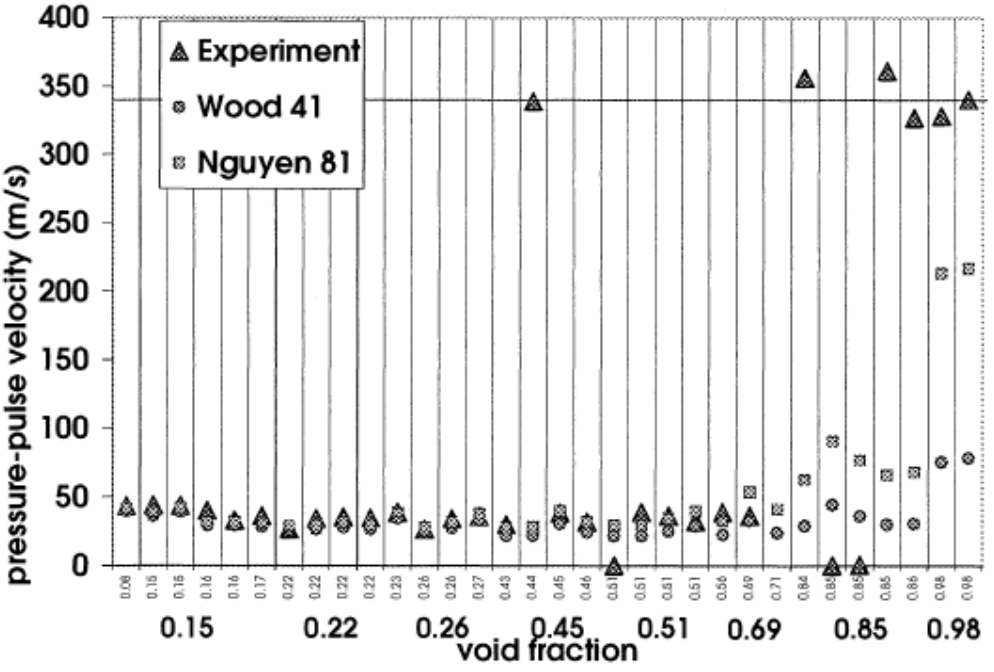


Figure 6.4: Comparison of experimental pressure-pulse velocity measurement with theory (Falk 1999)

The experimental results show good resemblance with Wood at low void fractions. These tests correspond to bubbly flows with a quite uniform distribution of gas and liquid, and little slip between the two phases. At high void fraction, however, the experimental results show little resemblance with theory. These tests correspond to stratified flows, wavy stratified flow and annular flows, where the cross-sectional distribution of gas and liquid is highly uneven. Gas and liquid is transported in separated phases with only a small fraction of the liquid phase entrained in the gas phase. The tests in the annular regime had void fractions of 0.98 and 0.99, and the pressure measurements revealed a pressure pulse speed of approximately 340 m/s. This corresponds to the acoustic speed in air, which indicates that liquid presence has little impact on the acoustic speed in this flow regime.

The flow through the compressor is typically modeled as an annular flow, where the liquid phase is divided between entrained droplets and a thin liquid film. According to the findings of Falk (1999) the pressure pulse velocity should therefore correspond to acoustic speed of the gas phase. However, different parts of the compressor will introduce variations in the flow regime. Rates of droplet deposition and atomization, and the degree of mixing of the two phases, will change throughout the machine, causing regions with different pressure pulse velocities. In the radial part of the impeller most of the liquid will be contained in the liquid film, due to extensive droplet deposition as the flow is accelerated through the impeller. In this region the pressure pulse velocity should be approximated with the acoustic speed of the gas. Other regions, like the diffuser, will have a larger degree of mixing between the two phases. The liquid phase exits the impeller as a jet-flow, and deceleration in the diffuser will cause break-up and atomization of the liquid flow. At the compressor discharge the flow is typically described as fully mixed. In these regions Wood's model is believed to give better results, and the propagation of pressure waves will therefore be significantly reduced. Determination of the pressure pulse velocity requires detailed knowledge of the different flow regime encountered in the machine is required. This information is currently missing. At this present, the liquid distribution in the different compressor components is only based on theoretical considerations, and not experimentally validated. All predictions of the pressure pulse velocity inside the centrifugal compressor are therefore associated with great uncertainty.

### 6.2.2 Attenuation of Pressure Pulses in Wet Gas Flows

When a pressure wave propagates through a medium, its intensity diminishes with the distance traveled. In idealized materials, the reduction in signal-amplitude is only due to spreading of the wave. Natural materials, however, all produce effects that further weaken the

signal. This weakening results from scattering and absorption, which is reflection and conversion of the wave energy to other forms of energy. The combined effect of scattering and absorption is called *attenuation*. Equation 6.2.2 expresses the attenuation of the pressure pulse amplitude:

$$P = P_0 e^{-ax} \tag{6.2.2}$$

P is the reduced pressure amplitude after the pressure wave has traveled a distance x from the initial location. The attenuation coefficient a is generally proportional to the square of the pressure pulse frequency, and it thus follows that high frequency fluctuations will be more affected by dampening than fluctuations of lower frequencies.

Multiphase effects will also affect the attenuation coefficient. The pressure pulse will be attenuated due to viscous effect between the different phases. If the pressure sensor is located away from the source, the addition in signal dampening may cause the pressure pulse to die out before it reaches the sensor. The attenuation of the pressure waves due to droplets can be explained as follows: Oscillating regions of gas with the same density will move together with little slip because they have the same inertia, and will respond equally to the pressure wave. However, if the oscillating gas is next to a water droplet, density differences causes slip between the two phases. The droplet will not respond as quickly as the gas, and the two phases will rub together causing frictional hetaing to occur. This convert kinetic energy into heat, and the amplitude of the oscillation will be reduced. (Leighton, Jiang and Baik 2012).

Leighton, Jiang and Baik (2010) investigated liquid impact on pressure pulse attenuation by comparing sound wave attenuation inside pipes containing bubbly water and water droplet fog. A speaker or a sonar source at one end of the pipe generated sound waves, while a microphone or a hydrophone in the other end of the pipe was used to measure the corresponding signal. Figure 6.5 shows the effect of the droplets on the pressure signal. Figure a) shows the microphone signal 5 seconds before fog was poured into the pipe, and figure b), c) and d) shows the microphone signal 5s, 50s and 100s after pouring the fog. Before fogging (a) the pressure pulse generated by the speaker is clearly visible. After fogging, in figure b), c) and d), the amplitude of the signal decreases to a very small value, and then returns back as the fog gradually disappears. When the signal is at its minimum, it is 30dB less than prior to fogging (Leighton, Jiang and Baik 2012).

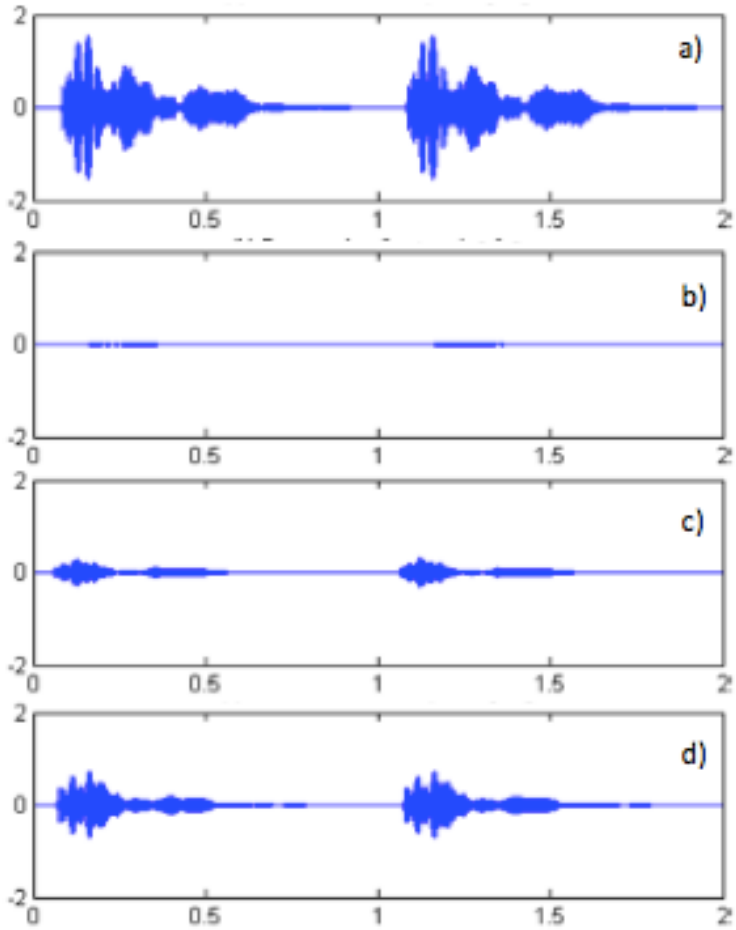


Figure 6.5: Microphone signal shown on oscilloscope (Leighton, Jiang and Baik 2012)

Falk (1999) found the attenuation to be quite different in the different regimes. Stratified flows had the largest attenuation coefficient, but for bubbly flows, the higher frequencies were much more affected. In bubbly flows all frequencies above 10-20 Hz where effectively dampened out just a few meters below the shock tube, while stratified flows contained frequency components up to 100 Hz. Due to very low liquid rates in wet gas compression, there will be no regions of bubbly flows. However, entrained droplets in the gas phase will contribute to viscous attenuation of the pressure fluctuations in the same manner as gas bubbles flowing in a liquid phase. This was shown experimentally by Brenne, et al.(2005). They investigated the performance of a centrifugal compressor operating under wet gas conditions. Fast response pressure sensors were located at the inlet and discharge of the compressor. Figure 6.6 shows the dry gas and wet gas frequency spectra measured at the compressor discharge. The figure clearly shows how liquid injected into the process gas attenuates pressure components of high frequency. The dampened pressure fluctuations were believed to originate from the passing of impeller blades.

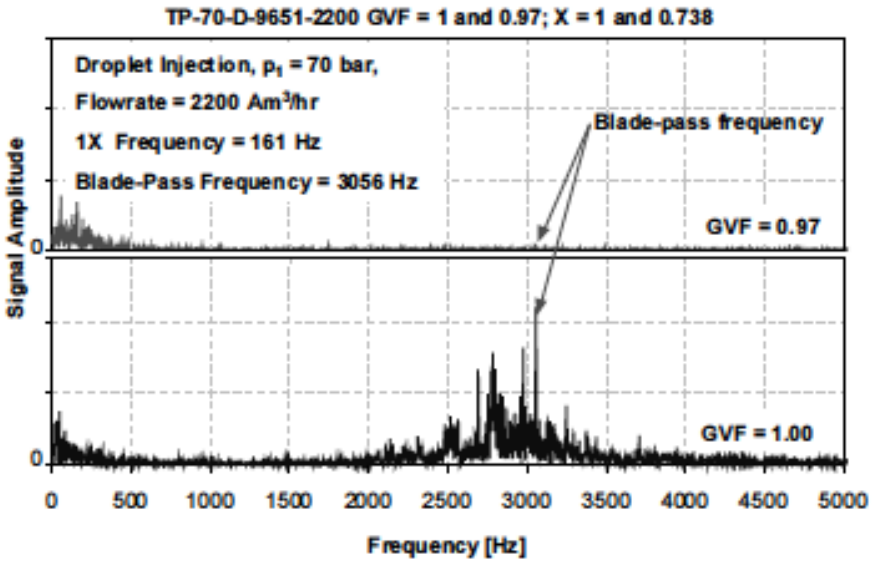


Figure 6.6: Dry and wet frequency spectra with droplet injection (Brenne, et al. 2005)

The frequency spectra of the pressure signal measured at the compressor inlet showed less dampening. This is not surprising. The pressure pulsations propagating through the highly turbulent and chaotic diffuser flow regime will experience high rates of droplet entrainment. In the impeller the droplets will are forced to deposit on the liquid film, and the droplet entrainment will be lower. As a consequence there will be more viscous dissipation of pressure pulses propagating downstream than upstream.

The characteristic frequencies of rotating stall and surge is much lower than the frequencies evaluated above. Pressure pulse attenuation due to liquid injection may thus not seem like a problem when detecting stall and surge. However, results of Falk (1999) indicated that regardless of flow regime, all frequencies above 100 Hz were dampened out in multiphase flow. Depending on the rotational speed, rotating stall may cause pressure fluctuations well above 100 Hz, and detection will thus be affected. The results presented in the report by Brenne et al (2005) do not reveal anything about the unstable characteristics of the compressor. All the pressure measurements correspond to stable operation, and it is therefor difficult to make any assumptions on how pressure fluctuations corresponding to rotating stall and surge will be attenuated. However, according to Bakken (2013), the compressor was operated in the unstable region, but the pressure sensors located at the inlet and discharge failed to measure the expected pressure fluctuations. To avoid similar problems it was decided to install the pressure transducers in the diffuser wall at the wet gas compressor rig at NTNU. Further experiments should measure the pressure fluctuations both within the machine and in the piping at the inlet and discharge. This would reveal how the pressure

signal is attenuated through the machine, and also indicate whether or not pressure transducers installed in the inlet or discharge piping can be used to detect stall and surge in wet gas compression.

### 6.2.3 Generation of Pressure Fluctuations in Liquid Films

The increase in pressure pulse attenuation and the variations in pressure pulse propagation speed are of most concern if the pressure sensor is located away from the source of the pressure pulsations. Grüner (2012) chose to install the pressure sensors in the diffuser, where the instabilities originated. Fast responding piezoresistive pressure sensors were flush mounted in the diffuser wall, and a reversed pitot probe was inserted in the core flow. The dry and wet gas frequency spectra from the flush-mounted pressure sensors were presented in figure 6.1 a)-d). By comparing the spectra it is evident that the liquid presence affects the measurements. The figures reveal a significant amplification of low frequency components. The amplification increases with increasing liquid fraction, and make it very difficult to detect incipient surge and stall. There might be several reasons for this amplification, but the presence of the liquid film is believed to be a key factor. This assumption is also confirmed by evaluating measurement from the pitot probe. The sensing part of the pitot probe was located outside the liquid film, and the measurements were therefore unaffected by the film. Figure 6.7 shows that noise, and amplification of random frequencies is much more apparent when the pressure is measured beneath the film.

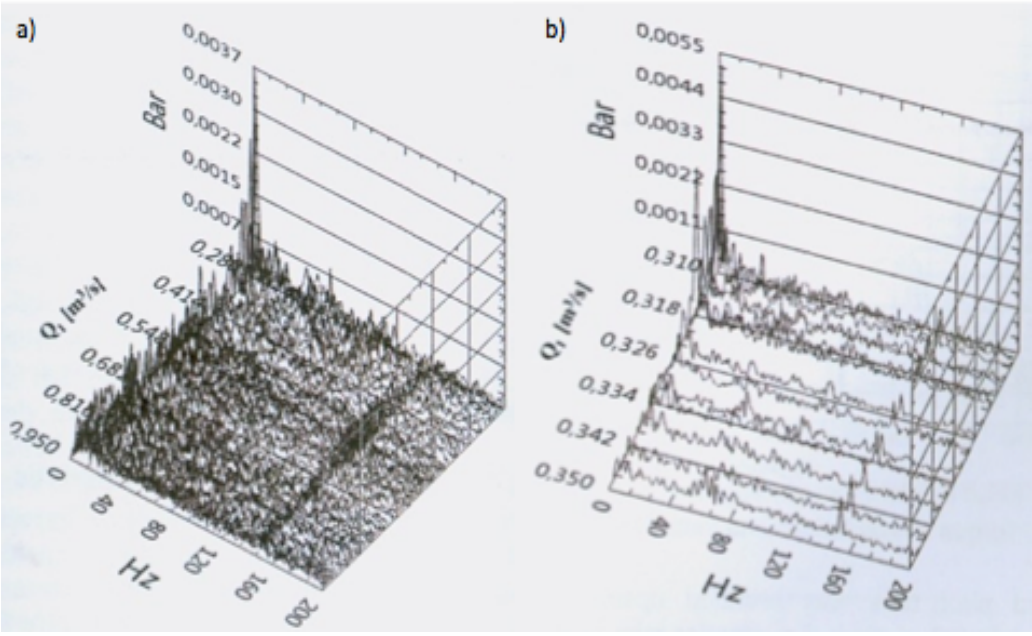


Figure 6.7: Frequency spectrums of wet gas evolution into surge measured by a) flush-mounted pressure transducer and b) reversed pitot probe (T. Grüner 2012)

The dynamic behavior of the film, i.e. surface waves, film turbulence and fluctuating velocity components, is believed to generate additional pressure components, which will contribute to the total surface pressure. The generation of surface waves at the gas and liquid interface is particularly important to the wall pressure. Surface waves will affect the hydrostatic pressure in the film, the film flow structure, wall friction and film-turbulence, and increase the fluctuations in normal and stream-wise velocity components. The magnitude of wave-induced pressure fluctuations depends on the wave structure at the gas-liquid interface, which again depends on gas and liquid flow rates.

WAVE-INDUCED TURBULENCE

Surface waves have significant impact on the generation of turbulent eddies. In single-phase flows, turbulence is typically generated near the wall in the form of burst that generate larger eddies. The turbulence energy is transferred from larger eddies to smaller eddies and is then eventually dissipated through friction. This process is much more complex in film flows, and the free surface will have competing effects depending on film waviness. A smooth surface tends to damp out any abrupt disturbances coming from near the wall, while a wavy surface will have the opposite effect, and induce fluctuations in film thickness and both normal and stream-wise velocity components. The significance of each mechanism depends on the wave amplitude, and other parameters such as the gas and liquid Reynolds numbers. The inherent characteristics of film flows makes is difficult to initiate and maintain turbulence in smooth films at small Reynolds number. However, once the film becomes wavy and turbulent, the turbulent intensity distributions are amplified and generally greater than those of single-phase flow (Karimi and Kawaji 1999).

Karimi and Kawaji (1999) investigated the flow characteristics and circulatory motion in wavy films. Flow visualization experiments revealed the occurrence of circulatory motions with significant velocities normal to the tube wall under large interfacial waves. Fluctuations in the normal velocity components will have a significant impact on the pressure measured at the wall. The inertia of the flow causes an impact or dynamic pressure to be generated on surfaces perpendicular to the direction of flow. Normal velocity fluctuations will generate normal loads that are added to the pressure signal. Pressure sensors flush mounted at the wall will not only measure fluctuations in static pressure, but also report on the dynamic pressure fluctuations generated in the film. This is indicated in equation 6.2.3.

$$P_{wall} = P_{stat} + P_{dyn} = P_{stat} + \frac{1}{2}\rho V_N^2 \qquad (6.2.3)$$

The magnitude of the dynamic pressure fluctuations depends on the turbulent intensity, and the generation of turbulent eddies, which again is dependent on the size and frequency of surface waves. According to Karimi and Kawaji (1999) several vortices of varying sizes may exist simultaneously under a single large wave, but the eddy-size is limited by the local film thickness. Figure 6.8 shows a sketch of this eddy formation.

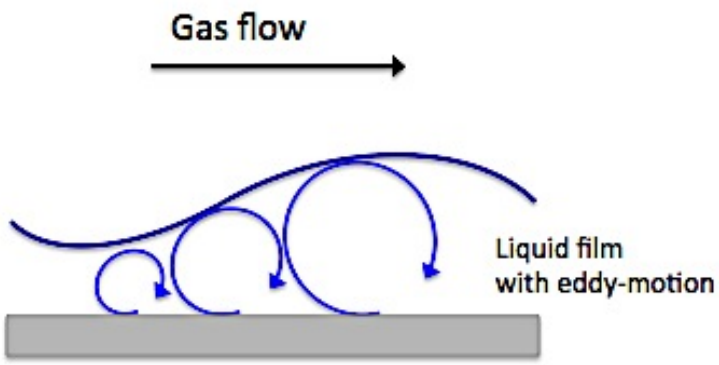


Figure 6.8: Vortices in wavy annular flows

Larger waves allow for large eddies, which again will generate larger normal velocities. The fluctuations in dynamic pressure are therefore expected to be more profound in regions with large interfacial waves compared to regions with small waves and ripples. Large amplitude waves are in general less frequent than small ripple waves (Asali and Hanratty 1993). The wave-induced pressure fluctuations should therefore be most apparent in the low frequency region, which agrees well with the wet gas frequency spectra in figure 6.1. Figure 6.1d) clearly shows significant amplification of random low-frequency pressure components, while components of higher frequencies only have small amplitudes. It is also reasonable to assume the presence of normal velocity components in the case of dry gas compression. However, as dynamic pressure increases linearly with density, the impact on the wall pressure will be much smaller.

TRANSPORT OF WAVE-INDUCED MOMENTUM

Karimi and Kawaji (1999) also investigated the transport of wave-induced momentum in laminar and turbulent films. Instantaneous velocity profiles and film thickness were measured simultaneously to determine how the effect of surface waves was transmitted through the film. The results are summarized in figure 6.9. The figure shows the transient profiles of film thickness fluctuations and local stream-wise velocities at different normalized distances from the wall. Under smooth-laminar conditions (a) only small ripple waves form at the interface, and there are almost no stream-vise velocity fluctuations in the film. In the wavy-laminar

regime (b) the amplitude of the waves are much larger, and the effects of the waves can be sensed even close to the wall. At laminar-to-turbulent transition condition (c) the film can be divided into two distinct regions. In the laminar portion to the left, interfacial waves do not cause any significant changes in the velocity close to the wall, but as the flow becomes turbulent, the effects from the waves is observed deep into the film. In fully turbulent wavy films (d) interfacial waves induce significant changes in the stream-vise velocity component close to the wall.

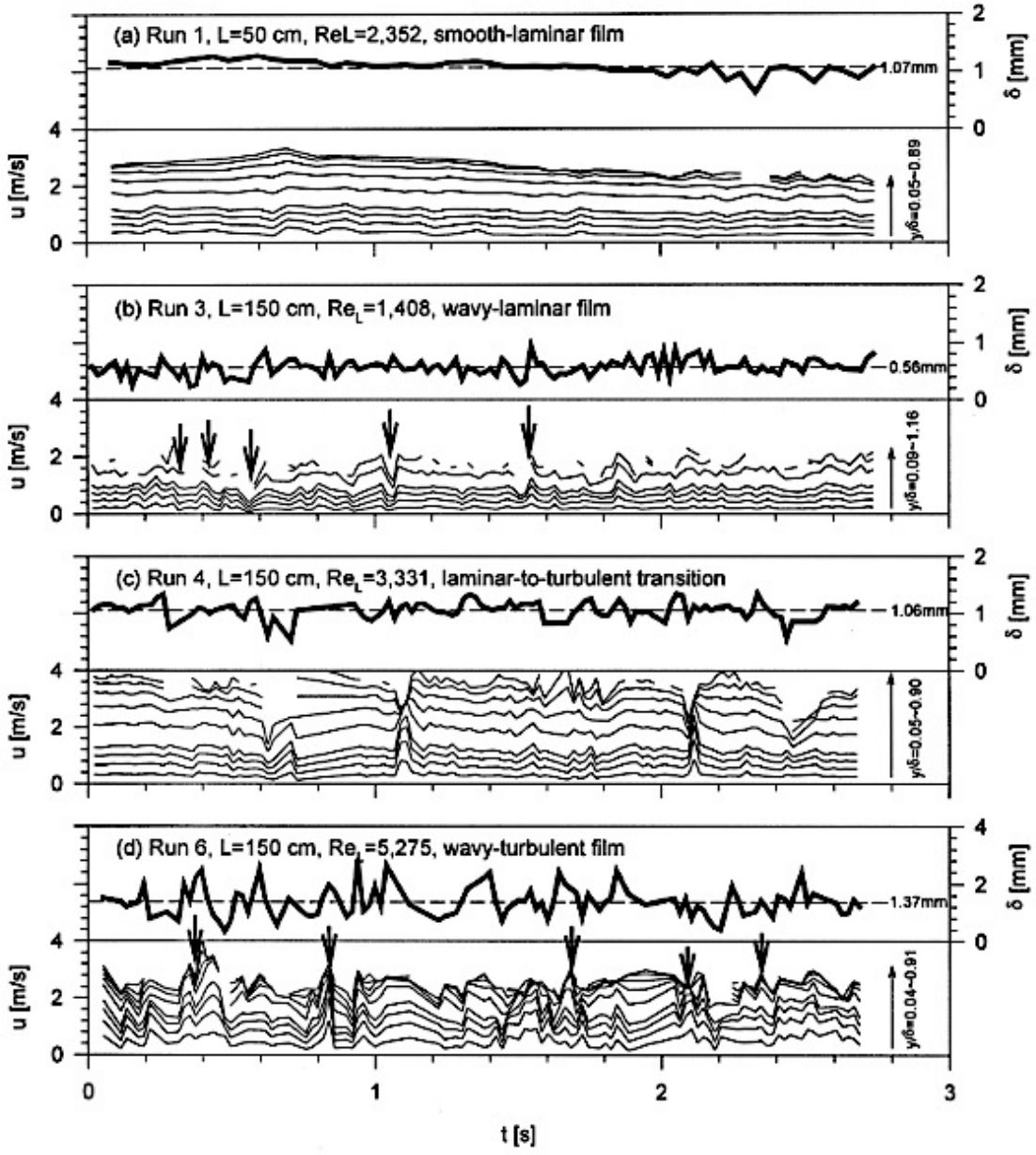


Figure 6.9: Simultaneous measurements of liquid film thickness and local stream-wise velocity fluctuations for different flow conditions (Karimi and Kawaji 1999)

When considering wet gas compression, the liquid film is believed to be fully turbulent throughout the machine. There may exist a small region of laminar flow in the anterior part of the impeller, but transition to turbulence is rapid. Based on findings of Karimi and Kawaji (1999), it can thus be argued that surface waves will have significant impact on the flow dynamic at the compressor wall. Wave-induced momentum will penetrate deep into the film, and the effects will be easily sensed at the compressor surface. Figure 6.9 only show the wave impact on variations in stream-vise fluctuations, but it seems reasonable to expect that normal components will be affected in the same manner.

WAVE-INDUCED GAS PHASE INSTABILITIES

At last, before leaving this topic, it should also be mentioned that film waviness can introduce occasional instabilities in the gas. Several papers have reported on the occurrence of local boundary layer separation and flow reversal in flows over solid wavy walls, and it has also been suggested that separation may appear near the troughs of interfacial waves in the case of wavy film flows (Zilker and Hanratty 1979), (Buckles, Hanratty and Adrian 1985). This may induce significant fluctuations in the local gas phase velocity, and generate corresponding fluctuations in the pressure.

Hagiwara et al. (1988) made simultaneous measurements of liquid film thickness, wall shear stress and gas flow turbulence in horizontal wavy two-phase flow. Their results revealed a remarkable correspondence between the gas flow velocity and the propagation of large waves. A gradual decrease followed by a rapid increase in the gas velocity was observed just before large wave peaks was detected. The instantaneous minimum value of the gas velocity was reduced to only 5-10% of its mean value. Hagiwara et al. (1988) used tuft probes to visualize the gas-phase flow near the interface. This is illustrated in figure 6.10.

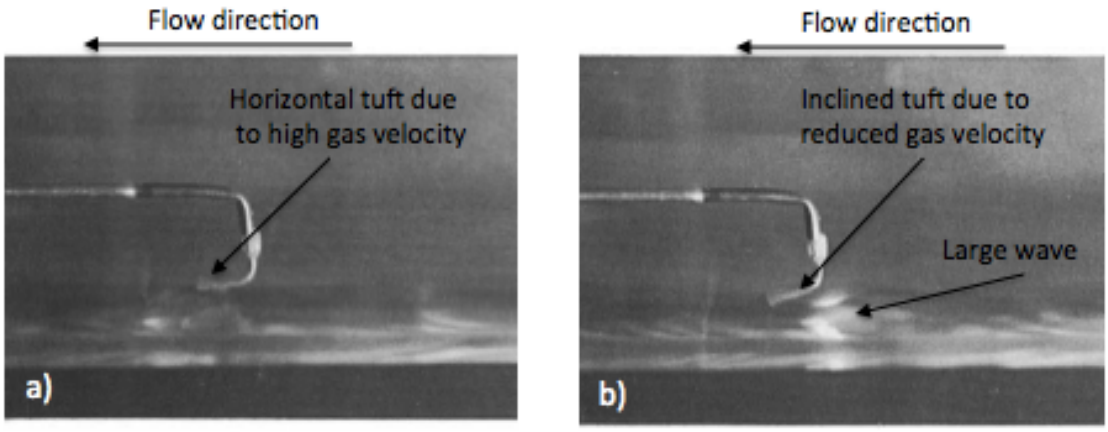


Figure 6.10: Interfacial waves tufts: a) ripple wave; b) large wave (Hagiwara, et al. 1988)

Figure 6.10a) shows a photograph of the tuft probe in the case of ripple waves, while 6.10b) shows the tuft probe when a large wave approaches. In figure a) the tuft is pointing downstream, which indicates that the gas velocity is high even close to the interface. In figure b) on the other hand, the tuft tends to point to the interface, which demonstrates the significant velocity retardation occurring in front of large waves.

## 6.3 LIQUID IMPACT ON PRESSURE SENSORS

Liquid presence may also affect the performance of the pressure sensor. Different measurement techniques may react differently, and therefore have different suitability for measuring in wet gas flows. A literature search has been conducted in order to document wet gas impact on piezoelectric and piezoresistive pressure sensors, pressure sensitive paints and surface stress sensitive films. The literature found was limited, and the author was not able to find much relevant research. Mail correspondence, telephone conversation and also meeting with spokespersons from different sensor producers have given valuable information, but experimental validation of the wet gas performance was unfortunately not obtainable.

### 6.3.1 PIEZOELECTRIC AND PIEZORESISTIVE PRESSURE SENSORS

Kyte (2013) and Hoel (2013) recommended the use of flush-mounted piezoelectric and/or piezoresistive pressure sensors for unsteady pressure measurements in wet gas compressors. Flush-mounted sensors generally yield the minimal response time, limited only by the mechanical response of the sensing diaphragm, or the sensing crystal in the case of piezoelectric sensors. This arrangement is therefore the ideal when measuring rapidly varying pressures. As long as the senor is properly installed, and the acting fluid do not cause corrosion or in other ways harms the sensor material, the performance of these sensors should not be affected by liquid. The sensitivity, linearity, response time and so on, will thus be the same whether the acting fluid is a gas or a liquid. However, even though the sensor itself is unaffected by liquid, liquid presence may amplify the effects of poor mounting and also cause increased levels of flow-induced vibrations. These effects are not directly related to the sensor performance, but will indirectly affect the measurement. The sensors will also measure the actual pressure beneath the liquid film, and cannot distinguish between the pressure fluctuations in the gas phase, and components contributed by the liquid

LIQUID IMPACT ON MOUNTING ERRORS

Poor mounting of the sensor may cause significant errors in the measurement. If the sensing membrane is not perfectly in flush with the model surface, the resulting cavity will cause vortex formation, flow separation and a highly chaotic flow regime above the sensor. Lin and Rockwell (2001) investigated the flow dynamic of turbulent flows past open cavities. Their results showed the emergence of small- and large-scale vortical structures when the turbulent boundary layer separated at the leading edge of the cavity. The flow pattern within the cavity was dominated by circulatory motion, and pressure measurements inside the cavity showed that the large vortices induced ordered pressure fluctuations (Lin and Rockwell 2001).
Cavity effects will give measurement errors in both dry gas and wet gas flows. The vortex formation and circulatory motion inside the cavity will generate normal velocity components, which again will result in normal loads at the sensor surface. However, in wet gas flows the cavity is filled with liquid, and the fluctuations concerned with the liquid phase. This is shown in figure 6.11.

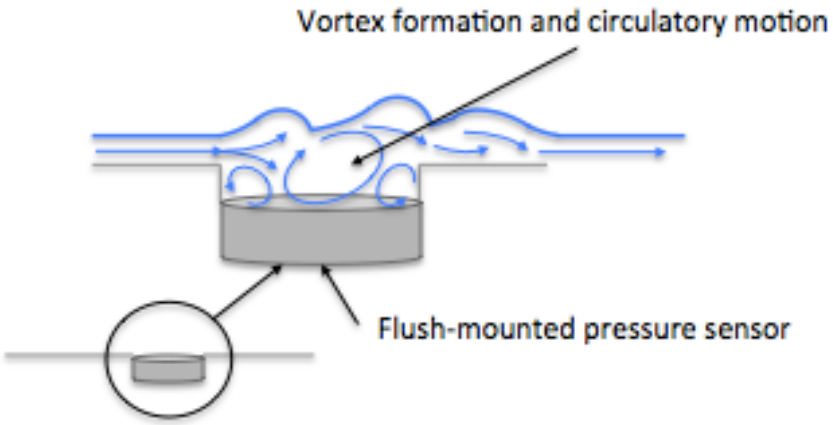


Figure 6.11: Wet gas flow past cavity

The velocity fluctuations generate dynamic pressure components normal to the sensor. Because of density difference in between gas and liquid, the amplitudes of the dynamic pressure will be much higher in wet gas flows, and the measurement error will be correspondingly larger. The density difference also causes the liquid to respond slower to the gas, and the fluctuations are therefore expected to lie in a lower frequency range

LIQUID IMPACT ON VIBRATION

Liquid presence may also have significant impact on flow-induced vibration, and this has received a lot of attention in recent years. Phase interactions in multiphase pipes may lead to unacceptable levels of vibration causing damages to the pipes system. Flow-induced vibrations in multiphase pipelines have characteristic excitation forces depending on the flow

regime, and amplitudes and frequencies of the flow-induced vibration responses will differ in the different regimes. Chenquan et al. (2010) investigated flow-induced vibration in horizontal pipes, and their results revealed strong vibration in the annular regime due to turbulence in the liquid film. Brenne et al. (2005) measured the effects of two-phase flow on the vibration response of a centrifugal compressor. The liquid impact on vibration was insignificant a small liquid fractions, but at GMF below 0.61 the wet gas spectrum showed large peaks in the subsynchronous range that did not appear in the dry gas spectrum. This is shown in figure 6.12, and indicates that liquid presence will have an impact on low-frequency components. Brenne et al. (2005) only investigated cases where liquid was uniformly distributed at the pipe inlet, but indicated that uneven distributions were likely to produce more significant two-phase effects on the vibration response of the machine.

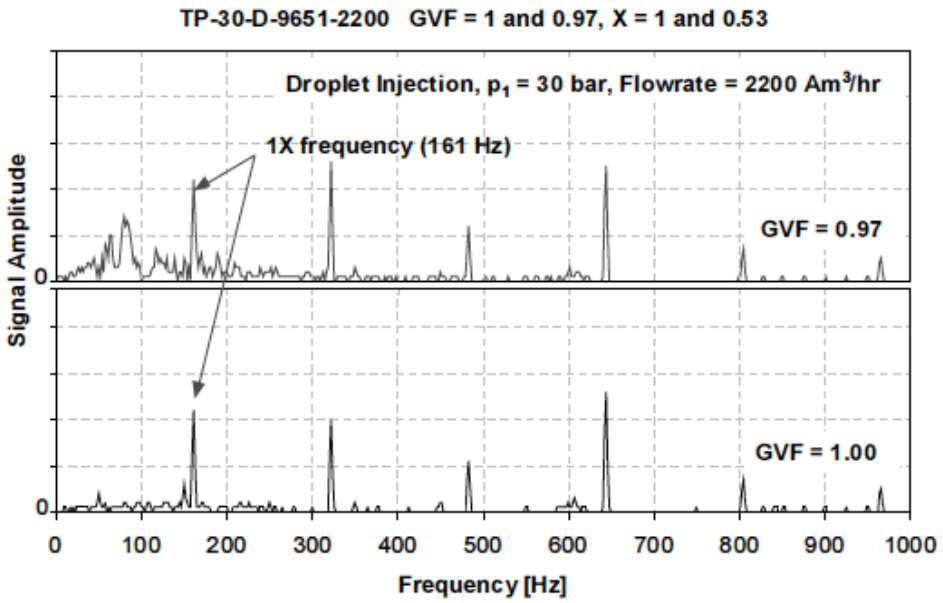


Figure 6.12: Vibration response of centrifugal compressor exposed to wet gas (Brenne, et al. 2005)

Pressure sensors are sensitive to acceleration and vibration, especially in the direction of their axis. The inertia of the mass of the diaphragm and transmitting plates in front of the piezoelectric transduction element will produce a force when accelerated or exposed to vibrations. The produced signal is superimposed on the pressure output, causing an undesired error. This can severely disturb the measurement, particularly if the sensor is subjected to strong vibration while trying to measure small pressures. Acceleration/vibration-compensated pressure sensors have been design in order to solve this problem. However, in order to apply optimal compensation, it is important to be aware of the multiphase impact vibration.

### 6.3.2 Pressure Sensitive Paints and Surface stress Sensitive Films

Forelines (2013) and Palluconi (2013) recommended the use of fast porous paint for measuring stall and surge phenomena. The PSP method is suitable for dry gas application, but liquid presence will affect the quality of the measurement. The paint responds to changes in oxygen concentration at the painted surface, and anything that impedes $O_2$ migration to the surface will therefore affect the performance of the paint. The presence of the liquid film will result in a slower response, and a reduced sensitivity. The response time is increased because of additional time required for the oxygen to move through the film. This will also affect the sensitivity because of less time available for the paint to interact with the oxygen. Conventional polymer-based PSP have been demonstrated under water and in very humid environments without any physical effect in the coating. However, the response time under water or in organic media is usually several seconds for full response. Forlines (2013) and Palluconi (2013) could not give any certain estimation on how much the Fast-porous paint would be affected by the liquid. The changes in sensitivity and response time will depend on the thickness of the liquid film and also the velocity of the gas phase, and extensive experimental testing is therefore required in order to determine the wet gas characteristics of the paint. However, when considering application in wet gas compressors, it seems unlikely that the oxygen will have time to migrate through the liquid film before being swept through the machine. The prospects of using PSP for investigating wet gas stall and surge are therefore poor, but no certain conclusions can be made before the paint is tested.

Neither Forelines (2013) nor Palluconi (2013) was aware of any other techniques used to measure high-resolution unsteady pressure in liquid or highly humid media. However, they were open to the idea of maybe using stress sensitive. Since this technology is sensitive to shear and not $O_2$ concentration, the presence of the liquid film should not cause any problems. However, the film will not distinguish between shear generated by the gas phase and contributions due to the liquid film, and just as piezoelectric and piezoresistive pressure sensors the reported pressure will consist of both gas phase components and components introduced by the liquid. The contrast markers used to indicate the direction of the flow would also report on the motion in the liquid film instead of the gas phase motion. However, knowledge of the liquid streamlines would be of great value in order to understand how the liquid is distributed in the compressor, and gas phase motion and the motion in the liquid film are also closely connected.

Using S3F requires optical access to the flow, as the technique involves imaging of contrast markers and measurement of luminescent intensity. Figure 6.13 and 6.14 illustrates two

different possibilities for installation in the diffusor. In figure 6.13 the film is located at the hub side surface, and transparent cover plates at the shroud side provide optical access. This configuration would not be optimal as the water droplets and the liquid film will distort the excitation and emission light, and also interfere with the imaging of contrast markers. Another possibility is to install the film at the same side you will be imaging through. This configuration is shown in figure 6.14, and would eliminate optical effects due to the liquid phase. Forelines (2013) and Palluconi (2013) also agreed that this would be the best solution, but the film needs to be made of a semi see-through material in order to detect the contrast markers at the liquid interface.

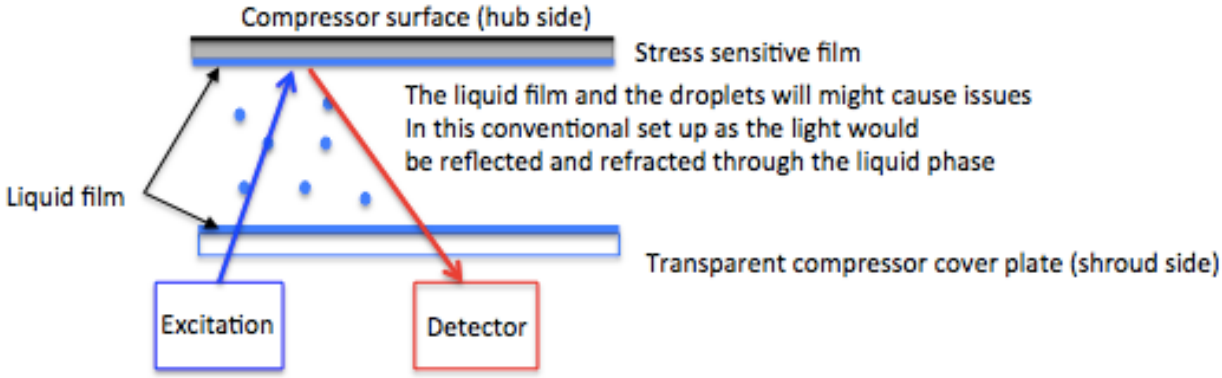


Figure 6.13: S3F installed at the diffuser hub

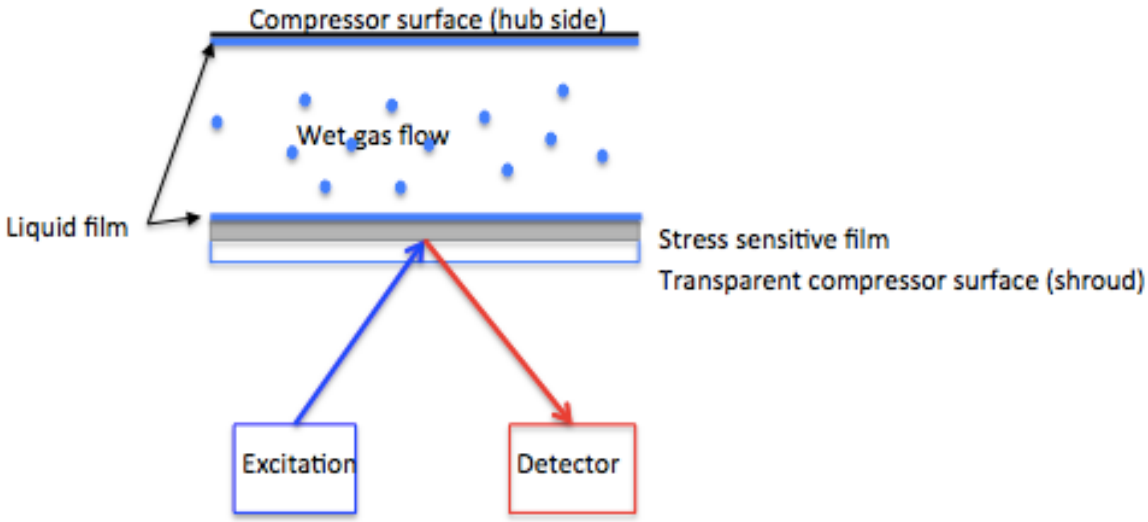


Figure 6.14: S3F installed at the diffuser shroud

### 6.3.3 Improving the Pressure Data

Evident from research presented in chapter 6.3 liquid presence will significantly contribute to the pressure signal. These are physical consequences of the liquid, and cannot be avoided by choosing a different sensor or measuring system. However, correct adjustment of the pressure data can help eliminate some of the random pressure components generated by the liquid, and this will be helpful in order to identify the frequencies that are specifically related to the dynamic characteristic of the flow. The technique of spectra averaging is normally used to decrease the variance of the computed spectrum. The procedure requires several spectra taken at the same operating point. Each point of the final spectrum is then computed by taking the mean of the corresponding points of all the spectra. In the process any random features are averaged out, while characteristic features common to all spectra remain. This is illustrated in figure 6.15.

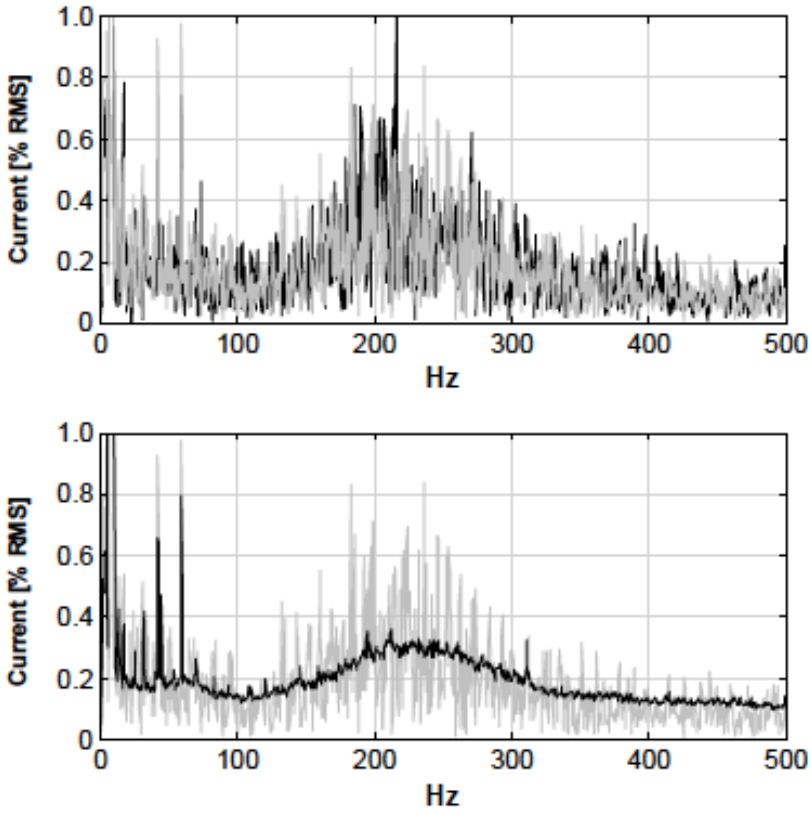


Figure 6.15: Individual output current spectra for identical operating points (above), and an averaged spectrum (below) (Orkisz, et al. 2009)

When considering wet gas stall and surge detection, averaging of frequency spectra will preserve the frequency corresponding to the onset of instability and also other frequencies specially related to the dynamic characteristic of the flow. Frequency components due to random pressure fluctuations generated by the liquid will be cancelled out.

# 7 EXPERIMENTAL INVESTIGATION OF PRESSURE MEASUREMENTS

The pressure sensors used for dynamic measurements in centrifugal compressors are typically installed in flush with the compressor surface. This arrangement yields the best response times, and are therefor ideal when measuring rapidly varying pressure. However, if flush mounted in wet gas flows, the sensing membrane of theses sensor will lie beneath the liquid film, and the measurement will be influenced by the flow dynamic in the film. This chapter describes the set-up and procedure of an experiment conducted to investigate how a thin liquid film will influence the surface pressure. The experiment is considered as a part of a larger survey needed in order to validate the ability of flush mounted fast-response dynamic pressure sensors to measure pressure fluctuations in wet gas flow.

The chapter is divided into five main parts. The first part presents the focus and background of the experiments. The second part gives a description of the test facility, while the third part describes the test variables and experimental procedure. Part four gives a brief discussion of the expected surface pressures, and the fifth and final part suggests some additional test rig options.

## 7.1 BACKGROUND AND FOCUS OF EXPERIMENT

The literature search performed in the pre-project and also the findings presented in chapter 6 serves as the background and motivation for planning this experiment. Results from the investigation of wet gas stall and surge performed at the facility for wet gas compression at NTNU indicates that liquid causes the inception of instability to be delayed, and changes the evolution of the instability. However, the wet gas frequency spectra also showed excessive amplification of random low-frequency pressure components. This made early stage detection of stall and surge very difficult, as the characteristic stall and surge frequencies were “buried” in noise. The amplitudes and number of the random frequency components increased with increasing liquid flow rate, and it is therefore reasonable to relate the phenomenon to the dynamic behavior of the liquid phase. At high liquid fractions these random components were dominating the frequency spectrum. Chapter 6 presented several multiphase mechanisms that

could contribute to the additional frequency components. However, the experimental foundation was limited. There were few experiments investigating the multiphase effects on surface pressure, and very little information on wet gas impact on pressure sensor performance. In order to validate the ability of flush-mounted pressure sensor to measure pressure fluctuations in wet gas flows, it thus follows that extensive testing is required. The influence of the liquid film, droplets and interaction between the phases must be determined in order to assure that the sensors are able to detect the onset of unstable compressor operation, and also to avoid any misinterpretations of the pressure signal due to contributions from the liquid phase.

The main focus of this experiment is to investigate how a flush-mounted pressure sensor will respond to pressure fluctuations in a gas phase when the sensor is installed beneath a thin liquid film. Will peaks corresponding to dry gas variations be recognized through the film, or will the measurements be dominated by pressure components generated in the liquid film? To what degree will film thickness, surface ripples and large interfacial waves affect the surface pressure? And last but not least: is it possible to identify any dependencies between the gas phase fluctuations and the dynamic of the liquid film? The type of flow regime created in the test pipe will not resemble the flow regime inside the compressor. The velocities are too low, it is very little droplet entrainment, and the flow path is not curved. However, the results are still relevant, and will help reveal whether or not flush mounted pressure sensors can be used to investigate the inception and evolution of aerodynamic instabilities in wet gas compressors. Will they report the actual pressure in the core flow, or will film-effects dominate the signal? If the latter were true, traditional stall and surge prediction methods would be misleading. These guidelines are developed based on dry gas compression. The spectral content of the pressure signal that characterizes rotating stall and incipient surge is therefore related to the aerodynamic characteristic of gases.

## 7.2 DESCRIPTON OF TEST RIG

The proposed test rig consists of a straight, horizontal and transparent pipe section connected to the inlet piping of the wet gas compressor rig. A simple sketch of the experimental set-up is given in figure 7.1. Ambient air, and water from a separate supply, is fed through the test pipe. The flow rates are adjusted in order to obtain the correct flow regime in the test pipe. As the focus of the experiments is to investigate how a liquid film will affect the surface pressure, the flow is kept in the stratified and wavy stratified regime. Two holes are drilled into the test pipe at the same axial position. One hole is located in the top surface, while the other is located in the bottom surface. Fast-response dynamic pressure sensors are mounted

through these holes. The sensors are installed in such a way that the sensor sensing diaphragm is perfectly in flush with the pipe surface. During testing pressure fluctuations are generated in the gas phase just upstream of the pressure sensors. The upper sensor will be unaffected by water, while the bottom sensor will be covered by a liquid film. The difference between the two measurements yields the liquid impact on the pressure measurement.

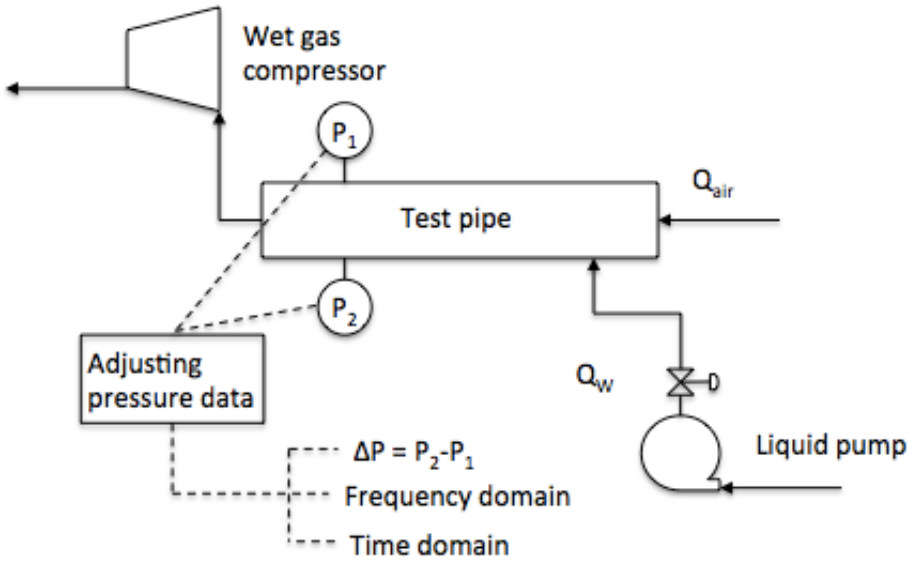


Figure 7.1: Experimental set-up

It may be argued that a curved test pipe would be more appropriate as the compressor flow path is curved. However, in order to isolate the influence from the film it is important that the flow conditions, apart from the presence of the liquid, are similar at the two surfaces. Having a curved path would give different geometries at the two sensor locations, and comparing the measurements would be pointless. While the flow in the bottom part experiences a concave surface, the flow in the upper part would experience a convex surface, and visa versa. The flow field in the two cases will be very different, and generate different pressure profiles.

Figure 7.2 shows a more detailed sketch of the test pipe. The different pipe sections, i.e. the pressure measurement section, the water film injection module and section for generation of pressure fluctuations, are indicated in this figure.

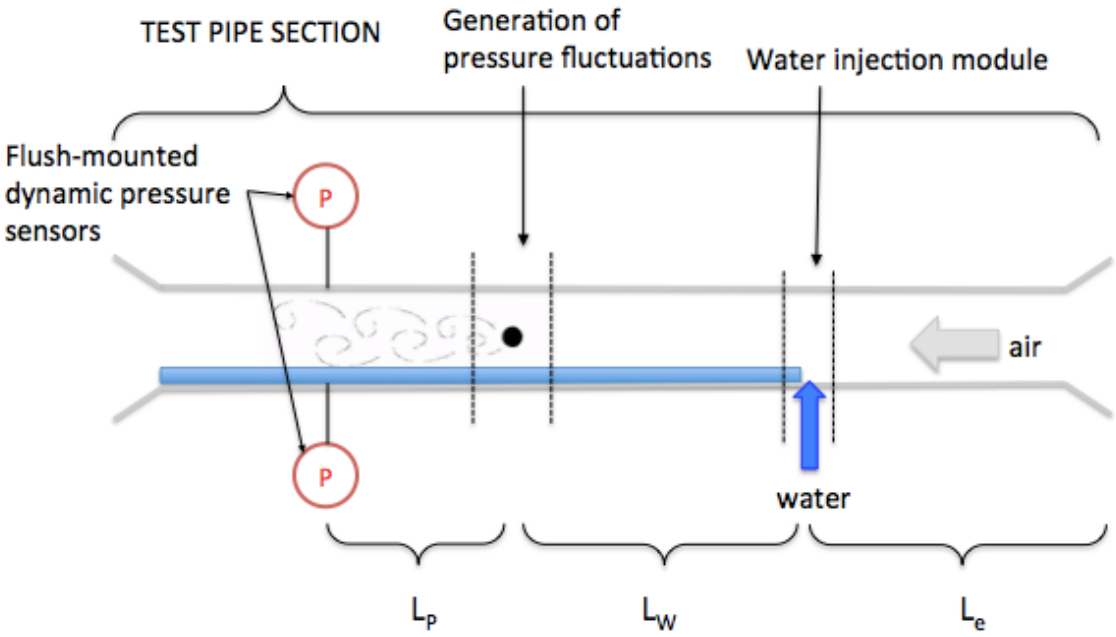


Figure 7.2: Test pipe

### 7.2.1 Choice of Test Pipe Design

Choosing the correct pipe material, dimension and cross-sectional geometry is important in order to get good results. The pipe dimensions are summarized in Table 7-1.

| | |
|---|---|
| Length (L) | ≈ 5.0m |
| Height (h) | 0.2m |
| Depth (b) | 0.1m |
| $L_e$ | 1.0m |
| $L_w$ | 2.0m |
| $L_p$ | 1.0m |

Table 7-1: Test pipe dimensions

The choice of pipe dimensions is based on the following test requirements:

PIPE MATERIAL

In order to ensure that the correct flow regime is obtained, the pipe should be made of a transparent material. Optic access to the flow will enable visualization of the dynamic

characteristic of the liquid film, and also makes measurement of the film thickness very easy. If possible color should be added to the liquid in order to make it easy to distinguish between the two phases.

SIZE OF PIPE CROSS-SECTION

The size of the pipe cross-section must be carefully chosen in order to achieve sufficiently high air velocities in the pipe. Generation of interfacial waves depends upon the gas velocity: the higher the gas velocity the larger and steeper the waves According to the flow regime map in figure 2.5 the superficial gas velocity should be kept in the range of 3 m/s < $U_{sg}$ < 20 m/s. At higher velocities the flow becomes annular, and at lower rates very little surface waves are generated. The gas volume flow is limited by the compressor flow rate, but by changing the cross sectional area, high velocities can be obtained in the test pipe. The size of the pipe cross-section must also allow for a sufficient distance between the film surface and the top surface. The distance need to be large enough to ensure that top surface pressure sensor under no circumstances is exposed to water. During testing the flow will stay in the stratified regime, and the liquid phase will thus be concentrated in the bottom of the pipe. However, interfacial waves due to interfacial shear causes droplets atomization at the air-water interface. If distance between the sensor and the gas-liquid interphase is to small, there is a risk of droplets being transported to the upper surface affecting the top surface pressure measurement.

GEOMETRY OF CROSS-SECTION

When considering the film thickness measurements, having a rectangular cross-sectional area would be favorable. This geometry gives a uniform film thickness across the bottom surface, and the film thickness above the bottom pressure sensor is thus obtained simply by measuring the liquid level at the sidewalls. If flow area is circular, increasing the gas rates will soon causes the liquid surface to start bending around the pipe circumference making film thickness calculations more complex. Having a rectangular cross-section is also favorable when considering size. In order to achieve large velocities, a small sectional area is necessary. However, in order to minimize the liquid impact at the top surface, the distance between the top and bottom surfaces must be sufficiently large. Both of these requirements can be met by having rectangular cross section with a small depth and large height.

PIPE LENGTH

There are also some requirements to the pipe length. The test pipe must be long enough to accommodate the section creating pressure fluctuations, the pressure sensors, the inlet section

where liquid is introduced, as well as a sufficient spacing between the different sections. The magnitude of this spacing is difficult to predict, but the initial values are given in table 7-1. In order to ensure that the wanted flow regime is achieved in the different pipe sections, the pipe dimensions must then be validated experimentally.

### 7.2.2 The Water Injection Module

Water is introduced in the airflow as a water film uniformly coating the bottom surface of the test pipe. This pattern is achieved by injecting the water through a slit in the bottom surface of the pipe. Figure 7.3 and 7.4 show some illustrative sketches of the water injection module.

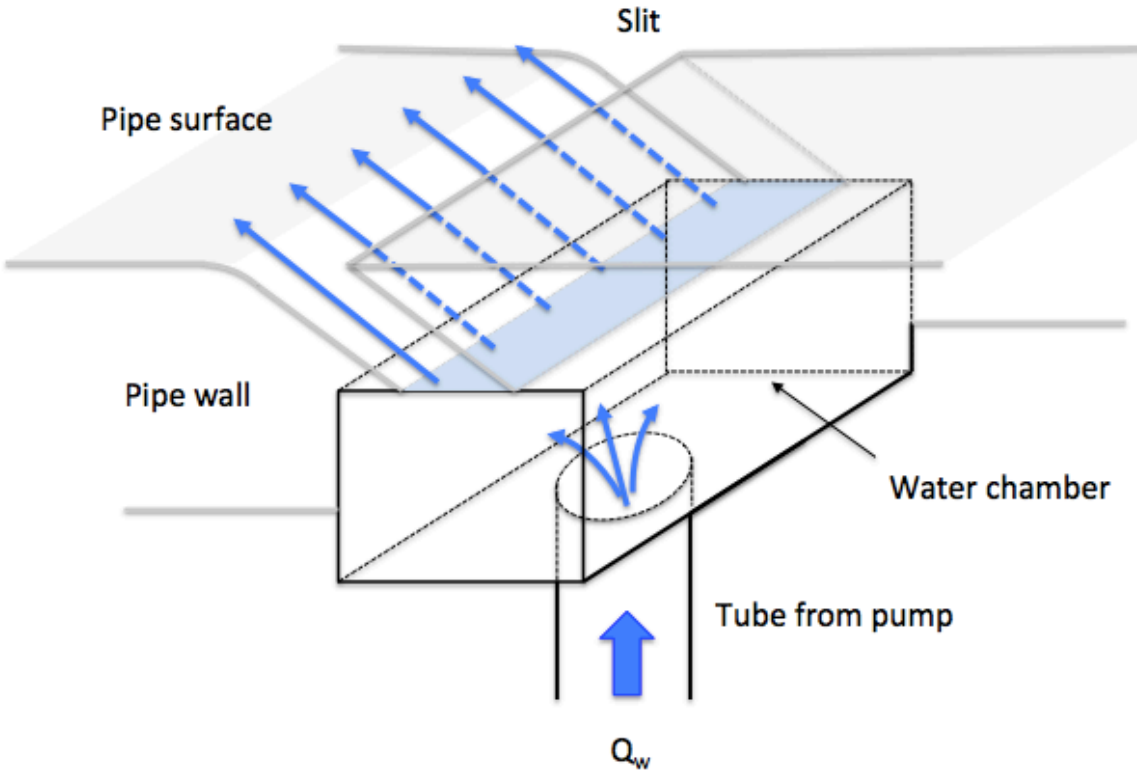


Figure 7.3: Water injection module

The water injection module is supplied with water from a liquid pump. During testing water will flow from the water supply system, into a water injection chamber, through the slit, and into the bottom of the test pipe. The injection chamber is partly embedded in the test pipe wall. During testing the chamber is filled with water, and provides a uniform water flow into the slit. The water exits the slit in an inclined direction, causing a smooth film development in the bottom of the pipe.

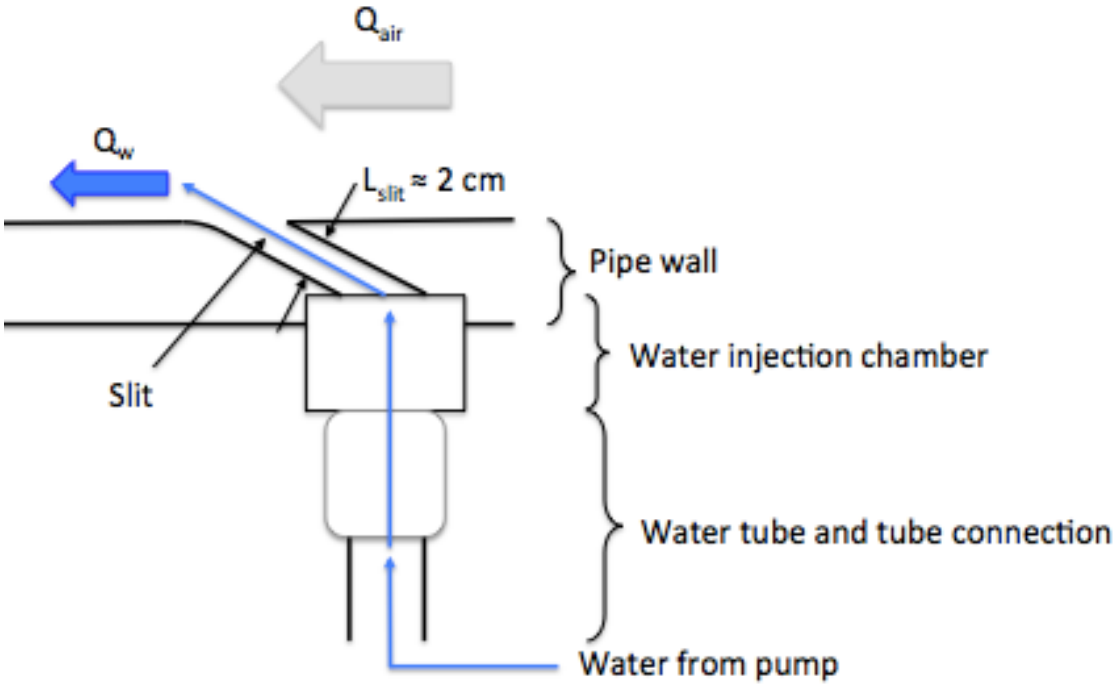


Figure 7.4: Water film pattern injection, seen from the side

Equilibrium between the air and the water film can be reached in two ways. Figure 7.5 shows the film development in the two cases.

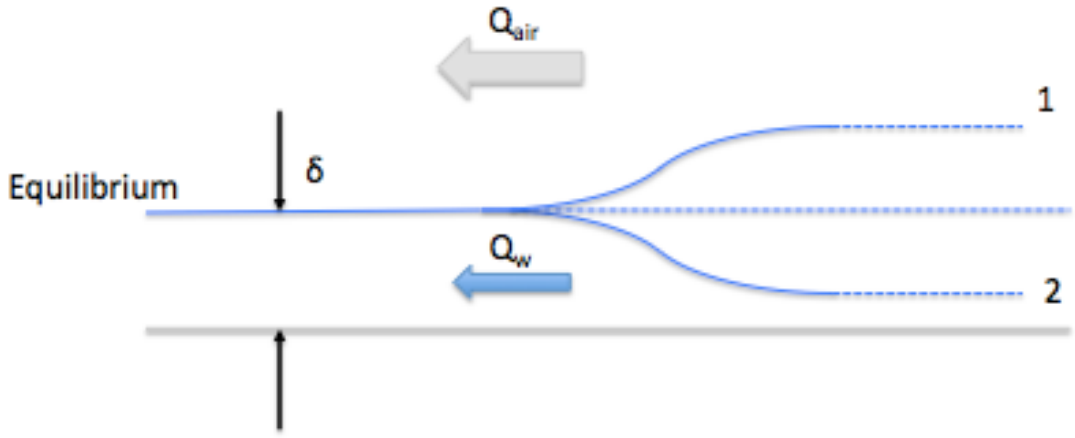


Figure 7.5: Equilibrium in stratified two-phase flows

1. The water enters with a too low velocity, $V_{w,\,inlet} < V_{w,\,eq.}$, and in order to reach equilibrium conditions the water is accelerated downstream of the injection point. This causes the film thickness to decrease toward the equilibrium point.

2. The water enters with a too high velocity, $V_{W, inlet} > V_{W, eq.}$ This means that the water is decelerated downstream of the injection point, with a corresponding increase in the film thickness.

There is also a third possibility, a special case: if the water enters at the equilibrium velocity, the water film thickness will be adjusted to the equilibrium value almost immediately after the water injection.

The type of scenario expected in the test pipe will depend on the dimension of the slit. If the slit is very narrow, the water velocity into the pipe must be very high in order to achieve the correct water flow rate. This implies that the second scenario will be dominating. At the opposite, if the slit is wide, the same water flow rates can be achieved with a much smaller water velocity at the inlet. In this case the first scenario is likely to occur. Compared to acceleration, deceleration of the water phase will result in a much more chaotic flow field, and also cause significant film atomization. Depending on the velocity of the air, these effects might not settle before the flow reaches the pressure sensors, and thereby expose the upper sensor to water. It was therefore chosen to scale the slit according to the thickest water film tested in the experiment. By doing this the inlet velocity of the water will always be less than or equal to the equilibrium velocity, and deceleration of water is avoided. The size of the slit was set to 2 cm. Testing film thicknesses over this value is not considered as very relevant. The internal compressor flow pattern is characterized as annular multiphase flow where the liquid flows as a thin film on internal walls and a dense droplet spray in the core. The focus of the experiment is thus to evaluate the influence thin films only.

The air and water flow rates, and also the cross sectional area of the pipe, will determine the thickness and velocity of the water film when equilibrium is reached. High air rates, and correspondingly high air velocities, will increase the interfacial friction between the two phases. This will affect the water film by dragging it faster through the pipe. If the water flow rate is kept constant, it thus follows that the water film thickness decreases. At the opposite, if the air flow rate is held constant, increasing the water flow rate will increase the water level in the pipe. In this experiments various water film thickness will be tested at constant air flow rate by changing the water flow through the pipe. The water flow rate is determined by the pump discharge pressure and the static pressure in the test pipe. This is indicated in equation 7.2.1 and 7.2.2.

$$P_{pump} - P_{pipe} = \Delta P_{f,water} = f(\dot{Q_w}, \rho_W, L_{tube}, L_{slit} \ldots) \quad (7.2.1)$$

$$\dot{Q}_w = f\left(P_{pump} - P_{pipe}\right) \quad (7.2.2)$$

The pressure difference between the pump discharge and test pipe must cover the pressure drop in the tubing between the pump and the pipe, the pressure drop in the injection chamber, and the pressure drop over the slit. As indicated in equation 7.2 1, this pressure drop will be a function of the water flow rate and the geometrical dimensions of the water supply system. However, as the geometrical dimensions and the pressure in the pipe are kept constant, the water flow rate is changed by changing the pump pressure.

### 7.2.3 The Pressure Fluctuation Generation

In order to investigate how the pressure sensors respond to pressure fluctuations in the gas flow, a device that generates these fluctuations of different amplitudes and frequencies, must be implemented in the test pipe. This can be achieved in a very simple manner by installing a blunt body, for instance a small cylinder, in the gas phase upstream of the pressure sensors. When the gas passes the cylinder, a boundary layer will form at the cylinder surface. At the front surface of the cylinder the flow will stay attached to the cylinder surface, but as the flow moves towards the rear, the boundary layer separates creating a wake flow with vortices and eddies behind the cylinder.

Two-dimensional circular cylinder flows have been well studied because of the phenomenon of vortex shedding. This process, which occurs for a wide range of fluid speeds, properties and cylinder sizes, is characterized by a repeating pattern of swirling vortices generated by unsteady separation of the flow past the cylinder. When the boundary layer separates from the cylinder surface, the resulting shear layer becomes unstable. It rolls up into a vortex in the wake region and the vortex is eventually shed from the cylinder. The shear layer from the opposite side of the cylinder then repeats the process, and a vortex with an opposite sense of rotation is shed downstream. The arrangement of alternating vortices travelling downstream in the wake, illustrated in figure 7.6, is called a Kármán vortex sheet (Heseltine 2003).

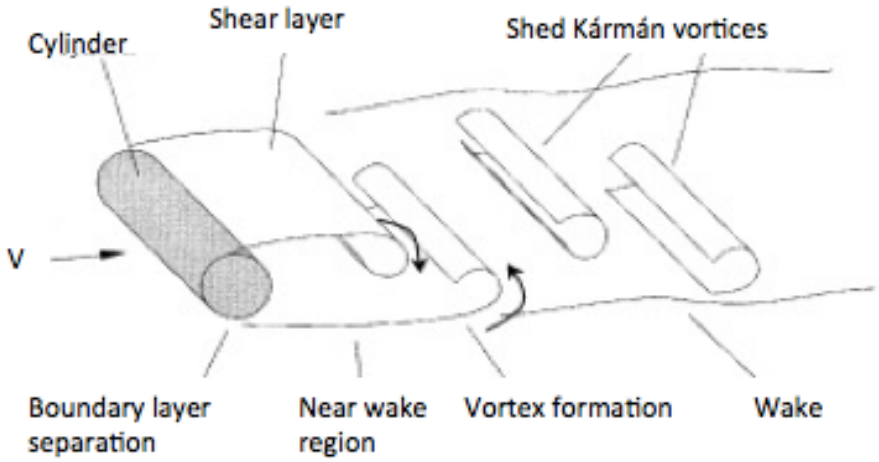


Figure 7.6:Vortex shedding behind circular cylinder (Heseltine 2003)

In order to generate pressure fluctuations with different frequencies, the vortex shedding frequency must be varied. This can be done by changing the cylinder diameter and/or changing the velocity of the air. The vortex shedding frequency, f, is non-dimensionalized as the Stouhal number, St. The definition is given in equation 7.2.3. The Reynolds number in flows past blunt bodies is given in equation 7.2.4 (Heseltine 2003).

$$St = \frac{fd}{V_\infty} \tag{7.2.3}$$

$$Re_d = \frac{\rho V_\infty d}{\mu} \tag{7.2.4}$$

Vortex shedding behind a circular cylinder occurs for a wide range of Reynolds number. However, at certain Reynolds numbers vortex formation may cease, and other flow patterns occur. Depending on the wake characteristics, the flow can be divided into different Reynolds number regimes. Figure 7.7 show how the Stouhal number varies with Reynolds number for flow past a circular cylinder.

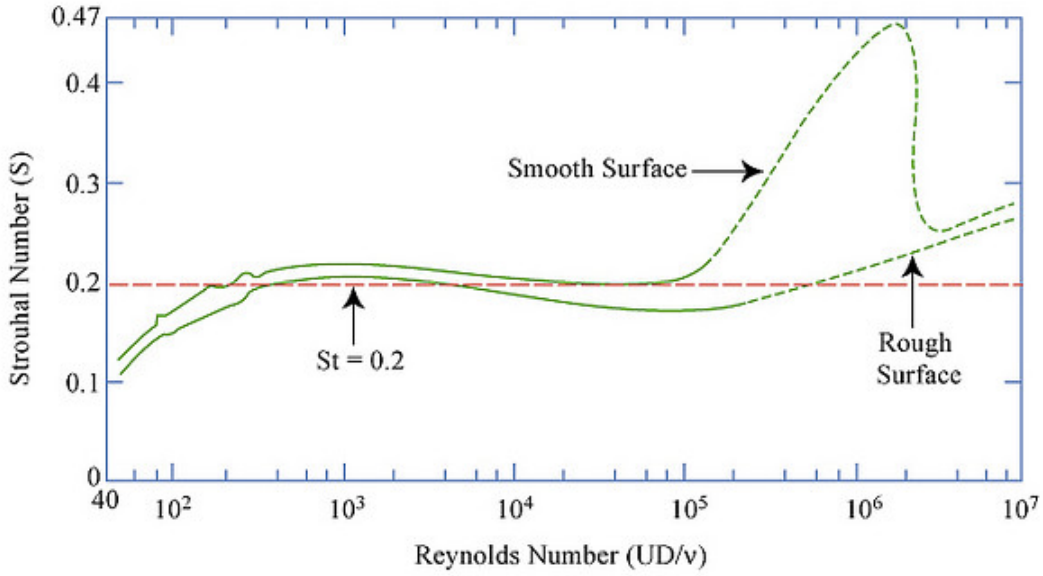


Figure 7.7: Stouhal number plotted versus Reynolds number (MITOpenCourseWare 2005)

If $250 < Re_d < 2x10^5$, the Stouhal number is almost constant. This regime is called the sub critical regime and equation 7.2.5 gives a relationship between the vortex shedding frequency, the cylinder diameter and the free-stream velocity (Heseltine 2003).

$$f = 0.198\left(\frac{V_\infty}{d} - \frac{19.7\mu}{\rho}\right) \tag{7.2.5}$$

The last term in the brackets is much smaller than the first term, and equation 7.2.5 can be simplified to yield:

$$f \approx 0.2\frac{V_\infty}{d} \tag{7.2.6}$$

The amplitude of the fluctuating pressure in the vortex street wake has a close connection to the vortex shedding process. There is a strong link between the magnitude of the pressure fluctuation and the intensity or energy of the vortices generated: The higher the vortex energy, the larger the pressure amplitudes. The vortex energy is proportional to the kinetic energy of the flow, and it can therefore also be assumed that the same will hold for the magnitude of the pressure fluctuations. It thus follows that increasing the velocity of the air will induce stronger pressure fluctuations.

$$\Delta P \propto \frac{1}{2}\rho V_\infty^{\ 2} \tag{7.2.7}$$

The vortex shedding frequency and the vortex energy is also dependent on the blockage ratio, β, of the flow obstacle. In general it has been shown experimentally that the shedding frequency decreases with increasing blockage ratio, while the vortex energy increases with increasing blockage ratio (Shakouchi, Tian and Ida 2002). According to Hans and Windorfer (2002) the blockage ratio should be around 0.25 in order to generate pressure amplitudes with sufficient amplitude to make reliable measurements in a gas flow.

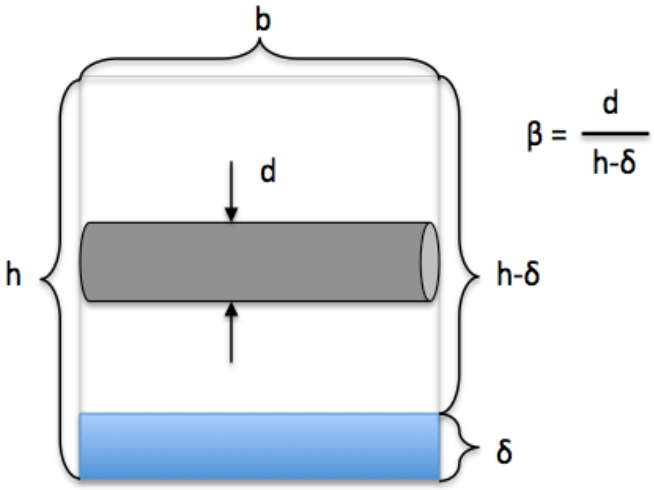


Figure 7.8: Test pipe cross section

Figure 7.8 gives an explanation of the blockage ratio in stratified flows. In this experiments the water film will be thin, meaning that δ << h. The blockage ratio can thus be approximated according to equation 7.2.8.

$$\beta \approx \frac{d}{h} \tag{7.2.8}$$

By using different cylinder diameters, the possible frequency and pressure amplitude range is extended. However, in this experiments it has been chosen to have a fixed cylinder diameter, and change the vortex shedding characteristics by just controlling the air flow rate. In order to generate pressure amplitudes of sufficient size, the blockage ratio is set to 0.25, which means that the cylinder diameter, d, is set to 0.05 m. If the resulting pressure amplitudes turn out to be to small, the cylinder is just switched with a bigger one. In order to generate vortices with a stable separation point, and also to improve the frequency control, the cylinder should have a rough surface. This is indicated in figure 7.7, and was also shown experimentally by Hans and Windorfer (2002).

There are many ways of generating pressure fluctuations in the air. The method with the cylinder is a very simple one, and will also generate a flow regime in the air that to some extent can simulate the flow regime inside the compressor at rotating stall. The flow in the test pipe will separate as it moves past the cylinder, and a wake with stagnant flow will develop in the pipe behind the cylinder. The vortices shed from the cylinder surface will generate alternating regions of high and low pressure that passes by the pressure sensor, and affects the surface pressure measured by the sensor. In rotating stall the pressure fluctuations also results from regions of stagnant flow passing over the pressure sensors. The pressure difference and the velocities in the case of the compressor are much higher than those achieved in the test pipe, but the structure of the flow, i.e. boundary layer separation and vortex generation, will be present in both of the cases. However, there are one major draw-back with this method: the amplitude and frequency of the generated pressure fluctuations is dependent on the air flow rate. Ideally one would also like to be able to apply the same pressure signal to different flow conditions, but this is not possible with the method described in this chapter. If large air flow rates are high, the frequency and amplitude of the pressure fluctuation will be correspondingly high. Oppositely, if the air flow rate is low, the generated pressure signal will have a small amplitude and low frequency. Other combinations of flow rates, frequency and amplitudes call for a different pressure generation method. One such method is briefly described in chapter 7.5.1.

### 7.2.4 Pressure Sensor

Two pressure sensors are installed adjacent to each other, one in the bottom surface, beneath the water film, and one in the top surface. The installation point is located a certain distance, $L_P$, downstream of the vortex generator. This is done in order for the vortex sheet to fully develop, and also to allow for sufficient phase interactions between the air and the water film. Fluctuations in the air will most likely affect the dynamics of the water film. However, due to inertia and velocity differences between the two phases, the attenuation and propagation speed of these fluctuations will not necessarily be the same. By having some distance between the cylinder and the sensors, these effects would have time to evolve, and could be captured by the pressure measurements. As a starting value, $L_p$, has been set to 1.0 m.
The pressure sensor needs to meet several requirements. First of all the sensor must be able to measure in both air and water. One of the sensors will be exposed to water, and it is important that the characteristics of the sensor, i.e. the frequency response, linearity and sensitivity, are not affected by water. If this is the case, variations in the measurements may still arise even though the actual pressure at the two sensing elements is the same. This will highly

complicate the process of comparing the pressure signals from the two sensors, and make it very difficult to isolate the pressure components stemming from the water film.

Secondly there are also requirements regarding the sensitivity and frequency range of the sensor. The amplitude of the pressure fluctuations caused by the vortex generation is expected to be quite small, less than 1 kPa (Hans and Windorfer 2003). The sensor must be able to detect the pressure fluctuations in the air, and also the possible components stemming from ripples, disturbance waves and turbulence in the water film. Since the film is quite thin, these pressure amplitudes are also expected to be small. In order to resolve these small-scale fluctuations the sensor needs to be very sensitive. It will need to have a very small threshold value, and also be able to measure small pressure variations with high accuracy. The sensor also needs to have a wide frequency range. The vortex shedding frequency will determines the main frequency in the flow. This frequency will be quite low, up to 2-300 Hz. However, other frequencies may also appear due to turbulent motion in the water film and the air. In order to get the full picture on how the pressure is affected by water, the pressure sensor should also be able to pick up on these frequencies as well.

Based on the specification listed above, a piezoelectric low pressure transducer, Kistler 7261A, was chosen for the experiments. This pressure is sensor designed for measuring dynamic and short-term static pressures from vacuum to 10 bar. The sensor has a very high sensitivity and a very low threshold value. The measured pressure acts through a stainless steel diaphragm on a quartz crystal sensing element, which then transforms the pressure into an electrostatic charge. The diaphragm is welded flush and hermetically to the stainless steel transducer body. The quartz element is mounted in a highly sensitive arrangement in a quartz chamber, which is welded hermetically to the sensor body. The sensor comes with optional screw-on cover and hose nipple for easy connection to the measured pressure. However, if both the cover and the hose nipple are mounted, the frequency response of the sensor is considerably reduced due to the Helmholtz resonator effect. In order to maximize the natural frequency of the sensor, these additional components are therefore discarded. The senor is thus mounted in the pipe wall with the diaphragm in flush with the pipe surface. The sensor is designed for measuring in air, but according to Kyte (2013) the sensor itself is waterproof, and simple adjustment can be made in order to protect the connector from water. One possibility is to use an epoxy coating. Figure 7.9 shows a picture of the sensor, and the datasheet are found in Appendix H.

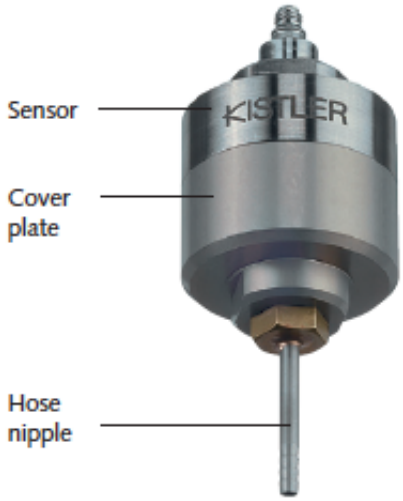


Figure 7.9: Kistler 7261A (Kistler)

Kistler 7261A is a charge mode sensor, and recalled from chapter 4.1.5, this means that the output needs signal conditioning prior to being analyzed. The high-impedance charge output must be converted to a low-impedance voltage signal, and also needs external amplification and filtering. In the case of Kistler 7261A, this is achieved by using a charge amplifier. There are both advantages and disadvantages of using this type of system. The high impedance output have the potential of being contaminated by environmental influences such as cable movement, electro-magnetic signals and radio frequency interference, prior to being conditioned. Furthermore it is not recommended to use charge-amplified systems above 50 or 100 kHz as the feedback capacitor in the system exhibits filtering characteristics above this range (see figure 4.7). However, a major benefit with external electronics is that the characteristics of the sensor are variable and can be changed by switching components in the external signal conditioner. Depending on the choice of charge amplifier, Kistler 7261A can detect pressure variations down to 0.25 Pa. Additionally, since the cable length between the sensor and the charge amplifier can be kept very short, the risk of signal noise is not significant, and the frequency limit is not a problem as the frequencies being investigated is in the lower range, well below 50 kHz.

Using the extremely sensitive Kistler 7261A allows for very accurate measurements of the pressure fluctuations at the two surfaces. The sensor will capture larger pressure peaks, due to the passing of a vortex, but also smaller pressure variations due to turbulence and interfacial waves. By comparing the two measurements detailed knowledge of how the water film affects the surface pressure can be obtained.

## 7.3 TEST VARIABLES AND EXPERIMENTAL PROCEDURE

### 7.3.1 TEST PROCEDURE

Two main variables are changed during the experiment: the air flow rate, $\dot{Q}_{air}$, and the water film thickness, δ. The experimental procedure for each air flow rate is as follows:

1. The compressor is adjusted to obtain the correct air flow rate in the test pipe

2. Liquid is introduced in the pipe by opening the valve between the liquid injection module and the liquid pump.

3. The pump settings are adjusted according to the desired film thickness and corresponding water flow rate. Introducing liquid in the pipe will affect the air flow rate, and some smaller adjustment of air and liquid flow rates will be necessary in order to achieve the correct flow rates.

4. For each choice of film thickness the surface pressure at the bottom and top surface is recorded, and the data presented in time and frequency domain. The pressure difference between the to sensors, ΔP, is also calculated, and the result plotted in time and frequency domain.

The surface pressure is measured at 5 different air flow rates and with three different water film thicknesses. The resulting test matrix is displayed in figure 7.10.

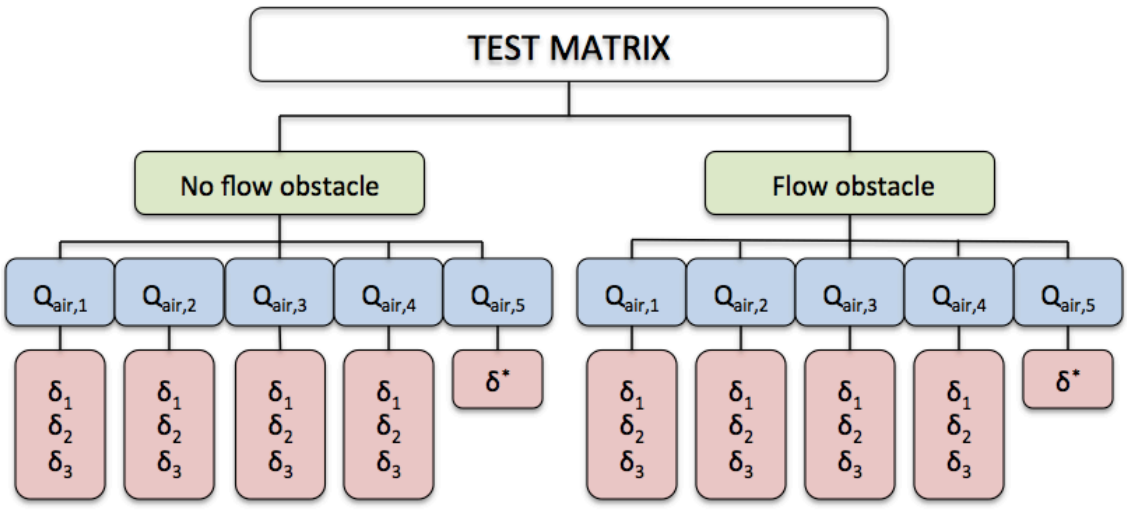


Figure 7.10: Test matrix

As indicated in the figure the tests are also conducted without the cylinder inserted in the flow. There are two reasons for doing this. Firstly, when considering wet gas compression, testing without the cylinder can help indicate the amount of signal noise due to the liquid phase that could be expected during stable operation of the machine. By testing without the cylinder, it is possible to isolate the effects of variations in film thickness, surface ripples and larger disturbance waves. The magnitude of these effects is not expected to be large, but if the aim is to measure the pressure in the air, they may still contribute to significant "noise" in the pressure signal. It is therefore useful to investigate how these parameters will contribute to the surface pressure, both in terms of pressure amplitude, but also regarding the frequency of these pressure components. If the cylinder is inserted in the air stream these effects might be lost, as the resulting air fluctuations will affect the dynamic of the water film, and most likely dominate the behavior of the film.

Secondly, useful information can also be gained by comparing the measurements with and without the cylinder, but with the same air flow rate and film thickness. In case of the pressure sensor located beneath the water film, the difference between the measurements will yield the total effect of both aerodynamic instabilities in the air stream and the interactions between the air and the water film. The result of this comparison will be very useful if trying to identify a characteristic pressure response to aerodynamic instabilities in multiphase flows.

### 7.3.2 Air Flow Rates

In order to generate waves of different size and shaped the velocity of the air must be varied. This is achieved by changing the air flow rate through the compressor. The air flow rate is changed by changing the compressor speed. The compressor speed changes the suction pressure at the compressor inlet. Increasing the speed reduces the suction pressure, which again results in a higher the flow rate.

Figure 7.11 and equation 7.3.1-3 expresses the relationship between the pressure, velocity and flow rate at the compressor inlet and in the test pipe. This is Bernoulli's equation and mass conservation taken from the ambient air to the compressor inlet, with the assumption of incompressible flow and no friction. By reducing the suction pressure, the velocity of the air at the compressor inlet increases. This will then result in a larger air flow rate, and a larger velocity of the air in the test pipe.

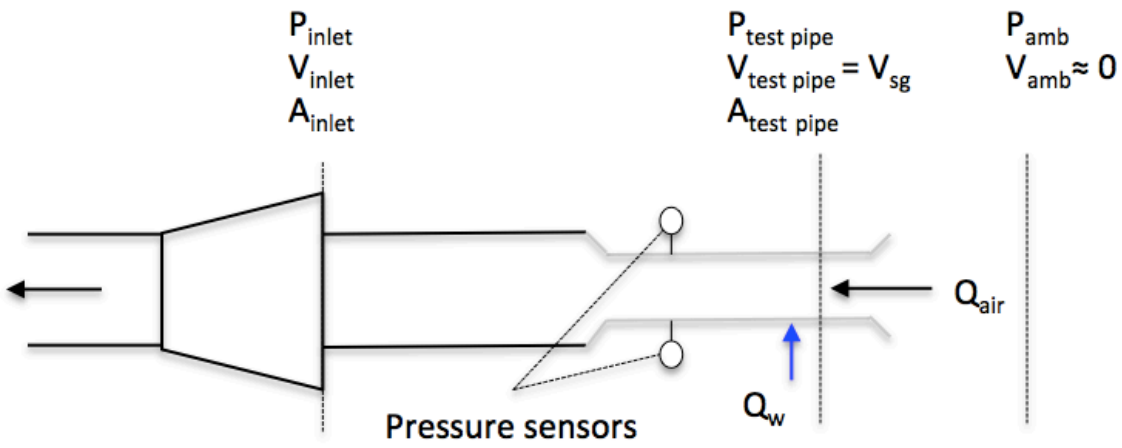


Figure 7.11: Pressures and velocities in different sections

$$P_{amb} \approx P_{inlet} + \frac{1}{2}\rho_{air}V_{inlet}^2 \tag{7.3.1}$$

$$\dot{Q}_{air} = V_{inlet}A_{inlet} = V_{test\ pipe}A_{test\ pipe} \tag{7.3.2}$$

$$P_{amb} \approx P_{inlet} + \frac{1}{2}\rho_{air}\left(\frac{\dot{Q}_{air}}{A_{inlet}}\right)^2 = P_{inlet} + \frac{1}{2}\rho_{air}\left(\frac{A_{test\ pipe}}{A_{inlet}}\right)^2 V_{test\ pipe}^2 \tag{7.3.3}$$

Table 7-2 gives a list of the chosen air flow rates and the corresponding velocities of the air. The actual velocities of the air downstream of the liquid injection module will be somewhat higher than the ones indicated in the table. Some of the pipe cross section is occupied by the water film, resulting in a smaller area available for the air. In order to satisfy continuity it thus follows that the velocity of the air must increase. However, since the film is kept thin, this increment will not be that significant, and as a first approximation, the velocity of the air is substituted by the superficial velocity of the air. Figure 7.12 shows the air flow rates in the flow regime map.

| $Q_{air}$ [$m^3/s$] | $V_{sg}$ [m/s] |
|---|---|
| 0.05 | 2.5 |
| 0.10 | 5.0 |
| 0.20 | 10.0 |
| 0.40 | 20.0 |
| 0.50 | 25.0 |

Table 7-2: Air flow rates and superficial air velocities

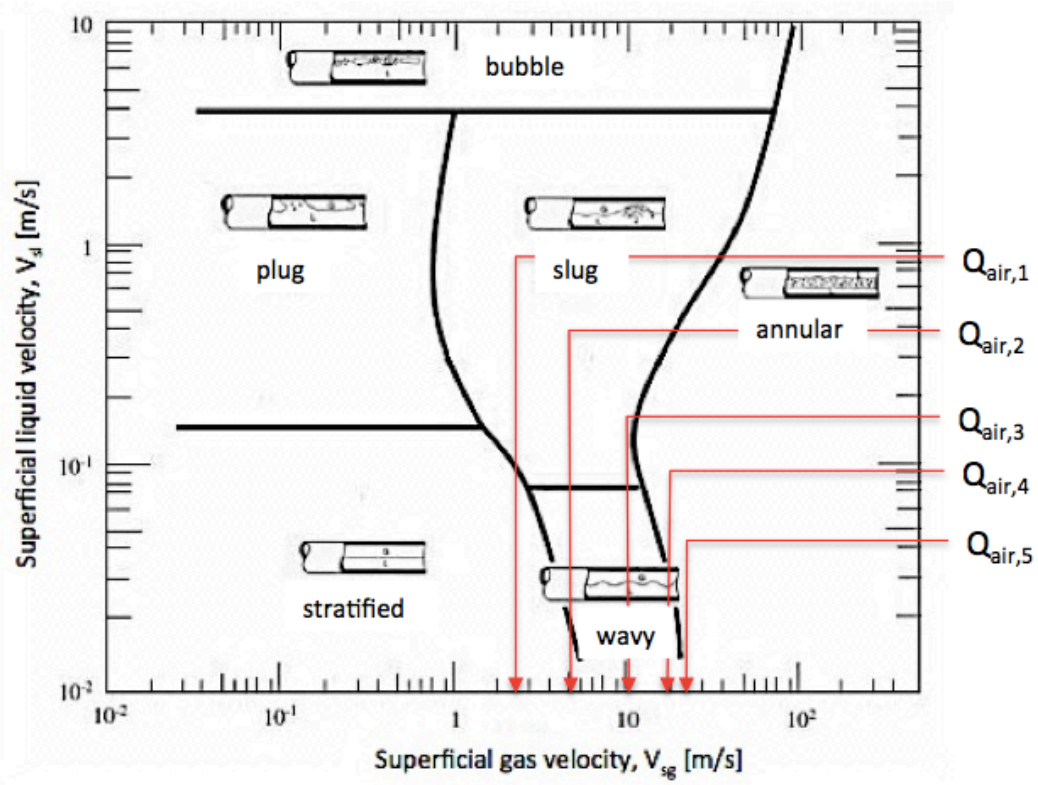


Figure 7.12. Flow regime map with test flow rates indicated

Beaufort scale, which relates wind speed to observed conditions at sea, can be used to predict the type of waves expected in the pipe. At small velocities, up to approx. 3 m/s, only ripples, wavelets and small wavelets will appear at the water surface. As the velocity increases these wavelets develops into breaking waves with increasing wavelengths and amplitudes, and when the velocity reaches 18 m/s the water surface is dominated by large roll waves. Velocities in the range of 20-25 m/s will generate steep waves with overhanging crests and

considerable impact from tumbling of the waves. Evident from table 7-2 the whole spectra of waves will be covered in the experiments. This is also clear from the figure 7.12, which indicates the different flow rates in a flow regime map. The chosen flow rates covers the whole wavy region.

In order to keep the flow in the stratified region, the superficial velocity of the air should not exceed 20 m/s. At higher rates the flow becomes annular, and the sensor in the top surface is at risk of being exposed to water. However since the pipe cross section is rectangular, and the height is two times the width, it is reasonable to assume that the transition to annular flow will be delayed to a larger flow rate. Nevertheless, caution must be taken when introducing water at the highest rate, in order to ensure that no water is transferred to the upper surface.

The velocity of the air will also affect the vortex shedding frequency and the Reynolds number past the cylinder. Increasing the velocity increases both the frequency and the amplitude of the pressure fluctuations. Table 7-3 gives the Reynolds number and the vortex shedding frequency for the different flow rates. The calculation is based upon the superficial velocity of the air.

| $Q_{air}$ [$m^3/s$] | $Re_d$ | $f_{vortex}$ [Hz] |
|---|---|---|
| 0.05 | 1.0E04 | 10 |
| 0.10 | 2.0E04 | 20 |
| 0.20 | 4.0E04 | 40 |
| 0.40 | 8.0E04 | 80 |
| 0.50 | 1.0E05 | 100 |

Table 7-3: Air flow rate, Reynolds number and vortex shedding frequency

### 7.3.3 WATER FILM THICKNESS

The dynamic of the liquid film depends on the velocities of air and water, but also on the film thickness. The size of the turbulent structures in the film, the wave pattern at the air-water interface, and also the transport of wave induced momentum through the film, will all change if the film thickness changes. A thicker film will allow for larger and steeper surface waves compared to a thin film. By using different film thicknesses, different wave patterns are

generated, and the resulting effect in terms of surface pressure can be explored. When considering film turbulence, the characteristics of the energy containing large-scale eddies are limited by the film thickness. The thicker the film, the larger eddies, and the larger the time scale of the turbulent motion. It is therefore reasonable to believe that film turbulence, in the case of thick films, will generate pressure components with a lower frequency compared to thinner films. It is also expected that the amplitudes of this pressure component will be larger in thicker films as the film contains more kinetic energy than the thinner films. This however, also depends on the velocity of the water.

In order to reveal dependencies between the surface pressure and the film thickness, three different water film thicknesses will be tested for each air flow rate: a very thin film, an intermediate value, and a thicker film. The selected values are listed in table 7-4. The table also indicates how the film thickness will affect the velocity of the air.

| δ [mm] | Increment of air velocity [%] |
|---|---|
| 5 | 2.6 |
| 10 | 5.3 |
| 15 | 8.1 |

Table 7-4: Film thicknesses

| $Q_{air}$ [$m^3/s$] | $Q_{w,1}$ (δ = 5mm) [$m^3/s$] | $Q_{w,2}$ (δ = 10mm) [$m^3/s$] | $Q_{w,3}$ (δ = 15mm) [$m^3/s$] |
|---|---|---|---|
| 0.05 | 2.6050E-05 | 6.3330E-05 | 1.0686E-04 |
| 0.10 | 5.6360E-05 | 1.3373E-04 | 2.2315E-04 |
| 0.20 | 2.7807E-04 | 6.1088E-04 | 9.6773E-04 |
| 0.40 | 5.6934E-04 | 0.00124 | 0.00196 |
| 0.50 | N/A | N/A | N/A |

Table 7-5: Water flow rates at different air flow rates,

Table 7-5 gives an approximate value of the corresponding water flow rates at the different air flow rates. These values are obtained by solving the hold-up equation for stratified flow in Matlab. The derivation of the equations and the Matab functions and script can be found in appendix C-G. Evident from the table 7-5 the water rates are very small, and caution must be taken when adjusting the pump. The film thickness increases very rapidly with flow rates the, especially at low air rates. At high air rates and thick films, the flow will enter the annular regime, at least if using the flow regime maps as a guideline. It is therefor not calculated any water flow rates for the highest air rate, and also regarding $Q_{air}$ =0.4 it is not yet known if it is possible to create a film flow pattern with this flow rate, or if the droplet generation is to high. This must be tried and tested as the experiment is conducted.

| $V_{s,air}$ [m/s] | $V_{s,w}$ ($\delta$ = 5mm) [m/s] | $V_{s,w}$ ($\delta$ = 10mm) [m/s] | $V_{s,w}$ ($\delta$ = 15mm) [m/s] |
|---|---|---|---|
| 2.5 | 1.30E-03 | 3.17E-03 | 5.34E-03 |
| 5.0 | 2.82E-03 | 6.69E-03 | 0.011 |
| 10 | 0.014 | 0.031 | 0.048 |
| 20 | 0.029 | 0.062 | 0.098 |
| 25 | N/A | N/A | N/A |

Table 7-6: Superficial air and water velocities

Table 7-6 gives the superficial velocities for air and water at the different film thicknesses. If substituting the values into the flow regime map, it is evident that some of the cases will be outside the stratified and wavy stratified region. This is also seen in figure 7.13 on the next page. However, due to the special cross sectional geometry of the pipe it is expected to take larger water rates before the upper surface is wetted. There are also quite large uncertainties regarding the calculated water flow rates, both due to the choice of wall friction model and interfacial friction model, and also because of the geometry of the pipe. The friction model that was chosen is developed for circular pipes, but the test pipe in this case is rectangular. Furthermore, the correction factor used when calculating the interfacial friction is chosen based upon “common sense”, and the choice has not been experimentally validated. The calculated water flow rates should thus only be used a starting value.

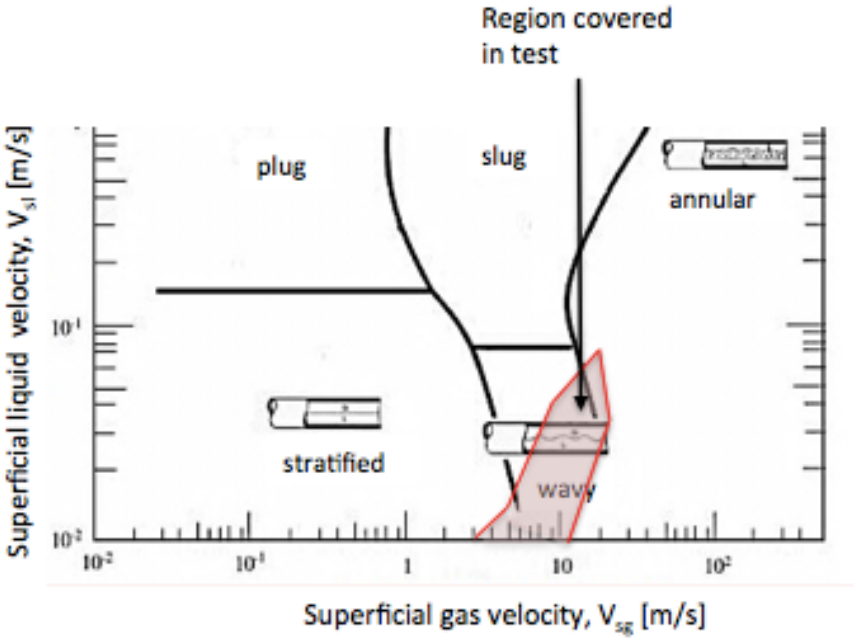


Figure 7.13: Tested region in flow regime map

### 7.3.4 Adjusting the Pressure Data

After the sensor output has been conditioned and further turned into a digital signal through a analog-to digital converter, the results can be manipulated in order to generate the frequency spectra and the transient history of the surface pressures. For each test case the two pressures, $P_{air}$ and $P_w$, and also the difference between the measurement, $\Delta P = P_w - P_{air}$, is plotted in the time and frequency domain. Some adjustment must be made when representing the signal in the time domain, as there will be a phase delay between the two signals. Due to the alternating nature of the vortex shedding process, the surface pressure contribution due to the passing of vortexes will be in opposite phases at the two adjacent surfaces. This means that when one sensor measures a pressure peak, the other sensor will measure a pressure trough. If this is not accounted for when plotting the pressure difference versus time, the result will be very misleading.

When physical phenomena are represented in the form of a frequency spectrum, the physical description of the internal processes becomes much simpler. The frequency spectrum will clearly show the main oscillating behavior, but also harmonics, visible as distinct spikes or lines. This can provide insight into the different mechanisms that generate the entire signal. The frequency spectrum is obtained by applying the Fourier transform, $P(t) \rightarrow P(\omega)$, to the transient pressure signal. The theory behind this transform will not be included in this thesis, but the general idea is illustrated in figure 7.14.

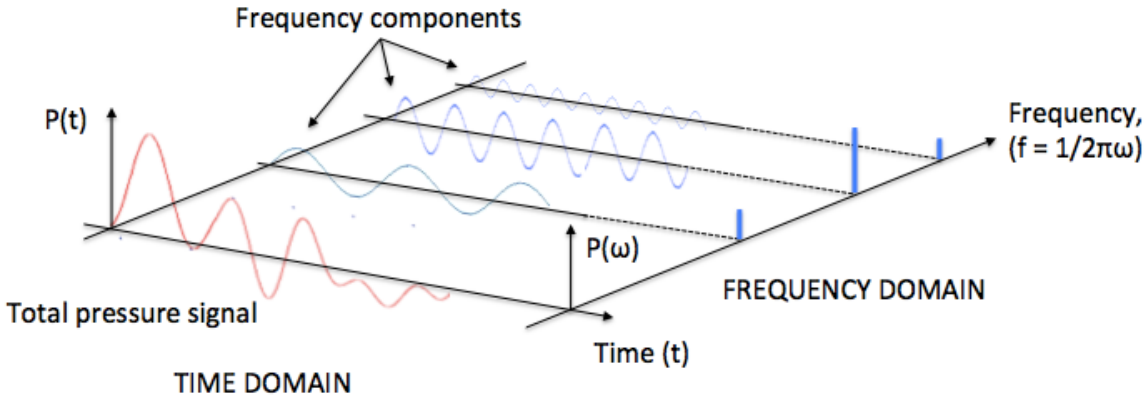


Figure 7.14: Explanation of time and frequency domain

$P(\omega)$ is the frequency spectrum, and it identifies the individual frequency components obtained from the transform. A sinusoidal function in the time domain is a single frequency component in the frequency domain. If a sinusoidal signal is modulated in amplitude, frequency, or phase, additional frequency components appear on either side of the unmodulated discrete frequency in the frequency domain. These additional components are called "sidebands" and they are distributed over a wider band of frequencies as the rate of modulation is increased.

The Fourier transform of a random waveform is also random, and some kind of averaging is required in order to create a clear picture of the underlying frequency content. This can be achieved by dividing the data into time-segments of a chosen duration, and do the transform on each one. Then the magnitudes of the frequency components of the transforms are summed into an average transform. When considering the two surface pressures, it would be interesting to generate both averaged frequency spectra and un-averaged ones. Comparing un-averaged frequency spectra will give an idea of how the water film affects the amount of signal noise. If the noise is significantly increased, more attention should be given the averaging process in the case of wet gas compression in order to improve the measurements. The averaged spectra can be used to identify any characteristic frequencies generated by the water film. This result can be useful if trying to develop alternative guidelines to predict rotating stall and surge based on the characteristic response of the liquid phase, instead of the characteristic response of the gas phase. Averaged values should be used when calculating and plotting ΔP in time and frequency domains. Otherwise there is a risk of random noise to dominate the plots, and making it very difficult to recognize any distinct frequencies.

## 7.4 TEST EXPECTATIONS

Due to time constraints and some delays at the new wet gas impeller rig, the author was not able to carry out the experiment. There will therefore not be presented any results, but as a compensation there will be a short summary of some of the test expectations.

### 7.4.1 TOP SURFACE PRESSURE MEASUREMENTS

The pressure fluctuations measured at the upper surface is expected to resemble the time history and frequency spectrum given in figure 7.15a) and b). The characteristic frequency, recognized as a distinct peak in the frequency spectrum, will be half the vortex shedding frequency due to the alternating shedding process.

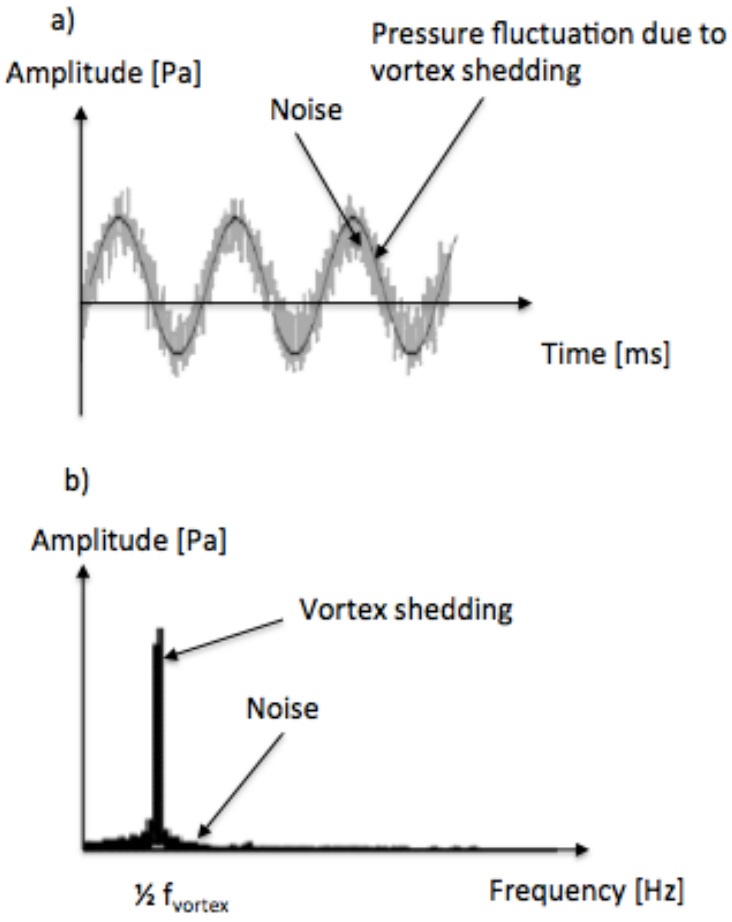


Figure 7.15: Top surface pressure measurement represented in a) time domain and b) frequency domain

As the air flow rate increases both the frequency and the amplitude of the pressure fluctuation increases. Changing the water film thickness should have minimal consequences for the upper surface pressure. The only consequence is that the air velocity varies slightly, but as seen from table 7-4 this is at most 8% and will not cause significant changes. However, if increasing the film thickness also results in significant droplet generation, and wetting of the upper surface, the impact on the surface pressure can be significant. Theoretically, if the all the kinetic energy of the droplet it converted to pressure energy, a droplet with a normal velocity component of 1 m/s will cause an impact pressure of approx.~ $\frac{1}{2}\rho_w V_n^2 = 500Pa$, if hitting the sensor in a normal direction. As explained before, this scenario should not happen, and will be avoided by carefully controlling the water flow rate.

Due to turbulent motion in the air, and also because the pressure sensor is extremely sensitive, some noise in the measurements should be expected. The magnitude of this noise will increase as the air flow rate increases due to a corresponding increase in the turbulent energy in the flow. However, since the amplitude of the main fluctuation also increases, the resulting noise-to-signal ratio will not be that affected. All in all, the amplitude of the frequency components due to noise are expected to be small compared to the component caused by the vortex shedding. This is also indicated in figure 7.15 a) and b). In the frequency spectrum the noise appears as additional frequency components at both sides of the vortex shedding frequency, and in the time domain the noise is recognized as small fluctuations superimposed on the main pressure fluctuations. However, as the magnitude of noise s small, it is easy to identify the main dynamic caused by vortex shedding.

### 7.4.2 Bottom Surface Pressure measurments

The pressure fluctuation measured at the bottom surface is expected to be much more affected by variations in air flow rate and water film thickness. How drastic these changes will be, is hard to predict, and a good answer would require actually performing the experiment first. However, as an indication, just the passing of a wave with an amplitude of 10mm will cause pressure increase of approx. 100 Pa. This is quite a lot when considering that the pressure amplitude due to the vortex shedding will be in the range of 500-800 Pa (Hans and Windorfer 2003). In addition turbulent motion in the film, will also contribute to the total surface pressure. These pressure components stems from fluctuations in normal velocity components in the film, but compared to fluctuations in air the resulting pressure variation will be much bigger due to the large density difference between air and water. Figure 7.16a) and b) gives an idea of how the pressure measured at the bottom surface.

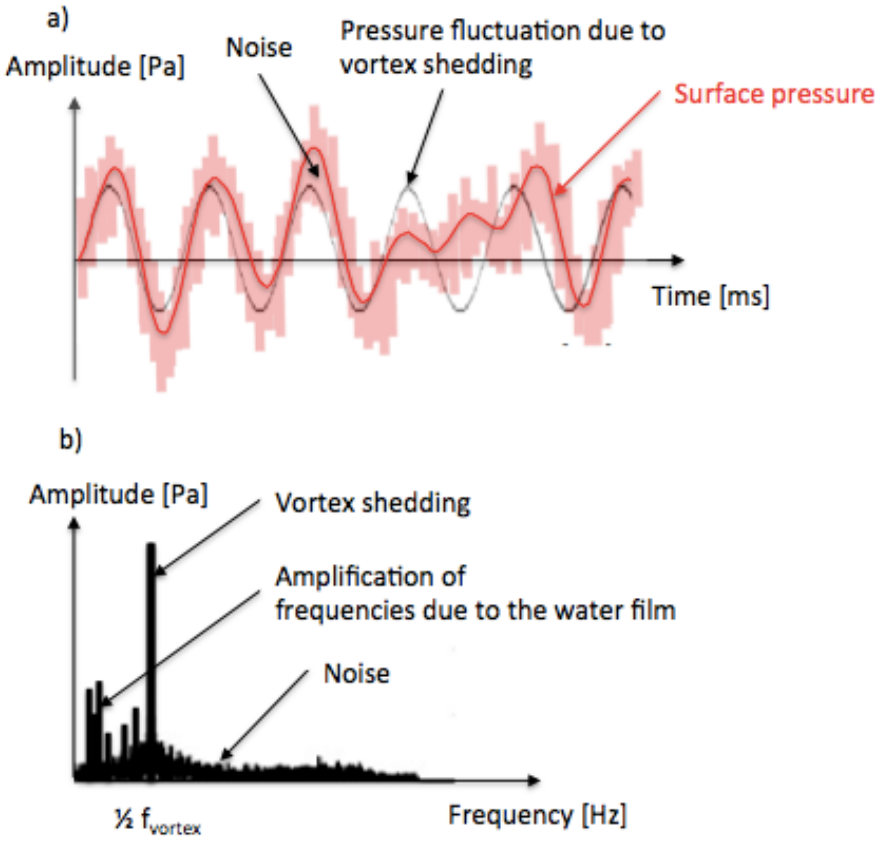


Figure 7.16: Bottom surface pressure measurement represented in a) time domain and b) frequency domain

As explained earlier in the chapter, the size of the waves and also the turbulent energy in the film increases with increasing air velocity and water film thickness. It thus follows that the water film is expected to have more impact on the surface pressure as the air flow rate and water film thickness increases. Depending on flow dynamic in the liquid film one might come across flow conditions where it becomes difficult to identify the vortex shedding frequency due to large amplification of random frequencies. The time domain representation of the pressure signal will also be very chaotic. In contrast to figure 7.15a), where the dominating pressure fluctuation in the air can be recognized, the pressure signal will seem un-periodic with random peaks and no characteristic trend. Signal filtering and averaging of the spectra of the pressure signal will help eliminating amplifications of random frequencies and signal noise, and also reveal any characteristic frequency components related to the water film.

When comparing the pressure measurements at the two surfaces the difference is expected to increase with increasing water flow rate and film thickness.

## 7.5 TESTRIG OPTIONS

### 7.5.1 USING A LOUDSPEAKER TO GENERATE PRESSURE FLUCTUATIONS

Instead of using the cylinder to generate a fluctuating pressure, a loudspeaker and an amplifier/subwoofer placed in the vicinity of the air intake could serve as the pressure generator. In contrast to the cylinder method, this alternative allows for independently controlling the pressure amplitude and frequency without having to change the air flow rate. The characteristics of the pressure signal, i.e. the frequency and the amplitude, are determined by the choice of sound and volume from the loudspeaker. This means that all types of combinations of frequency, amplitude, air flow rates and film thicknesses can be tested. By playing different sinus tones (sound with only one frequency), the frequency responses of the two pressure sensors can also be obtained, and by comparing the measurements, the influence of the liquid film, if any, can be identified. Figure 7.17 shows a simple sketch of the experimental set-up.

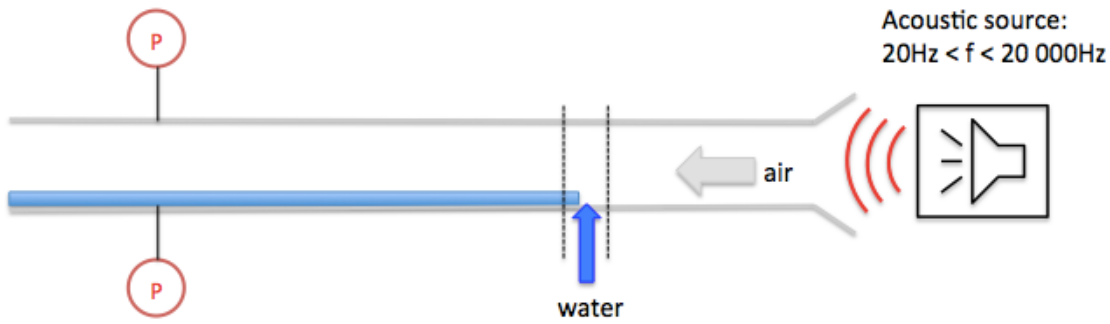


Figure 7.17: Pressure generation with loudspeaker

The loud speaker alterative was given quite a lot of attention due to the prospect of having total control of the pressure signal, and also due to the simplicity of the experimental set-up. However, as always, there are also draw-backs concerning this method. Firstly, the air flow in the test pipe will not have the same chaotic and unstable behavior that results from placing the cylinder in the flow. There will be no vortices, regions of stagnant flow, boundary layer separation or similar flow dynamics that can simulate the internal compressor flow during unstable operation. Hence the flow will not show any resemblance to the internal compressor flow, which was one of the main benefits with the cylinder option. Secondly, generating pressure oscillation with sufficient amplitudes requires high volumes. In order to generate a pressure peak of 500 Pa the volume from the loudspeaker must be approx. 150dB. This is well above the threshold of pain, and could possibly harm the ears if not proper protection is provided. In comparison the vuvuzela plastic horn, which has become a symbol of South

African football after the 2010 football world cup, can produce sound levels up to 120 dB at 1 m from the device opening. The third problem with using acoustics is the generation of vibrations especially at low frequencies. The loudspeaker produces highly periodic pressure oscillation that may coincide with the natural frequency of the compressor piping or the water supply system. If the pedestal of the acoustic source is not well isolated, the vibrations may be transmitted through the floor to test pipe and affect the performance of the pressure sensors, or alternatively induce vibrations in the liquid supply system that may affect the injection of water. Another problem is the attenuation of sound waves due to droplets in the air. Ideally there will be no droplet entrainment in the test pipe at the pressure sensor location. However, at high air flow rates, especially at the water injection point, it is reasonable to expect some droplets to be formed, and this may significantly dampen the pressure signal, in particular the sound waves of high frequency.

After comparing benefits and draw-backs attributed the two different pressure generation techniques it was chosen to focus on the method using the cylinder. However, changing between the two systems requires almost no adjustments, just removing the cylinder and placing the loudspeaker in front of the pipe. Hence, in order to obtain as much information on pressure measurement in wet gas flows, both of the method should be applied.

### 7.5.2 Testing Other Pressure Sensors

The proposed test rig can also be used to validate other pressure sensors, and testing the pressure sensor used at the wet gas impeller rig would be of particular interest. This would be very beneficial when analyzing pressure data from the wet gas compressor tests. If the pressure components induced by the water film can be excluded from the frequency spectra it will be much easier to interpret the transient pressure signature of the compressor. Four different pressure sensors, similar to those used for stall and surge detection at the wet gas impeller rig at NTNU, are listed below.

KISTLER 7031

Kistler 7031 is a piezoelectric pressure sensor for measuring dynamic and quasistatic pressures up to 250 bar at temperatures up to 200 °C. This sensor was recommended by Kyte (2013), and is equivalent to the dynamic sensor used by K-lab for measuring pressure fluctuations with amplitudes of 200-2000 mbar. Similar Kistler sensors, with a natural frequency of ~80 kHz, were also installed for unsteady pressure measurement in the diffuser in the old wet gas impeller rig at NTNU (Grüner and Bakken 2010). Figure 7.18 shows a picture of the sensor. The datasheet can be found in Appendix I.


Figure 7.18: Kistler 7031 (Kistler)

KULITE XCL-152 and KULITE XTL-190

Kulite XCL-152 and Kulite XTL-190 were recommended by Hoel (2013). Both sensors feature the leadless technology described in chapter 4.2.5. The sensors have a high natural frequency, an adequate pressure range, and are well suited for both dynamic and static measurements. The waterpower laboratory at NTNU has had good experiences with Kulite pressure sensors. They have for instance used the Kulite XTE-190 (similar to XTL-190) for measuring fluctuations in the surface pressure inside of water turbines. In these experiments the sensor was installed flush-mounted at the turbines blades. Datasheets on Kulite XCL-152 and Kulite XTL-190 are given in Appendix J and K.

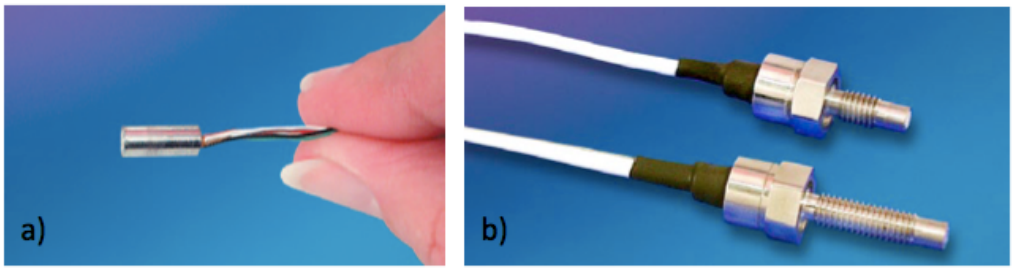


Figure 7.19: Kulite sensor a) XCL-152 and b) XTL-190 (Kulite Semiconductor Products, Inc.)

PCB MODEL 102A05

This sensor is currently being installed at the new impeller rig at NTNU. The sensor utilizes the ICP pressure probe that is shown in figure 4.3. The sensor consists of a high sensitivity acceleration compensated quartz element and an integrated current source follower amplifier joined together as an inseparable assembly. The datasheet is given in Appendix L.

Compared to the Kistler 7261A the sensors described above have a much higher pressure-range and a higher natural frequency, but they are less sensitive and have a higher threshold value. As a result, the sensor will perhaps not pick up on the smallest pressure fluctuations in the test pipe. However if the air flow rate is large enough, the main trends, i.e. passing of vortexes and large interfacial waves, should be detected. If the results obtained with the

different sensors are very contradicting, meaning that some of the sensors show much more impact from the liquid film than others, it is reasonable to assume that the performance of these sensors are directly affected by the water. Furthermore, if the results also differs significantly from the main trends in the results obtained with Kistler 7261A, there are even more indications leading towards this assumption. If this is the case, these sensors are not suitable for measuring in multiphase flows, and should not be used for pressure measurement in wet gas compressors. If using the loudspeaker configuration, the test rig may also be used to test the frequency response of the different pressure sensors. This will of course require very high volumes in order for the pressure amplitudes to be sufficiently large.

Finally, it must also be mentioned that the test rig is ideal for testing the wet gas performance of pressure sensitive paint and surface stress sensitive films. Mail and telephone correspondence with Innovative Solutions Inc. revealed that little research have been conducted on this particular topic, and it would be very interesting to investigate whether or not PSP and S3F is compatible with wet gas flows. By inserting a patch of paint or film at the bottom surface close to the pressure sensor location, the wet gas performance of the paint and the film can be determined.

# 8 WET GAS SURGE DETECTION IN SUBSEA COMPRESSORS

The useful operation range of compressors, both centrifugal and axial, is limited. By choking at high mass flow, when sonic velocity is reached in some component, and at low mass flows by the onset of rotating stall and surge. Surge and stall limits the compressor performance and efficiency, and can damage the compressor and auxiliaries due to the large thermal and mechanical loads involved. Vibration induced by unstable operation may also propagate to the rest of the compression system, and cause damage to connected pipelines. The economical consequences of surge and breakdown of the compression system are massive. In particular if the system is installed subsea. Successful implementation of subsea compressors thus depends on safe and reliable anti-surge systems that prevent the machine from unstable operation.

This chapter investigates different topics related to subsea anti-surge control in subsea wet gas compression. Focus is given surge avoidance and surge detection schemes. The chapter is divided into three main parts. The first part compares traditional and modern anti-surge techniques. The second part investigates wet gas impact on anti surge control, while the third part focus on the use of pressure measurements for surge detection in subsea wet gas compression.

## 8.1 TRADITION VS. MODERN TECHNIQUES

Surge control for industrial applications, especially in the gas transmission industry, is predominantly based on surge avoidance schemes. This is currently the safest and reliable technique. According to Gravdahl and Egeland (1999) surge avoidance is believed to be in a mature phase, with only incremental improvement emerging in the future. However, results from a patent search conducted by Helvoirt in 2007 suggest otherwise. According to van Helvoirt (2007) technological efforts focus mainly on surge avoidance techniques, and much less on surge detection methods. The most recent patents focus on specific applications, which imply that surge avoidance technology is in a research perfection stage rather than a development, matured or declining stage.

Regarding surge detection, findings of van Helvoirt (2007) indicate poor prospects for future commercial use. Even though the technique has the potential of increasing compressor efficiency and operability, the corresponding reduction in safety and reliability, have resulted in this method finding little acceptance. This is particularly true in the gas transmission industry, where system reliability and safety are of primary concern. Different compressors exhibit different behaviors and signature patterns during incipient surge. The detection techniques will therefore be specific to a certain compression system, and any attempt to implement the same technique to a different type of compressor or compression system will most likely fail. It thus follows that a major restriction in surge detection is the lack of general solution that can be applied to almost all compressors and compression system, and also work adequately over the entire operation range. Surge detection also depends on finding a proper control-value to compare the signal measured when the machine is at incipient surge. This is difficult and requires extensive compressor testing at different operating conditions (Botros and Henderson 1994).

As mentioned in chapter 3.5.4 surge detection also imposes much stricter requirements on measurement accuracy and response time for actuators and sensors. Surge detection allows for operation close to the surge line, and the time gap between sensing actual flow conditions and activating proper countermeasures are reduced to a minimum. If the time delay between detection of surge and activation of the countermeasures is too big, and/or if the mechanical components that prevent the system from surging, i.e. the anti-surge valve, react to slow, deep surge may develop before the control system is able to react.

## 8.2 WET GAS SURGE CONTROL

Surge control is obviously a challenging task, and even more so in the case of wet gas compressions. By introducing liquid in the flow, both the inception and the evolution of flow instabilities become much more complex, the liquid flow alters the gas flow due to phase interactions, and also has significant impact in the boundary layer stability. The wavy surface of liquid films increases the surface roughness experienced by the gas phase, and momentum is transferred between the phases due to droplet deposition and film atomization. In addition, there will be droplet coalescence and fragmentations, and the inertia of the liquid phase will cause acceleration and deceleration of liquid films and liquid fragments in the flow field. A fully description of the different flow mechanisms, and how they affect the stability of the machine, is currently not obtained, and this lack of knowledge is considered as a severe drawback when trying to design a surge control system. There is also a lack of a general model that corrects the compressor characteristics for variations in GMF, not to mention the

problems related to measurements in multiphase flow. Any changes in the measurement accuracy will have direct impact on the performance of the control system. If the accuracy of flow, pressure or temperature measurements are reduced, the performance of the anti surge control will be correspondingly affected. If the changes are significant, the consequences in terms of safe compressor operation may be severe. All these complications needs to be further investigated, and taken into account, in order to choose the best surge control system.

### 8.2.1 Determination of Wet Gas Surge Line

Surge control based on surge avoidance requires detailed knowledge of the location of the surge line. Compressor performance maps for dry gas compression can be predicted analytically, but the surge limit must be determined experimentally at all operating conditions. This requires a substantial amount of testing in order to cover all combinations of flow, compressor speed and pressure ratio. When liquid is introduces in the system, both the compressor characteristics as well as the surge limit will change. It has been shown experimentally that liquid presence has a tendency of delaying surge to lower flows, but detailed knowledge about how the surge line is affected by variation in GMF, is not yet obtained. There exist no correction parameter or analytical method to correct the compressor characteristics for variations in GMF, and in order to determine the wet gas surge line it thus follows that the surge limit also must be verified experimentally for all GMFs encountered. The addition of an extra process variable has a huge impact of the amount of testing needed. At all combinations of gas composition, flow rates, pressures and temperatures encountered, the compressor surge limit also needs to be tested at all possible GMFs.

Even if the wet gas surge line is determined at normal conditions, wear and tear of the machine will over time result in degradation of the compressor performance with corresponding changes in the compressor characteristic and surge limit. Liquid presence will affect how the compressor is worn, and make it very difficult to predict the effects on the surge limit. Dry gas compressors are also subjected to degradation, but due to substantial research, this field is much better understood. Several mechanisms cause the degradation of compressors (Kurz and Brun 2000):

- Fouling is caused by the adherence of particles to impeller blades and annulus surfaces. The adherence is caused by oil or water mists. The result is a build-up of material that causes increased surface roughness and to some degree changes the shape of the impeller blade.

- Hot corrosion is the loss of material from flow path components caused by chemical reactions between the component and certain contaminants, such as salts, mineral acids or reactive gases. The products of these chemical reactions may adhere to the compressor components as scale.

- Erosion is the abrasive removal of material from the flow path by hard particles impinging on flow surfaces.

- Abrasion is caused when a rotating surface rubs on a stationary surface. The material removal will typically increase seal or tip gaps.

Some of the effects, like fouling and scale, can be reversed by cleaning or washing the compressor. Others however, like erosion, abrasion or very severe fouling or scale, will require adjusting, repair or replacement of components. If the compressor is installed subsea, this is a massive task that will include shutdown of the entire compression system and elevation of the compressor. In order so save cost, the most likely scenario is therefore that the machine is kept running without repairs, adjustments or replacements until breakdown. The performance of the machine, and also the location of the surge line, is thus expected to vary substantially from start-up to shutdown. This makes surge control based on surge avoidance difficult.

### 8.2.2 Flow, Pressure and Temperature Measurements

Flow meters are routinely used in surge control systems to compare the surge line flow rate to the actual flow rate. Flow rate changes quickly when the compressor is at incipient surge, and measuring flow will therefore have a high sensitivity in detecting surge. Flow measurements are more challenging in wet gas flows compared to dry gas flows. Both gas and liquid flow rates must be determined, and this is difficult to achieve due to the non-uniform liquid distribution and the fundamental physical differences between the two phases. The industry has found the development of reliable and accurate methods a difficult task, but through extensive experimental testing, wet gas flow meter manufacturers have come up with several promising solutions. The marketed wet gas meters is typically grouped into three generic types (Trostel 2010):

- The first design uses a differential pressure meter with the additional measurement of a permanent pressure loss. The relationship between the two pressure measurements gives enough information to predict the gas flow rate and the liquid flow rate.

- The second group consist of designs using two different gas meters with different responses to wet gas flow in series. By comparing the two meter-outputs, the two flow rates can be determined.

- The last generic design is uses a differential pressure meter with phase fraction devices embedded in the meter body. The typical phase fraction devices are gamma ray, microwave and capacitance devices. By cross-referencing the output from the multiple instruments, gas and liquid flow rates, and also water rates, can be determined.

Wet gas flow meters are slower and more inaccurate than the typical dry gas flow meters. The signal need more processing, and additional algorithms must be included in the transmitter to account for the liquid fraction. This is of major concern when considering application in wet gas surge control. Due to the stringent requirements in response time and accuracy, finding a solution that meets the specifications is big a challenge. According to Bjørge (2012) multiphase meters have been tested for flow measurement in sub sea compression systems. The minimum response time achieved was around 300ms, which is three times the recommended value. However, attempting to meter wet gas flow with a dry gas flow meter can cause many problems. First of all, as the location of the surge line depends on GMF, both gas and liquid flow rates must be measured to determine the available surge margin. This is not possible with dry gas flow meters. Secondly, it has been discovered that liquid presence in a gas flow causes differential pressure meters (e.g. orifice, cone or Venturi meters) to produce a higher differential pressure than would exist if the gas flowed alone. This causes an over-measurement of the gas flow, which can extend to more than 10% (Trostel 2010). Recalling chapter 3.5.1, the surge margin is typically chosen as 10% of the surge limit flow, and that using a gas flow meter can therefore result in running dangerously close to the surge line.

Temperature and pressure at both suction and discharge must also be measured. In a surge avoidance scheme this is used alongside flow measurements, or together with the compressor speed, to determine the available surge margin. In surge control based on surge detection, monitoring variations in pressure or temperature along with time derivatives or frequency of oscillations, are typical techniques to detect the onset of unstable operation. The pressure measurements are typically made with high frequency pressure sensors, while typical temperature measurement instrumentation includes thermocouples, thermistors and resistance temperature devices (Brun and Nored 2008).

The importance of high accuracy in flow, pressure and temperature measurements was highlighted in chapter 3.5.4. As measurement uncertainty increases, the control system is at

more risk of over predicting or under predicting surge. Adding liquid to the flow increases the measurement uncertainty, and causes inaccurate and noisy measurements. If temperature and pressure measurements are provided from instrumentation installed at the pipe wall or at the inner surfaces of the compressor, the measurements will be disturbed due to impact from the liquid film. To avoid the influence from the liquid film, the sensing elements can be mounted on probes, and inserted into the core flow outside the liquid film. However, due to entrained droplets constantly hitting the probes, measurement will still be affected. The sensor openings are also at risk of being clogged by the droplets, or in the worst case destroyed by the droplet impact. Insertion types of devices are in general associated with reduced reliability, as they are more susceptible to damage (Brun and Nored 2008). Turbulence in the flow can cause the element to break off, and if the probe is installed near the compressor inlet, there is also the risk of the element being ingested by the compressor. This can cause significant damage to the machine. Insertion type of devices are therefore not suitable, particularly subsea, where robust instrumentations is needed in order to minimize maintenance.

Due to the slower response time of wet gas meters, and also the higher pressure and temperature measurements uncertainty, wet gas compressors are considered as more vulnerable to surge compared to dry gas compressors.

### 8.2.3 Choosing anti-Surge Control System

Surge control based on surge avoidance is the dominant way to coping with surge in all industrial compression systems. System safety and reliability are of primary concern, as the economical consequences associated with surge and break down of the compression system are massive. This is particularly true regarding the gas-distribution industry, where the compressors are responsible of transporting natural gas worth billions of NOK every day. The amount of variations in pressure and flow rates encountered in theses types of systems are also substantial, and consequently operating close to the surge line is a big risk.

Liquid presence introduces new challenges in the field of anti surge control. There is the problem of not knowing the exact location of the surge line at different GMF and how liquid affects performance degradation, and also the challenges associated with flow, pressure and temperature measurements in wet gas flows. All these issues will affect the performance of surge control system, and traditional methods are not necessarily the best alternative any longer. If the surge line is determined for all GMF's, increasing the surge margin can be used to compensate for the reduction in measurement quality. However, even with a large surge margin, the amount of uncertainty regarding flow, temperature and pressure measurements,

and also regarding how liquid affects stability and degradation of the machine, will still cause a significantly reduction in safety and reliability. The approach will also limit the compressor operating range and reduce the performance of the machine. Areas of high pressure rise and efficiency will be excluded from the operating envelope, which means that compression becomes more energy demanding.

Surge control based on surge detection could eliminate some of the problems mentioned above. If a general surge precursor is found, and a safe and reliable detection system is developed, this could be used instead of a traditional avoidance scheme. At the current time, no such surge precursor has been identified. Admittedly, Grüner (2012), Sørvik (2012) and also Dahl (2011), observed an expanding annulus ring of reversed water flow at the shroud side of the impeller inlet at incipient surge. However, attempting to use this as a general precursor would require substantial testing on order to validate the generality of the phenomena. Secondly, one would also need to develop reliable instruments capable of detecting this liquid ring.

The appearance of characteristic pressure fluctuations could also be used as a surge precursor. This approach is by far the most tried and tested method in detection schemes for dry gas surge control. Unfortunately it has been shown that the inception and evolution of rotating stall and surge, and thus the characteristic pressure signature at incipient surge, depends on GMF. This means that the pre-determined control variable used to recognize incipient surge must be adjusted according to GMF, which again requires accurate measurements of gas and liquid flow rates. Extensive compressor testing would be needed to establish how the surge signature varies with GMF, and regarding the problems related measuring wet gas flow rates, a detection scheme will suffer the same drawbacks as a conventional avoidance scheme. The liquid contribution to the pressure measurements is also a major drawback. If the pressure sensors are flush mounted in the compressor walls or in the inlet or discharge piping, the liquid film will contribute to the surface pressure, and affect the sensors ability to detect pressure fluctuations in the gas. Experimental results presented in chapter 6 indicate that the spectral content of the pressure signal is significantly affected by liquid, especially in the lower range of GMF. Frequency spectrum of dynamic pressure measurements obtained at the test facility for wet gas compression at NTNU rig showed amplification of random frequencies that made it almost impossible to detect the onset of unstable operation. Conducting the experiment described in chapter 7, will give a more detailed picture of the liquid contribution to the pressure measurement.

Because of the severe consequences accompanying compressor surge, particularly in the gas distribution industry and especially in subsea installations, and also due to the lack of a reliable detection system, surge control solely based on surge detection is considered too big of a risk. Despite the many drawbacks regarding surge avoidance, this approach still seems like the safest and therefore best alternative. The solution is by no means optimal, and in the future, if further research results in finding a general and easy detectable stall and surge precursor, one would benefit from changing to a detection-based system. At the time being, there is also possible to improve the avoidance scheme by using a combination of the two techniques. Surge avoidance would be the main technique, and the anti-surge valve would be opened according to the available surge margin. However, as an addition, dynamic pressure sensors could be installed in the inlet or discharge piping, or flush mounted in the compressor walls, to report on the flow conditions inside the machine. Whether liquid is present or not, prevailing flow mechanisms such as boundary layer separation, impeller and diffuser rotating stall would generate significant pressure transient in the compressor and connecting piping, and the pressure measurements could thus be used to reflect the actual condition of the flow. The lack of a general stall precursor means that the frequency spectra should not be used to control the anti-surge valve. However, by detecting the occurrence of different flow abnormalities one would be more able to estimate the lifetime of the compressor, and also to predict what type of damages to expect in the machine. This would be very beneficial when considering minimizing maintenance. The time required to repair or replace the compressor could be significantly reduced if the condition of the machine at shut down is known in forehand. By installing dynamic pressure sensors in the compression system the condition monitoring of the machine could be significantly improved. This will result in more detailed real-time condition information of the compressor, improved documentation of the historical condition progress and better diagnosis and remaining lifetime estimations. As a consequence the maintenance planning can be optimized, which again increases the production.

## 8.3 OPTIMAL SENSOR FOR STALL AND SURGE DETECTION

The 3-dimensional, turbulent and inherently unsteady nature of compressor flow fields makes pressure measurements inside centrifugal compressors a demanding task. By the addition of liquid, the flow also becomes non-homogenous, which significantly increases the flow-complexity and makes pressure measurements exceedingly difficult. Experimental results presented in chapter 6 indicate that the liquid will contribute to the pressure measurements, and therefore affect the ability of pressure sensors to detect fluctuations in the gas phase. The overall impact depends on the distribution and the dynamic behavior of the liquid phase, and will thus vary throughout the compressor. Choosing an optimal location to install the sensor is

therefore considered as key to get good measurements. The quality of the pressure measurements is a direct result of the choice of sensor. Success in using pressure to detect flow abnormalities, and to identify dynamic changes occurring in the flow field prior to rotating stall and surge, will therefore depend on choosing the correct pressure sensor.

### 8.3.1 Sensor Requirements

Many aspects must be considered before deciding upon a particular sensor. The sensor must be optimized according to the particular pressure and frequency range, and also meet specifications to external conditions. If the sensor is used outside its environmental range, the performance can be significantly reduced, and the sensor can also be damaged. In subsea installations, a high sensor stability, ruggedness and expected lifetime, is critical, and the sensor's ability to operate in harsh environments is therefore a decisive factor.
When measuring in wet gas flows there are additional challenges due to the liquid impact on the measurement, and when used in rotating machinery the pressure signal needs extra conditioning to distinguish between periodic instabilities and turbulent fluctuations. The different sensor requirements are discussed in the next paragraphs.

PRESSURE RANGE

Even though the machine should not be operated in surge, or with rotating stall present, the anti-surge system might fail, and unstable conditions occur. The pressure sensor is installed detect these situations, and indicate any flow abnormalities that could possibly harm the machine. The sensor must therefore be able to measure at all conditions, both stable and unstable. Recalling equation 3.4.1 and 3.4.2, the pressure amplitudes associated with rotating stall and surge are proportional to the fluid density and the square of the compressor speed. The amplitudes will thus vary significantly depending on the operating conditions of the machine. There pressure amplitude will also differ from rotating stall to surge, and also between the different degrees of surge. It thus follows that the sensor should have a wide pressure range to cover all possible conditions. It is difficult to suggest a specific pressure range without having any details on the compressor operating range. The Kistler sensors used at K-lab had a pressure range of 0-250 bar, and were calibrated to measure pressure fluctuations of 200-2000 mbar (Kyte 2013). However, laboratory testing and subsea installation are two very different things. In laboratory testing flow rates, and operating conditions are carefully controlled, while the variations in pressure and flow rates encountered in the transport compressors for natural gas are substantial. The requirements to the sensor pressure range will increase correspondingly.

SENSITIVITY

In order to detect flow instabilities at an early stage, and to resolve these small-scale pressure fluctuations with high accuracy, the sensor needs to be very sensitive. Results obtained at the test facility for wet gas compression at NTNU, showed pressure components with amplitudes well below 150 mbar appearing in the frequency spectrum when the compressor entered the unstable region (T. Grüner 2012).

FRENQUENCY RANGE

Rotating stall is recognized as regions of stagnant flow travelling around the circumference of the compressor at 10-90% of the shaft speed. The characteristic flow pattern induces pressure fluctuations with the same characteristic frequency, and depending on the compressor speed these frequencies may approach several hundreds of hertz. The pressure frequencies corresponding to surge are much lower. Only a few hertz compared to those of rotating stall. The pressure sensor must be able to detect all modes of unstable operations, and the frequency range must therefore at least cover the region associated with rotating stall and surge. However, boundary layer separation, turbulence and other flow phenomena may also cause amplification of higher frequency components, and in order to closely monitor the flow, the frequency range should be as wide as possible. The frequency range of a particular sensor depends on the dynamic characteristics of the sensor. In electro-mechanical pressure sensors the upper usable frequency limit is usually taken as 1/3 of the natural frequency or the resonant frequency of the sensor (Gautschi 2002). The pressure sensors used at K-lab, and also the ones installed at wet gas compressor rig at NTNU, had a natural frequency of approx. 80 kHz (Kyte 2013), (T. Grüner 2012).

ENVIRONMENTAL ENVIRONMENTS

The challenging subsea environment demands high quality equipment. Sensors intended for permanent installations must exhibit excellent long-term stability, reliability and durability. The sensors will be exposed to large variations in flow and pressure, and depending on the ocean depth the sensor will also be exposed to high absolute pressures. The sensors must function in this environment without loss of performance, and this imposes stringent requirements to robustness. Solid casings, seals and covers must be constructed in order to protect the sensing elements and internal electronics, and care must be taken when choosing the materials due to salt, dissolved $O_2$, $CO_2$ and other corrosive substances in the seawater. There will also be variations in temperature, GMF, hydrocarbon composition and water content, and the flow will also contain glycols and other substances. Furthermore, if the flow is not filtered before entering the compressor, the flow may also contain sand, wax, asphaltenes and hydrates that may damage the sensing diaphragm.

Depending on the choice of installation location, the sensor may also be exposed to high levels of vibrations. Finding pressure sensors that can operate under these conditions and still provide accurate measurements is challenging, but it is a critical part of the realization of subsea compression.

WET GAS PREFORMANCE

If the properties of the sensor, meaning the sensitivity, frequency response, linearity etc., changes when exposed to liquid, the sensor will not produce reliable measurements in a wet gas flows, and the sensor cannot be used for surge detection in wet gas compressors. However, this is not considered as a big problem, as most sensors intended for application in turbomachinery can handle both gas and liquid. Leadless technology silicon diaphragm pressure transducers can be used with any media that is compatible with stainless steel and silicon dioxide. As long as the liquid is not aggressive and causes structural damages to the sensor, the performance of the sensor is unaffected. The problems related to pressure measurements in wet gas flows are therefor generally not due to the sensor itself, and cannot be avoided by choosing a different sensor.

### 8.3.2 Choosing the Location of Pressure Sensors in Wet Gas Compressors

The choice of sensor location will also significantly affect the quality of the pressure measurements. The pressure sensor can be mounted in the inlet or discharge piping, in the diffuser wall, or in the impeller blades. It can be located in the top of the pipe, or in the bottom, at the diffuser hub side or shroud side, and at the impeller blade suction side or pressure side. Due to the large variations in the dynamic behavior of gas and liquid between the different compressor components, the measurements will vary significantly between the different installation locations. When considering measurements in the impeller, this configuration will also require means of data transmission from rotating to stationary frames.

The liquid impact on the pressure measurement will depend on the location of the sensor. By avoiding areas with large liquid fractions, and also the regions with the waviest films and the highest film turbulence, the liquid contribution to the pressure signal can be minimized. This requires detailed knowledge of the liquid distribution and the prevailing flow mechanisms and phase interactions in the different compressor components. At present time this is unknown, but future wet gas compressor testing may provide the necessary information. The new wet gas impeller currently being installed at the test facility for wet gas compression at NTNU is equipped with transparent cover plates at both the diffuser and impeller shroud, and also has a transparent inlet module. This design gives allows for visual perception of the flow field in

the different compressor components, which will be very useful to determine the liquid flow path. By adding color to the liquid it will be easier to distinguish between the different phases, and by using high-speed camera the development from stable to unstable operation can be observed in slow motion and the different flow mechanisms studied in details.

Not knowing the liquid distribution in the compressor makes it very difficult to determine where to install the sensor. However, operating compressors will in general have the sensors installed in the inlet or discharge piping, and not inside the machine. If the sensors are installed inside the machine they will be exposed to larger and more variable loads. The intensity of structural vibration will be much greater, and depending on the flow conditions the sensor may also be exposed to shocks and other extreme flow conditions. If the shock or vibration environment contains significant energy at frequencies above 1/3 the resonance frequency of the transducers, it is possible to excite the resonance of the diaphragm. Then, unless the medium provides significant damping, the diaphragm may be broken (Kulite Semiconductor Products, Inc.). Compared to installation outside the machine, the expected lifetime of sensor installed inside the machine is therefore significantly reduced.

When taking liquid effects into account, there are additional aspects that must be considered. Due to low velocities compared to those encountered in the impeller and diffuser, the film turbulence and waviness of the liquid film will be much smaller in the pipeline compared to inside the compressor. Because of gravity the liquid phase will be concentrated in the bottom of the pipe, and by installing the sensor in the top surface, the liquid contribution to the pressure measurement can be minimized. However, as explained in chapter 6.2.2, droplets entrained in the gas phase will significantly increases the attenuation of pressure fluctuations. Wet gas compressor tests at K-lab showed that acoustic signals were efficiently dissipated by liquid. In general this is a positive effect, but the phenomena might also affect the ability of the result pressure sensor to detect the characteristic pressure fluctuations of incipient surge or rotating stall. If the flow instabilities are generated in the impeller or diffuser, there is a risk of the corresponding pressure fluctuations being dampened out before reaching the sensor. This will reduce the sensors ability to detect instabilities at an early stage, as only the largest pressure amplitudes will propagate through the machine. These fluctuations will also be dampened, causing the pressure sensor to under-predict the condition of the machine. The report by Brenne et al. (2005) did not provide any results where the compressor was operated in the unstable region, and further testing should therefore investigate how, or if, liquid will significantly dampen the pressure frequencies corresponding to stall and surge. By installing pressure sensors in both the inlet and discharge piping as well as inside the machine, and then

compare the measurement at different operation conditions, the pressure attenuation through the machine can be determined.

If a very robust and durable pressure sensor were available, or for laboratory testing in, the sensors could also be installed in the diffuser wall. In the compressor tests conducted by Grüner (2012) the pressure sensors were mounted at the hub-side of the diffuser. However recalling chapter 6.1, the measurements were significantly affected by liquid. Considering all the film effect discussed in chapter 6.2.3, and also the inherently unstable compressor flow, this is not a surprise. Due to deceleration the diffuser flow is particularly vulnerable to separation, and even though the compressor is operated within the stable region this may periodically occur along the diffuser flow path. Boundary layer separation causes generation of vortexes and eddies in the gas phase, which will significantly increase the magnitude of surface waves and turbulence in the liquid film. This will affect the pressure measured at the diffuser surface, and result in amplification of random frequencies and increased amount of noise. It is very difficult to avoid these effects, but one possible solution could be to develop a sensor that measures both pressure and another parameter that corrects the pressure measurements for the liquid effects. In chapter 6.2.3 it was explained how large surface waves increases the shear measures at the solid surface. This could perhaps be utilized in a sensor. If the sensor measures both pressure and shear, variations in shear could be linked to variations in wave height, and the results could be used to eliminate the impact of the interfacial waves on the pressure measurement.

Another, and perhaps more realistic approach is to minimize the liquid impact by installing the sensor at locations where the liquid film is very thin or where the amount of film turbulence and surface waves is at a minimum. Due to inertia differences between the gas and liquid, one might expect the liquid phase to be concentrated at the hub-side rather than the shroud-side. In this case minimizing liquid impact on the pressure measurements could be realizes by mounting the pressure sensor at the shroud side of the diffuser. However, according to Bakken (2013), a liquid jet-flow corresponding to the one illustrated in figure 8.1 was observed in the wet gas compressor tests conducted at the old impeller rig. This type of flow path makes avoiding liquid very difficult. Regardless of whether the sensor is mounted in at the diffuser hub-side or shroud side, the measurements will be affected by the jet flow.

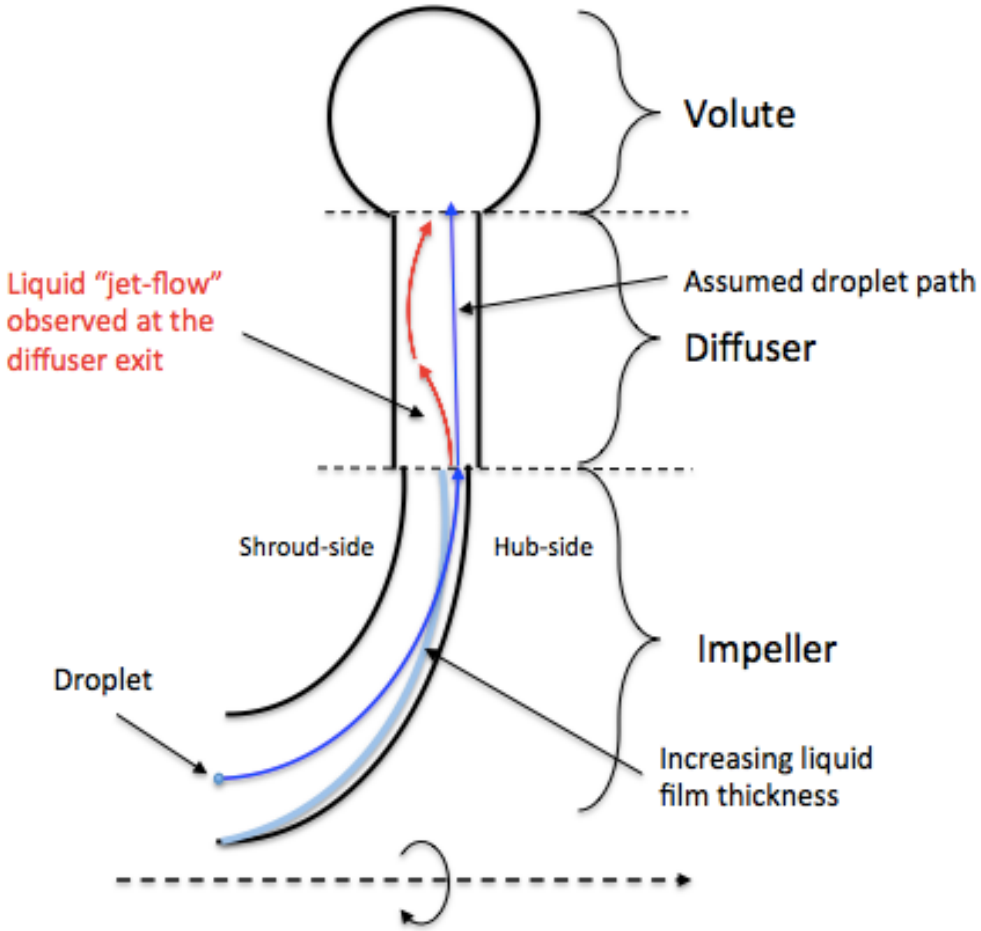


Figure 8.1: Droplet flow path

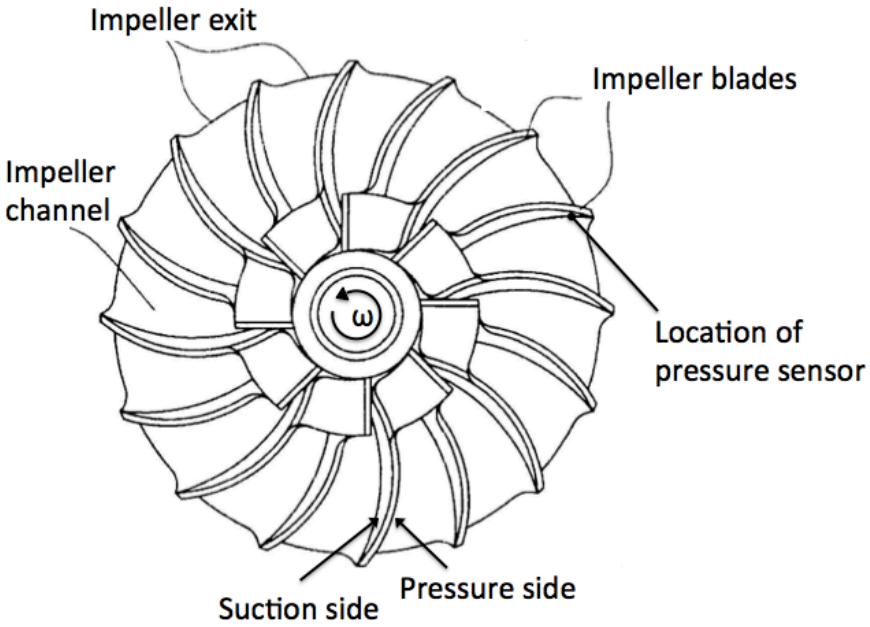


Figure 8.2: Installation of pressure sensor in the impeller

Installing the pressure sensors in the impeller is the final option. If the sensor is mounted to at the suction side of the blade in the radial portion of the impeller close to the exit, the influence of the liquid could perhaps be reduced. Figure 8.2 shows the location of the sensor. When the flow is accelerated through the impeller, the liquid droplets will be forced to deposit on the pressure side of the impeller blade. As the flow moves through the impeller, more and more of the droplets will deposit causing the liquid to be concentrated in this part of the impeller. At the suction side of the blade, close to the exit, the liquid concentration is believed to be at a minimum. This approach has not been attempted yet, and must be tested experimentally before any conclusions can be taken. It is also not considerer as suitable for industrial application, but meant as a possibility in laboratory testing.

### 8.3.3 Choice of Pressure Measurement Technique

Many instruments, with different advantages and disadvantages, have been invented to measure pressure. Pressure range, sensitivity, dynamic response and cost all vary by several orders of magnitude from one instrument design to the next, and the suitability of different sensors to a particular application will differ correspondingly. Four different measurement techniques have been explained in this thesis: Piezoelectric and piezoresistive pressure sensors were described in chapter 4, while pressure sensitive paint (PSP) and surface stress sensitive films (S3F) were introduced in chapter 5. PSP and S3F offers great advantage compared to conventional techniques since they can measure the global surface pressure. However, they are only used for laboratory testing, and not suitable for continuous monitoring and application in control systems.

Electromechanical sensors such as piezoelectric and piezoresistive pressure sensors, are the typical choice when measuring unsteady pressure in turbomachines. Both sensors offer fast response, high sensitivity, wide pressure and frequency range, good stability and ruggedness, and also the ability to withstand harsh environments without loss of performance. There are minor differences in strain sensitivity, temperature sensitivity, stability and ruggedness, but the main differences between the two sensors are the dynamic characteristics and the requirements to external power supply. Piezoelectric pressure sensors have a superior dynamic performance, and respond extremely quickly to pressure changes. They can measure quasistatic pressures, but in contrast to piezoresistive sensors, they are not able to measure truly static events. Piezoelectric sensors are also active devices, while piezoresistive sensors, on the other hand, require power from an external source to produce an output. Compared to piezoelectric pressure sensors, piezoresistive pressure sensors are also more sensitive to electric and magnetic fields, and also to radiation. When considering the liquid impact on the

pressure measurement, piezoelectric and piezoresistive pressure sensors can measure in both gas and liquid, and the choice of technique is arbitrary. The liquid contribution to the measurement is a direct result of the dynamic behavior of the liquid phase, and not related to the sensor performance. Regarding subsea applications, features like high sensitivity, wide pressure range, excellent dynamic performance, good stability, reliability and ability to withstand harsh environments, indicate that both piezoelectric and piezoresistive pressure sensors are good alternatives. The signal processing should be accomplished internal to the sensor sensors due to reductions in signal quality if the high impedance output is transmitted over long distances. However, even with internal processing, both piezoelectric and piezoresistive have inherent limitations such as transmission loss and susceptibility to noise. This makes subsea sensing a challenge.

Trying to get an overview of the state of the art of the different sensing techniques has been a real challenge. The sensor marked is large, and rapidly increasing, with numerous different sensor manufacturers and brands. Technical improvements, hybrid solutions and new techniques are constantly being developed, and attempting to identify the best sensor among thousands of different designs seems close to impossible. To narrow down the problem, it was thus chosen to focus on a few techniques, but if more time were available, fiber-optic sensing would have been added to the list. The technique uses light rather than electricity, and standard optical fiber in place of copper wire. Fiber-optic sensors have been described as excellent candidates for subsea sensing. The output signal is immune to electromagnetic interference and radio frequency interference, which gives fiber-optic sensors better remote sensing capabilities compared to those of electromechanical sensors. Fiber-optic sensors are also sensitive, robust and resistant to harsh environments, and due to their small size and cylindrical geometry, they are easy to integrate in different structures (Fidanboylu and Efendioglu 2009). Because of time constraints the technique was not investigated in this thesis, but this should be given focus in future work.

# 9 SUMMARY OF THE MAIN FINDINGS

This chapter summarizes the main findings described in this report, and presents conclusions that can be drawn from the work conducted.

## 9.1 PRESSURE MEASUREMENTS TECHNIQUES

Stall and surge are complex phenomena, and sophisticated measurement techniques are required in order to detect and investigate the different flow mechanisms involved. Incipient surge and rotating stall generate characteristic pressure frequencies, and spectral analysis of the pressure signal can therefore be used to detect and distinguish between the different instabilities. In order to capture when and where instabilities occur, and also how the instabilities develop, the pressure sensing system must be very sensitive and have a very fast response. Four different techniques have been evaluated in this report. This includes piezoelectric and piezoresistive pressure sensors, and pressure sensitive paints (PSP) and surface stress sensitive films (S3F). The different methods have different advantages and disadvantages, and the main findings are summarized below:

- Piezoelectric and piezoresistive pressure sensors have many of the same advantages. Both sensors have a very fast response, a wide pressure and frequency range and a high sensitivity. The sensors are very stable, and features both high reproducibility and high linearity. They are robust, and capable of measuring in harsh environments with little loss of performance. This makes them very reliable, and also suitable for implementation in anti-surge control systems.

  When comparing the two techniques, the difference in dynamic characteristics is most significant. Piezoelectric sensors are more sensitive and have a faster response. However, they cannot measure truly static events, and have a limited performance in the low-frequency range. This is a disadvantage in surge detection as characteristic surge frequencies are in the lower frequency range. Only a few hertz depending on the compression system. Piezoresistive sensors can measure both static and dynamic pressures.

- On the downside, piezoelectric and piezoresistive sensors are intrusive methods, and if not care is taken during installation, the sensors may disturb the flow. Furthermore, the sensors will only provide *point* measurements. Measuring the full-field pressure will therefore require arrays of embedded pressure taps, and a substantial amount of drilling in the compressor walls.

- PSP and S3F are used to measure global surface pressures. The main advantages of these two techniques are that they are non-intrusive and have a very high spatial resolution. Fast-response PSP have been used to measure unsteady pressure in centrifugal compressors, and the technique show great potential for experimental investigation of unstable compressor operations. S3F also measures shear tension, and allow for simultaneous pressure measurements and visualization of the surface flow. This is very useful, especially when investigating the physics of complex flow fields.

- On the downside, PSP and S3F have a slower response, and are also less sensitive when compared to piezoelectric and piezoresistive pressure sensors. They will therefor have a more limited frequency range, and provide less accurate measurements. However, the techniques are in an early stage of development, and improvements are expected in the future. The PSP and S3F methods require optical access to the model surface and an imaging device of high pixel resolution. The techniques are not meant for continuous monitoring and cannot be implemented in control systems.

## 9.2 LIQUID IMPACT ON PRESSURE MEASUREMENTS IN WET GAS FLOWS

The initiation and evolution of rotating stall and surge are highly complicated. The two phenomena are well investigated in dry gas compression, but when considering wet gas compression, the experimental and theoretical foundation is very limited. Experimental results from the test facility for wet gas compression at NTNU indicate that the liquid has a stabilizing effect on the compressor. The compressor was instrumented with flush-mounted piezoresistive pressure sensors in the diffuser wall, and spectral analysis of the pressure signal showed that the liquid presence causes the instabilities to be delayed to lower flow rates, and altered the evolution of the instability. However, the results also revealed a significant amplification of random pressure frequencies in the lower frequency-range. The magnitude of the amplification increased with liquid fraction, and was dominating the frequency spectrums at low GMFs. Frequencies of higher amplitudes were dampened out. This observation

suggests that the liquid may cause suppression and/or enhancement of certain frequencies, and also introduce additional frequencies that are specifically related to the dynamic characteristic of the liquid phase. This may cause misinterpretation of wet gas frequency spectra, and effort must therefore be made to determine how liquid affects pressure and pressure measurements in wet gas flows. A literature study was conducted in order to identify different multiphase mechanisms that may influence the pressure. Liquid impact on the performance of the pressure measuring system was also investigated. The most important findings are summarized below:

- The dense droplet fields in annular flows have significant impact on the propagation of pressure pulses in wet gas flows. The pressure pulses will be attenuated due to viscous effect between the different phases. High frequency components will be most affected, but experiments have also shown significant dampening of frequencies down to 100 Hz. This is important when considering stall and surge detection. If the pressure sensor is located away from the source of the instability, the dampening may cause the pressure pulse to die out before it reaches the sensor.

- The presence of the liquid film is believed to be the main reason of the amplification of random frequencies. The dynamic behavior of the film, i.e. surface waves, film turbulence and fluctuating normal velocity components, will generate additional pressure components and significantly affect the pressure measurement at the compressor surface. The magnitude and size of the surface waves is of particular importance. Large waves will have significant impact on the film flow structure close to the solid wall, and also increase the turbulent intensity in the film. Large surface waves are will generate large eddies in the film, which again results in large normal velocities in the film.

  It has also been shown that wavy films can introduce occasional instabilities in the gas. Flow separation may appear near the troughs of larger interfacial waves, and this may induce significant fluctuations in the local gas phase velocity, and generate corresponding fluctuations in the pressure.

- The performance of piezoelectric and piezoresistive sensors is not affected by the liquid phase. As long as the senor is properly installed, and the acting fluid do not cause corrosion or in other ways harms the sensor material, the sensors should not be affected by liquid. The sensitivity, linearity, response time and so on, will thus be the same whether the acting fluid is a gas or a liquid. However, even though the sensor itself is

unaffected by liquid, liquid presence may amplify the effects of poor mounting and also cause increased levels of flow-induced vibrations. These effects are not directly related to the sensor performance, but will indirectly affect the measurements.

- The performance of PSP will be significantly reduced by the presence of liquid. The pressure measurement is based on the paint response to changes in oxygen concentration at the painted surface, and anything that impedes $O_2$ migration to the surface will therefore affect the measurement. The presence of the liquid film will result in a slower response, and a reduced sensitivity. Fast response PSP has not been tested in wet gas flows, but the prospects of applying the method in wet gas compression are poor.

- The performance of S3F is not directly affected by liquid, but the liquid film and the droplet field will cause reduced optical access to the test surface. However, if the film is applied on the back of the transparent cover, the problems may be avoided.

The physical consequences of the liquid phase cannot be avoided by choosing a different pressure sensor. Furthermore, when the sensor is installed at the compressor surface, it will measure the actual pressure beneath the liquid film, and cannot distinguish between the pressure fluctuations in the gas phase and the contribution from the liquid film. The guidelines used to predict and distinguish between rotating stall and surge are based on characteristic flow patterns in the gas phase. In order to apply these guidelines in wet gas compression, it is therefore important to eliminate the influence from the liquid, or at least be able to recognize the pressure components that are specifically related to the liquid phase. This will require detailed knowledge how liquid, and the different phase interactions between gas and liquid, affects pressure measurements in the wet gas flow. The literature search gave some information, but only indicated general trends. The behavior of the liquid phase, hence the impact on the pressure, will differ significantly depending on the flow regime and also the physical properties of the gas and liquid. Extensive wet gas testing will therefore be necessary to explore the different phenomena. The experiment described in chapter 7 is one step in this direction. The experiment will give a better understanding of how a thin liquid film will affect measurement of surface pressure in wet gas flows, and thus will be very valuable when investigating stall and surge phenomena in wet gas compressors in the future.

## 9.3 LIQUID IMPACT OM ANTI-SURGE CONTROL IN SUBSEA COMPRESSORS

The economical consequences from surge and failure in the compression system are massive. In particular if the system is installed subsea. Safe running of the compressor thus depends on reliable anti-surge systems preventing the compressor from unstable operations. There are three main methods for dealing with surge: surge avoidance, surge detection and surge suppression. Surge avoidance is the safest and most conservative technique. The compressor operating point is kept in a safe distance away from the surge line by applying an appropriate surge margin. The surge margin significantly limits the capabilities of the compressor. The peak pressure rise for constant speed, representing the peak performance of the compressor, is located close to the surge line and cannot be reached when the safety margin is introduced. Regions of high efficiency lie close to, or may even encompass the surge line, and are also excluded from the operating envelope. However, due to requirements in safety and reliability, surge control for industrial applications, especially in the gas transmission industry, is predominantly based on this technique.

Due to the complex nature of the aerodynamics in the centrifugal compressor, surge control is a challenging task. However, when liquid is introduced in the flow the situation is even worse. Liquid changes the inception and evolution of the instabilities, but a fundamental understanding of the different multiphase mechanisms, and how they affect compressor stability is currently missing. This is a major drawback when trying to design a surge control system. Liquid presence will also introduce other problems, and those described in this report are summarized below:

- In order to determine the available surge margin, the surge limit must be known. In wet gas compression the location of the surge line will depend on the liquid fraction, and there exist no correction parameter or analytical method to correct the compressor characteristics for variations in GMF. The surge limit must be verified experimentally at all operating conditions, and this will require extensive testing.

- Even if the wet gas surge line is determined at normal conditions, wear and tear of the machine will over time result in degradation of the compressor performance with corresponding changes in the compressor characteristic and surge limit. Liquid presence will affect how the compressor is worn, and make it very difficult to predict the effects on the surge limit.

- Liquid reduces the accuracy of flow, pressure and temperature measurements. These process variables are used to determine the compressor operating point, and accurate measurements are essential in order for the surge control system to work properly.

The problems just listed will significantly reduce the performance of the anti surge system. In particular a surge avoidance scheme, which depends on both accurate knowledge of the surge line, and accurate knowledge of the operating point. However, the alternatives are not better. Surge control based on surge detection requires a general surge precursor, and a reliable detection system, and this is not developed for wet gas compressors. Despite the drawbacks regarding surge avoidance, this approach is therefor the safest alternative. However, as an addition to the avoidance scheme, dynamic pressure sensors could be installed in the compression system to improve the condition monitoring of the machine. This would give more detailed real-time condition information of the compressor, an improved documentation of the historical condition progress, and a better diagnosis and remaining lifetime estimation. As a consequence the maintenance planning could be optimized, which would increases the running time of the compression system.

The harsh subsea environment, and also the need for a permanent solution that can operate without loss of performance for a long period of time, imposes stringent requirements to pressure sensor robustness. The sensor should also be sensitive, and have a large frequency and pressure range to report on all types of instabilities in the compressor flow. The location of the sensor is also important. When considering liquid impact on the pressure measurement, the sensor should be installed in regions where the liquid film is very thin or where the amount of film turbulence and surface waves is at a minimum. At the same time, due to attenuation of pressure pulses in wet gas flows, the sensor should not be located to far from where the instabilities originate. The typical choice would be to install the sensor in the inlet or discharge piping. This is beneficial both in terms of environmental impact and the impact from the liquid film, but not when considering pressure pulse attenuation. Another possibility would be to install the sensor inside the compressor. This however requires an extremely robust sensor, and also knowledge of the liquid distribution inside the machine. Finding a reliable sensor that meets all these requirements is a challenge. However, this is a challenge that must be overcome in order to ensure that the sub sea compressors can be relied upon to operate continuously in deep water for long periods of time. Piezoresistive or piezoelectric sensors is one possibility, but theses sensors have inherent limitation such as transmission loss and susceptibility to noise that makes remote sensing a challenge.

# 10 RECOMMENDED WORK AND CONCLUDING REMARKS

Identifying problems and asking questions forms the basis for all development and innovative thinking, and is an important part of doing research. In many ways this thesis has led to more questions than answers, and in the process of writing the report several areas in need of more research have been identified. However, some problems are more critical than others, and should be prioritized:

- The liquid impact on pressure and pressure measurements in wet gas flows must be determined. The dynamic behavior of both gas and liquid phases will contribute to the pressure signals, and in order to indicate the aerodynamic conditions in the compressor, it is necessary to distinguish between the different contributions. The experiment described in chapter 7 is one step in this direction. Performing this experiment, and also plan and conduct other experiments that investigate pressure fluctuations in wet gas flows, should have high priority. The presence of the liquid film is believed to be most significant if the pressure sensors are installed inside the compressors. If the sensors are installed in the pipeline in the vicinity of the compressor, attenuation of the pressure pulses due to the dense droplet field will be of more concern. Both phenomena should be explored.

- Only four different pressure measurement techniques have been described in this report. In order to come up with an optimal solution, both for continuous monitoring of subsea compression systems and for application in laboratory testing, more techniques should be evaluated. As previously mentioned, fiber-optic sensors is a technique with great prospects. Optical fibers are used for temperature measurements in subsea cables, and the technology can also be used to measure the pressure.

- Determination of how the liquid distribution inside the compressor is also considered as essential to the development of wet gas compressors. Knowledge of the droplet flow path and development and dynamics of the liquid film will significantly improve the understanding of wet gas stall and surge, and also be key when choosing the best location to install pressure sensors and other measuring devices. Incipient surge and rotating stall

is expected to affect the dynamic characteristics of the liquid phase and change the liquid flow path through the compressor. Identification of characteristic changes in the liquid distribution could therefore be used as new guidelines to predict and distinguish between different modes of compressor operations.

During the literature search the author came across some interesting YouTube videos that really showcase how a liquid may respond to changes in external conditions. The videos show the characteristic behavior of a liquid jet when exposed to pressure oscillations of variable frequencies and amplitudes. The videos is by no means modeling the flow inside the compressor, but it is still interesting to see how only small changes in pressure can cause significant changes in the liquid flow. The video also suggests that vibrations in the compressor may induce characteristic patterns in the liquid phase. The link to one of the videos can be found in the Bibliography

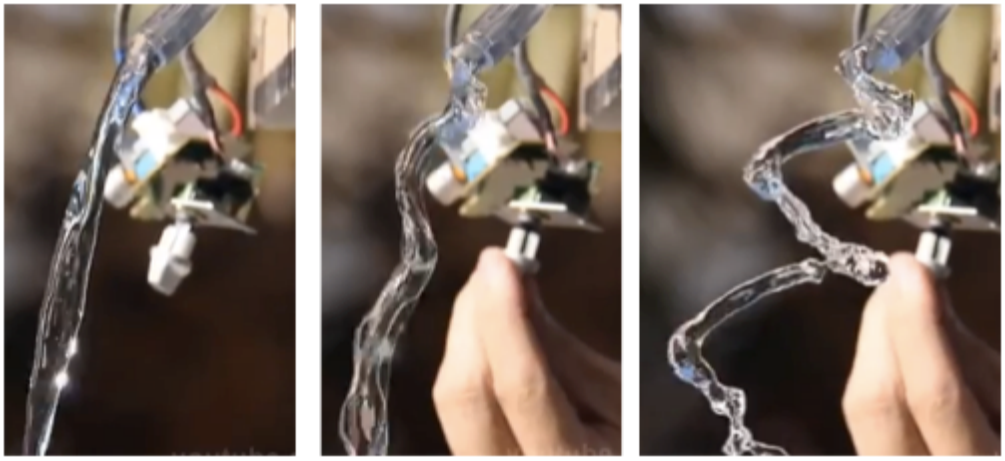

Figure 10.1: Liquid response to pressure oscillations with increasing amplitude (YouTube)

# 11 Bibliography


Abe, S., K. Okamoto, and H. Madrame. "The Development of PIV–PSP Hybrid System Using Pressure Sensitive Particles." *Measurement Science and Technology* (Institute of Physics Publishing) 15, no. 6 (2004).

Ahmed, S. A. "Control of Stall in Radial Diffuser Using Rough Surfaces." *Canadian Aeronautic Space Journal* 54, no. 1 (2008).

Asali, J. C. , and T. J. Hanratty. "Ripples Generated on a Liquid Film at High Gas Velocities." *International Journal of Multiphase Flow* (Pergamon Press Ltd.) 19, no. 2 (1993).

Tropea, C., A. L. Yarin, and J. F. Foss. *Handbook of Experimental Fluid Mechanics.* Springer, 2007.

Bakken, L. E., interview (meetings at NTNU) by M. R. Jellum. (Spring 2013).

Barlian, A. Alvian, Woo-Tae Park, Joseph R. Mallon Jr, Ali J. Rastegar, and Beth L. Pruitt. "Review: Semiconductor Piezoresistance for Microsystems." *Proceedings of the IEEE* (IEEE, Institute of Electrical and Electronics Engineering) 97, no. 3 (March 2009): 513-552.

Bertin, J. J., and R. M. Cummings. *Aerodynamics for Engineers.* 5th Edition. Pearson International, 2009.

Bjørge, T., interview (meeting at NTNU) by M. R. Jellum. (November 2012).

Botros, K. K., and J. F. Henderson. "Developments in Centrifugal Compressor Surge Control - A Technology Assessment." *Journal of Turbomachinery* (ASME) 116, no. 2 (April 1994): 240-249.

Boyce, M. P. *Gas Turbine engineering Handbook.* 3rd Edition. Gulf Professional Publishing, 2001.

Boyce, M. P. "Principals of Operation and Performance of Centrifugal Compressors." *The 22nd Turbomachinery Symposium.* Dallas, 1993.

Bratland, O. *Pipe Flow 2 - Multiphase Flow Assurance.* 2010.

Brenne, L., T. Bjørge, J. L. Gilarranz, J. M. Koch, and H. Miller. "Performance Evaluation of Centrifugal Compressor Operating Under Wet Gas Conditions." *The 34th Turbomachinery Symposium.* Houston, 2005.

Brennen, C. E. *Fundamentals of Multiphase Flow.* Cambridge University Press, 2005.

Brun, K., and M. G. Nored. *Application Guideline for Centrifugal Compressor Surge Control Systems.* Gas Machinery Research Council, 2008.

Buckles, J. J., T. J. Hanratty, and R. J. Adrian. "Separated Turbulent Flows over a Small Amplitude Wave." *The 2nd International Symposium on Applications of Laser Anemometry to Fluid Mechanics.* 1985.

Chenquan, H., W. Changming, G. Yanfeng, and S. Tianming. "Noninvasive Flow Regime Identification for Wet Gas Flow Based on Flow-Induced Vibration." *Chinese Journal of Chemical Engineering* 18, no. 5 (2010).

Cumpsty, N. A. *Compressor Aerodynamics.* Longman Scientific and Technical, 1989.
de Jager, B. "Rotating Stall and Surge Control: A survey." *The 34th Conference on Decision and Control.* New Orleans, 1995.

Dou, H. S., and S. Mizuki. "Analysis of the Flow in Vaneless Diffusers with Large Width-to-radius Ratios." *Journal of Turbomachinery* (ASME) 120, no. 1 (1998).

Falk, K. "Pressure Pulse Propergation in Gas-Liquid Pipe Flow; Modeling, Experiments and Field Testing." PhD Thesis, Department of Petroleum Engineering and Applied Geophysics, NTNU, 1999.

Ferrara, G., L. Ferrara, and L. Baladassarre. "Rotating Stall in Centrifugal Compressor Vaneless Diffuser: Experimental Analysis of Geometrical Parameter Influence on Phenomenon Evolution." *International Journal of Rotating Machinery*, 2004.

Fidanboylu, K., and H. S. Efendioglu. "Fiber Optic Sensors and Their Application." *5th International Advanced Technology Symposium*, May 2009.

Fonov, S., G. Jones, J. Crafton, V. Fonov, and L. Goss. "The Developmemt of Optical Techniques for Measurements of Pressure and Skin Friction." *Measurement Science and Technology* (Institute of Physics Publishing) 17, no. 6 (2006).

Forelines, A., interview (mail correspondance and phone call) by M. R. Jellum. *Innovative Solutions. Inc* (February 2013).

Fraden, J. *Handbook of Modern Sensors.* 3rd Edition. Springer, 2004.
Gautschi, G. *Piezoelectric Sensorics.* Springer, 2002.

Gravdahl, J. T., and O. Egeland. *Compresor Surge and Stall - Modeling and Control.* Springer, 1999.

Grüner, T. G. , L. E. Bakken, L. Brenne, and T. Bjørge. "An Experimental Investigation of Airfoil Perfomance in Wet Gas Flow." *ASME Turbo Expo 2008.* Berlin: ASME, 2008. 575-584.

Grüner, T. G. *Wet Gas Compression.* PhD Thesis, NTNU, Trondheim: NTNU, 2012.

Grüner, T. G., and L. E. Bakken. "Wet Gas Impeller Test Facility." *ASME Turbo Expo 2010: Power for Land, Sea and Air.* ASME, 2010.

Gregory, J. W. "Unsteady Pressure Measurements in a Turbocharger Compressor Using Porous Pressure-Sensitive Paint." MSc Thesis, Department of Aeronautics and Astronautics, Purdue University, 2002.

Gregory, J. W., and J. P. Sullivan. "Effect of Quenching Kinetics on Unsteady Response og Pressure-Sensitive Paint." *American Institute of Aeronautics and Astronautics (AIAA)* 44, no. 3 (March 2006).

Gregory, J. W., K. Asai, M. Kameda, T. Liu, and J. P. Sullivan. "A Review of Pressure-sensitive Paint for High-speed and Unsetady Aerodynamics." *Proceedings of the Institution of Mechanical Engineers.* SAGE publications, 2008.

Gyarmathy, G., A. Inderbitzin, and T. Staubli. 2000. http://www.hslu.ch/t-fmf_2000_visualization_rotating_stall_full_size_water_model_singlestage_centrifugal_compressor.pdf (accessed Mars 2013).

Hagiwara, Y., E. Esmaeilzadeh, H. Tsutsui, and K. Suzuki. "Simultaneous Measurement of Liquid Film Thickness, Wall Shear Stress and Gas Flow Turbulence of Horizontal Wavy Two-Phase Flow." *International Journal of Multiphase Flow* (Pergamon Press) 15, no. 3 (1988).

Hans, V., and H. Windorfer. "Comparison of Ultrasound and Pressure Measurements in Vortex Flow Meters." *Measurement* (Elsevier) 33, no. 2 (2003).

Hayami, H., M. Hojo, M. Matsumoto, S. Aramaki, and K. Yamada. "Application of Pressure Sensitive Paint Measurement to a Low-Solidity Cascade Diffuser of a Transonic Centrifugal Compressor." *Journal of Visualization* (The Visualization Society of Japan and Ohmsha, Ltd.) 5, no. 1 (2002).

Heeley, D. *Understanding Pressure and Pressure Measurements.* Application note, Freescale Semiconductor, 2005.

Heseltine, J. L. *Flow Around a Circular Cylinder With a Free End.* MCs Thesis, Department of Mechanical Engineering, University of Saskatchewan, University of Saskatchewan, 2003.

Hoel, C. O., interview (mail correspondance and meeting at NTNU) by Marie Rennemo Jellum. *Coba Måleteknikk AS* (February 11, 2013).

Innovative Scientific Solutions, Inc. http://www.psp-tsp.com/index.php?id=135 (accessed Mars 2013).

Innovative Sientific Solutions, Inc. http://www.psp-tsp.com/pdfs/Pressure-Sensitive%20Paint.pdf (accessed February 2013).

Ishide, M., D. Sakaguci, and H. Ueki. "Suppression of Rotating stall by Wall Roughness Control in Vaneless Diffusers of Centrifugal Blowrs." *Journal of Turbomachinery* (ASME) 123, no. 1 (2000).

Jellum, M. R. "Wet Gas Compressor Stall and Surge." Project Thesis, Department of Energy and Process Engineering, NTNU, 2012.

Kang, J.-S., and S.-H. Kang. "Stall Inception in a Vaneless Diffuser of a Centrifugal Compressor." *ASME Turbo Expo 2003.* Atlanta: ASME, 2003. 693-701.

Karimi, G., and M. Kawaji. "Flow Chracteristics and Circulatory Motion in Wavy Falling Films With and Without Counter-Current Gas Flow." *International Journal of Multiphase Flow* (Elsevier Science Ltd.) 25 (1999).

Kimura, F., et al. "Dual Luminophore Polystyrene Microspheres for Pressure-Sensitive Luminescent Imaging." *Measurement Science and Technology* (Institute of Physics Publishing) 17, no. 6 (2006).

Kistler. http://www.kistler.com/no/en/innovation/technology/piezoresistivetechnology (accessed February 2013).

Kon, S., K. Oldham, and R. Horowitz. "Piezoresistive and Piezoelectric MEMS Strain Sensors for Vibration Detection." *Sensors and Smart Structures Technologies for Civil, Mechanical, and Aerospace Systems.* SPIE, 2004.

Kulite Semiconductor Products, Inc. http://www.kulite.com/technology.asp?p=2-6 (accessed February 2013).

Kurz, R., and K. Brun. "Degradation in Gas Turbine Systems." *Journal of Engineering for Gas Turbines and Power* (ASME) 123, no. 1 (November 2000).

Kyte, J., interview (mail correspondance) by M. R. Jellum. *Scanditest Norge AS* (January 2013).

Leighton, T. G., J. Jiang, and K. Baik. "Demonstration Comparing Sound Wave Attenuation Inside Pipes Containing Bubbly Water and Water Droplet Fog." *Journal of Acoustical Society of America* (Acoustical Society of America) 131, no. 3 (2012).

Lin, J.-C., and D. Rockwell. "Organized Oscillation of Initailly Turbulent Flow Past a Cavity." *Journal of the American Instritute of Aeronautics and Astronautics* 39, no. 6 (2001).

Liu, C. *Foundation of MEMS.* 2nd Edition. Pearson Eductaion, Inc., 2006.

Mandhane, J. M., G.A. Gregory, and K. Aziz. "A Flow Pattern Map for Gas-Liquid Flow in Horizontal Pipes." *International Journal of Multiphase Flow* (Pergamon Press) 1, no. 4 (1974).

MITOpenCourseWare. http://www.flickriver.com/photos/mitopencourseware/4150128499/ (accessed April 2013).

Nabavi, M. "Unsteady and Pulsating Pressure and Temperature: A Riview of Experimental Techniques." *Scientific Instruments* (The American Institute of Physics), 2010.

Navarra, K. R. "Development of the Pressure-Sensitive-Paint Technique for Advanced Turbomachinery Applications." McD Thesis, Department of Mechanical Engineering, Virginia Polytechnic Institute and State University, 1997.

Norwegian Petroleum Directorate. http://www.npd.no/en/Publications/Facts/Facts-2012/Chapter-7/ (accessed May 2013).

Nu-Way Energy. http://www.nuwayenergy.co.nz/product-range/roots-api-617-type-h-centrifugal-compressor (accessed May 2013).

Orkisz, M., M. Wnek, Joerg P., K. Ruetten, and E. Jellum. "Selected Data Analysis Techniques for Equipment Monitoring Using Drive's Control Signals." *International Symposium on Diagnostics For Electrical Machines, Power Electronics and Drives.* 2009.

Palluconi, S., interview (mail correspondance) by M. R. Jellum. *Innovative Solutions Inc.* (February 2013).

PCB Piezotronics. http://www.pcb.com/TechSupport/tech_gen (accessed Janury 2013).

Saravanamuttoo, H. I. H., G. F. C. Rogers, H. Cohen, and P.V. Straznicky. *Gas Turbine Theory.* 6th Edition. Pearson International, 2009.

Sørvik, L. A. "Validation of Wet Gas Surge Phenomena." MSc Thesis, NTNU, 2012.

Schlichting, H., and K. Gersten. *Boundary Layer Theory.* 8th Edition. Springer, 2000.

Shakouchi, T., D. Tian, and T. Ida. "Behaviour of Vertical Upward Gas-Liquid Two-Phase Flow Past Obstacle in Rectangular Channel (Effect of Blockage Ratio)rectangular." *International Journal of the Japanese Society of Mechanical Engineering* 45, no. 3 (2002).

Thermal-FluidsCentral. https://www.thermalfluidscentral.org/encyclopedia/index.php/Pressure_measurements_and_instrumentation (accessed May 2013).

Trostel, B. "Solving the Wet Gas Flow Measurement Challenge." *Pipeline & Gas Journal* 237, no. 7 (2010).

Tsung, T.-T., and L.-L. Han. "Evaluation of Dynamic Performance of Pressure Sensors Using a Pressure Square-like Wave Generator." *Measurement Science and Technology* (Institute of Physics Publishing) 15, no. 6 (2004).

Tri-Sen Turbomachinery Controls. http://tri-sen.com/2012/06/08/incipient-surge-in-a-centrifugal-compressor/ (accessed February 2013)

van Helvoirt, J. "Centrifugal Compressor Surge, Modeling and Identification for Control." PhD Thesis, Eindhoven University of Technology, 2007.

Wilson, J. *Sensors.* http://www.sensorsmag.com/sensors/pressure/pressure-measurement-principles-and-practice-969 (accessed May 2013).

*YouTube.* http://www.youtube.com/watch?v=3BdVxxEhKgo (accessed Mars 2013).

Zilker, D. P., and T. J. Hanratty. "Influence of the Amplitude of a Solid Wavy Wall on a Turbulent Flow, Part 2, Separated Flows." *Journal of Fluid Mechanics* (Cambridge University Press Ltd.) 90, no. 2 (1979).

# APPENDIX

## A) BOUNDARY-LAYER SEPARATION

In physics and fluid mechanics, a boundary layer is the layer of in the immediate vicinity of a bounding surface where the effects of viscosity are significant. According to theory, boundary layer separation may occur when a flow is subjected to an adverse pressure gradient. If the boundary layer travels far enough against an adverse pressure gradient the speed of the boundary layer relative to the solid surface may fall to almost zero. The fluid flow becomes detached from the surface, and instead takes the forms of eddies and vortices (Schlichting and Gersten 2000). The compressor flow is vulnerable to boundary layer separation. The static pressure increases through the machine, which means that the flow will experience an adverse pressure gradient. When boundary layer separation occurs, being in the diffuser or in the blading in the impeller, the compressor performance drops due to increased friction causing a loss of kinetic energy. The stability of the machine is also affected due to a degraded aerodynamic performance.

### THEORETICAL FOUNDATION

Boundary layer separation is primarily caused by an adverse pressure gradient that is imposed on the boundary layer by the outer invicid flow. The location of the separation is governed by the pressure distribution in the outer flow and friction at the wall. The phenomenon can be explained by considering the flow past a blunt body, for instance a circular cylinder. This is illustrated in figure A.1.

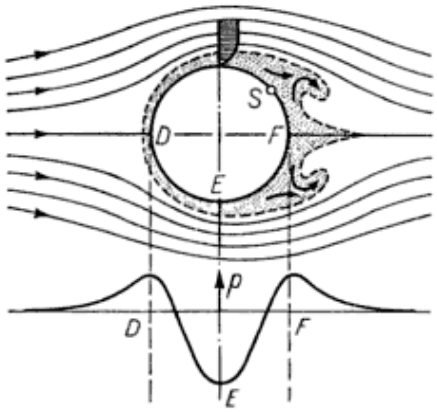


Figure A.1: Separation of the boundary layer and vortex formation at a circular cylinder (Schlichting and Gersten 2000)

A particle within the boundary layer experiences the same pressure distribution as the invicid outer flow, and the freestream pressure therefore gives the pressure distribution around the cylinder. The flow is accelerated from point D to E, and decelerated from E to F. The pressure distribution around the body is obtained by substituting the velocity field of the outer flow into the Bernoulli equation. Moving from D to E pressure is transformed into kinetic energy, resulting in an favorable pressure gradient. From E to F, kinetic energy is transformed into pressure again, which gives an adverse pressure gradient. A particle within the boundary layer, especially the particles directly at the wall, will also be subjected to strong frictional forces. In figure A.1 the particle at the wall looses so much of its kinetic energy to friction that it cannot manage to get over the "pressure mountain" from E to F. It is retarded, becomes standstill, and is then pushed into backwards motion by the pressure distribution of the outer flow. The process changes the flow portrait at the back of the cylinder with vortexes forming from the reversed flow. The pressure distribution is also drastically changed (Schlichting and Gersten 2000).

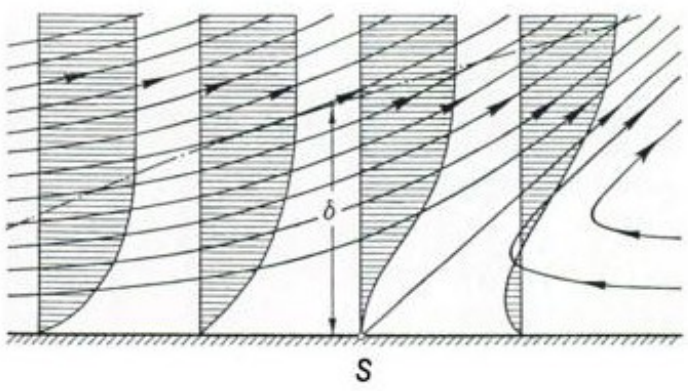


Figure A.1: Boundary-layer separation (Schlichting and Gersten 2000)

Figure A.2 illustrates the flow portrait close to separation. As a result of the backflow close to the wall, a strong thickening of the boundary layer takes place. Boundary layer mass-flow is transported into the outer flow, and then accelerated. Kinetic energy is transferred from the outer flow to the separated boundary layer, and thus causes the overall effect of decelerating the invicid outer flow. The position of separation is given by the condition that the velocity gradient perpendicular to the wall vanishes, i.e. the wall shear stress $\tau_w$ is zero. This is expressed mathematically in equation A.1 (Schlichting and Gersten 2000).

$$\tau_w = \mu \left(\frac{\partial u}{\partial y}\right)_w = 0 \qquad (A.1)$$

FLOW SEPARATION IN CHANNEL FLOWS

Boundary layer separation can also occur for internal flows. It can result from such causes such as a rapidly expanding duct of pipe. Separation occurs due to an adverse pressure gradient encountered as the flow expands. In order to satisfy the continuity equation, the velocity must drop when the cross-sectional area increases. In the outer flow, the kinetic energy is transformed to pressure, thus pressure increases in the direction of the flow. This is exactly what happens in the diffuser. The flow within the boundary layer experiences the same pressure increase as the outer flow, but due to strong friction forces at the wall it may not be able to overcome the adverse pressure gradient. If the channel expands too rapidly, thus causing a too steep pressure gradient, the flow will separate. Figure A.3 and A.4 illustrates channel flow without separation and with separation respectively. This corresponds to a diffuser with good and bad performance.

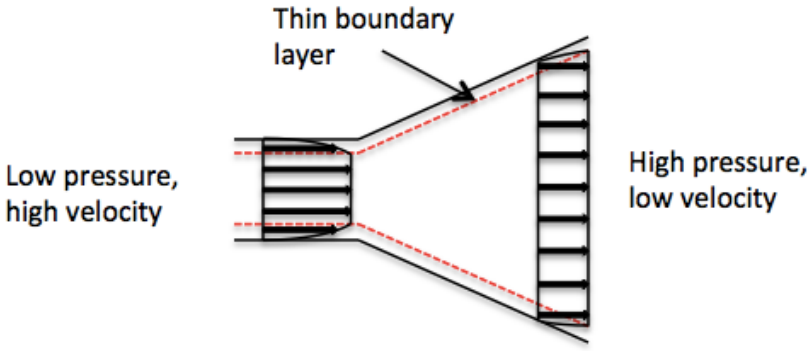


Figure A.2: Diffuser with good performance, i.e. diverging channel without separation

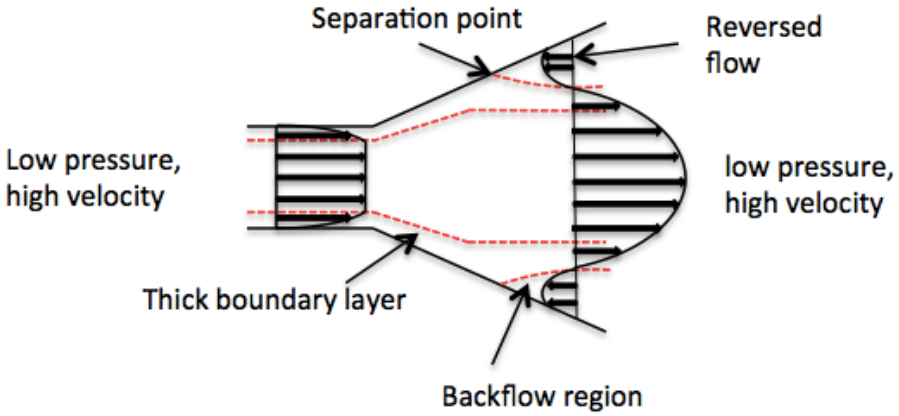


Figure A.3: Diffuser with poor performance, i.e. diverging channel with separated boundary layer

BOUNDARY LAYER SEPARATION IN FLOW PAST AIRFOIL

Boundary layer separation may also occur in flow past airfoils, or in the blading in the impeller channels. The same theory as for flow past a circular cylinder or flow in a diverging channel can be applied in order to explain the phenomena. The curvature of the upper surface of the blade results in a favorable pressure gradient in the frontal part, and an adverse pressure gradient at the rear end. At small angles of attack, as illustrated in picture a) in figure 3.6, the flow past the airfoil stays attached at both lower and upper side. The kinetic energy of the boundary layer is big enough to overcome both the friction, and the adverse pressure gradient at the trailing edge. As the angle increases, the expansion, and thus the pressure gradient increases. It becomes too steep, and the boundary layer can no longer stay attached to the upper surface. A separated region develops at the trailing edge of the airfoil, and moves towards the leading edge as the angle is further increased. Picture b) in figure A.5 illustrates the separated flow at the upper surface of an airfoil. Large vortexes forms and inhibit the outer flow from flowing smoothly past the airfoil.

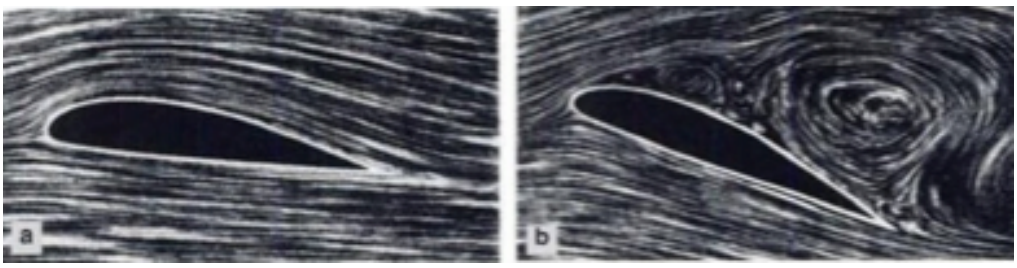


Figure A.4: Flow past airfoil (Schlichting and Gersten 2000)

# B) ADVANTAGES AND DISADVANTAGES WITH PIEZOELECTRIC AND PIEZORESISTIVE PRESSURE SENSORS

The advantages and disadvantages of piezoelectric and piezoresistive pressure sensors are summarized in table B-1 and B-2.

| ADVANTAGES | DISADVANTAGES |
|---|---|
| - Very fast response<br>- Very high stress sensitivity<br>- Wide pressure and frequency range<br>- Good pressure resolution<br>- Good linearity of the dependence of the output on the measurands<br>- High reproducibility<br>- Very good stability<br>- Extremely high rigidity (ruggedness)<br>- Good ability to withstand harsh environment<br>- Wide temperature range<br>- Low temperature dependency<br>- High degree of miniaturization<br>- Very compact design<br>- Insensitive to electric and magnetic field, and to radiation | - Unable toe measure truly static events<br>- Intrusive method<br>- Provides point measurements only |

Table B-1: Advantages and disadvantages of piezoelectric pressure sensors (Nabavi 2010) and (Gautschi 2002)

| ADVANTAGES | DISADVANTAGES |
|---|---|
| - Fast response<br>- High stress sensitivity<br>- Very wide frequency and pressure range<br>- Good pressure resolution<br>- Good linearity of the dependence of the output on the measurands<br>- High reproducibility<br>- High rigidity (ruggedness)<br>- Good ability to withstand harsh environment<br>- Very high degree of miniaturization<br>- Very compact design<br>- Wide temperature range<br>- High accuracy<br>- Favorable SNR (signal-to-noise ratio) | -Temperature and humidity dependency<br>- Sensitive to electric and magnetic field, and also to radiation<br>- Require an external energy source to produce output signal<br>- Intrusive method<br>- Provides point measurements only |

Table B-2: Advantages and disadvantages of piezoresistive pressure sensors (Nabavi 2010)

# C) THE HOLD-UP EQUATION

The equations presented in this Appendix are based on lecture notes from Ole Jørgen Nydal, professor in multiphase pipe flow at NTNU. The hold-up equation in stratified flows is retrieved by making a steady state force balance in the pipe. Since the test pipe is horizontal, the gravitational forces can be eliminated. This is illustrated in figure C.1

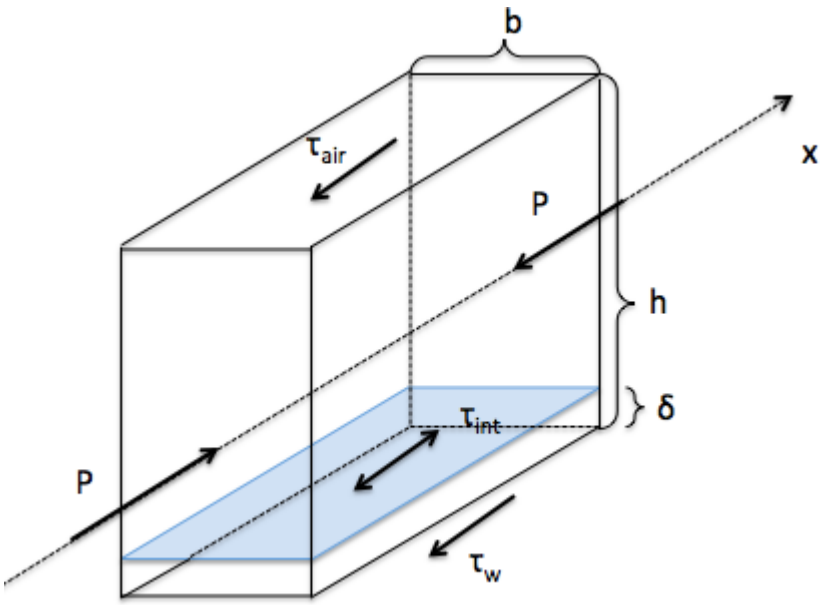


Figure C.1: Force balance in horizontal stratified flow

By evaluating the two phases separately, two force equations can be written. One for the air, and one for the water film:

$$0 = \alpha_{air}\frac{dp}{dx} - F_{air} - F_{int} \qquad C.1$$

$$0 = \alpha_{w}\frac{dp}{dx} - F_{w} + F_{int} \qquad C.2$$

The pressure drop is the same in both phases, and by substituting equation C.1 into C.2 the force balance is reduced to equation C.3. This is hold-up equation for horizontal stratified flows.

$$0 = -F_{int} + \alpha_{air}F_{w} - \alpha_{w}F_{air} \qquad C.3$$

By expressing the area fraction $\alpha_{air}$ and $\alpha_w$ according to figure C.1, equation C.3 can be rewritten as equation C.4

$$0 = -F_{int} + \frac{h-\delta}{h}F_w - \frac{\delta}{h}F_{air} \qquad C.4$$

$F_{air}$ and $F_w$ is the wall friction for air and water, while $F_{int}$ is the interface friction:

$$F_i = \frac{\tau_{int}S_{int}}{A_{tot}}\ , \qquad F_{air} = \frac{\tau_{air}S_{air}}{A_{tot}}\ , \qquad F_w = \frac{\tau_w S_w}{A_{tot}}$$

$S_{int}$ is the interface perimeter while $S_{air}$ and $S_w$ is the wall perimeter for air and water. By evaluating figure C.1 it thus follows that:

$$S_{int} = b\ , \qquad S_{air} = 2(h-\delta) + b, \qquad S_w = 2\delta + b, \qquad A_{tot} = bh$$

The wall shear stresses, $\tau_{air}$ and $\tau_w$ is expressed in terms of the friction factor and the density and velocity of the two phases:

$$\tau_{air} = \frac{1}{8}\lambda_{air}\rho_{air}V_{air}^2, \qquad \tau_w = \frac{1}{8}\lambda_w\rho_w V_w^2,$$

The wall forces, $F_{air}$ and $F_w$, can then be written as

$$F_{air} = \frac{1}{2}\rho_{air}\lambda_{air}V_{air}^2\frac{S_{air}}{4A_{tot}} = \frac{1}{2}\rho_{air}\lambda_{air}\left(\frac{\dot{Q_{air}}}{b(h-\delta)}\right)^2\left(\frac{2(h-\delta)+b}{4bh}\right) \qquad C.5$$

$$F_w = \frac{1}{2}\rho_w\lambda_w V_w^2\frac{S_w}{4A_{tot}} = \frac{1}{2}\rho_w\lambda_w\left(\frac{\dot{Q_w}}{b\delta}\right)^2\left(\frac{2\delta+b}{4bh}\right) \qquad C.6$$

The interface shear stress can also be formulated as a wall shear stress, and the resulting interface force is given by equation C.7.

$$\begin{aligned} F_i &= \frac{1}{2}\rho_{air}\lambda_{int}(V_{air}-V_w)^2\frac{S_{int}}{4A_{tot}} \\ &= \frac{1}{2}\rho_{air}\lambda_{int}\left(\frac{\dot{Q_{air}}}{b(h-\delta)} - \frac{\dot{Q_w}}{b\delta}\right)^2\left(\frac{b}{4bh}\right) \end{aligned} \qquad C.7$$

The next step is to calculate the two different wall factors, $\lambda_w$, $\lambda_{air}$. There are many different empirical correlations available, but it was decided to use Haalands correlation, as this gives an explicit expression for $\lambda$

$$\frac{1}{\sqrt{\lambda}} = -1.8log\left[\left(\frac{\varepsilon/D_h}{3.7}\right)^{1.11} + \frac{6.9}{Re_{D_h}}\right] \qquad C.8$$

Since the test pipe is made of plastic it ha a very smooth surface, and the surface roughness, ε, is therefore set to zero. Equation C.9 gives the simplified expression. Appendix D explains how to calculate the Reynolds number for the air and the water in stratified flows.

$$\frac{1}{\sqrt{\lambda}} = -1.8log\left(\frac{6.9}{Re_{D_h}}\right) \qquad C.9$$

The interface friction factor is estimated based on the friction factor for the air. It has been decided to assume that $\lambda_{int}$ is proportional to $\lambda_{air}$,

$$\lambda_{int} = c_{int}\lambda_{air} \qquad C.10$$

The proportional constant has been set to 1 in the stratified regime (for $Q_{air,1}$ and $Q_{air,2}$) and 5 in the wavy stratified regime. This is to take into account the additional interface friction due to surface waves.

| $Q_{air}$ | $c_{int}$ |
|---|---|
| 0.05 | 1 |
| 0.10 | 1 |
| 0.20 | 5 |
| 0.40 | 5 |
| 0.50 | 5 |

By substituting eq. C.6, C.7, C.8 and C.10 into the hold-up equation C.4, the water flow rate at different air flow rates can be determined.

# D) CALCULATION OF REYNOLDS NUMBER FOR AIR AND WATER

When calculating the Reynolds number in stratified flow, the gas and liquid phases are treated separately. Due to high slip, the gas flow can be modeled as a closed channel flow, while the liquid film flow can be modeled as an open channel flow. The Reynolds number is given by equation D.1. The hydraulic diameter is defined according to equation D.2. A is the flow area, while P is the wetted perimeter.

$$Re = \frac{VD_h}{\upsilon} \tag{D.1}$$

$$D_h = \frac{4A}{P} \tag{D.2}$$

According to figure C.1, it tus follows that

$$D_{h,w} = \frac{4A_w}{S_w} = \frac{4\delta b}{2\delta + b} \tag{D.3}$$

$$D_{h,air} = \frac{4A_{air}}{S_{air} + S_{int}} = \frac{4(h-\delta)b}{2(h-\delta) + 2b} \tag{D.4}$$

The velocities of the air and the water can be expressed in terms of flow rate and flow area:

$$V_w = \frac{\dot{Q}_l}{\delta b} \tag{D.5}$$

$$V_{air} = \frac{\dot{Q}_q}{(h-\delta)b} \tag{D.6}$$

By substituting eq. D.3-6 into eq. D.1, the Reynolds number for the air and the water can be calculated:

$$Re_l = \frac{4\dot{Q}_l}{\upsilon_l(2\delta + b)} \tag{D.7}$$

$$Re_g = \frac{4\dot{Q}_g}{\upsilon_g(2(h-\delta) + 2b)} \tag{D.8}$$

## E) MATLAB FUNCTION FOR AIR AND WATER FRICTION FACTORS

```
function [ l_air ] = haaland_air(Q_air, delta)

% DESCRIPTION:
% Calculates the friction factor for the air
%
% PARAMETERS:
%
% Input:
%       Q_air = air flow rate
%       delta = liquid film thickness
%
% Output:
%       l_air: air friction factor
%
% Constants:
%       b = channel width
%       h = channel height
%       v_air = kinematic viscosity air
%       e = surface roughness
%
% Calculated values:
%       D_air = hydraulic diameter air
%       Re_air = Air flow Reynolds number

b = 0.1;
h = 0.2;
v_air = 15.11*10^(-6);
e = 0;

D_air = (4*(h-delta)*b)/(2*((h-delta)+b));
Re_air = 4*Q_air/(v_air*((2*((h-delta))+b)));

f=-1.8*log(((e/D_air)/3.7)^1.11 + (6.9/Re_air));
l_air=(1/f)^2;

end
```

```
function [l_w] = haaland_w( Q_w, delta )

% DESCRIPTION:
% Calculates the friction factor for the water
%
% PARAMETERS:
%
% Input:
%       Q_w = water flow rate
%       delta = liquid film thickness
%
% Output:
%       l_w: water friction factor
%
% Constants:
%       b = channel width
%       v_w = kinematic viscosity of water
%       e = surface roughness
%
% Calculated values:
%       D_w = hydraulic diameter water
%       Re_w = Water Reynolds number

b = 0.1;
v_w = 1.004*10^(-6);
e = 0;

D_w = (4*delta*b)/((2*delta +b));
Re_w = 4*Q_w/(v_w*((2*delta)+b));

f=-1.8*log(((e/D_w)/3.7)^1.11 + (6.9/Re_w));
l_w=(1/f)^2;

end
```

## F) MATLAB FUNCTION FOR HOLD-UP EQUATION

```
function [ a ] = water_flow_rate( Q_air, Q_w, l_air,
l_w, delta, c_i)

% DESCRIPTION:
% Calculates the hold-up equation:
%
% 0 = -F_i+((1-alfa_w)*F_w)-(alfa_w*F_air)
%
% If water flow rates and water film thickness
% matches, the function returns zero
%
% PARAMETERS
% Input:
%       Q_air = qair flow rate
%       Q_w = water flow rate
%       l_air = air friction factor
%       l_w = water friction factor
%       delta = water film thickness
%       c_i = interfacial friction constant
%
% Output:
%       a = a number that indicates if the water flow
%      rate is correct:
%
%       a < 0 too low water flow rate
%       a > 0 too high water flow rate
%       a = 0 correct water flow rate
%
% Constants:
%       rho_air = air density
%       rho_w = water density
%       b = channel width
%       h = channel height
%
% Calculated values:
%       s_air = wetted perimeter air
%       s_w = wetted perimeter water
%       s_i = air/water interface
%       alfa_w = water area fraction (hold-up)
%       F_air = air friction
%       F_w = water friction
%       F_i = interfacial friction

rho_air = 1.205;
rho_w = 998.3;
b = 0.1;
```

```
h = 0.2;
s_air = 2*(h-delta)+b;
s_w = b+(2*delta);
s_i = b;
alfa_w = delta/h;


F_air = 0.5*rho_air*l_air*(Q_air/((1-
alfa_w)*b*h))^2*(s_air/(4*b*h));

F_w =
0.5*rho_w*l_w*(Q_w/(alfa_w*b*h))^2*(s_w/(4*b*h));

F_i = 0.5*rho_air*c_i*l_air*((Q_air/((1-
alfa_w)*b*h))-(Q_w/(alfa_w*b*h)))^2*(s_i/(4*b*h));

a = -F_i+((1-alfa_w)*F_w)-(alfa_w*F_air);

end
```

## G) MATLAB SCRIPT FOR WATER FLOW RATE CALCULATION

```
% DESCRIPTION:
% Script that calculates the correct water flow rate,
% and also makes a plot of the hold-up equation
% versus the water flow rate. The correct flow rate
% is reached as the hold-up equation goes towards
% zero.

% NEW PARAMETERS:
% V_air = velocity of air at chosen air flow rate
% Q_w_max = max water flow rate. Calculated by
% assuming that the water cannot have a larger
% velocity than the air.
% step = increment of water flow rate for each
% calculation
% N = total number of steps
% i = index for vectors

b = 0.1;
h = 0.2;
Q_air = 0.05;
c_i = 1;
delta = 0.005;

V_air = Q_air/(b*(h-delta));
Q_w_max = V_air*b*delta;
step = 0.00000001;
N = Q_w_maks/step;
Q_w = 0;

for i = 1:1:N

    flow_rate(i) = Q_w;
    a(i) =
water_flow_rate(Q_air,Q_w,haaland_air(Q_air,delta),ha
aland_w(Q_w,delta),delta,c_i);

    if abs(a(i)) <0.001
       Q_w = flow_rate(i)
       break
    end
   Q_w = Q_w + step;
end

plot(flow_rate, a)
clear flow_rate a
```

# H) – L) DATASHEETS OF DIFFERENT PRESSURE SENSORS

H) Kistler 7261A

I) Kistler 7031

J) Kulite XCL-152

K) Kulite XTL-190

L) PCB model 102A05

APPENDIX H)

KISTLER
measure. analyze. innovate.

# Piezoelectric Low Pressure Sensor

**Type 7261**

## Very High Sensivity – Pressure Range 10 bar

Low pressure quartz transducer for dynamic and short term static pressure measurements from vacuum to 10 bar. High resonant frequency and flush welded diaphragm.

The charge signal of the transducer is transformed into a proportional output voltage in a charge amplifier. Within wide limits, the output voltage does not depend on the length of the transducer cable.

- Very high sensitivity
- Very robust

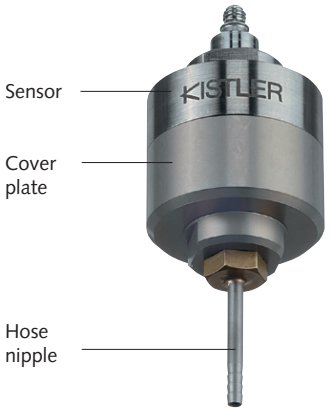


### Description

The measured pressure acts through the diaphragm on the quartz crystal measuring element which transforms the pressure into an electrostatic charge. The stainless steel diaphragm is welded flush and hermetically to the stainless steel transducer body. The quartz elements are mounted in a highly sensitive arrangement (transversal effect) in the quartz chamber, which is welded hermetically to the body. The screw-on cover and the hose nipple simplify in many cases the connection to the measured pressure.

### Application

The low pressure transducer Type 7261 is suited for fast dynamic pressure measurements if used without cover. In case both cover and nipple are mounted, the frequency response is reduced considerably due to the Helmholtz resonator effect. Quasi-static measurements of several minutes duration are possible under appropriate conditions.

Typical applications:

- Dynamic and quasi-static pressure measurements, e.g. in pipes of blowers or compressors for investigating the dynamic behaviour of the air columns
- Pressure measurements in carburettors of combustion engines and in pneumatic control circuits and fluidics
- Measurement of pressure pulses in automatic oil firing plants
- Measurement of sound pressure in rough environment

### Technical Data

| | | |
|---|---|---|
| Measuring range | bar | –1 ... 10 |
| calibrated partial ranges | bar | 0 ... 1 |
| | bar | 0 ... –1 |
| Overload | bar | 12 |
| Threshold | | |
| with charge amplif. Type 5015 | bar | ≈$1x10^{-5}$ |
| with charge amplif. Type 5018 | bar | ≈$2{,}5x10^{-6}$ |
| Sensitivity | pC/bar | 2 200 |
| Natural frequency | kHz | ≈13 |
| with cover | kHz | ≈2,5 |
| with hose nipple Type 1227 | kHz | ≈0,35 |
| Linearity | %FSO | ≤±0,8 |
| Hysteresis | %FSO | <0,5 |
| Dead volume | $cm^3$ | 1,5 |
| Insulation resistance | Ω | >$5x10^{13}$ |
| Capacitance | pF | 24 |
| Acceleration sensitivity | bar/g | <$10^{-3}$ |
| Temperature coefficient of sensitivity | %/°C | –0,02 |
| Operating temperature range | °C | –40 ... 240 |
| Shock resistance | g | 2 000 |
| Weight | kg | 0,18 |

1 bar = $10^5$ N·$m^{-2}$ = 1,019... at = 14,50... psi;
1 at = 1 kp · $cm^{-2}$ = 1 kgf · $cm^{-2}$ = 0,980665 bar, 1 psi = 0,06894... bar;
1 in = 25,4 mm

7621_000-053e-01.13

KISTLER
measure. analyze. innovate.

## Dimensions

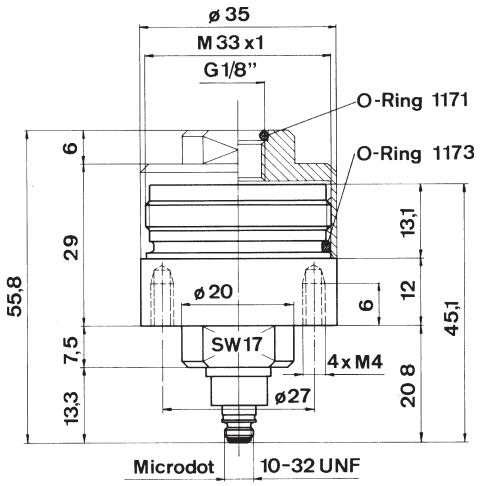


Fig. 1: Dimensions, Type 7261

## Mounting

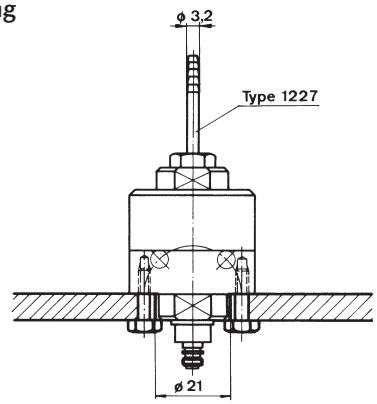


Fig. 2: Measured pressure connection with hose nipple

Usually the transducer Type 7261 is not mounted on the test object but connected by a hose (Fig. 2). For this purpose the hose nipple Type 1227 (including O-ring seal Type 1171) is supplied (Fig. 3). For measuring fast pressure variations, the connecting hose or pipe should be short and of adequate crosssection. For this case it is recommended to use a 1/8" gas pipe that is screwed directly into the cover.

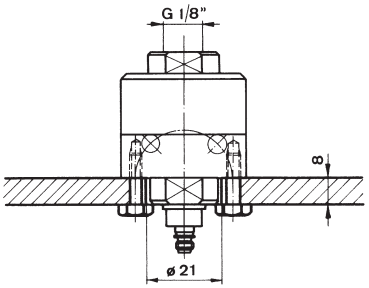


Fig 3: At quick pressure deviations direct pressure line G1/8"

If flush mounting is desired, the thread M33x1 may be used (Fig. 4, left half) or the transducer may be introduced with its front part into a bore of 33 mm ø and fixed with a flange (Fig. 4, right half). In all cases the o-ring Type 1173 is used for sealing. The four threaded holes M4 may be used for fixing the transducer (Fig. 2 and 3). It is recommended to use a thermo-shrink-sleeve to seal and secure the Microdot-connection of the transducer cable.

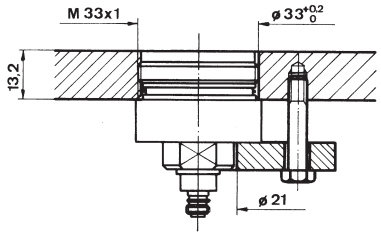


Fig. 4: Mounting with flange

| Included Accessories | Type/Art. No. |
|---|---|
| • Hose nipple | 1227 |
| incl. o-ring seal | 1171 |

**Optional Accessories**

- None

**Ordering Code**

| | |
|---|---|
| • Ultrahigh sensitive low pressure transducer for measuring smallest pressure fluctuations | **Type 7261** |

# APPENDIX I)



**Quarz-Drucksensor, beschleunigungskompensiert**
**Capteur pression à quartz, avec compensation d'accélération**
**Quartz Pressure Sensor, Acceleration-Compensated**

**7031**

Quarz Drucksensor zum Messen dynamischer und quasistatischer Drücke bis 250 bar bei Temperaturen bis 200 °C. Der eingebaute Beschleunigungssensor kompensiert Störsignale die durch Schock oder Vibration in Richtung der Sensorachse entstehen.

Capteur de pression à quartz pour mesurer des pressions dynamiques et quasistatiques jusqu'à 250 bar à des températures jusqu'à 200 °C. L'accéléromètre incorporé compense les signaux d'interférence provenant des chocs et vibrations dans la direction de l'axe du capteur.

Quartz pressure sensor for measuring dynamic and quasistatic pressures up to 250 bar at temperatures up to 200 °C. The built-in accelerometer compensates interference signals produced by shock or vibration in the direction of the sensor axis.

- Beschleunigungskompensiert
  Compensé aux accélération
  Accceleration compensated
- Hohe Empfindlichkeit
  Haute sensibilité
  High sensitivity
- Temperaturen bis zu 200 °C
  Températures jusqu'à 200 °C
  Temperatures up to 200 °C

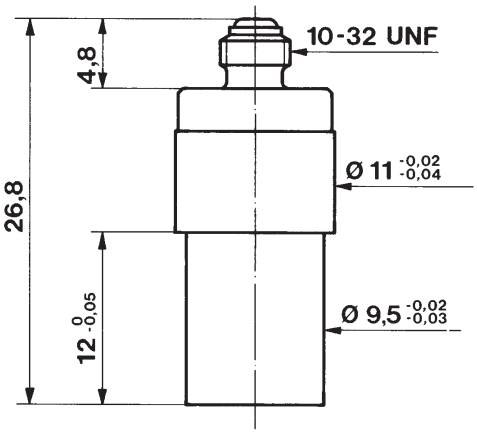



**2:1**

## Technische Daten — Données techniques — Technical Data

| | | | | |
|---|---|---|---|---|
| **Bereich** | **Gamme** | **Range** | bar | 0 ... 250 |
| **Kalibrierte Teilbereiche** | **Gamme partielles étalonnées** | **Calibrated partial ranges** | bar | 0 ... 25 |
| | | | bar | 0 ... 2,5 |
| **Überlast** | **Surcharge** | **Overload** | bar | 350 |
| **Empfindlichkeit** | **Sensibilité** | **Sensitivity** | pC/bar | ≈ –55 |
| **Eigenfrequenz** | **Fréquence propre** | **Natural frequency** | kHz | ≈80 |
| **Linearität** | **Linéarité** | **Linearity** | %FSO | ≤ ±1 |
| **Beschleunigungsempfindlichkeit** | **Sensibilité aux accélérations** | **Acceleration sensitivity** | bar/*g* | <0,0001 |
| **Betriebstemperaturbereich** | **Gamme de température d'utilisation** | **Operating temperature range** | °C | -150 ...200 |
| **Temperaturkoeffizient der Empfindlichkeit** | **Coefficient de température de la sensibilité** | **Temperature coefficient of sensitivity** | %/°C | 0,02 |
| **Isolationswiderstand** | **Résistance d'isolement** | **Insulation resistance** | TΩ | ≥10 |
| **Stossfestigkeit** | **Résistance au choc** | **Shock resistance** | *g* | 5000 |
| **Kapazität** | **Capacité** | **Capacitance** | pF | 20 |
| **Gewicht** | **Poids** | **Weight** | g | 10,8 |
| **Stecker,** Teflon-Isolator | **Connecteur,** isolateur en téflon | **Connector,** teflon insulator | | 10-32 UNF |

1 N (Newton) = 1 kg·m·s$^{-2}$ = 0,1019... kp = 0,2248... lbf; 1 kp = 1 kgf = 9,80665 N; 1 inch = 25,4 mm; 1 kg = 2,2046... lb; 1 Nm = 0,73756... lbft

***** In all Kistler documents, the decimal sign is a comma on the line (ISO 31-0:1992).

## Beschreibung

Der zu messende Druck wirkt über die Membrane auf das Quarzkristall-Messelement, das den Druck p (bar) in eine elektrische Ladung Q (pC = pico-Coulomb) umwandelt. Die Membrane aus rostfreiem Stahl ist mit dem Sensorgehäuse aus rostfreiem Stahl hermetisch und bündig verschweisst. Das durch die Masse des Sensors bei Beschleunigung (Schock oder Vibration) erzeugte Signal wird durch das Signal mit umgekehrten Vorzeichen eines eingebauten Beschleunigungssensors kompensiert.

Der Stecker-Anschluss ist mit dem Gehäuse verschweisst, jedoch ist sein Teflon-Isolator nicht völlig dicht.

## Description

Par l'intermédiaire du diaphragme, la pression agit sur l'élément de mesure à quartz qui transforme la pression p (bar) en charge électrique Q (pC = pico-Coulomb). Le diaphragme en acier inoxydable est soudé hermétiquement, au ras du front, au boîtier en acier inoxydable. Les signaux dûs aux accélérations (choque ou vibrations) sont compensés par un signal de polarité inverse provenant d'un accéléromètre compensateur incorporé.

La prise électrique est soudée au boîtier, cependant son isolateur en téflon n'est pas rigoureusement étanche.

## Description

The measured pressure acts through the diaphragm on the quartz crystal measuring element, which transforms the pressure p (bar) into an electric charge Q (pC = pico-Coulomb). The stainless steel diaphragm is welded flush and hermetically to the stainless steel sensor housing. The signal produced by acceleration (shock or vibration) due to the sensor mass, is compensated by a signal of inverse polarity yielded by the built-in accelerometer.

The connector is welded to the body, but its teflon insulator is not absolutely tight.

000-051m-07.96 (DB03.7031m)

## Anwendung

Der Drucksensor Typ 7031 eignet sich besonders für die Messung schneller Druckverläufe an stark vibrierenden Messobjekten. Dieser Sensor ist rund 10 mal weniger vibrationsempfindlich als der Standardsensor Typ 601A. Bei besonders beschränkten Einbauverhältnissen oder sehr hohen Messfrequenzen ist der Drucksensor 6031 zu verwenden.

## Application

Le capteur type 7031 est adapté à la mesure de variations rapides de pression dans des dispositifs vibrant. Ce capteur est à peu près 10-fois moins sensible aux vibrations que le capteur standard type 601A. On choisit le capteur miniature 6031 pour des dispositifs à dimensions réduites ou pour les fréquences très élevées.

## Application

The quartz pressure sensor Type 7031 is suited for dynamic pressure measurements on heaving vibrating objects. This sensor is about 10 times less sensitive to vibrations than the standard Type 601A. For very high frequencies or reduced mounting space the sensor 6031 is used.

## Montage

Der Sensor kann mittels eines Montagenippels (Fig. 1) oder eines Steckernippels (Fig. 2) im Messobjekt oder dem Adapter montiert werden. Bei der Montage nach Fig. 2 werden Sensor und Steckernippel zu einer Montageeinheit zusammengeschraubt. Die Trennfläche kann mit “Loctite” gedichtet werden.

Siehe auch Datenblätter für:

| | |
|---|---|
| Werkzeuge | 4.012 |
| Adapter | 4.016 |
| Steckernippel | 4.014 |
| Kabel | 15.035 |

## Montage

Le capteur peut être monté directement dans le dispositif de mesure ou dans l’adaptateur à l’aide d’un écrou de montage (fig. 1) ou d’un écrou connecteur (fig. 2). Pour le montage selon fig. 2, le capteur et l’écrou connecteur forment une unité. La jonction capteur - écrou connecteur peut être rendue étanche avec du “Loctite”.

Voir aussi les notices techniques suivantes:

| | |
|---|---|
| Outillage | 4.012 |
| Adaptateurs | 4.016 |
| Ecrous connecteurs | 4.014 |
| Câbles | 15.035 |

## Mounting

The sensor can be mounted directly into the measuring object or the adapter by means of a mounting nut (fig. 1) or a connecting nipple (fig. 2). When mounted with a connecting nipple, the latter is preassembled with the sensor to a mounting unit. The junction between nipple and sensor can with sealed by “Loctite”.

See also datasheets for:

| | |
|---|---|
| Tools | 4.012 |
| Adapters | 4.016 |
| Connecting nipples | 4.014 |
| Cables | 15.035 |

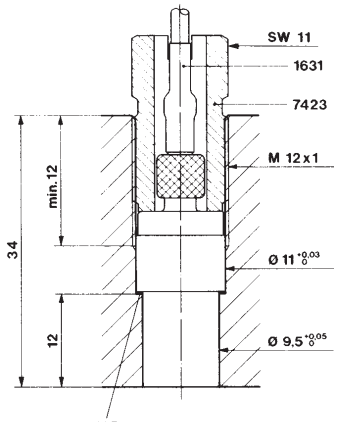


Fig. 1:

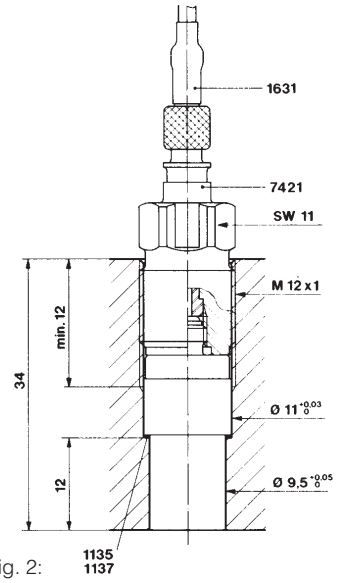


Fig. 2:

| **Zubehör** | *Typ* |
|---|---|
| Cu-Dichtung | 1135 |
| Ni-Dichtung | 1135A |
| Teflon-Dichtung | 1137 |
| Schlüssel für Steckernippel 7421 | 1303 |
| Stufenbohrer | 1333 |
| Ausziehwerkzeug für 10-32 UNF | 1311 |
| Montagenippel SW8 | 7423 |
| Steckernippel 10-32UNF/10-32UNF | 7421 |
| Steckernippel 10-32UNF/BNC | 7401 |
| Steckernippel 10-32UNF/TNC | 7411 |
| Steckernippel luftgekühlt 10-32UNF/10-32UNF | 7461 |
| Schrumpfschlauch für Stecker | 1021 |
| Montageadapter M14 x 1,25 | 7501 |
| Montageadapter M5 | 7503 |
| Kühladapter M18 x 1,5 | 7505 |
| Kühladapter M14 x 1,25 | 7507 |

| **Accessoires** | *Type* |
|---|---|
| Joint en cuivre | 1135 |
| Joint en nickel | 1135A |
| Joint en téflon | 1137 |
| Clé pour écrou connecteur 7421 | 1303 |
| Aléseuse progressive | 1333 |
| Outil extracteur pour 10-32 UNF | 1311 |
| Ecrou de montage OCW8 | 7423 |
| Ecrou connecteur 10-32UNF/10-32UNF | 7421 |
| Ecrou connecteur 10-32UNF/BNC | 7401 |
| Ecrou connecteur 10-32UNF/TNC | 7411 |
| Ecrou connecteur refroidi par air 10-32UNF/10-32UNF | 7461 |
| Gaine thermorétractable pour connecteur | 1021 |
| Adaptateur de montage M14 x 1,25 | 7501 |
| Adaptateur de montage M5 | 7503 |
| Adaptateur refroidi M18 x 1,5 | 7505 |
| Adaptateur refroidi M14 x 1,25 | 7507 |

| **Accessories** | *Type* |
|---|---|
| Copper seal | 1135 |
| Nickel seal | 1135A |
| Teflon seal | 1137 |
| Key for connecting nipple 7421 | 1303 |
| Step drill | 1333 |
| Extraction tool 10-32 UNF | 1311 |
| Mounting nut WS8 | 7423 |
| Connecting nipple 10-32UNF/10-32UNF | 7421 |
| Connecting nipple 10-32UNF/BNC | 7401 |
| Connecting nipple 10-32UNF/TNC | 7411 |
| Connecting nipple air cooled 10-32UNF/10-32UNF | 7461 |
| Heat-shrink tubing for connector | 1021 |
| Mounting adapter M14 x 1,25 | 7501 |
| Mounting adapter M5 | 7503 |
| Cooling adapter M18 x 1,5 | 7505 |
| Cooling adapter M14 x 1,25 | 7507 |

000-051m-07.96 (DB03.7031m)

# APPENDIX J)

## SHORT LENGTH IS® PRESSURE TRANSDUCER

### XCL-152 SERIES

- High Natural Frequency
- Available 5 PSI To 1000 PSI
- Short Body
- Patented Leadless Technology **VIS®**

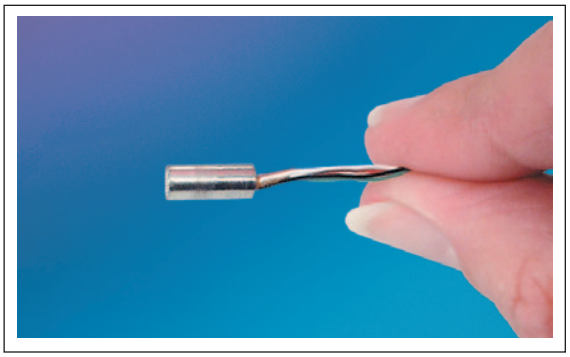

The XCL-152 design features Kulite's patented leadless technology. This allows for a very rugged package suited for probes, pressure rakes and other similar test set ups. This transducer is well suited for both dynamic and static pressure measurements in benign or harsh environments.

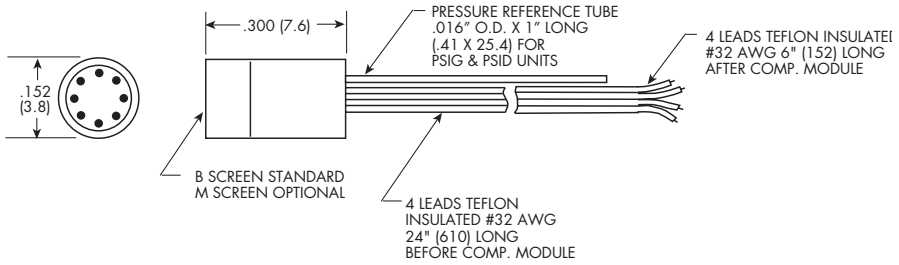


| WIRING | |
|---|---|
| COLOR | DESIGNATION |
| RED | + INPUT |
| BLACK | – INPUT |
| GREEN | + OUTPUT |
| WHITE | – OUTPUT |

NOTE: FOR INTERNAL COMPENSATION CONSULT FACTORY

CONSULT FACTORY FOR SPECS. ON SEALED GAGE

| | | | | | | | | |
|---|---|---|---|---|---|---|---|---|
| **INPUT**<br>Pressure Range | 0.35<br>5 | 0.7<br>10 | 1.7<br>25 | 3.5<br>50 | 7<br>100 | 17<br>250 | 35<br>500 | 70 BAR<br>1000 PSI |
| Operational Mode | Absolute, Gage, Sealed Gage, Differential | | | | | Absolute, Sealed Gage | | |
| Over Pressure | 2 Times Rated Pressure With No Change In Calibration | | | | | | | |
| Burst Pressure | 3 Times Rated Pressure | | | | | | | |
| Pressure Media | All Nonconductive, Noncorrosive Liquids or Gases (Most Conductive Liquids and Gases - Please Consult Factory) | | | | | | | |
| Rated Electrical Excitation | 10 VDC/AC | | | | | | | |
| Maximum Electrical Excitation | 15 VDC/AC | | | | | | | |
| Input Impedance | 1000 Ohms (Min.) | | | | | | | |
| **OUTPUT**<br>Output Impedance | 1000 Ohms (Nom.) | | | | | | | |
| Full Scale Output (FSO) | 100 mV (Nom.) | | | | | | | |
| Residual Unbalance | ± 5 mV (Typ.) | | | | | | | |
| Combined Non-Linearity, Hysteresis and Repeatability | ± 0.1% FSO BFSL (Typ.), ± 0.5% FSO (Max.) | | | | | | | |
| Resolution | Infinitesimal | | | | | | | |
| Natural Frequency (KHz) (Typ.) | 150 | 175 | 240 | 300 | 380 | 550 | 700 | 1000 |
| Acceleration Sensitivity % FS/g<br>Perpendicular<br>Transverse | $1.5x10^{-3}$<br>$2.2x10^{-4}$ | $1.0x10^{-3}$<br>$1.4x10^{-4}$ | $5.0x10^{-4}$<br>$6.0x10^{-5}$ | $3.0x10^{-4}$<br>$4.0x10^{-5}$ | $1.5x10^{-4}$<br>$2.0x10^{-5}$ | $1.0x10^{-4}$<br>$9.0x10^{-6}$ | $6.0x10^{-5}$<br>$6.0x10^{-6}$ | $4.5x10^{-5}$<br>$3.0x10^{-6}$ |
| Insulation Resistance | 100 Megohm Min. @ 50 VDC | | | | | | | |
| **ENVIRONMENTAL**<br>Operating Temperature Range | -65°F to +250°F (-55°C to +120°C) | | | | | | | |
| Compensated Temperature Range | 80°F to +180°F (25°C to +80°C) Any 100°F Range Within The Operating Range on Request | | | | | | | |
| Thermal Zero Shift | ± 1% FS/100°F (Typ.) | | | | | | | |
| Thermal Sensitivity Shift | ± 1% /100°F (Typ.) | | | | | | | |
| Steady Acceleration | 10,000g. (Max.) | | | | | | | |
| Linear Vibration | 10-2,000 Hz Sine, 100g. (Max.) | | | | | | | |
| **PHYSICAL**<br>Electrical Connection | 4 Leads 32 AWG 30" Long | | | | | | | |
| Weight | .6 Gram (Nom.) Excluding Module and Leads | | | | | | | |
| Pressure Sensing Principle | Fully Active Four Arm Wheatstone Bridge Dielectrically Isolated Silicon on Silicon Patented Leadless Technology | | | | | | | |

*Note: Custom pressure ranges, accuracies and mechanical configurations available. Dimensions are in inches. Dimensions in parenthesis are in millimeters.*
*Continuous development and refinement of our products may result in specification changes without notice - all dimensions nominal. (D)*

*KULITE SEMICONDUCTOR PRODUCTS, INC. • One Willow Tree Road • Leonia, New Jersey 07605 • Tel: 201 461-0900 • Fax: 201 461-0990 • http://www.kulite.com*

# APPENDIX K)

## MINIATURE RUGGEDIZED IS® PRESSURE TRANSDUCER

### XTL-190 (M) SERIES

- Easy Installation
- Patented Leadless Technology **VIS®**
- High Natural Frequency
- Intrinsically Safe Applications Available (i.e. IS-XTL-190)

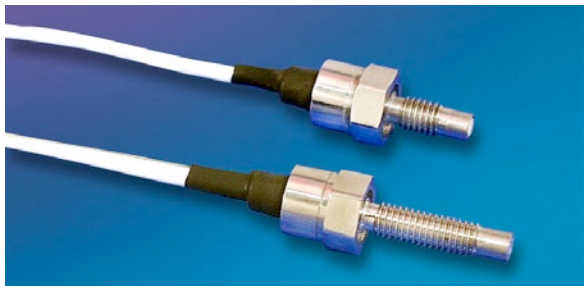

The ruggedness of this sensor has not compromised its performance. It was designed for ease of installation and will operate properly in any medium compatible with 15-5 SS or $SiO_2$. Its Patented Leadless construction makes it possible for the sensing unit to be installed in such a way that will not compromise its high natural frequency.

**OPTIONAL CONNECTOR VERSION**

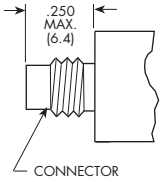


NOT AVAILABLE ON DIFFERENTIAL UNIT

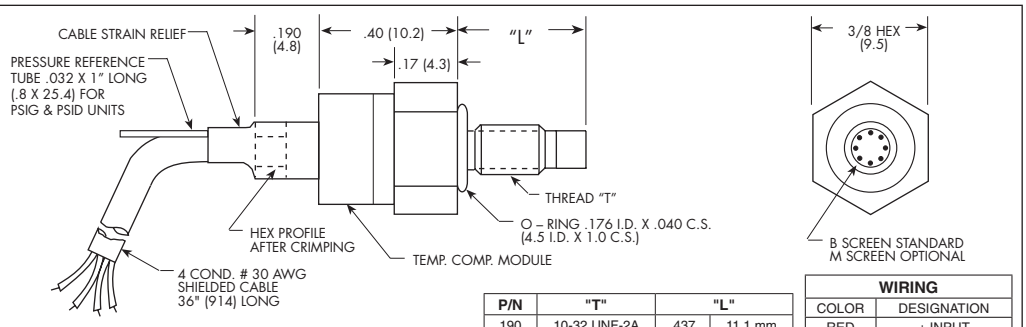


CONSULT FACTORY FOR SPECS. ON SEALED GAGE

| P/N | "T" | "L" | |
|---|---|---|---|
| 190 | 10-32 UNF-2A | .437 | 11.1 mm |
| 190M | M5 x .8 | .437 | 11.1 mm |
| 190 | 10-32 UNF-2A | .760 | 19.3 mm |
| 190M | M5 x .8 | .760 | 19.3 mm |

| WIRING | |
|---|---|
| COLOR | DESIGNATION |
| RED | + INPUT |
| BLACK | - INPUT |
| GREEN | + OUTPUT |
| WHITE | - OUTPUT |

| | | | | | | | | | |
|---|---|---|---|---|---|---|---|---|---|
| **INPUT**<br>Pressure Range | 0.35<br>5 | 0.7<br>10 | 1.7<br>25 | 3.5<br>50 | 7<br>100 | 17<br>250 | 35<br>500 | 70<br>1000 | 140 BAR<br>2000 PSI |
| Operational Mode | Absolute, Gage, Sealed Gage, Differential | | | | | Absolute, Sealed Gage | | | |
| Over Pressure | 2 Times Rated Pressure to a Maximum of 3000 PSI (210 BAR) | | | | | | | | |
| Burst Pressure | 3 Times Rated Pressure to a Maximum of 5000 PSI (350 BAR) | | | | | | | | |
| Pressure Media | All Nonconductive, Noncorrosive Liquids or Gases (Most Conductive Liquids and Gases - Please Consult Factory) | | | | | | | | |
| Rated Electrical Excitation | 10 VDC/AC | | | | | | | | |
| Maximum Electrical Excitation | 15 VDC/AC | | | | | | | | |
| Input Impedance | 1000 Ohms (Min.) | | | | | | | | |
| **OUTPUT**<br>Output Impedance | 1000 Ohms (Nom.) | | | | | | | | |
| Full Scale Output (FSO) | 100 mV (Nom.) | | | | | | | | |
| Residual Unbalance | ± 5 mV (Typ.) | | | | | | | | |
| Combined Non-Linearity, Hysteresis and Repeatability | ± 0.1% FSO BFSL (Typ.), ± 0.5% FSO (Max.) | | | | | | | | |
| Resolution | Infinitesimal | | | | | | | | |
| Natural Frequency (KHz) (Typ.) | 150 | 175 | 240 | 300 | 380 | 550 | 700 | 1000 | 1400 |
| Acceleration Sensitivity % FS/g<br>Perpendicular<br>Transverse | <br>$1.5x10^{-3}$<br>$2.2x10^{-4}$ | <br>$1.0x10^{-3}$<br>$1.4x10^{-4}$ | <br>$5.0x10^{-4}$<br>$6.0x10^{-5}$ | <br>$3.0x10^{-4}$<br>$4.0x10^{-5}$ | <br>$1.5x10^{-4}$<br>$2.0x10^{-5}$ | <br>$1.0x10^{-4}$<br>$9.0x10^{-6}$ | <br>$6.0x10^{-5}$<br>$6.0x10^{-6}$ | <br>$4.5x10^{-5}$<br>$3.0x10^{-6}$ | <br>$2.0x10^{-5}$<br>$2.0x10^{-6}$ |
| Insulation Resistance | 100 Megohm Min. @ 50 VDC | | | | | | | | |
| **ENVIRONMENTAL**<br>Operating Temperature Range | -65°F to +350°F (-55°C to +175°C) | | | | | | | | |
| Compensated Temperature Range | +80°F to +180°F (+25°C to +80°C) Any 100°F Range Within The Operating Range on Request | | | | | | | | |
| Thermal Zero Shift | ± 1% FS/100°F (Typ.) | | | | | | | | |
| Thermal Sensitivity Shift | ± 1% /100°F (Typ.) | | | | | | | | |
| Steady Acceleration | 10,000g. (Max.) | | | | | | | | |
| Linear Vibration | 10-2,000 Hz Sine, 100g. (Max.) | | | | | | | | |
| **PHYSICAL**<br>Electrical Connection | 4 Conductor 30 AWG Shielded Cable 36" Long | | | | | | | | |
| Weight | 4 Grams (Nom.) Excluding Cable | | | | | | | | |
| Pressure Sensing Principle | Fully Active Four Arm Wheatstone Bridge Dielectrically Isolated Silicon on Silicon Patented Leadless Technology | | | | | | | | |
| Mounting Torque | 15 Inch-Pounds (Max.) 1.7 N-m | | | | | | | | |

*Note: Custom pressure ranges, accuracies and mechanical configurations available. Dimensions are in inches. Dimensions in parenthesis are in millimeters.*
*Continuous development and refinement of our products may result in specification changes without notice - all dimensions nominal. (F)*

*KULITE SEMICONDUCTOR PRODUCTS, INC. • One Willow Tree Road • Leonia, New Jersey 07605 • Tel: 201 461-0900 • Fax: 201 461-0990 • http://www.kulite.com*

APPENDIX L)

# Model 102A02

# ICP® Dynamic Pressure Sensor

# Installation and Operating Manual

**For assistance with the operation of this product , contact the Division of PCB Piezotronics, Inc.**

**Division toll-free** 888-684-0015

**24-hour SensorLine**[SM] 716-684-0001

**Fax** 716-686-9129

**E-mail** pressure@pcb.com

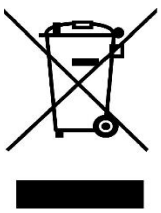

PCB PIEZOTRONICS INC.
PRESSURE DIVISION

PCB PIEZOTRONICS INC.
A PCB GROUP COMPANY

**Warranty, Service, Repair, and Return Policies and Instructions**

**The information contained in this document supersedes all similar information that may be found elsewhere in this manual.**

**Total Customer Satisfaction** – PCB Piezotronics guarantees Total Customer Satisfaction. If, at any time, for any reason, you are not completely satisfied with any PCB product, PCB will repair, replace, or exchange it at no charge. You may also choose to have your purchase price refunded in lieu of the repair, replacement, or exchange of the product.

**Service** – Due to the sophisticated nature of the sensors and associated instrumentation provided by PCB Piezotronics, user servicing or repair is not recommended and, if attempted, may void the factory warranty. Routine maintenance, such as the cleaning of electrical connectors, housings, and mounting surfaces with solutions and techniques that will not harm the physical material of construction, is acceptable. Caution should be observed to insure that liquids are not permitted to migrate into devices that are not hermetically sealed. Such devices should only be wiped with a dampened cloth and never submerged or have liquids poured upon them.

**Repair** – In the event that equipment becomes damaged or ceases to operate, arrangements should be made to return the equipment to PCB Piezotronics for repair. User servicing or repair is not recommended and, if attempted, may void the factory warranty.

**Calibration** – Routine calibration of sensors and associated instrumentation is recommended as this helps build confidence in measurement accuracy and acquired data. Equipment calibration cycles are typically established by the users own quality regimen. When in doubt about a calibration cycle, a good "rule of thumb" is to recalibrate on an annual basis. It is also good practice to recalibrate after exposure to any severe temperature extreme, shock, load, or other environmental influence, or prior to any critical test.

PCB Piezotronics maintains an ISO-9001 certified metrology laboratory and offers calibration services, which are accredited by A2LA to ISO/IEC 17025, with full traceablility to N.I.S.T. In addition to the normally supplied calibration, special testing is also available, such as: sensitivity at elevated or cryogenic temperatures, phase response, extended high or low frequency response, extended range, leak testing, hydrostatic pressure testing, and others. For information on standard recalibration services or special testing, contact your local PCB Piezotronics distributor, sales representative, or factory customer service representative.

**Returning Equipment** – *Following these procedures will insure that your returned materials are handled in the most expedient manner*. Before returning any equipment to PCB Piezotronics, contact your local distributor, sales representative, or factory customer service representative to obtain a Return

Materials Authorization (RMA) Number. This RMA number should be clearly marked on the outside of all package(s) and on the packing list(s) accompanying the shipment. A detailed account of the nature of the problem(s) being experienced with the equipment should also be included inside the package(s) containing any returned materials.

A Purchase Order, included with the returned materials, will expedite the turn-around of serviced equipment. It is recommended to include authorization on the Purchase Order for PCB to proceed with any repairs, as long as they do not exceed 50% of the replacement cost of the returned item(s). PCB will provide a price quotation or replacement recommendation for any item whose repair costs would exceed 50% of replacement cost, or any item that is not economically feasible to repair. For routine calibration services, the Purchase Order should include authorization to proceed and return at current pricing, which can be obtained from a factory customer service representative.

**Warranty** – All equipment and repair services provided by PCB Piezotronics, Inc. are covered by a limited warranty against defective material and workmanship for a period of one year from date of original purchase. Contact PCB for a complete statement of our warranty. Expendable items, such as batteries and mounting hardware, are not covered by warranty. Mechanical damage to equipment due to improper use is not covered by warranty. Electronic circuitry failure caused by the introduction of unregulated or improper excitation power or electrostatic discharge is not covered by warranty.

**Contact Information** – International customers should direct all inquiries to their local distributor or sales office. A complete list of distributors and offices can be found at www.pcb.com. Customers within the United States may contact their local sales representative or a factory customer service representative. A complete list of sales representatives can be found at www.pcb.com. Toll-free telephone numbers for a factory customer service representative, in the division responsible for this product, can be found on the title page at the front of this manual. Our ship to address and general contact numbers are:

PCB Piezotronics, Inc.
3425 Walden Ave.
Depew, NY 14043 USA
Toll-free: (800) 828-8840
24-hour SensorLine[SM]: (716) 684-0001
Website: www.pcb.com
E-mail: info@pcb.com

*DOCUMENT NUMBER: 21354*
*DOCUMENT REVISION: B*
*ECN: 17900*

# OPERATION MANUAL FOR ICP® PRESSURE SENSORS Models 102A02, A05, A07, A09 Models 112A21, A22, A23



## 1.0 INTRODUCTION

The series of miniature pressure sensors described by this operating guide is designed for low pressure, high resolution applications and features acceleration compensation.

Uses include monitoring of low pressure hydraulic and pneumatic phenomena in the presence of shock and vibration such as on jet engines, compressors, turbines and other operating machinery, high intensity sound and turbulence measurements, and many other industrial R & D applications.

## 2.0 DESCRIPTION

This series is comprised of six sensor models having high sensitivities, but differing in mechanical configuration.

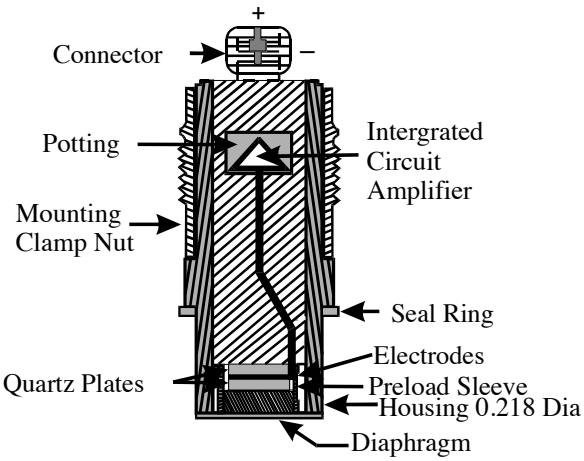


**Typical ICP® Probe Style Sensor**

Each model utilizes the basic ICP® pressure probe as shown in above figure. The pressure probe consists of the Model 112A high sensitivity acceleration-compensated quartz element and an IC source follower amplifier joined together as an inseparable assembly.

Refer to "General Guide to ICP® Instrumentation" G-0001B for a complete treatment of the ICP® concept.

Models 112A21, 112A22 and 112A23 are in the basic probe configuration as shown in Figure 1, and are installed with a hollow clamp nut with 5/16-24 external threads. The housings of these models are at electrical ground potential.

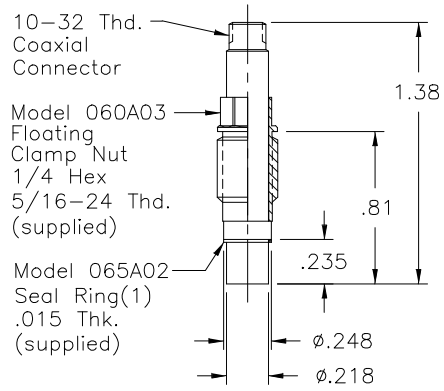


**Series 111: Probe Style Sensor**

The Model 102A05 utilizes the same basic pressure probe, mounted in a 3/8-24 threaded mounting adaptor with shoulder seal. The probe is assembled into the adaptor at the factory in an "off ground" configuration, i.e., the probe body is electrically insulated from the external mounting adaptor body. Do not attempt to disassemble probe and adaptor.

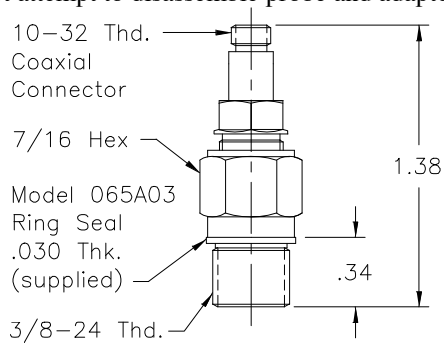


**Model 102A05 Thread Mount Design, Ground-Isolated Sensor**

Models 102A02, 102A07, and 102A09 utilize the same inner probe design but in a 3/8-24 threaded adaptor with floating clamp nut to allow adjustment of diaphragm depth where it is necessary to adapt to various wall thicknesses. These models are supplied only in low pressure (100 and 50 psi) versions and are also "off ground".

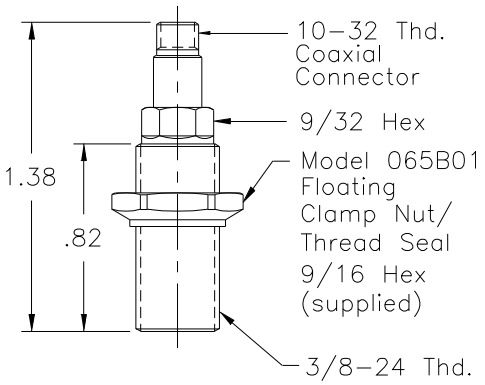


**102A's: Thread Mount with Floating Clamp Nut, Ground-Isolated Sensor**

## 3.0 INSTALLATION

This manual contains outline and installation information for your specific model in this series. Prepare mounting ports in accordance with the installation drawing for the specific model, paying particular attention to sealing surfaces. These surfaces must be smooth and free from chatter marks, nicks and other irregularities which could preclude a pressure-tight seal.

Seals are provided with each sensor and should always be used. Extra seals for all standard models are in stock at the factory. Replace seals when they become unserviceable.

In some cases, e.g., where flash temperatures such as those generated by combustion processes are present, it may be necessary to thermally insulate the diaphragm to minimize spurious signals generated by these effects.
Common black vinyl electrical tape has been found to be an effective insulating material in many cases. One or more layers may be used across the end of the diaphragm without affecting response or sensitivity.

A silicone rubber coating approximately .010" thick has also been proven effective in many applications. General Electric RTV type 106 silicone rubber is recommended. Apply the rubber coating and allow to cure in accordance with the manufacturer's instructions.

Although ICP® sensors have low output impedance and in general are not affected by moisture, in extreme environments it is good practice to protect cable connections with shrink tubing.

It is not necessary to use low-noise coaxial cable with this sensor series. In fact, a Model 070A09 solder connector adaptor that allows the use of ordinary two-wire cable is desired.

## 4.0 OPERATION

It is only necessary to supply the sensor with a 2 to 20 mA constant current at +20 to +30 VDC through a current-regulating diode or equivalent circuit. (See Guide G-0001B for powering and signal utilization information pertaining to all ICP® instrumentation).

Most of the signal conditioners manufactured by PCB have an adjustable current feature allowing a choice of input currents from 2 to 20 mA. In general, for lowest noise (best resolution) choose the low current ranges and for driving long cables (to several thousand feet) use the higher current, up to 20 mA maximum.

To operate system using a PCB signal conditioner:

1. Switch power on.

2. Wait several minutes for the IC amplifier to turn on and stabilize.

3. Proceed with measurements.

## 4.1 OPERATINGCONSIDERATION FOR MODEL 112A23

The Model 112A23 features a low-noise amplifier which, based on a peak-to-peak broadband noise factor of 50 μV, results in a resolution of .001 psi.

Defined for practical purposes as the minimum readout signal, the resolution is based on the sensitivity of 50 mV/psi and a low noise amplifier of 50 μV peak noise.

Thus, 50 μV/50mV = .001 psi resolution

The output bias voltage of the Model 112A23 is 5.0 volts, half the bias voltage of most PCB pressure sensors. This will cause the bias monitor meter on PCB power supplies to read at the low end of the green band.

## 5.0 POLARITY

This sensor series produces a positive-going output voltage for increasing pressure input.

## 6.0 LOW FREQUENCY RESPONSE

The low frequency response of an ICP® system is determined by:

1. The discharge time constant of the sensor, and,

2. If AC-coupled at power unit, the coupling time constant.

Consult Section 7.0 in Guide G-0001B for detailed explanation of low frequency characteristics of ICP® instruments.

## 7.0 CALIBRATION

Piezoelectric sensors are dynamic devices, but static calibration methods may be employed if discharge time constants are sufficiently long. Generally, static methods are not employed below several hundred seconds discharge time constant.

To employ static methods, directly couple the sensor to the DVM readout using a T-connector from the XDCR jack or use the Model 484B in the "calibrate" mode. Apply pressure with dead weight tester and take readings quickly. Release pressure after each calibration point.

For the shorter discharge time constant series, a rapid pressure step must be generated by a pneumatic pressure pulse calibrator or dead weight tester and readout is by recorder or storage oscilloscope.

PCB offers a complete recalibration service. Consult factory for details.

## 8.0 MAINTENANCE

The miniature size sealed construction precludes field maintenance. Should service be required, return unit to factory with note describing problem.

| Model Number | ICP® PRESSURE SENSOR SPECIFICATIONS | Revision: B |
|---|---|---|
| 102A02 | | ECN #: 14825 |

| Performance | ENGLISH | SI | |
|---|---|---|---|
| Measurement Range (for ± 5 V output) | 100 psi | 690 kPa | |
| Useful Overrange (for ± 10V output) | 200 psi | 1379 kPa | [1] |
| Sensitivity (±10 mV/psi) | 50 mV/psi | 7.3 mV/kPa | |
| Maximum Pressure | 1 kpsi | 6900 kPa | |
| Resolution | 2 mpsi | 0.014 kPa | |
| Resonant Frequency | ≥250 kHz | ≥ 250 kHz | |
| Rise Time | ≤2 μ sec | ≤2 μ sec | |
| Low Frequency Response (-5 %) | 0.5 Hz | 0.5 Hz | |
| Non-Linearity | ≤1.0 % FS | ≤1.0 % FS | [2] |
| **Environmental** | | | |
| Acceleration Sensitivity | ≤0.002 psi/g | ≤ 0.0014 kPa/(m/s²) | |
| Temperature Range (Operating) | -100 to +275 °F | -73 to +135 °C | |
| Temperature Coefficient of Sensitivity | ≤0.03 %/°F | ≤ 0.05 %/°C | |
| Maximum Flash Tempurature | 3000 °F | 5400 °C | |
| Maximum Shock | 20000 g pk | 196000 m/s² pk | |
| **Electrical** | | | |
| Output Polarity (Positive Pressure) | Positive | Positive | |
| Discharge Time Constant (at room temp) | ≥1 sec | ≥1 sec | |
| Excitation Voltage | 20 to 30 VDC | 20 to 30 VDC | |
| Constant Current Excitation | 2 to 20 mA | 2 to 20 mA | |
| Output Impedance | <100 ohms | <100 ohms | |
| Output Bias Voltage | 8 to 14 VDC | 8 to 14 VDC | |
| Electrical Isolation | 100000000 ohms | 100000000 ohms | |
| **Physical** | | | |
| Sensing Geometry | Compression | Compression | |
| Sensing Element | Quartz | Quartz | |
| Housing Material | Stainless Steel | Stainless Steel | |
| Diaphragm | Invar | Invar | |
| Sealing | Welded Hermetic | Welded Hermetic | |
| Electrical Connector | 10-32 Coaxial Jack | 10-32 Coaxial Jack | |
| Weight | 0.39 oz | 11.0 gm | |

CE [3]

*All specifications are at room temperature unless otherwise specified.*
*In the interest of constant product improvement, we reserve the right to change specifications without notice.*

ICP® is a registered trademark of PCB Group, Inc.

## OPTIONAL VERSIONS

Optional versions have identical specifications and accessories as listed for the standard model except where noted below. More than one option may be used.

**H** - Hermetic Seal

| | | |
|---|---|---|
| Sealing | Welded Hermetic | Welded Hermetic |

**M** - Metric Mount
Supplied Accessory : Model 065A42 Floating clamp nut and thread seal, M10 x 1.0 thd. (1) replaces Model 065B01

**N** - Negative Output Polarity

**S** - Stainless Steel Diaphragm

| | | |
|---|---|---|
| Diaphragm | 316L Stainless Steel | 316L Stainless Steel |

## NOTES:

[1] For +10 volt output, minimum 24 VDC supply voltage required. Negative 10 volt output may be limited by output bias.
[2] Zero-based, least-squares, straight line method.
[3] See PCB Declaration of Conformance PS023 for details.

## SUPPLIED ACCESSORIES:

Model 065B01 Floating clamp nut and thread seal 3/8-24 thd (1)

| Entered: DBJ | Engineer: MEM | Sales: JMM | Approved: GKH | Spec Number: |
|---|---|---|---|---|
| Date: 4/9/02 | Date: 4/9/02 | Date: 4/9/02 | Date: 4/9/02 | 6371 |

PCB PIEZOTRONICS
PRESSURE DIVISION
3425 Walden Avenue, Depew, NY 14043

Phone: 716-684-0001
Fax: 716-686-9129
E-Mail: pressure@pcb.com

| APPLICATION | | |
|---|---|---|
| NEXT ASS'Y | USED ON | VAR |
| | | |

| REVISIONS | | | | |
|---|---|---|---|---|
| REV | DESCRIPTION | ECN | DATE | APP'D |
| A | UPDATE DRAWING | 15123 | 3/29/02 | |

8495



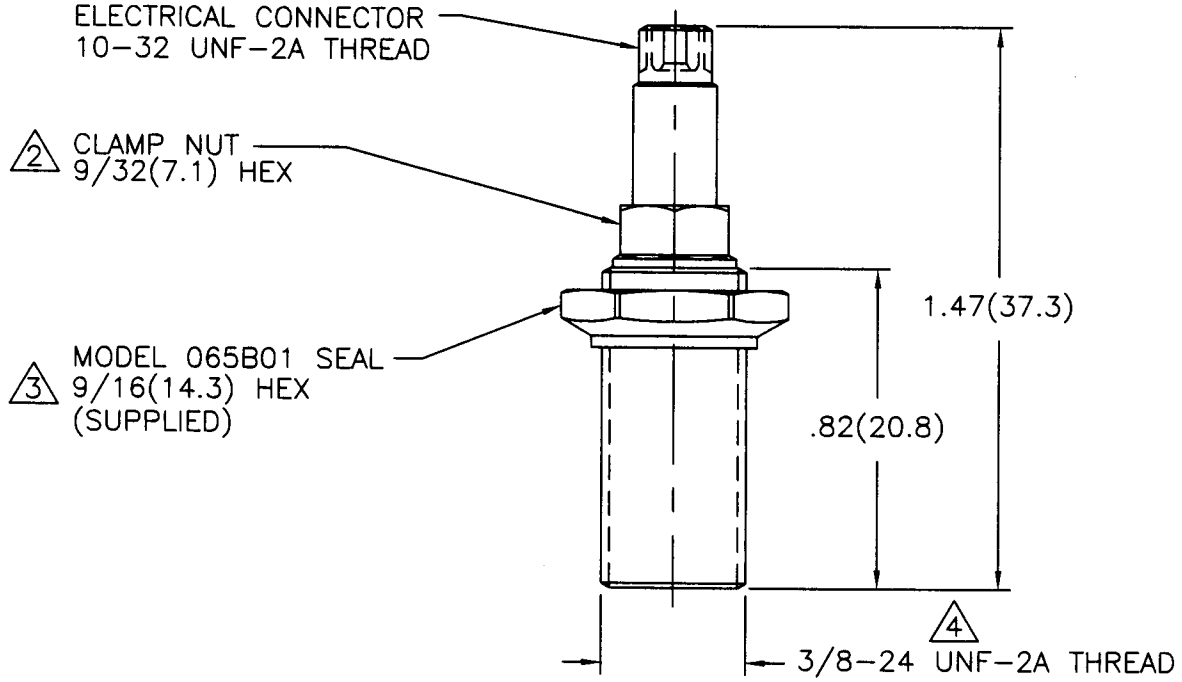


MOUNTING HOLE PREPARATION:

ø.332 THRU
TAP 3/8-24 UNF-2B
THRU

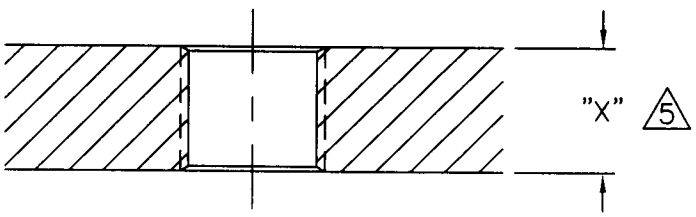


5 LENGTH TO SUIT USER REQUIREMENTS.

4 COAT THREADS OF SENSOR WITH TEFLON THREAD SEALANT IF REQUIRED. (FOR VACUUM TIGHT SEAL ONLY)

3 ADJUST MODEL 065B01 SEAL TO APPROXIMATE POSITION REQUIRED.

2 USE 9/32(7.1) NUT DRIVER TO TURN SENSOR INTO TAPPED HOLE. NORMAL LOCATION OF DIAPHRAGM FACE IS FLUSH WITH INSIDE SURFACE. RECESS .010(0.25) FOR ABLATIVE COATING IF DESIRED. WHILE HOLDING SENSOR WITH NUT DRIVER, TIGHTEN SEAL TO OBTAIN PRESSURE-TIGHT SEAL AND LOCK SENSOR IN PLACE. RECOMMENDED MOUNTING TORQUE 20-25 INCH POUNDS(226-282 NEWTON CENTIMETERS).

1.) THIS SENSOR IS A SEALED ASSEMBLY AND MUST BE RETURNED TO THE FACTORY SHOULD SERVICE BECOME NECESSARY.

| UNLESS SPECIFIED TOLERANCES | |
|---|---|
| DIMENSIONS IN INCHES<br>DECIMALS XX ±.01<br>XXX ±.005<br>ANGLES ±2 DEGREES | DIMENSIONS IN MILLIMETERS (IN PARENTHESIS)<br>DECIMALS XX ±0.3<br>XXX ±0.13<br>ANGLES ±2 DEGREES |
| FILLETS AND RADII<br>.003 - .005 | FILLETS AND RADII<br>(0.07 - 0.13) |
| DD011 REV. B 03/13/98 | |

| | | | | | | |
|---|---|---|---|---|---|---|
| DRAWN | DBJ | 3/29/02 | MFG | JMS | 4/8/02 |
| CHK'D | DM | 4/4/02 | ENGR | WSH | 4/10/02 |
| APP'D | WEM | 4/8/02 | DM | DPC | 4/8/02 |

TITLE: INSTALLATION DRAWING
MODEL 101A & 102A02, A07, A09, A12
PRESSURE SENSORS

PCB PIEZOTRONICS
3425 WALDEN AVE. DEPEW, NY 14043
(716) 684-0001 EMAIL: SALES@PCB.COM

| CODE IDENT. NO. | DWG. NO. |
|---|---|
| 52681 | 8495 |
| SCALE: 2X | SHEET 1 OF 1 |